Colloids in Ultra-Low Dielectric Media

Surface Forces and Self-Assembly

Soumi Banerjee

Thesis committee

Promotor

Prof. Dr M.A. Cohen Stuart
Professor of Physical Chemistry and Colloid Science
Wageningen University

Co-promotor

Dr J.M. Kleijn
Assistant professor, Laboratory of Physical Chemistry and Colloid Science
Wageningen University

Other members

Prof. Dr C.G.P.H. Schroën, Wageningen University
Prof. G.J.T. Tiddy, The University of Manchester, United Kingdom
Prof. G.-J. Witkamp, Delft University of Technology, the Netherlands
Dr P. Jaeger, The University of Hamburg-Harburg, Germany

This research was conducted under the auspices of the Graduate School for Socio-Economic and Natural Sciences of the Environment (SENSE).

Colloids in Ultra-Low Dielectric Media

Surface Forces and Self-Assembly

Soumi Banerjee

Thesis

submitted in fulfilment of the requirements for the degree of doctor
at Wageningen University,
by the authority of the Rector Magnificus
Prof. Dr M.J. Kropff,
in the presence of the
Thesis Committee appointed by the Academic Board,
to be defended in public
on Wednesday 2 October 2013
at 4 p.m. in the Aula.

Soumi Banerjee
Colloids in Ultra-Low Dielectric Media
Surface Forces and Self-Assembly
272 pages

PhD thesis, Wageningen University, Wageningen, The Netherlands (2013)
with references, with summaries in English and Dutch.

ISBN: 978-94-6173-685-7

Contents

Chapter 1

Introduction

1.1 General introduction

Colloidal interactions in apolar media and how these interactions are influenced by surfactants are the subject matter of this thesis. The two main aspects covered are surface forces and surfactant self-assembly in low dielectric solvents such as hexane and liquid CO_2. The aspects discussed have direct relations to the application of liquid CO_2 as a dry-cleaning medium.

Dry-cleaning is a process of removing soils and stains from fabrics and garments using a non-aqueous solvent with additives. Traditional dry-cleaning methods employ organic solvents such as perchloroethylene (PERC), which is toxic and environmentally harmful. PERC is classified as carcinogenic to humans (IARC Group 2A classification) and an ozone layer depletant, air pollutant and a groundwater contaminant. There are increasing legal restrictions on the use of PERC or other conventional dry-cleaning solvents, i.e., chlorinated fluorocarbons and hydrocarbons. As a result, the present research on dry-cleaning involves replacement of PERC and similar solvents as the dry-cleaning medium and looking for an alternative solvent which is environmentally benign, non-toxic, and economical.

Carbon dioxide is a possible candidate. It is non-toxic, non-flammable, ecologically sound, cheap, and available on a large scale. An important differ-

ence between dry cleaning with PERC or other currently used solvents, and dry-cleaning with CO_2 is that carbon dioxide dry cleaning needs a substantially higher pressure (45 - 60 bar) than atmospheric pressure. Therefore, a new process for dry-cleaning has to be developed. Literature on dry-cleaning using liquid CO_2 revealed that removal of oily soil was comparable or in some cases better than PERC, however, detergency of small particulate soil (size less than 20 μm) was inadequate compared to the cleaning performance of PERC. Higher input of mechanical action could not improve the cleaning performance of particulate soil in liquid CO_2 and as a result the perspectives of liquid CO_2 as a dry cleaning solvent remained limited. This is the backdrop of the research undertaken in this thesis. The aims are summarized below.

1.2 Aim of this Research

Understanding the physico-chemical aspects of dry-cleaning in liquid CO_2 is the overall aim of this thesis. The effects of adding cleaning aids such as water or alcohol on the soil removal process have been dealt with fundamentally. Another goal was to investigate the effect of surfactant on these processes. The final aim was to propose design guidelines for a CO_2 soluble surfactant.

1.3 Outline of this thesis

The research carried out to approach the above-mentioned aims can broadly be classified into two parts. The first part deals with measuring the interaction forces between model surfaces in a model apolar solvent, i.e., n-hexane. The interaction forces have been measured with colloidal probe atomic force microscopy and the results are described in Chapters 3 - 5. The second part (Chapters 6 - 8) contains experiments in liquid CO_2. Moreover, the experimental results are complimented with a self-consistent field based theoretical model. To provide context, a review of current literature and some critical analysis is presented in Chapter 2 to provide the knowledge on the current state-of-the-art. At the end of this thesis, a general discussion followed by

a summary is given. The content of the thesis Chapters is briefly outlined below.

In Chapter 2 we focus on describing the problem definition from colloidal perspectives. This Chapter contains a review of the dry-cleaning process/ industry followed by a discussion of the complexity of the problem at hand at various length scales: from macro to micro down to the nano-length scales. We give an overview of the surface forces that are important and the role of the additives such as water, alcohol and surfactant in altering these forces.

Chapter 3 experimentally underpins the effects of water in mediating the surface forces between the interacting model fabric and soil surfaces through a model apolar solvent. The role of roughness and softness of the interacting surfaces on the kinetics, magnitude and range of the force have been addressed.

In Chapter 3 it is shown that water results in a higher adhesion force, by forming capillary bridges, and this could be one of the reasons behind poor detergency of particulate soil in liquid CO_2 dry-cleaning since water is always present in this process. Hence, we wanted to study if a surfactant can reduce the capillary forces to increase the soil removal efficiency. To this end, a surfactant formulation was designed in hexane. This was further tested in a pilot scale dry-cleaning apparatus. The results have been summarized in Chapter 4.

Chapter 5 provides further insights into the effects of surfactant mesophases, such as reverse micelles and lamellar phases, on the force of interactions between model surfaces. It was argued that the oscillatory force-distance curves originate from long-range ordering of mesophases between the confined surfaces.

In Chapter 6, experiments and modeling on the real system, i.e. liquid CO_2, are presented. The surface force measurements on the model (hexane) system and the detergency experiment in the liquid CO_2 have indicated that cleaning efficiency can indeed be improved by the use of surfactants. However, finding a surfactant for liquid CO_2 is challenging. Liquid CO_2 near the critical pressure and temperature is a poor solvent and hence solubility of surfactants in this medium is low. The quest for a suitable surfactant molecule

was done following a systematic selection approach based on the hypothesis of fractional free volume, then testing its solubility first in the model solvent, and followed by testing in the liquid CO_2 system, measuring its interfacial activity at the water-liquid CO_2 interface, and finally studying its self-assembly in liquid CO_2 in the presence of water. The surfactant chosen was a low molar mass, branched hydrocarbon, polyoxyethylene non-ionic (C_iEO_j). The common name of this surfactant is Igepal CA520.

The experimental study of water-liquid CO_2 interfaces with or without the surfactant is difficult: first, the interface is not always readily accessible as it requires high-pressure instrumentation, and, secondly, even when the system is accessible, wetting and adsorption studies at such interfaces are difficult to perform. Hence, gaining molecular insight requires the use of complimentary methods, such as theoretical modeling. With this vision and to gain molecular understanding in the liquid CO_2 system, from this point onwards we have taken a combined approach of experiments and modeling.

Understanding interfacial activity of the surfactant at the water-liquid CO_2 interface demands knowledge of the pristine water-liquid CO_2 interface. Hence we first discuss in detail in Chapter 6, the interfacial and wetting behaviour of the water-CO_2 biphasic system at various pressures. For the modeling, we employ the numerical tool of the self-consistent field (SCF) theory of Scheutjens and Fleer (SF).

These studies were further extended to a surfactant containing system as described in Chapter 7. This Chapter addresses the interfacial and bulk behavior of the surfactant-water-liquid CO_2 system. The partial phase behavior of the surfactant in liquid CO_2 as well as in water has been mapped using the SF-SCF theory. The thermodynamics of self-assembly has also been described. The model has been compared with the experimental findings, and is found to describe the system satisfactorily.

Finally, X-ray scattering was used to study the phase behaviour of Igepal CA520 in liquid CO_2. Water was used to drive the self-assembly. The results, which unambiguously demonstrate the presence of surfactant aggregates are presented in Chapter 8.

At the end of the thesis a general discussion is presented where we reflect on the major findings of this work. Some additional observations have been added to this chapter, and guidelines for the design of a suitable surfactant for liquid CO_2 are provided. Although the findings are directly linked to the application of dry-cleaning, the outcome of this thesis can also be extended to other fields of research, such as tertiary oil recovery, oil based paints and geological storage of CO_2.

Chapter 2

Colloidal Interactions in Liquid CO_2: A Review [a]

Liquid CO_2 is a viable alternative for the toxic and environmentally harmful solvents traditionally used in dry-cleaning industry. Although liquid CO_2 dry-cleaning is being applied already at a commercial scale, it is still a relatively young technique which poses many challenges. The focus of this review is on the causes of the existing problems and directions to solve them. After presenting an overview of the state-of-the-art, we analyse the detergency challenges from the fundamentals of colloid and interface science. The properties of liquid CO_2 such as dielectric constant, density, Hamaker constant, refractive index, viscosity and surface tension are presented and in the subsequent sections their effect on CO_2 dry-cleaning operation are delineated. We show, based on theory, that the van der Waals forces between a model soil (silica) and model fabric (cellulose) through liquid CO_2 are much stronger compared those across water or the traditional dry-cleaning solvent perchloroethylene (PERC). Prevention of soil particle redeposition in liquid CO_2 by electrostatic stabilization is challenging and the possibility of using electrolytes having large anionic parts is discussed. Furthermore, the role of different additives used

[a] This chapter is published as: Soumi Banerjee, Stevia Sutanto, J. Mieke Kleijn, Maaike. J.E. van Roosmalen, Geert-Jan Witkamp, Martien A. Cohen Stuart, Adv. Colloid Interface Sci., 175, 2012, 11-24.

in dry-cleaning, such as water, alcohol and surfactants, is reviewed. Water is used as an aid to remove polar soils, but it also enhances adhesion between fabric and soil by forming capillary bridges. Its role as a minor component in liquid CO_2 is complex as it depends on many factors, such as the chemical nature of fabrics and soil, and also on the state of water itself, whether present as molecular solution in liquid CO_2 or in phase separated droplets. The phenomena of wicking and wetting in liquid CO_2 systems are predicted from the Washburn-Lucas equation for fabrics of various surface energies and pore sizes. It is shown that nearly complete wetting is desirable for good detergency. The effect of mechanical action and fluid dynamic conditions on dry-cleaning are analysed theoretically. From this it follows that in liquid CO_2 an order of magnitude higher Reynolds number is required to exceed the binding forces between fabric and soil than in PERC or water, mainly due to the strong van der Waals forces and the low viscosity of CO_2 at dry-cleaning operational conditions.

2.1 Introduction

Liquid and supercritical (sc) carbon dioxide are gaining importance as an alternative to toxic organic solvents in various industrial processes such as dry-cleaning[1] , dying of polyester,[2] extraction of natural materials,[3] emulsion polymerization,[1] nanoparticle synthesis,[4] enzymatic catalysis,[5] photo-resist drying[6] and metal extraction.[7] CO_2 is environmentally benign, non-flammable, inexpensive, does not leave any traces in the products and is available on a large scale. An important difference with respect to the currently used solvents is that CO_2 needs a substantially higher pressure than atmospheric. In dry-cleaning this has the advantage that it is quite easy to separate the CO_2 from the detergent formulation and the soil after the cleaning process; in addition, the CO_2 spontaneously evaporates from the fabrics during depressurization, so no additional energy intensive drying step is needed (and no heat damage occurs).

Carbon dioxide has a relatively low critical point, at 304 K and 73.8 bar.

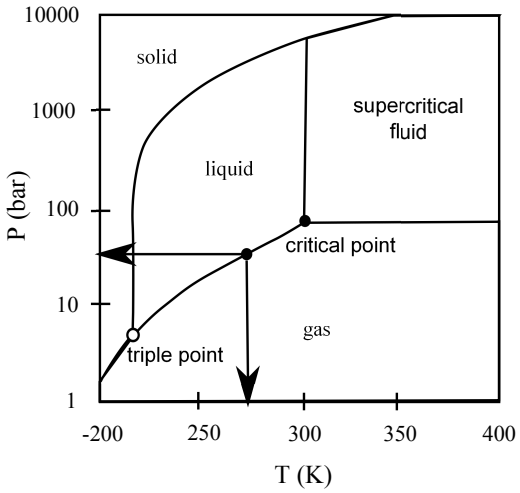

Figure 2.1: *The pressure-temperature phase diagram of* CO_2*. The critical pressure and temperature are 73.8 bar and 304 K, respectively. Above the critical point,* CO_2 *is in the supercritical state. The black dot on the gas - liquid boundary represents the pressure and temperature usually applied in dry-cleaning, i.e. ca 45 bar and 283 K. (Adapted from Leitner*[8]*)*

Above the critical temperature and pressure it is in the supercritical state (see Figure 2.1), where it displays liquid like density and gas like viscosity.[1]

In dry-cleaning operation, the liquid state of CO_2 is preferred over the supercritical state. During the washing process, the pressure and temperature combination is maintained at values such that the system always stays at the two-phase boundary line (Figure 2.1), i.e. the liquid CO_2 stays in equilibrium with the saturated CO_2 gas. The presence of the gas-liquid interface has been reported to be beneficial for cleaning as soil particles can be trapped at the high energy gas-liquid interface. In addition, the gas-liquid biphase is necessary to achieve mechanical action in the washing process in a rotating system; we will come back to this in Section 2.3.

Research on dry-cleaning with liquid CO_2, replacing the traditionally used harmful and toxic cleaning agent perchloroethylene (PERC, $Cl_2C{=}CCl_2$), started in 1973.[9] Chemically, liquid CO_2 and PERC are very different molecules and hence the fluid dynamics and the cleaning efficiencies of these

solvents are also very different. The research in CO_2 dry-cleaning has been mainly focused on two areas: the optimization of the cleaning equipment (solvodynamics) to make it most suitable to use with liquid CO_2 and the design of a detergent (including surfactants) to improve the cleaning efficiency in the liquid CO_2 medium.

In the context of textile cleaning in a given liquid, it is useful to distinguish between three kinds of dirt (soil) that have to be removed:

(i) Substances that are soluble in the pure solvent (ii) Substances that are insoluble but can be solubilized with the help of additives (iii) Particulate soil: particles attached to or trapped in the textile matrix.

The removal of (i) is obviously a solubility issue: which molecules are soluble in the given liquid and why, and what influence do pressure and temperature have? For (ii), substances are needed that improve the solvent quality (co-solvents) or that form pools that remain suspended in the liquid and in which the dirt can dissolve. These pools include small stabilised droplets of a second liquid immiscible with the main one, or micelles formed by suitable amphiphiles. Liquid and additive together form the wash liquor. In order to successfully remove (i) and (ii), it is needed that the wash liquor can reach the dirt on the textile surface, i.e. full penetration (wicking) into the porous textile material has to occur readily.

For the successful removal of (iii), the forces that keep particles bound to a fibrous material have to be modified or overcome. Trapping forces originate from the elasticity of the textile fibres; friction forces originating from the roughness of the fabric and particle surfaces; surface forces acting between particle and textile surfaces and can have various contributions, such as H-bridges, dispersion (van der Waals) forces and electrostatic forces. Surface forces can be modified by changing the state of the surfaces, e.g., by adsorption of suitable additives, or by changing the pressure or temperature. However, as long as the surface forces remain attractive, particles can only be removed by the action of external forces, such as viscous drag by bulk liquid or by a moving three-phase contact line. A discussion of particle removal therefore involves a discussion of many physicochemical aspects: fibre swelling and elasticity,

surface forces in solutions and two-phase systems, viscous drag, and capillary forces exerted by bubbles and droplets. Hence, various interfaces play roles, so that we have to consider interfacial tensions and adsorption on all of these, but friction forces are also important, implying that we also must discuss the flow of liquid and the motion of contact lines and the effects of additives on these.

For the further development of CO_2 dry-cleaning (i.e., finding suitable additives as well as optimizing the machine design), a thorough understanding of the interaction forces between colloidal bodies in apolar media is needed. We think that there is a gap between the currently employed technology and the fundamental understanding of the dry-cleaning and hence a dovetailing is necessary to increase the cleaning performance of liquid CO_2. Keeping this in mind, in this review we focus on different aspects of the science behind dry-cleaning: first we identify the challenges associated with liquid CO_2 in relation to the interaction forces between soil particles and fabric. We explore the roles of water and additives often found associated with the dry-cleaning formulation. We discuss current surfactant design concepts and show that most of these have been borrowed from water-based cleaning formulations, which may not be beneficial to have a breakthrough. Finally, the effects of mechanical action and fluid dynamic conditions on dry-cleaning are analysed theoretically.

2.2 State of the art: dry-cleaning with liquid CO_2

Substantial efforts have been made by both the academic and industrial community to employ CO_2 in the cleaning of clothing, mechanical parts, the surface of microelectronics components, membranes and filters.[10–12] Understanding the problems associated with liquid CO_2 dry-cleaning requires knowledge of the detergency process in general. Historically, washing processes were developed and optimized for water, the most often employed cleaning medium. Extensive research, both fundamental and applied, has been carried out by various groups of scientists and many scientific reviews can be found in the

literature focusing on various aspects of detergency in aqueous systems.[13–19]

Research indicated that in water-based systems the main challenge lies in removing the apolar soil from the fabric. The main components in body soil (also called sebum) are fatty acids, triglycerides, cholesterol, wax esters and squalene, which are medium to high molecular weight apolar components.[20,21] It is also known that fatty acids like oleic acid, which remain after each cycle of cleaning, can polymerize and then become higher in molecular weight, thereby increasing the difficulties in removing them from the garment in subsequent cycles.[22] The approach here is to add an amphiphilic component (surfactant), which tends to accumulate on interfaces between water and apolar materials, and can also solubilise apolar molecules in water. Particulate soil (e.g. clay, soot) is often also quite readily detached by surfactants. Detached (dispersed) particles have to be kept away from the fabric during the wash by means of anti-redeposition agents.

Understanding of dry-cleaning in CO_2 is far less developed. Only a few papers and reports can be found on dry-cleaning in liquid CO_2.[23–28] Studies by van Roosmalen *et al.*[24–27] indicate that the removal of non-polar soils in CO_2 is comparable to that in PERC, whereas the removal of particulate soil in CO_2 is lower. Particles are bound to the textile surface by various forces such as electrostatic and/or van der Waals forces. In addition, they may be mechanically bound by being trapped between fibres. Particle removal can be improved by applying mechanical action, exceeding the binding forces between the particles and the fibres without damaging the textiles. The binding forces may be decreased by the addition of surfactants. For the removal of relatively large particles (e.g. sand), mechanical action is the most important factor whereas for small particles ($<20\ \mu$m, e.g. carbon black and clay) a combination of mechanical action and surfactants is probably required.[24]

The European DETECTIVE (2000-2004 LIFE) project[28] evaluated the feasibility of liquid CO_2 as a replacement of PERC. Numerous CO_2 textile washing experiments were conducted in full scale machines with different commercial detergents, pre-spotting agents and mechanical agitation levels. Several advantages of liquid CO_2 textile cleaning compared to PERC dry cleaning

were identified with respect to textile behaviour, like less dimensional change of sensitive fabrics, less color loss of the fabrics, less direct bleeding of color from one fabric to the other, and less loss of textile fibers during the cleaning cycle leading to a longer garment lifetime. It was reported that the washing performance of CO_2 was lower compared to that of PERC and other solvents (hydrocarbon, cyclosiloxane and water); CO_2 textile dry-cleaning alone could not remove all the soils, especially the insoluble particulate ones. The commercially available detergents for liquid CO_2 textile cleaning do increase the cleaning performances, but the results depend on the type of stain. One of the reported drawbacks was redeposition.

Despite all these studies, the mechanism of detergency in liquid CO_2 is at best partly understood. The proposed mechanism for removal of apolar soils, mainly fats, oils and greases, is dissolution. For removal of CO_2 insoluble soils (polar soils, mainly sugars and salts) the mechanism is probably solubilisation by surfactants with the addition of a co-solvent or water or using a pre-spotting agent. Pre-spotting agents are chemical mixtures that are used in all dry-cleaning processes and are brought into contact with the stained area before the washing process. Finally, insoluble particles have to be removed by detachment and dispersion and this turns out to be problematic.

Another challenge in particulate soil cleaning in liquid CO_2 is the problem of redeposition of the soil particles during the wash. If after the detachment the soil particles are not stabilized in the washing liquor, they often get deposited elsewhere on the garments.[29] In water-based cleaning, the problem of redeposition is solved by the incorporation of anti-redeposition agents in the formulation. Anti-redeposition agents are surfactants or water soluble polymeric stabilizers such as sodium carboxymethyl cellulose, polymeric cellulose acetate and polyvinyl alcohol compounds.[29] The principal modes of action of these anti-redeposition agents are stabilization by increasing the electrostatic repulsion between soil particles and steric stabilization. In dry-cleaning with CO_2, charge stabilization of particulate soil is almost impossible, because of its low dielectric constant. Moreover, steric stabilization is difficult, as most polymers are insoluble in CO_2 unless the density of the CO_2 and hence the

pressure is sufficiently high. The stabilization of particles in dense CO_2 is discussed in Section 2.6.3 and possible solutions to prevent redeposition in CO_2 dry-cleaning are given in Section 2.9.

2.3 Properties of liquid CO_2

The environmentally benign dry-cleaning solvent liquid CO_2 has many advantages which have been described in the introduction section of this review. However, there are several disadvantages associated with liquid CO_2 that make dry-cleaning a difficult job. Dry-cleaning with CO_2 employs a pressure and temperature at which the CO_2 is in the liquid state (Figure 2.1). Given the proximity of the critical point, CO_2 is a strongly compressible fluid. Its density changes with pressure, as shown in Figure 2.2a. The variation of its physicochemical properties with density, i.e. dielectric constant, refractive index, Hamaker constant, viscosity and interfacial tension, is depicted in Figure 2.2b.

CO_2 molecules are linear and symmetric. They have no dipole moment and a low polarizability[30] ($\sim 2.6 \times 10^{-24}$ cm^3), resulting in a low zero frequency dielectric constant and a low Hamaker constant (Figure 2.2b). The low cohesive energy density of CO_2[31] close to its critical temperature, even at reasonable pressure, is responsible for its poor solubilizing capacity. For this reason dry-cleaning using CO_2 is a challenging task. However, CO_2 is not entirely inert: it has a quadrupole moment[32] (-4.1×10^{-26} e.s.u.) and can act as H-acceptor in hydrogen bonds. Therefore, hydrogen bond donors have a modest solubility in liquid CO_2

The density of CO_2 is 850 - 900 kg m^{-3} at the operating conditions for dry-cleaning. Apart from the properties mentioned so far, CO_2 also has a very low viscosity: about 10^{-4} Pa s at 45 bar and 10 °C (cf. at 1 bar and room temperature, water has a viscosity of 0.001 Pa s). As a result the momentum transfer in liquid CO_2 is low and attainment of sufficient mechanical action in liquid CO_2 cleaning is a challenge. In addition, in textile cleaning the mechanical action is created by the drum rotation (the paddles on the inside of the drum lift the wash load to the top of the drum from where it falls

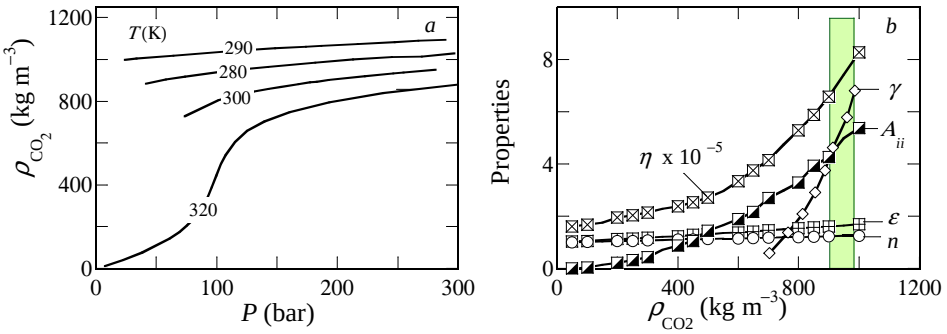

Figure 2.2: *(a) Density of liquid* CO_2 *as a function of pressure at various temperatures as indicated. Data taken from Diller et al.*[33] *(b) Physico-chemical properties of* CO_2 *with increasing density. The dielectric constant and refractive index values have been calculated using the equations of states for* CO_2 *after Ely et al.*[34] *The viscosity (Pa s) data has been derived from the data of Diller et al.*[33] *The surface tension (mN* m^{-1}*) data has been plotted from the data reported by Quinn.*[35] *The Hamaker constants (*A_{ii}*) is expressed in the units of kT. The highlighted region indicates the industrially relevant density range of liquid* CO_2 *for dry-cleaning. The variation of* CO_2 *density as a function of pressure and temperature is given in (a).*

to the bottom) and the mechanical energy generated is proportional to the difference in density between the liquid and gas in the cleaning machine. The difference in density for CO_2 is 720 kg m^{-3} at 10 °C (strongly depending on temperature) as opposed to PERC, for which the density difference is 1600 kg m^{-3} (rather independent on temperature). This means that the mechanical energy employed during CO_2 textile cleaning at 5 °C is less than half of that employed during PERC dry-cleaning (neglecting any differences in drum size). This effect leads to a lower cleaning performance of CO_2 in comparison to that of PERC.[28]

Knowledge of the interfacial properties of liquid CO_2 is also important for dry-cleaning applications. Although surface tension and wettability play a major role in fluid transport along the interfaces, these properties are less explored and the information available in the scientific literature is scarce. We could not find any information on contact angles of liquid CO_2 on typical fabric surfaces and data on surface tension are limited as well. The variation

of surface tension with the density of liquid CO_2 has been reported by Quinn[35] and is shown in Figure 2.2. The surface tension of liquid CO_2 has been reported to vary from 16.5 to 0.59 mN m^{-1} in the temperature range of -52 to 25 °C.[35,36] Jianxin *et al.*[36] compared their experimentally measured values to values calculated from semi-empirical and statistical theories based on the equation of state. Their measurements and calculations are limited because the effect of pressure on the surface tension of liquid CO_2 was ignored. From Figure 2.2 it can be seen that the surface tension of liquid CO_2 in the pressure and temperature range of dry-cleaning operation is $\sim 3-4$ mN m^{-1} which implies that liquid CO_2 should be a completely wetting solvent for most surfaces, which is advantageous for dry-cleaning.

2.4 Particle-fibre interaction forces

In this section we examine the forces that are important for the removal of soil particles from fabric in liquid CO_2 dry-cleaning and where possible, we compare with such forces in water and PERC. We consider in particular dispersive (van der Waals) and electrostatic interactions, the so-called DLVO (Derjaguin, Landau, Verweij and Overbeek) forces.[37] Other interactions between soil and fabric, such as H-bonding and specific interactions (chemical affinity), may exist but are difficult to assess. First, we calculate the dispersive forces between a soil particle and fabric in liquid CO_2, water and PERC.

2.4.1 Dispersive interactions

The van der Waals interaction energy between soil (component 1) and fabric (component 2) interacting through solvent (component 3) has been calculated from the sphere-plate model using the following equation:[38–41]

$$V = \left[-\frac{A_{132}}{6}\left(\frac{2R(R+d)}{d(d+2R)} - \ln\frac{d+2R}{d}\right)\right]\left[\frac{1}{1+14\frac{d}{\lambda_L}}\right]\left[\frac{1}{1+\frac{B}{d}}\right] \qquad (2.1)$$

where R is the radius of the soil particle and d is the distance between the soil and the fabric surface, λ_L is the London wavelength (assumed 100 nm)[42] and B is the roughness parameter, the value of which is assumed to be 2 nm.[39,40,42] The composite Hamaker constant[41] (A_{132}) is calculated from the equation,

$$A_{132} = \left(\sqrt{A_{11}} - \sqrt{A_{33}}\right) - \left(\sqrt{A_{22}} - \sqrt{A_{33}}\right) \tag{2.2}$$

In the above equation, the individual Hamaker constants interacting through vacuum are represented as A_{ii} and have been calculated from the Lifshitz approximation[41] as,

$$A_{ii} = \frac{3}{4k_BT}\left(\frac{\epsilon_i - \epsilon_{vac}}{\epsilon_i + \epsilon_{vac}}\right)^2 + \frac{3h\vartheta_e}{16\sqrt{2}}\frac{\left(n_i^2 - n_{vac}^2\right)^2}{\left(n_i^2 + n_{vac}^2\right)^{\frac{3}{2}}} \tag{2.3}$$

In this equation, ϑ_e is the maximum electronic ultraviolet absorption frequency[41] and ε_i and n_i are the dielectric constant and refractive index, respectively. For CO_2, ε_i and n_i have been calculated using the following equations:[34,43]

$$\frac{n^2 - 1}{n^2 + 2} = 0.07016\rho_r + 1.412 \times 10^{-4}\rho_r^2 - 3.171 \times 10^{-4}\rho_r^3 \tag{2.4}$$

$$\rho_r = \frac{\rho}{\rho_c} \tag{2.5}$$

$$\varepsilon - 1 = 0.2386\rho_r + 0.02602\rho_r^2 \tag{2.6}$$

In which ρ, ρ_c and ρ_r are the bulk, critical and reduced densities respectively. The values thus obtained agree with the values reported in literature by Keyes *et al.*[44] and Besserer *et al.*[45] ($\varepsilon_i = 1.6$ and $n_i = 1$ at 850-900 kg m^{-3} respectively). For water, PERC, silica (model soil) and cotton (model fabric) the values of ε_i and n_i were directly taken from literature. For the radius of the soil particle we used 3 μm.

In Figure 2.3 the van der Waals interaction energy as a function of

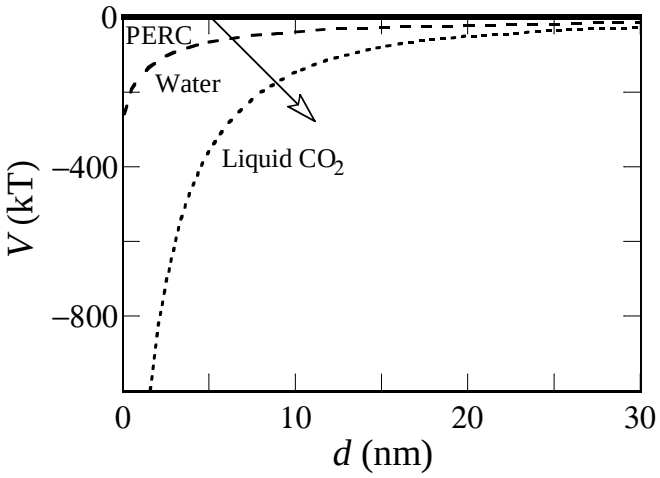

Figure 2.3: *Van der Waals interaction energy between a model soil particle (silica, radius 3 μm) and fabric (cellulose) in PERC, water and liquid* CO_2.

particle/fabric separation d is compared for the three solvents: in PERC there is almost no van der Waals attraction between fabric and soil whereas there is a strong interaction between the two when CO_2 is the liquid medium. Probably this is one of the reasons for poor particle removal in liquid CO_2 dry-cleaning.

2.4.2 Electrostatic interactions

Classically, the effect of surface charge on the interaction between particles and macroscopic surfaces in apolar media has been considered using a generalized DLVO model.[37] In apolar media the surface charge density on any dispersed particle is low and the potential at the slip plane of the particle (the zeta potential) is also low. The Debye length,[41] which is the characteristic thickness of the electric double layer around a charged particle, is large (typically on the order of microns),[46] making the overlap of neighbouring double layers likely, although the repulsive forces are extremely weak. The Debye length ($1/\kappa$) can

be written as,[42]

$$\frac{1}{\kappa} = \sqrt{\frac{\varepsilon\varepsilon_0 k_B T}{2N_A e^2 I}} \tag{2.7}$$

where e is the elementary charge, ε the relative dielectric constant of the apolar medium, ε_0 the vacuum permittivity, k_B the Boltzmanns constant, T the temperature, N_A Avogadros number and I the ionic strength. As can be seen from this equation, the Debye length in apolar media is large due to the low electrolyte dissociation (low I) and not directly due to the low dielectric constant ε of the apolar medium. For liquid CO_2, the Bjerrum length λ_B, which is the distance of separation at which the electrostatic interaction between two unit charges is comparable to the thermal energy ($k_B T$), would also be large.[42,47] This length is given by,

$$\lambda_B = \frac{e^2}{4\pi\varepsilon\varepsilon_0 k_B T} \tag{2.8}$$

The typical Bjerrum length[47] for a solvent with a dielectric constant of 2 is 25-30 nm compared to 0.7 nm for water with dielectric constant 80. This means that in liquid CO_2 dissolved salts (if any) would hardly dissociate.

The high van der Waals forces and lack of electrostatic stabilization of the particles lead to the redeposition associated with liquid CO_2 cleaning. Electrostatic stabilization of particle suspensions in liquid CO_2 may be enhanced by specific adsorption of ionic species at the particle surface and effective shielding of individual charges by large moieties (to prevent ion pair formation). The effect of the size and structure of ions on ion-pair formation and dissociation can be explained from the Fuoss equation,[42] which relates the dissociation constant (K_D) with the radius (a) of the ions and the dielectric constant of the apolar solvent:

$$K_D = \frac{10^3}{\frac{4}{3}\pi a^3 N_A} \exp\left(\frac{-e^2}{4\pi\varepsilon\varepsilon_0 k_B T}\frac{1}{a}\right) \tag{2.9}$$

In the literature one finds the use of aluminium diisopropylsalicylate, tetra (isoamyl) ammonium picrate and calcium stearylcyclohexyl-benzene sulphon-

ate as electrolytes for apolar media, owing to their large anionic parts (high polarizability). However, electrostatic stabilization in CO_2 at a pressure of 50 bar, relevant for dry-cleaning, has not been reported till date. A breakthrough in particle stabilization through the route of electrostatic stabilization would help to decrease the redeposition.

Addition of water as a minor component together with a suitable surfactant can play a significant role in liquid CO_2 dry-cleaning by providing a route to reduce the redeposition of soil. Self-association of surfactants in liquid CO_2 would lead to the formation of reverse micelles. The polar cores of the reverse micelles are known to solubilize water as mentioned earlier. Water trapped inside the reverse micelles can carry additional ions.[48] We will come back to this in Section 2.6.

2.5 Structural and mechanical properties of fabric

In general, fibre surface irregularities and cross-over points play a role in the collection of dirt. If surface roughness would have a great influence on soil retention, one would expect polyester fabrics with their smooth surfaces to retain less soil and thus easier to clean than cotton and wool fabrics with scales.[18] However, for wool better cleaning results have been obtained in liquid CO_2 than for cotton and polyester.[24] Apparently, the effect of surface roughness of the fibres on the washing results is limited and other characteristics, like chemical nature, flexibility and porosity, are more important. In water-based cleaning it is known that cotton gets plasticized in water and swells, leading to a fast diffusion of water inside the fibres. A study by Beltrame *et al.*[49] has indicated that cotton and polyester (polyethylene teraphthalate, PET) behave in completely different ways when dipped in sc CO_2, cotton behaving in a much more glassy way, making the dyeing of cotton in sc CO_2 technically challenging. The state of fabrics (glassy or rubbery) seems to be relevant for dry-cleaning as well, but the effect has not been reported anywhere in literature so far. Like in sc CO_2, in liquid CO_2 cotton fabrics are expected to be less flexible than in water. The effect of the viscoelasticity of fabrics could

be crucial for particle removal depending on the time scales involved in the detergency process and should be investigated in future.

What has been investigated to some extent is the effect of the CO_2 dry-cleaning process on the physical and mechanical properties of fabrics. Rombaldoni *et al.*[50] investigated the change in properties of six different wool and wool/cashmere fabrics. Their results showed that the combined effect of CO_2, surfactant, small quantities of water and isopropyl alcohol resulted in loss of tension of the fabrics, swelling and changes in their structure. The swelling of the fibres resulted in thicker and fuller fabrics. A significant modification of the shear hysteresis was measured, i.e. the CO_2 dry-cleaning process resulted in a loss of elasticity of the fabrics under shear. However, no particular modifications were noted for bending and tensile properties or crease pressing performance and the changes in the properties of the fabrics were within acceptable limits for dry-cleaning applications. In the DETECTIVE final report[28] it was mentioned that in general fabrics exhibit less shrinking in CO_2 dry-cleaning compared to washing with PERC and water (38 different textile materials were investigated). The effect was attributed to the lower mechanical action in the CO_2 process.

2.6 Role of additives in liquid CO_2

So far we have discussed the three basic components involved in dry-cleaning: soil, fabric and solvent. Apart from these, a number of additives are commonly used in dry-cleaning, such as water, surfactants and alcohol. These additives will interact with the other three components in intricate ways and contribute somehow to the overall cleaning performance. In this section, we will delineate the role of some individual additives in dry-cleaning.

2.6.1 Water

In the dry-cleaning industry water is deliberately added to help increase the removal of polar soils.[25] Moreover, some water will always be present in the liquid CO_2 phase, introduced by the textile material itself since textiles absorb

moisture from the atmosphere and water can be introduced together with (body) soils as well. Water as a co-solvent has been hypothesized to increase the dielectric constant of liquid CO_2 and thereby enhancing the removal of the polar soils. However, only molecular dissolved water would contribute to this increase and the amount of water which can be solubilized in liquid CO_2 is small (in the order of 1000 ppm).[51] Water amounts exceeding this solubility limit can remain either as free water droplets or adsorbed by the textiles. An account on the equilibrium distribution of water in sc CO_2 can be found in reference 51. Estimation of the increase of the dielectric constant as a result of dissolved water-based on the linear mixing rule shows that it is negligible (from $\varepsilon = 1.6$ to 1.7 at the most). A more straightforward explanation for the beneficial effect of water is that in the presence of water droplets polar components of the soil can simply dissolve in these droplets. In addition, water present at the surfaces of particles or fibres can promote the dissociation of surface groups thereby providing stability against flocculation of particles and preventing redeposition.[42] However, van Roosemalen *et al.*[52] have shown that above a certain water content, the detergency process in liquid CO_2 becomes less effective. To understand this observation we first have to understand the interactions of water with the soil-fabric-liquid CO_2 system.

So far we have only focused on the DLVO type of interactions between the components, i.e., van der Waals and electrostatic interactions (Section 2.4). However, when water is introduced in the system other interactions such as capillary and hydrophobic interactions can become important.[53] For example, water can form capillary bridges between soil particles and fabric,[54] which makes detachment of particles more difficult and can increase redeposition of soil particles on the garments. Such a capillary bridge is schematically depicted in Figure 2.4.

When a homogeneous phase, in which one of the components is near its saturation point, is confined between two surfaces, a new phase can be formed by condensation. Condensation of water from a supersaturated mixture of water and apolar liquid is commonly discussed in terms of the classical theory of nucleation and growth.[55,56] The change in free energy (ΔG) due to

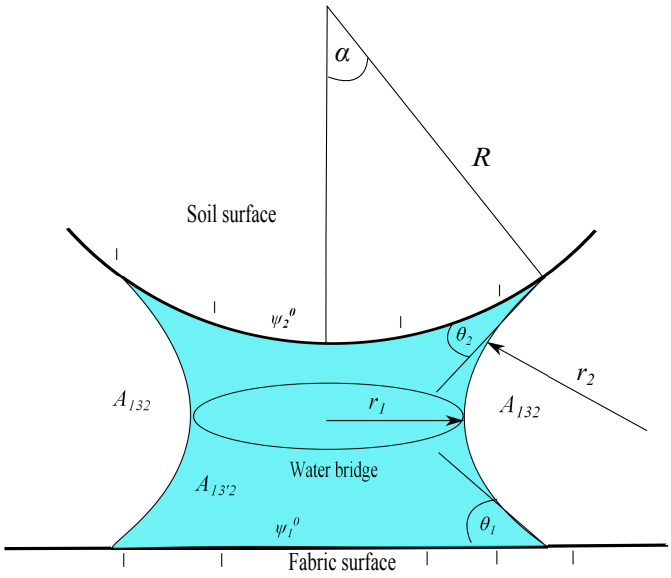

Figure 2.4: *Schematics of a capillary bridge between a soil particle (sphere) and a fabric surface (plate). The two radii of curvature of the capillary bridge are represented by r_1 (< 0) and r_2 (> 0); θ_1 and θ_2 are the contact angles of water with the fabric and the soil surface, respectively, and is the filling angle; ψ_1^0 and ψ_2^0 are the surface potentials of the fabric and soil respectively. The van der Waals forces will be governed by the composite Hamaker constants A_{132} and $A_{13'2}$. The former represents van der Waals interactions between particle and fabric through the apolar medium while the latter represents the interactions of the same bodies through the condensed water.*

condensation of water (denoted by W) in the confined space between cellulose and silica from an apolar liquid (C) can be expressed as[57]

$$\Delta G = -v\Delta G_v + A_{WC}\gamma_{WC} - A_{W-Cellulose}\left(\gamma_{W-Cellulose} - \gamma_{C-Cellulose}\right) + A_{W-Silica}\left(\gamma_{W-Silica} - \gamma_{C-Silica}\right) \tag{2.10}$$

where v is the volume of the water nucleus and $\triangle G_v$ is the free energy change due to the creation of new volume (water), the γ's and A's are the interfacial tensions and areas of the interfaces between water and apolar liquid (WC), water and cellulose (W-$Cellulose$), water and silica (W-$Silica$), apolar liquid and cellulose (C-$Cellulose$), and apolar liquid and silica (C-$Silica$), respect-

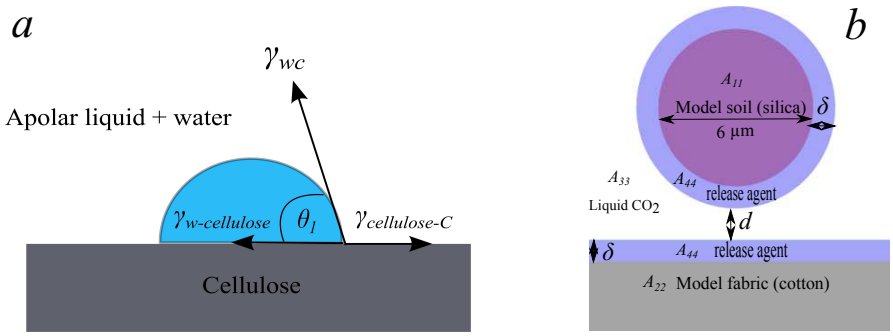

Figure 2.5: *(a) Energy balance for a water drop (W) nucleated from a water-saturated apolar liquid on a cellulose surface having a contact angle θ_1 (b) Schematic representation of soil and fabric modelled as a sphere and a plate immersed in liquid CO_2; at both surfaces a layer of thickness δ of a release agent is adsorbed.*

ively. Considering the energy balance at the three-phase contact point formed by the nucleated water drop, the cellulose surface and the apolar liquid (Figure 2.5), we get:

$$\gamma_{WC} \cos\theta_1 = \gamma_{cellulose-C} - \gamma_{W-cellulose} \tag{2.11}$$

with θ_1 the contact angle of water on the cellulose surface. Similarly, for the silica surface we arrive at

$$\gamma_{WC} \cos\theta_2 = \gamma_{C-silica} - \gamma_{W-silica} \tag{2.12}$$

θ_2 is the contact angle of water on the silica surface. Combining Equations 2.11-2.12 we get,

$$\Delta G = -v\Delta G_v + \gamma_{WC} \left(A_{WC} - A_{W-cellulose} \cos\theta_1 - A_{W-silica} \cos\theta_2\right) \tag{2.13}$$

From this equation it follows that above a certain critical v^* the bridge will grow spontaneously; if θ_1 and θ_2 are smaller than 90° capillary bridge formation is already for small values of v thermodynamically favourable.

Capillary bridges can also form between soil particles in the bulk medium and if the free energy of adhesion mediated by the capillary bridge formation is strong ($\gg k_BT$), the particles may irreversibly coagulate. The parts of the

soil and fabric surfaces that are in contact with water may get charged by dissociation of surface groups, which is thermodynamically favourable. This can lead to even stronger wetting by water giving rise to an enhanced capillary condensation. This may be one of the reasons behind the previously mentioned deterioration observed in soil removal efficiency by the addition of extra water.[52] However, there is still no experimental proof that capillary bridges occur in the fabric-soil system.

It is interesting - if not mandatory - to quantify the capillary forces. The expression for the capillary force (F_c) between a sphere (radius R) and a plate of the same material in a water-saturated medium is given by,[58]

$$F_c = 4\pi R\gamma_{WC}\cos\theta \tag{2.14}$$

where θ is the contact angle of water on both the surfaces. An order of estimate calculation (assuming $R = 10^{-6}$ m, $\gamma_{WC} = 0.04$ N m^{-1}, a bridge length of 10^{-8} m and complete wetting, i.e. $\cos\theta = 1$) reveals that the capillary energy can be as high as 10^6 k_BT. Equation 2.11 should be modified to account for the fact that in the real system of fabric and soil, water may have different contact angles with fabric and soil (Figure 2.4). The wettability or the contact angle will very much depend on the surface energy of the materials. Orr *et al.* have shown that there are certain combinations of these two contact angles θ_1 and θ_2 for which the capillary force may become repulsive.[58]

In a recent paper by Dickson *et al.*[59] it was reported that the water contact angle on glass surfaces in CO_2 increased from 70° to 100° when the pressure was increased from 1 to 240 bar. This was attributed to an increase of the interfacial tension between water and glass, $\gamma_{water-glass}$, and a decrease in $\gamma_{CO_2-\text{glass}}$ as a result of capping of the silanol groups on the glass surface by physisorbed CO_2. In addition, data on hard solid surfaces[60–62] revealed that CO_2 layers with a thickness of a few molecular diameters could remain bound to surfaces such as silica, activated carbon and zeolites due to van der Waals interactions between the surfaces and liquid CO_2. From these results the conclusion would be that it is easy to displace liquid water from fabric surfaces

in liquid CO_2. However, further wetting experiments on real and model fabric surfaces should be performed to determine if CO_2 has a similar interaction with fabric surfaces, whether the behaviour is fabric specific or generic and how the contact angle would affect the overall capillary force mediated by the presence of water in liquid CO_2.

2.6.2 Surfactants

The need to incorporate cleaning aids or surfactants in the dry-cleaning formulation using liquid CO_2 is generally acknowledged and the development of surfactants for commercial use in liquid CO_2 is ongoing. The research routes adopted so far can be divided into two categories, i.e. (i) synthesis of novel low cohesive energy density surfactants that can self-assemble in liquid CO_2 and (ii) formation of reverse micelles or water/ CO_2 microemulsions[63–65] using existing commercial surfactants. The quest for water/CO_2 microemulsions has mainly been inspired by the cleaning concepts applied in water-based systems. Since liquid CO_2 is an apolar medium, appropriate surfactants would self-assemble in CO_2 as reverse micelles or microemulsions (i.e. with a polar rather than an apolar core). The polar core of these reverse micelles would solubilize polar components of the soil and hence aid in the overall detergency. Although this route has been adopted by various research groups,[63–65] it remains debatable if it is a feasible cleaning concept in CO_2 dry-cleaning.

In water-based cleaning, wettability of apolar surfaces (oils, fabric covered with apolar body soil) by water is an issue. The strong tendency of surfactants to adsorb at these surfaces improves the wettability by lowering the surface tension of water (from 72.8 mN m^{-1} to 30 - 35 mN m^{-1}) as well as that of the water/apolar compound interfaces. Moreover, the formation of microemulsions facilitates the cleaning in water-based systems by causing ultra-low interfacial tension between oil and water (as low as 10^{-4} mN m^{-1}), thereby promoting enhanced solubilization of oily soil.[66] In contrast, at the operating conditions of dry-cleaning the surface tension of liquid CO_2 is already low (3 - 4 mN m^{-1}, see Figure 2.2). This promotes the wettability of any surface by liquid CO_2. Hence, in liquid CO_2 the function of surfactants as interfa-

cial tension lowering agents is not required. Moreover, one should expect the interfacial tension between CO_2 and oily soil to be low, both being apolar. Hence the formation of microemulsions rendering ultra-low interfacial tension between CO_2 and oily soil is not necessary either. The polar part of the soil can be removed by the incorporation of suitable polar additives such as alcohols.[25] To conclude, an amphiphile with affinity for the liquid CO_2/gas or CO_2/water interface is not necessarily a good detergent for liquid CO_2 systems.

From the above our conclusion is that one should aim for a release agent that can reduce the adhesion between the fabric and soil surfaces rather than for the development of a typical surfactant. Such a release agent should combine affinity for the solid (soil and fabric) and for CO_2 to be able to do the job: in Figure 2.5 (b) the principle is schematically depicted. Hence a potent release agent would have a CO_2-philic part and a fabric or soil-philic part. This approach is different from the prevailing routes taken so far encompassing the research of finding a cleaning aid for dry-cleaning using liquid CO_2.

The release agent should be able to creep in between soil and fabric, thus breaking any specific binding between the two. Another effect of adsorption of the release agent on both fabric and soil would be a reduction of the van der Waals attraction. In Figure 2.6 we show the calculated van der Waals interaction energy between fabric and soil by addition of the proposed release agent, assuming a 10 to 100 nm thick layer of the release agent at the fabric and soil surfaces, in comparison with the case that such an agent is absent.

The van der Waals interaction energy in the presence of an adsorbed release agent layer as shown in Figure 2.6 has been calculated using Equation 2.15.[67] The last two terms in Equation 2.15 represent the correction terms for retardation (captured by the parameter $\lambda_L = 100$ nm) and roughness (incorporated

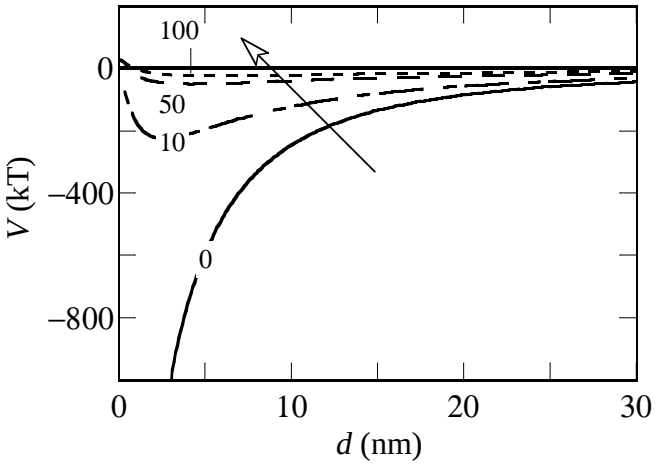

Figure 2.6: *Calculated van der Waals interaction energy between a spherical soil particle (radius 3 μm) and a flat fabric in liquid* CO_2 *with the addition of a release agent that adsorbs on both components (layer thickness 10-100 nm as indicated in the figure), compared to the case in the absence of such a release agent (0 nm).*

as $B = 2$ nm):

$$\begin{aligned} V = -\frac{1}{12}\Big[H_{14}\left(\sqrt{A_{11}}-\sqrt{A_{44}}\right) \\ +H_{42}\left(\sqrt{A_{44}}-\sqrt{A_{33}}\right)\left(\sqrt{A_{22}}-\sqrt{A_{33}}\right) \\ +H_{12}\left(\sqrt{A_{11}}-\sqrt{A_{44}}\right)\left(\sqrt{A_{22}}-\sqrt{A_{33}}\right)\Big]\left[\frac{1}{\frac{14d}{\lambda_L}}\right]\left[\frac{1}{(1+\frac{B}{d})}\right] \end{aligned} \tag{2.15}$$

where A_{44} represents the Hamaker constant of the surfactant layer (assumed to be homogeneous). H_{14}, H_{42} and H_{12} are the unretarded geometrical functions which are given by the following expressions[67]

$$H_{ij} = 2\ln\left(\frac{x}{1+x}\right)+\left(\frac{1}{1+x}\right)+\frac{1}{x} \tag{2.16}$$

for H_{14} and H_{42}:

$$x = \frac{d + \delta}{2R} \tag{2.17}$$

and for H_{12}:

$$x = \frac{d + 2\delta}{2R} \tag{2.18}$$

where the radius of the soil particle R is again taken as 3 μm and d is the distance between the release agent covered soil and fabric surfaces. The Hamaker constants A_{11} (soil, silica), A_{22} (fabric, cellulose) and A_{33} (CO_2) were calculated as before (see Section 2.4.1). A_{11} and A_{22} are on the order of 10^{-20} J and A_{33} is 10^{-22} J. The individual Hamaker constant for the release agent A_{44} was taken as 10^{-22} J, so of the same order of magnitude as that of CO_2, based on the argument that the release agent should have a CO_2-philic side for which $A_{44} \approx A_{33}$ is likely. It can be seen from Figure 2.6 that a layer thickness greater than 10 nm would be required to overcome the strong van der Waals attraction between fabric and soil in liquid CO_2 medium.

In the remaining part of this section we discuss some of the main findings of the last twenty years of research on surfactants for CO_2. The majority of this research has been focused on surfactants for sc CO_2, but are of importance for liquid CO_2 as well, and hence, we have included in this survey the supercritical state of the CO_2.

Earlier research has demonstrated that conventional surfactants used in water-based formulations are insoluble in liquid and sc CO_2.[68] It has been identified that in order to make the surfactants compatible, the cohesive energy densities of the surfactants should match to that of CO_2.[69] This should give rise to effective solvation of the tail portion of the surfactants and weaken the unfavourable tail-tail interaction,[70] so that upon addition of water they would form either an emulsion or a microemulsion system in CO_2. Hence, the need has been felt to synthesize a new class of molecules and this has been realized. Fluorosurfactants[71–74] and siloxanes[75,76] have been identified as potential candidates. However, a pressure as high as 100 bar is required to solubilize these surfactants in the CO_2 medium and therefore they do not have much promise as potential surfactants for the dry-cleaning industry. Moreover,

the use of fluorinated surfactants at an industrial scale is not a viable option as these are expensive and environmentally unfriendly. Hence, novel synthetic routes are being tried out by various researchers to synthesize new kinds of molecules.[70,77,78]

Recent research has shown that novel hydrocarbons such as poly(ether carbonate) copolymers[79] and peracetylated sugars[78,79] are soluble in liquid and sc CO_2, as well as some commercially available hydrocarbon surfactants.[80–82] We will come back to the mechanism of water/CO_2 emulsion stabilization using these novel surfactants later in this section.

Another class is formed by the so-called stubby surfactants that have methyl branching in the tail region. Several commercial varieties have been tested, such as Tergitol TMN[70] (polyoxyethylene 2,6,8-trimethyl-4-nonyl ether), and the results were compared to linear chain analogues.

These stubby surfactants form microemulsions in CO_2 without the use of a co-surfactant, and have been shown to solubilize lysozyme. Branching favours the tail-solvent interaction. The positive effect of branching on the solubility of stubby surfactants has also been explained in terms of the fractional free volume (FFV) theory.[70] In microemulsions the interfacial tail region of branched surfactants has a reduced fractional free volume relative to linear chain analogues, leading to less contact between water and CO_2, thereby creating a lower interfacial tension.[70]

For Tergitol TMN microemulsion phases in CO_2 (with the addition of water) have been found at pressures above 200 bar and in the temperature range from 35 to 70 °C.[70,83] However, Zhang *et al.*[84] showed that such microemulsions do not exhibit good detergency. This seems to corroborate our earlier argument that instead of focusing on the formation of microemulsions, more emphasis should be placed on the interactions of the additives (water and surfactants) with the solids (fabric and soil). Microemulsions do not necessarily contribute to the cleaning performance using liquid CO_2.

Mohamed *et al.*[85] have reported that custom made branching in anionic hydrocarbon surfactants such as AOT (sodium bis-(2-ethyl-1-hexyl) sulfosuccinate) can lead to the formation of reverse micelles in sc CO_2 without any

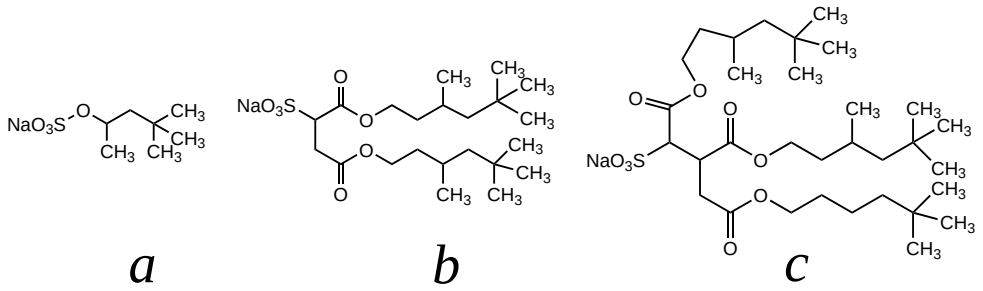

Figure 2.7: *Chemical structures of (a) SC4 (b) AOT4 (c) TC4.*

co-solvent, whereas linear chain AOT, which is a commercial surfactant, does not self-assemble in sc CO_2. Three different AOT based surfactants were investigated, namely SC4 (sodium 3,5,5-trimethylhexyl sulfate), AOT4 (sodium bis- (3,5,5-trimethyl-1-hexyl) sulfosuccinate) and TC4 (sodium 1,5-dioxo-1,5-bis (3,5,5 trimethylhexyloxy) carbonyl) pentane-2-sulfonate). These surfactants have a 3,5,5-trimethyl-1-hexyl chain in common with single, double and triple chains, respectively; branching was introduced by methylation of the chain ends (Figure 2.7). Eastoe *et al.* showed that triple chain branching turned out to be the most effective way to increase solubility in CO_2.[85] Small angle neutron scattering (SANS) data revealed that the reverse micelles in these systems are very small (close to 1.4-1.5 nm). One can argue whether these aggregates can really be called reverse micelles.

In another paper, Hollamby *et al.*[86] reported that when the dissolving power of CO_2 is improved by addition of a hydrocarbon, in particular heptane ($>$ 30 vol%), AOT (without any branching) can be solubilized in CO_2. Although this amount of heptane is much higher than that acceptable by the dry-cleaning industry, it opens up the opportunity to use commercially available anionic surfactants in CO_2 by improving the solvent quality using readily available hydrocarbons, within the boundaries of environmental demands. However, the effect on dry-cleaning performance or particle stabilization by enhancing the solubility of AOT-like surfactants in liquid CO_2 has not yet been shown on either lab or commercial scales. Similar to the approach of adding alkanes as cosolvents, van Roosmalen *et al.*[24] reported the use of alco-

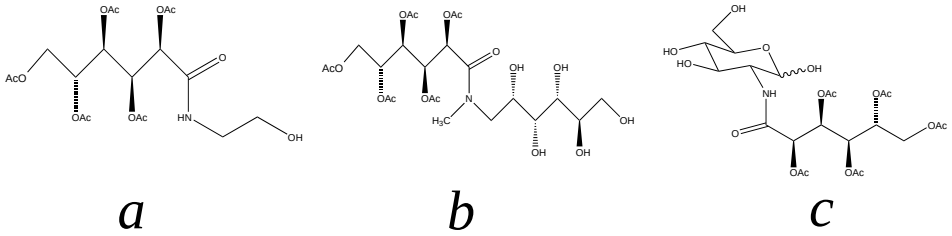

Figure 2.8: *Chemical structures of a) G1A (b) G2A (c) G3A.*

hols in liquid CO_2 as cleaning aids. Of all alcohols tested, 2-propanol (4 wt.%) gave the best results. The reason for the increased cleaning performance is not known.

Recently Bazito *et al.*[77] reported on three sugar based non-ionic surfactants, i.e. penta-O-acetyl-D-gluconamides of ethanolamine (G1A), N-methylglucamine (G2A) and D-glucosamine (G3A), which show even greater interfacial activity at the water-CO_2 interface in dense CO_2 system than their fluorinated analogues. These compounds are shown in Figure 2.8.

The CO_2-philic parts of these novel surfactants are peracetylated chains and the CO_2-phobic parts contain hydroxyl groups. The solubility of these sugar based surfactants was rationalized in terms of Lewis acid-base interactions between the peracetylated groups and CO_2.[77]

Suitabilities of commercial C_iEO_j type non-ionic surfactants have been explored for dry-cleaning application in liquid CO_2. The phase behaviour (solubility) of C_8EO_3, C_8EO_5 and C_6EO_5 in liquid CO_2 has been studied using a Cailletet apparatus between the pressure and temperature range of 2 to 100 bar and -13 to 37 °C. These studies indicate that the length of the EO chain is crucial for the solubility of these surfactants in CO_2, a higher EO chain length leading to phase separation at a lower temperature, whereas, the solubility remains relatively unaffected by the length of the hydrophobic tail.[87] Similar measurements have been shown to solubilize surfactants such as Triton X-100 (octylphenol ethylene oxide) and poly(ethylene glycol)-block-poly (propylene glycol)-block-poly(ethylene glycol) (PEG-PPG-PEG) in liquid CO_2 at pressure less than 100 bar and temperature between 25-30 °C.[88]

The effect of surfactants on the reduction of the water - CO_2 interfacial tension has also been explored. This interfacial tension is 30-35 mN m^{-1} at 50 bar and 14 °C[89] which is 75 % of the typical oil-water interfacial tension[90,91] (40 - 50 mN m^{-1}). Hence the tendency of adsorption of a surfactant at the CO_2-water interface would also be lower. da Rocha *et al.* reported an interfacial tension of 0.2 mN m^{-1} for a system comprised of the PDMS block copolymeric surfactant with PEO grafts ($PDMS_{24}$-g-EO_{22}) in dense CO_2.[92] However, the effect of lowering the surface tension on CO_2 dry-cleaning efficiency has not been investigated.

The authors are not aware of any commercial trials, which were taken to evaluate the performance of the surfactants mentioned in this section. Industrial CO_2 dry-cleaning employs a pressure of 45 - 60 bar and 10 °C, which is much lower than the pressure at which these surfactants have shown promise.

2.6.3 Steric stabilizers

Water-based cleaning formulations usually take care of the problem of redeposition by incorporating polymers into the formulation which get adsorbed onto the dirt particles thereby providing steric or electrostatic stabilization against deposition. Scientists have sought for electrostatic or steric stabilizers in dense CO_2 to stabilize emulsions or dispersions for industrial applications. Particle stabilization in liquid CO_2 using polymers is as challenging as finding a suitable surfactant for CO_2, essentially for the same reasons mentioned earlier. The key criterion for this is the solubility of the polymer in liquid CO_2, requiring solvation of the polymer chain segments by CO_2.[93] As explained in the previous sections, the solvent quality of CO_2 increases with increasing density (pressure): see Figure 2.2a and Figure 2.2b. Hence in systems where particles are stabilized by a polymer layer, a critical flocculation density (CFD) can be measured, below which the particles aggregate and the dispersion becomes unstable.[93] The CFD often coincides with the upper critical solution density (UCSD), where the solvent and the polymer possess similar cohesive energy. Above the UCSD, the polymer chains are well solvated by CO_2 and the polymer chains attain a random coil configuration. Upon lowering the

density by decreasing the pressure, polymer-polymer interactions prevail over the CO_2-polymer interaction and a coil to globule transition initiates phase separation and destabilization of the dispersion. This is essentially an entropy-driven phase separation, which is related to the differences in compressibility between the solutes and the solvents and similar to the lower critical solution temperature (LCST) in conventional solvents.

Application of polymeric stabilizers such as polydimethylsiloxanes, polyfluoroethers and polyfluoroacrylates for sc CO_2 (pressure $>$ 200 bar) has attained some momentum[75,94,95] but their use as soil stabilizer to prevent redeposition in CO_2 dry-cleaning has not been reported so far and looks quite challenging.

2.7 Capillary action (wetting/wicking) in liquid CO_2 systems

The physicochemical parameters described above all play a very complex role in the wettability and penetration of liquid CO_2 into the pores of the fabrics. Since fabric weaving varies across the fabric type, any generalized qualitative or quantitative analysis of liquid CO_2 penetration in the fabric pores will necessarily be an oversimplification. The wicking and wetting of various fabric types by water during the detergency process have been addressed by many authors.[14,96–98] The plethora of literature stands witness to the fact that the importance of these phenomena in the detergency process has long been realized; scientists have attempted to develop qualitative or quantitative expressions to describe these phenomena.[98–100] Although understanding of thermodynamics and kinetics of wetting, wicking, and redistribution of liquid CO_2 in the fabric pores are important, research in dry-cleaning has not put emphasis on understanding these processes and their effects on the efficiency of cleaning. Classically, fabrics have been modelled as a bundle of capillaries,[100] though it has been debated if this is a too oversimplified model. Generally, the characteristic parameters by which the transport kinetics and equilibrium distributions of liquids in a porous medium are controlled[98] are the average

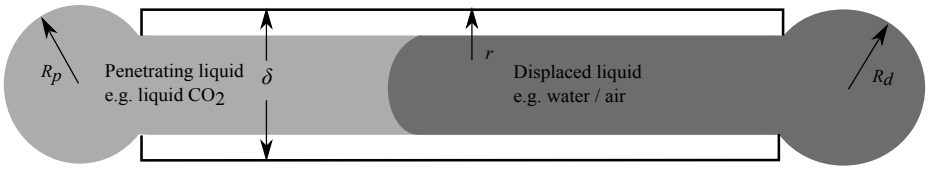

Figure 2.9: *Schematic representation of a capillary of radius r in a porous medium with a typical dimension δ. R_p and R_d represent the radii of curvature of the penetrating (in our case liquid CO_2) and the displaced fluid (air, water or other fluid) reservoirs of finite size (adopted from Marmur[98]).*

contact angles θ_p and θ_d of the penetrating (p) and displaced fluid (d) with the solid of which the porous medium consists, the radii of curvature of the liquid reservoirs R_p and R_d, the typical dimension of the porous medium (e.g. thickness) δ, and the typical pore size r, as shown in Figure 2.9.

The process of liquid flow through porous media has been fragmented into two processes which happen in tandem, the displacement process and the re-exposure process.[98] The displacement process refers to a situation where the capillary is full with an immiscible fluid from the beginning. In case of dry-cleaning with liquid CO_2, the immiscible fluid could be air, water or liquid polar oil. Water can be introduced into the system by various routes, e.g. from the textile or as an additive, as explained in the previous section. Hence before liquid CO_2 is wicked inside the capillary, it has to displace the liquid already present. The displaced liquid would come out as a drop with a finite curvature, as shown in Figure 2.9. The ratio R_p/r determines the criterion of capillary penetration: the process is driven by a pressure difference in the penetrating liquid (between the reservoir and the region adjacent to the meniscus in the capillary). If the liquid reservoir is small, as is the case in Figure 2.9, the local pressure is relatively high due to the strong curvature of the reservoir. As a result, the penetration process is enhanced. When the displaced liquid emerges out of the capillary, a drop is formed (radius R_d). The effect of the small radius of the displaced drop is opposite to that of the penetrating drop: the pressure in the displaced drop opposes the displacement process. The curvature of this drop passes through a maximum, which occurs when R_d/r

is approximately unity. Only after the point of maximum pressure (maximum curvature) is passed, displacement can proceed spontaneously.[98]

The re-exposure process is related to the typical dimension (δ) of the porous medium, i.e. the thickness of the porous walls of the capillary. The term re-exposure refers to the contact between the penetrating liquid with the fluid present in these porous walls. This unfavourable interaction may diminish the gain originating from the favourable contact between solid and penetrating liquid during the displacement process. The effect of re-exposure[98] is particularly important for thin-walled capillaries ($\delta/r \sim 10$). The re-exposure effect will be dominant for a fabric with high surface and bulk porosity.

In real systems the pore sizes vary across fabric types and also within one particular fabric. In general it is known that in case of small pores, the driving force for penetration is high but the penetration rate is low because of the increased viscous drag.[98] Hence large pores will be rapidly filled up at the beginning. Eventually, the liquid wicked in the large pores will redistribute itself into the finer pores albeit slowly. This may negatively affect the detergency process, because soil residing in the small pores will be less accessible to the washing liquor, which may result in poor removal. Marmur[98] summarized the penetration of a liquid drop into a thin porous medium (Figure 2.10) by a phase diagram (contact angle θ versus δ/r) showing that for $\delta/r > 0.5$ there are only two stable equilibrium states (complete penetration for contact angles below say 90° and no penetration for higher contact angles), whereas for smaller δ/r values a third state called basal penetration is possible. In this state the penetration of the drop is stopped by the re-exposure effect when the radius of the liquid inside the porous medium equals the radius of the base of the drop (stage 4 in Figure 2.10).

The kinetics of liquid CO_2 penetration in horizontal cylindrical capillaries has been estimated for various fabrics (by assuming different contact angles) by the Lucas-Washburn equation:[100]

$$\frac{l^2}{t} = \frac{\gamma_{lv} r \cos\theta}{2\eta} \tag{2.19}$$

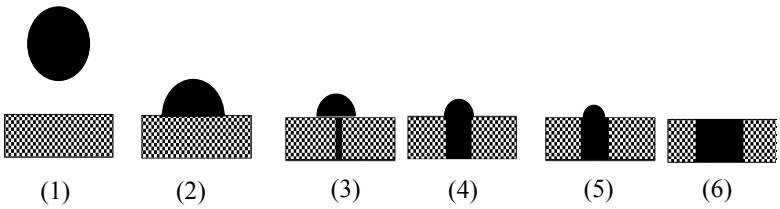

Figure 2.10: *Stages of the penetration of a drop into a thin porous medium. Adapted from Marmur*[98]

.

Where l is the length of the liquid column at time t, r is the pore radius, θ is the contact angle between liquid CO_2 and the fabric wall and η is the viscosity of liquid CO_2. The slope of the graph l^2/t versus r gives the velocity of the liquid CO_2 penetration inside the pores. As can be seen from Figure 2.11, this velocity strongly depends on the contact angle between liquid CO_2 and the fabric surface. For contact angles of 60 ° and higher, the velocity is significantly reduced. This implies that (nearly) complete wetting is crucial for detergency action. Following the above argument, dry-cleaning operation should take place near the critical point, as the gas/liquid interfacial tension of CO_2 is very low near the critical temperature and pressure. This would facilitate fast penetration (small η) and complete wetting ($\cos\theta = 1$). However, the low contact angle would also mean that the three phase contact line (formed by liquid and gaseous CO_2 and the surface) cannot exert strong forces which could result in an unfavourable condition for particulate soil removal. In addition, a too small density difference between the two CO_2 phases is detrimental for the mechanical action in rotating drum washing machines (see Sections 3).

2.8 Particle removal by shear forces

In previous sections the physicochemical aspects of dry-cleaning have been discussed and the magnitude of adhesion forces between soil particle and fabric in liquid CO_2 have been estimated. During dry-cleaning sufficient hydrodynamic - or better "solvodynamic"-force must be generated to achieve sufficient particle removal from the fabric matrix. In this section we estimate

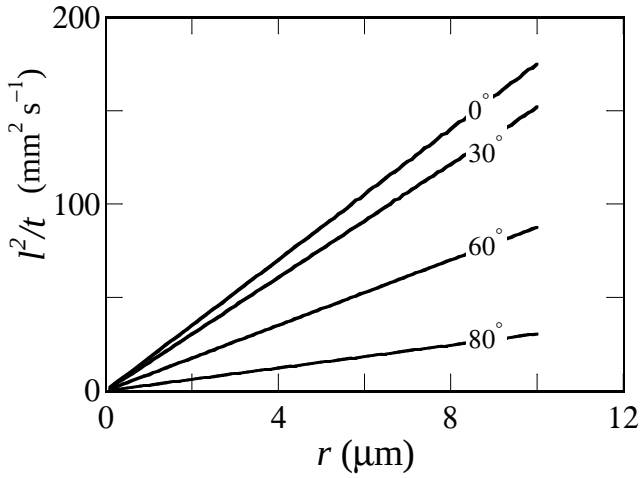

Figure 2.11: *l^2/t versus pore radius calculated from the Washburn-Lucas equation for penetration of liquid CO_2 into horizontal pores. The different curves correspond to different contact angles between liquid CO_2 and fabric. The interfacial tension for liquid/gas CO_2 and the viscosity of liquid CO_2 were taken from Figure 2.2 (3.5 mN m^{-1} and 1 $\times 10^{-4}$ Pa s, respectively, at operation conditions of dry-cleaning).*

the solvodynamic force required for particle removal in liquid CO_2 and compare it to that required in PERC and water. Again as a model we consider silica particles (now with radius R of 2 μm) attached to a cellulose surface. We assume that in shear flow the particles are mainly held on the fabric by van der Waals forces (at the primary minimum, the distance d between particle and surface is taken as 1 nm) and friction force. For particle removal the solvodynamic force must be equal to or greater than the sum of these two forces. The force balance is shown in Figure 2.12.

The van der Waals force (obtained by differentiating Equation 2.1 with respect to d) is given by

$$F_{adh} = F_{vdW} = \frac{A_{132}R}{6d^2} \tag{2.20}$$

The friction force equals μN, in which μ is the friction coefficient and N

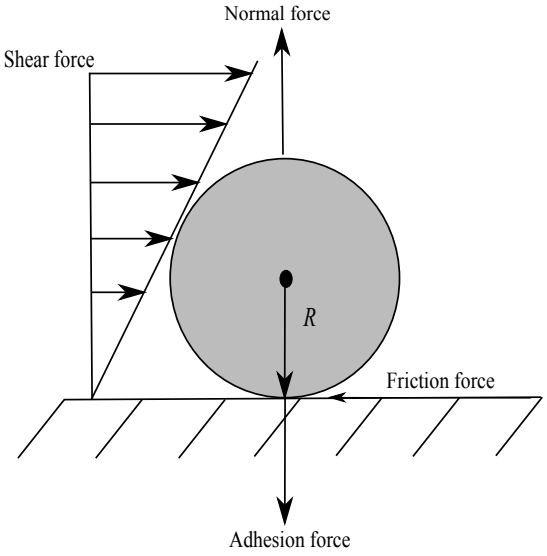

Figure 2.12: *Force balance around a particle in a parallel plate flow cell experiencing a drag/shear force. The particle is held by the van der Waals adhesion force and frictional force.*

is the normal force. The combination of van der Waals and friction forces is estimated to be approximately twice the adhesion force. The solvodynamic force is assumed to come from the shear force (F_{shear}) only; the effects of gravitational force, lift force and torque are assumed to be negligible. Thus, the criterion for removal of the particle from the surface is

$$F_{shear} = 2F_{adh} \tag{2.21}$$

For a spherical particle, the relation between the solvodynamic drag and the wall shear stress τ is given by[101]

$$F_{shear} = 32\tau R^2 \tag{2.22}$$

The wall shear stress is related to the wall shear rate $\dot{\gamma}$ by the viscosity of the fluid as

$$\tau = \eta\dot{\gamma} \tag{2.23}$$

and the flow velocity (v) around the particle can be written as

$$v = \dot{\gamma} R \tag{2.24}$$

From Equations 2.21 - 2.24 it follows that

$$v = \frac{2F_{\text{adh}}}{32\eta R} \tag{2.25}$$

The Reynolds number,[102] which is the ratio between the inertial force and the viscous force, is calculated from the flow velocity v, the hydraulic diameter of the flow channel D, and the density ρ and viscosity η of the fluid as

$$Re = \frac{Dv\rho}{\eta} \tag{2.26}$$

The hydraulic diameter (D) is the ratio between the cross-sectional area of the flow and the wetted perimeter and was estimated using a gap and width of 0.5 mm and 10 mm respectively.

For liquid CO_2 the density and viscosity are taken as 900 kg m^{-3} and 0.0001 Pa s, respectively, corresponding to a pressure of $\sim$ 50 bar (see Figures 2.2). Since the van der Waals force is related to the dielectric properties of the material (see Section 2.4), the solvodynamic force needed for particle release from the surface depends on the dielectric properties or the Hamaker constant of the fluid/system. This is illustrated in Figure 2.13.

From the plot of the Reynolds number versus composite Hamaker constant (A_{132})[41] in Figure 2.13, it is apparent that in liquid CO_2 a very high Reynolds number is needed to remove the soil from the fabric. In water the required Reynolds number is three orders of magnitude less and in PERC there is even a six orders of magnitude difference compared to liquid CO_2. This is due to (i) the large adhesion force with which the soil is attached to the fabric in liquid CO_2 and (ii) the extremely low viscosity of liquid CO_2 at the operating conditions for dry-cleaning. Hence generation of sufficient force in liquid CO_2 by mechanical action is a challenge.

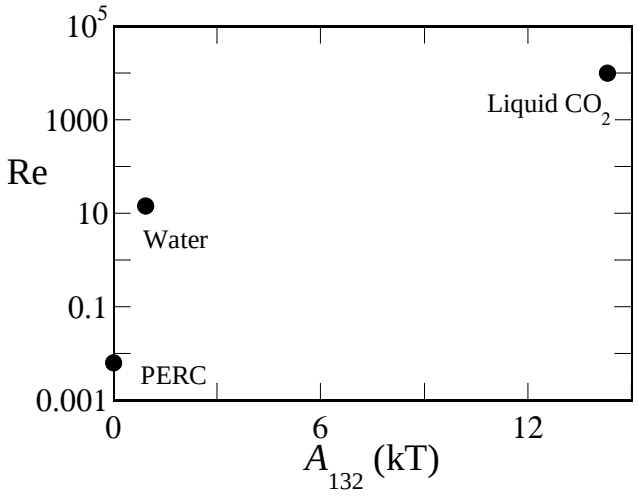

Figure 2.13: *Reynolds numbers required for detachment of a silica particle (2 μm radius) from cellulose versus the composite Hamaker constant. It is assumed that the particle in the liquid flow is held on the surface by van der Waals forces and friction forces only.*

2.9 Conclusion

CO_2 dry-cleaning technology has undergone significant technical development since it was invented in 1973. However, its commercialization is still difficult to be realized because of various problems. Issues include the redeposition problem, the low amount of mechanical action and the low solvent power that all lead to low (particulate) soil removal. In addition, the nature of dense CO_2 which requires high pressure equipment leads to high equipment costs. Nevertheless, CO_2 has a high potential to replace PERC for textile dry-cleaning. Development of effective surfactants and anti-redeposition methods, increasing the amount of mechanical action without textile deterioration are thus necessary. For progress a fundamental understanding of the cleaning principles and mechanisms in liquid CO_2 is essential.

Addition of water as a minor component together with a suitable surfactant can play a significant role in liquid CO_2 dry-cleaning by providing a route

to reduce the redeposition of soil. Self-association of surfactants in liquid CO_2 would lead to the formation of microemulsions or reverse micelles. Water trapped inside these structures can carry additional ions. This would be beneficial for two reasons, i.e. (i) the counterions can remain shielded inside the polar core of the reverse micelles and the tendency of forming ion pairs can be reduced, and (ii) the soil particles and also the fabric can acquire more charge than what is predicted from the dissociation of the surface groups. In either case (with or without surfactant) water would contribute towards charge driven interactions. These interactions could prove to be vital for both cleaning and prevention of soil redeposition.[29] However, research so far has shown that finding a surfactant which is capable of forming stable water-in-CO_2 microemulsions close to or below the critical pressure is a challenge. Designing of surfactants based on the routes which have already been tried has not yet resulted in finding the holy grail. Apart from the search for effective surfactants, a breakthrough in designing polymers capable of stabilizing particle dispersion in dense and liquid CO_2 will also benefit the dry-cleaning industry, by taking care of redeposition.

So far no data were found in literature regarding the mechanical movement of fabrics in CO_2 and how they behave in this medium. The highest level of mechanical action is produced in the motor powered rotating basket, but the washing performance in machines using this agitation method is still significantly lower than PERC. Thus it is needed to have a better insight into the dynamics of different agitation methods and their effect on the movement of garments, so that a higher mechanical action can be produced in a more efficient way.

Bibliography

[1] J. M. DeSimone. Practical Approaches to Green Solvents. *Science*, 297(5582):799–803, 2002.

[2] A. Hou, B. Chen, J. Dai, and K. Zhang. Using Supercritical Carbon Dioxide as Solvent to Replace Water in Polyethylene Terephthalate (pet) Fabric Dyeing Procedures. *J. Clean. Prod.*, 18(10–11):1009–1014, 2010.

[3] L. E. Laroze, B. Díaz-Reinoso, A. Moure, M. E. Zúñiga, and H. Domínguez. Extraction of Antioxidants from Several Berries Pressing Wastes using Conventional and Supercritical Solvents. *Eur. Food Res. Technol.*, 231:669–677, 2010.

[4] C. A. Fernandez, E. M. Hoppes, J. G. Bekhazi, C. Wang, R. J. Wiacek, M. G. Warner, G. E. Fryxell, J. T. Bays, and R. S. Addleman. Tuning and Quantifying the Dispersibility of Gold Nanocrystals in Liquid and Supercritical Solvents. *J. Phys. Chem. C*, 112(36):13947–13957, 2008.

[5] M. D. Romero, L. Calvo, C. Alba, A. Daneshfar, and H. S. Ghaziaskar. Enzymatic Synthesis of isoamyl acetate with Immobilized Candida Antarctica Lipase in n-hexane. *Enzyme Microb. Technol.*, 37(1):42–48, 2005.

[6] X. Zhang, J. Q. Pham, N. Ryza, P. F. Green, and K. P. Johnston. Chemical-mechanical Photoresist Drying in Supercritical Carbon Dioxide with Hydrocarbon Surfactants. *J. Vac. Sci. Technol. B Microelectron. Nanometer. Struct.*, 22(2):818–825, 2004.

[7] G. Heltai, B. Fehér, K. Percsich, B. Barabás, and I. Fekete. Application of Sequential Extraction with Supercritical CO_2, Subcritical H_2O, and an H_2O/CO_2 Mixture for Estimation of Environmentally Mobile Heavy Metal Fractions in Sediments. *Anal. Bioanal. Chem.*, 373:863–866, 2002.

[8] W. Leitner. Designed to Dissolve. *Nature*, 405:129–30, 2000.

[9] R. L. Maffei. Extraction and Cleaning Processess, 1997.

[10] T. Ito, Y. Otani, and H. Inomata. Performance of Air Filters Cleaned by Supercritical Carbon Dioxide. *Sep. Purif. Technol.*, 40(1):41–46, 2004.

[11] J. A. Keagy, Y. Li, P. F. Green, K. P. Johnston, F. Weber, J. T. Rhoad, E. L. Busch, and P. J. Wolf. CO_2 Promotes Penetration and Removal of

Aqueous Hydrocarbon Surfactant Cleaning Solutions and Silylation in Low-k Dielectrics with 3 nm Pores. *J. Supercrit. Fluids*, 42(3):398–409, 2007.

[12] M. Y. Lee, K. M. Do, H. S. Ganapathy, Y. S. Lo, J. J. Kim, S. J. Choi, and K. T. Lim. Surfactant-aided Supercritical Carbon Dioxide Drying for Photoresists to Prevent Pattern Collapse. *J. Supercrit. Fluids*, 42(1):150–156, 2007.

[13] D. Bajpai and V. K. Tyagi. Laundry Detergents: An Overview. *J. Oleo Sci.*, 56(7):327–340, 2007.

[14] B.J. Carroll. Physical Aspects of Detergency. *Colloids Surf A Physicochem Eng Asp*, 74:131–167, 1993.

[15] Y.-S. Chi and S. K. Obendorf. Aging of Oily Soils on Textile Materials: a Literature Review. *J. Surfactants Deterg.*, 1:407–418, 1998.

[16] J. W. Cleaver and B. Yates. Mechanism of Detachment of Colloidal Particles from a Flat Substrate in a Turbulent Flow. *J. Colloid Interface Sci.*, 44(3):464–474, 1973.

[17] J. C. Harris. Suspending Action by Detergents in the Presence of Substrate. *Text. Res. J.*, 29(2):99–118, 1959.

[18] G. M. Venkatesh, N. E. Dweltz, G. L. Madan, and R. H. Alurkar. A Study of the Soiling of Textiles and Development of Anti-Soiling and Soil Release Finishes: A Review. *Text. Res. J.*, 44(5):352–362, 1974.

[19] G. Ziskind, M. Fichman, and C. Gutfinger. Adhesion Moment Model for Estimating Particle Detachment from a Surface. *J. Aerosol Sci.*, 28(4):623–634, 1997.

[20] Y.-S. Chi and S. K. Obendorf. Effect of Fiber Substrates on Appearance and Removal of Aged Oily Soils. *J. Surfactants Deterg.*, 4:35–41, 2001.

[21] A. Varanasi, S. K. Obendorf, L. S. Pedersen, and R. Mejldal. Lipid Distribution on Textiles in Relation to Washing with Lipases. *J. Surfactants Deterg.*, 4:135–146, 2001.

[22] P. E. Choe and S. K. Obendorf. Chemical Changes in Unsaturated Oils upon Aging and Subsequent Effects on Fabric Yellowing and Soil Removal. *J. Am. Oil Chem. Soc.*, 71:17–30, 1994.

[23] Advanced CO_2 Cleaning as an Ecologocal Process Technology (ACCEPT). 2008.

[24] M. J. E. van Roosmalen, M. van Diggelen, G. F. Woerlee, and G. J. Witkamp. Dry-cleaning with High-pressure Carbon Dioxide-the Influence of Mechanical Action on Washing-results. *J. Supercrit. Fluids*, 27:97–108, 2003.

[25] M. J. E. van Roosmalen, G. F. Woerlee, and G. J. Witkamp. Dry-cleaning with High-pressure Carbon Dioxide–the Influence of Process Conditions and Various Co-solvents (Alcohols) on Cleaning-results. *J. Supercrit. Fluids*, 27(3):337–344.

[26] M. J. E. van Roosmalen, G. F. Woerlee, and G. J. Witkamp. Amino Acid Based Surfactants for Dry-cleaning with High-pressure Carbon Dioxide. *J. Supercrit. Fluids*, 32(1-3):243–254, 2004.

[27] M. J. E. van Roosmalen, G. F. Woerlee, and G. J. Witkamp. Surfactants for Particulate Soil Removal in Dry-cleaning with High-pressure Carbon Dioxide. *J. Supercrit. Fluids*, 30(1):97–109, 2004.

[28] Den Otter F. B. de walle F. B. Detective Final Report: L CO_2 Textile Cleaning. Demonstration Pilot Scale Testing of Textile Dry-cleaning with Sub/Supercrtical Carbon Dioxide. Technical report, 2005.

[29] A. J. O'Lenick. Soil Release Polymers. *J. Surfactants Deterg.*, 2:553–557, 1999.

[30] W. Q. Cai, T. E. Gough, X. J. Gu, N. R. Isenor, and G. Scoles. Polarizability of CO_2 Studied in Molecular-beam Laser Stark Spectroscopy. *Phys. Rev. A*, 36:4722–4727, 1987.

[31] K. Harrison, J. Goveas, K. P. Johnston, and E. A. O'Rear. Water-in-CarbonDioxide Microemulsions with a Fluorocarbon-Hydrocarbon Hybrid Surfactant. *Langmuir*, 10(10):3536–3541, 1994.

[32] A. D. Buckingham and R. L. Disch. The Quadrupole Moment of the Carbon Dioxide Molecule. *Proceedings of the Royal Society of London. Series A. Mathematical and Physical Sciences*, 273(1353):275–289, 1963.

[33] D. E. Diller and M. J. Ball. Shear Viscosity Coefficients of Compressed Gaseous and Liquid Carbon Dioxide at Temperatures between 220 and

320 K and at Pressures to 30 MPa. *Int. J. Thermophys.*, 6:619–629, 1985.

[34] J. W. Magee and J. F. Ely. Isochoric (p, v, t) Measurements on CO_2 and (0.98 CO_2 +0.02 ch_4) from 225 to 400 K and pressures to 35 MPa. *Int. J. Thermophys.*, 9:547–557, 1988.

[35] Elton L. Quinn. The surface Tension of Liquid Carbon Dioxide. *J. Am. Chem. Soc*, 49(11):2704–2711, 1927.

[36] P. Jianxin and L. Yigang. Estimation of the Surface Tension of Liquid Carbon Dioxide. *Phys. Chem. Liq.*, 47(3):267–273, 2009.

[37] J. Lyklema. *Fundamentals of Interface and Colloid Science.* Academic Press, London, 1991.

[38] J. Czarnecki. The Effects of Surface Inhomogeneities on the Interactions in Colloidal Systems and Colloid Stability. *Adv. Colloid Interface Sci.*, 24(0):283–319, 1985.

[39] J. Gregory. Approximate Expressions for Retarded van der Waals Interaction. *J. Colloid Interface Sci.*, 83(1):138–145, 1981.

[40] H. Sonntag and K. Strenge. *Coagualtion Kinetics and Structure Formation.* Plenum Press, New York, 1987.

[41] J. N. Israelachvili. *Intermolecular and Surface Forces.* Academic Press, London; San Diego, 1991.

[42] Ph. C. Van Der Hoeven and J. Lyklema. Electrostatic Stabilization in Non-aqueous Media. *Adv. Colloid Interface Sci.*, 42:205–277, 1992.

[43] J. E. Lewis, R. Biswas, A. G. Robinson, and M. Maroncelli. Local Density Augmentation in Supercritical Solvents: Electronic Shifts of Anthracene Derivatives. *J. Phys. Chem. B*, 105(16):3306–3318, 2001.

[44] F. G. Keyes and J. G. Kirkwood. The Dielectric Constant of Carbon Dioxide as a Function of Temperature and Density. *Phys. Rev.*, 36:754–761, 1930.

[45] G. J. Besserer and D. B. Robinson. Refractive Indexes of Ethane, Carbon Dioxide, and Isobutane. *J. Chem. Eng. Data*, 18(2):137–140, 1973.

[46] Kitahara A. and A. Watanabe. *Electrical Phenomena at Interfaces*, volume 15. Marcel Dekker, New York, 1984.

[47] S. Poovarodom and J. C. Berg. Effect of Particle and Surfactant Acid-base Properties on Charging of Colloids in Apolar Media. *J. Colloid Interface Sci.*, 346(2):370–377, 2010.

[48] K. P. Johnston, K. L. Harrison, M. J. Clarke, S. M. Howdle, M. P. Heitz, F. V. Bright, C. Carlier, and T. W. Randolph. Water in Carbon Dioxide Microemulsions: An Environment for Hydrophiles including Proteins. *Science*, 271(5249):624–626, 1996.

[49] Beltrame P. L., A. Castelli, E. Selli, A. Mossa, G. Testa, A. M. Bonfatti, and A. Seves. Dyeing of Cotton in Supercritical Carbon Dioxide. *Dyes Pigments*, 39(4), 1998.

[50] F. Rombaldoni, R. Demichelis, G. Mazzuchetti, A. Ferri, M. Banchero, and F. Dotti. Effect of Carbon Dioxide Dry-cleaning on Low-stress Mechanical Properties, Air Permeability and Crease Pressing Performance of Men's Suit Fabrics. *Text. Res. J.*, 79(13), 2009.

[51] The Mutual Solubilities of Water with Supercritical and Liquid Carbon Dioxides.

[52] van Roosmalen M. J. E. *Dry-cleaning with High Pressure Carbon Dioxide*. PhD thesis, TU Delft, 2003.

[53] Hugo K. Christenson. Non-DLVO Forces between Surfaces -Solvation, Hydration and Capillary Effects. *J. Dispersion Sci. Technol.*, 9(2):171–206, 1988.

[54] H. K. Christenson. Experimental Measurements of Solvation Forces in Non-polar Liquids. *J. Chem. Phys.*, 78(11):6906–6913, 1983.

[55] D. Turnbull. Kinetics of Heterogeneous Nucleation. *J. of Chem. Phys.*, 18(2):198–203, 1950.

[56] H. K. Christenson. Capillary Condensation in Systems of Immiscible Liquids. *J. Colloid Interface Sci.*, 104(1):234–249, 1985.

[57] E. Sahagún, P. García-Mochales, G. M. Sacha, and J. J. Sáenz. Energy Dissipation due to Capillary Interactions: Hydrophobicity Maps in Force Microscopy. *Phys. Rev. Lett.*, 98:176106–4, 2007.

[58] F. M. Orr, L. E. Scriven, and A. P. Rivas. Pendular Rings between Solids: Meniscus Properties and Capillary Force. *J. Fluid Mech.*, 67(04):723–742, 1975.

[59] J. L. Dickson, G. Gupta, T. S. Horozov, B. P. Binks, and K. P. Johnston. Wetting Phenomena at the CO_2 /Water/Glass interface. *Langmuir*, 22(5):2161–2170, 2006.

[60] J. H. Chen, D. S. H. Wong, C. S. Tan, R. Subramanian, C. T. Lira, and M. Orth. Adsorption and Desorption of Carbon Dioxide onto and from Activated Carbon at High Pressures. *Ind. Eng. Chem. Res.*, 36(7):2808–2815, 1997.

[61] O. Di Giovanni, W. Dörfler, M. Mazzotti, and M. Morbidelli. Adsorption of Supercritical Carbon Dioxide on Silica. *Langmuir*, 17(14):4316–4321, 2001.

[62] W. Gao, D. Butler, and D. L. Tomasko. High-Pressure Adsorption of CO_2 on NaY Zeolite and Model Prediction of Adsorption Isotherms. *Langmuir*, 20(19):8083–8089, 2004.

[63] J. Eastoe, Z. Bayazit, S. Martel, D. C. Steytler, and R. K. Heenan. Droplet Structure in a Water-in-CO_2 Microemulsion. *Langmuir*, 12(6):1423–1424, 1996.

[64] J. Eastoe, A. Dupont, A. Paul, C. Steytler D., and E. Rumsey. Design and Performance of Surfactants for Carbon Dioxide. In *Supercritical Carbon Dioxide*, volume 860 of *ACS Symposium Series*, pages 285–308. American Chemical Society, 2003.

[65] W. Ryoo, J. L. Dickson, V. V. Dhanuka, S. E. Webber, R. T. Bonnecaze, and K. P. Johnston. Electrostatic Stabilization of Colloids in Carbon Dioxide: Electrophoresis and Dielectrophoresis. *Langmuir*, 21(13):5914–5923, 2005.

[66] P. R. Garrett, D. Carr, D. Giles, G. Pierre-Louis, E. Staples, C. A. Miller, and B.-H. Chen. Solubilisation of Triolein by Microemulsions containing $c_{12}e_4$/Hexadecane/Water: Equilibrium and Dynamics. *J. Colloid Interface Sci.*, 325(2):508–515, 2008.

[67] B. Vincent. The van der Waals Attraction between Colloid Particles having Adsorbed Layers. II. Calculation of Interaction Curves. *J. Colloid Interface Sci.*, 42(2):270–285, 1973.

[68] Consan. K. A. and R. D. Smith. Observations on the Solubility of Surfactants and Related Molecules in Carbon Dioxide at 50°c. *J. Supercrit. Fluids*, 3(2):51–65, 1990.

[69] K. P. Johnston, D. Cho, S. R. P. DaRocha, P. A. Psathas, W. Ryoo, S. E. Webber, J. Eastoe, A. Dupont, and D. C. Steytler. Water in Carbon Dioxide Macroemulsions and Miniemulsions with a Hydrocarbon Surfactant. *Langmuir*, 17(23):7191–7193, 2001.

[70] W. Ryoo, S. E. Webber, and K. P. Johnston. Water-in-Carbon Dioxide Microemulsions with Methylated Branched Hydrocarbon Surfactants. *Ind. Eng. Chem. Res.*, 42(25):6348–6358, 2003.

[71] T. Hoefling, D. Stofesky, M. Reid, E. Beckman, and R. M. Enick. The Incorporation of a Fluorinated Ether Functionality into a Polymer or Surfactant to Enhance CO_2 -solubility. *J. Supercrit. Fluids*, 5(4):237–241, 1992.

[72] T. A. Hoefling, R. M. Enick, and E. J. Beckman. Microemulsions in Near-critical and Supercritical Carbon Dioxide. *J. Phys. Chem.*, 95(19):7127–7129, 1991.

[73] C. T. Lee, K. P. Johnston, H. J. Dai, H. D. Cochran, Y. B. Melnichenko, and G. D. Wignall. Droplet Interactions in Water-in-Carbon Dioxide Microemulsions Near the Critical Point: A Small-Angle Neutron Scattering Study. *J. Phys. Chem. B*, 105(17):3540–3548, 2001.

[74] D. A. Newman, T. A. Hoefling, R. R. Beitle, E. J. Beckman, and R. M. Enick. Phase Behavior of Fluoroether-functional Amphiphiles in Supercritical Carbon Dioxide. *J. Supercrit. Fluids*, 6(4):205–210, 1993.

[75] R. Fink and E. J. Beckman. Phase Behavior of Siloxane-based Amphiphiles in Supercritical Carbon Dioxide. *J. Supercrit. Fluids*, 18(2):101–110, 2000.

[76] P. A. Psathas, S. R. P. da Rocha, C. T. Lee, K. P. Johnston, K. T. Lim, and S. Webber. Water-in-Carbon Dioxide Emulsions with Poly(dimethylsiloxane)-Based Block Copolymer Ionomers. *Ind. Eng. Chem. Res.*, 39(8):2655–2664, 2000.

[77] Cássio F. L., Góes L. F., Pereira T. A., and Bazito R. C. New Peracetyleated Sugar-based Surfactants for Supercritical Carbon Dioxide. 2010.

[78] V. K. Potluri, J. Xu, R. Enick, E. Beckman, and A. D. Hamilton. Peracetylated Sugar Derivatives Show High Solubility in Liquid and Supercritical Carbon Dioxide. *Org. Lett*, 4(14):2333–2335, 2002.

[79] T. Sarbu, T. Styranec, and E. J. Beckman. Non-fluorous Polymers with Very High Solubility in Supercritical CO_2 Down to Low Pressures. *Nature*, 405(6783):165–168, 2000.

[80] J. Liu, B. Han, Z. Wang, J. Zhang, G. Li, and G. Yang. Solubility of Ls-36 and Ls-45 Surfactants in Supercritical CO_2 and Loading Water in the CO_2 /Water/Surfactant Systems. *Langmuir*, 18(8):3086–3089, 2002.

[81] An Investigation of Non-fluorous Surfactant Dynol-604 based Water-in-CO_2 Reverse Micelles by Small Angle X-ray Scattering. *J. Supercrit. Fluids*, 26(3):275–280, 2003.

[82] M. T. Stone, P. G. Smith, S. R. P. da Rocha, P. J. Rossky, and K. P. Johnston. Low Interfacial Free Volume of Stubby Surfactants Stabilizes Water-in-Carbon Dioxide Microemulsions. *J. Phys. Chem. B*, 108(6):1962–1966, 2004.

[83] M. Haruki, H. Yawata, M. Nishimoto, M. Tanto, S. I. Kihara, and S. Takishima. Study on Phase Behaviors of Supercritical CO_2 including Surfactant and Water. *Fluid Phase Equilib.*, 261(1-2):92–98, 2007.

[84] Han B. Zhang X. Cleaning using CO_2 -based Solvents. CLEAN- Soil, Air. *Water*, 35:223–9, 2007.

[85] A. Mohamed, K. Trickett, S. Y. Chin, S. Cummings, M. Sagisaka, L. Hudson, S. Nave, R. Dyer, S. E. Rogers, R. K. Heenan, and J. Eastoe. Universal Surfactant for Water, Oils, and CO_2. *Langmuir*, 26(17):13861–13866, 2010.

[86] M. J. Hollamby, K. Trickett, A. Mohamed, J. Eastoe, S. E. Rogers, and R. K. Heenan. Surfactant Aggregation in CO_2 /Heptane Solvent Mixtures. *Langmuir*, 25(22):12909–12913, 2009.

[87] T. E. Sandoval and M. P. Gárate. Measurement of the phase behaviour of the binary systems carbon dioxide (CO_2)+ non-ionic surfactants (C_iEO_j). *J. Chem. Thermodyn.*, 45(1):109–113, 2012.

[88] A. R. Anim-Mensah and I. Shamsuddin. Solubilization of TX-100 and PEG-PPG-PEG in Liquid Carbon Dioxide. *Sep. Sci. Technol.*, 45:1901–1907, 2010.

[89] T. Lafitte, B. Mendiboure, M. M. Piñeiro, D. Bessières, and C. Miqueu. Interfacial Properties of Water/CO_2 : A Comprehensive Description through a Gradient Theory-SAFT-VR Mie Approach. *J. Phys. Chem. B*, 114(34):11110–11116, 2010.

[90] J. L. Dickson. *Stabilization of Colloidal Dispersions in Supercritical Carbon Dioxide*. PhD thesis, 2005.

[91] P. G. Smith. *Stabilization of Dispersions in Carbon Dioxide and in Other Low-permittivity Media*. PhD thesis, 2006.

[92] S. R. P. da Rocha, K. L. Harrison, and K. P. Johnston. Effect of Surfactants on the Interfacial Tension and Emulsion Formation between Water and Carbon Dioxide. *Langmuir*, 15(2):419–428, 1999.

[93] J. L. Dickson, C. Ortiz-Estrada, J. F. J. Alvarado, H. S. Hwang, I. C. Sanchez, G. Luna-Barcenas, K. T. Lim, and K. P. Johnston. Critical Flocculation Density of Dilute Water-in-CO_2 Emulsions Stabilized with Block Copolymers. *J. Colloid Interface Sci.*, 272(2):444–456, 2004.

[94] J. L. Dickson, P. A. Psathas, B. Salinas, C. Ortiz-Estrada, G. Luna-Barcenas, H. S. Hwang, K. T. Lim, and K. P. Johnston. Formation and Growth of Water-in-CO_2 Miniemulsions. *Langmuir*, 19(12):4895–4904, 2003.

[95] T. A. Hoefling, R. R. Beitle, R. M. Enick, and E. J. Beckman. Design and Synthesis of Highly CO_2 -soluble Surfactants and Chelating Agents. *Fluid Phase Equilib.*, 83(0):203–212, 1993.

[96] E. Kissa. Wetting and Wicking. *Text. Res. J.*, 66(10):660–668, 1996.

[97] L. R Fisher and P. D. Lark. An Experimental Study of the Washburn Equation for Liquid Flow in Very Fine Capillaries. *J. Colloid Interface Sci.*, 69(3):486–492, 1979.

[98] A. Marmur. Penetration and Displacement in Capillary Systems of Limited Size. *Adv. Colloid Interface Sci.*, 39(0):13–33, 1992.

[99] A. Marmur. Kinetics of Displacement of a Liquid from a Capillary: the Effect of Limited Reservoirs. *Chem. Eng. Sci*, 44(7):1511–1517, 1989.

[100] E. W. Washburn. The Dynamics of Capillary Flow. *Phys. Rev.*, 17:273–283, 1921.

[101] M. Mercier-Bonin, K. Ouazzani, P. Schmitz, and S. Lorthois. Study of Bioadhesion on a Flat Plate with a Yeast/Glass Model System. *J. Colloid Interface Sci.*, 271(2):342– 350, 2004.

[102] Bird R. B., Stewart W. E., and Lightfoot E. N. *Transport Phenomena.* second edition.

Chapter 3

Effect of Surface Roughness and Softness on Water Capillary Adhesion in Apolar Media [a]

The roughness and softness of interacting surfaces are both important parameters affecting the capillary condensation of water in apolar media, yet are poorly understood at present. We studied the water capillary adhesion between a cellulose surface and a silica colloidal probe in hexane by AFM force measurements. Nano-mechanical measurements show that the Young's modulus of the cellulose layer in water is significantly less ($\sim$ 7 MPa) than in hexane ($\sim$ 7 GPa). In addition, the cellulose surface in both water and hexane is rather rough ($6 - 10$ nm) and the silica probe has a comparable roughness. The adhesion force between cellulose and silica in water-saturated hexane shows a time-dependent increase up to a waiting time of 200 s and is much (two orders of magnitude) lower than that expected for a capillary bridge spanning the whole silica probe surface. This suggests the formation of one or more smaller bridges between asperities on both surfaces, which is confirmed by a theoretical analysis. The overall growth rate of the condensate cannot

[a]This chapter is published as: Soumi Banerjee, Pieter Mulder, J. Mieke Kleijn and Martien A. Cohen Stuart, J. Phys. Chem. A, 2012, 116, 6481-6488.

be explained from diffusion mediated capillary condensation alone; thin film flow due to the presence of a wetting layer of water at both the surfaces seems to be the dominant contribution. The logarithmic time dependence of the force can also be explained from the model of the formation of multiple capillary bridges with a distribution of activation times. Finally, the force-distance curves upon retraction show oscillations. Capillary condensation between an atomically smooth mica surface and the silica particle show less significant oscillations and the adhesion force is independent of waiting time. The oscillations in the force-distance curves between cellulose and silica may stem from multiple bridge formation between the asperities present on both surfaces. The softness of the cellulose surface can bring in additional complexities during retraction of the silica particle, also resulting in oscillations in the force-distance curves.

3.1 Introduction

Capillary condensation is scientifically intriguing as well as industrially relevant.[1,2] Ever since the discovery of the surface force apparatus (SFA) and atomic force microscope (AFM), measurements of capillary forces and other solvent related surface forces, such as solvation and structural forces between surfaces, have been attempted by various research group.[3–12] With AFM it is possible to probe both the equilibrium and time-dependent behaviour of capillary condensation. As the distance between the tip and sample surface is decreased beyond a critical distance, a curved meniscus is formed, giving rise to capillary forces that can be attractive, repulsive or zero[13] depending on the system parameters such as contact angle, filling angle, and radii of curvature. The sample surface and the AFM tip can be kept in contact or at close proximity for various times and the growth of the capillary bridge can be studied quantitatively. Moreover, the distance between the tip and the sample can be changed at various speeds and the bridge formation or rupture can be followed in real time. Depending on the time scale of evaporation or condensation of the bridge, equilibrium or kinetic parameters can be extracted using

models assuming constant radius of curvature of the capillary bridge (in case of equilibrium) or constant volume of the bridge (kinetic) at all tip-sample separations.[14]

Classically, capillary condensation has been described by the theories of homogeneous or heterogeneous (i.e. in presence of surfaces) nucleation and growth.[15] It was hypothesized that a dense liquid phase, formed by small to medium sized molecules such as water or oil or by macromolecules such as polymers, gets phase separated from a mixture in which the concentration of the condensing phase is low. The force due to a capillary bridge (f_c) has two components,[14] i.e. a surface tension term (F_γ) and a volume term ($f_{\Delta P}$), and can be written as,

$$f_c = f_\gamma + f_{\Delta P} = 2\pi r\gamma + A_c\Delta P \tag{3.1}$$

where r is the radius of the capillary bridge, γ is the interfacial tension between the condensate and the bulk fluid, A_c is the cross-section area and ΔP is the difference in Laplace pressure across the curved meniscus. The mechanism of phase separation (capillary condensation) has been reported to be diffusion controlled following the model of Kohonen *et al.*,[6] with the time scale of growth in the range of milliseconds to seconds. However, meniscus formation has also been observed for highly viscous and non-volatile lubricants where diffusion is virtually excluded. In these cases, growth time scales are of the order of minutes.[14–16] For these cases the kinetics of bridge formation has been related to the balance between the Laplace pressure and the disjoining pressure of the films around the interacting bodies. In this chapter we report the capillary condensation of water from hexane between a cellulose surface and a silica particle. We discuss our results by taking into consideration various parameters such as the roughness and softness of the cellulose layer, and the presence of a wetting water film on the surfaces. The model system chosen here can be used to gain insight into the process of dry-cleaning of dirty fabrics in an apolar medium such as liquid CO_2. Like hexane, liquid CO_2 is a low dielectric constant medium, which always contains trace amounts of water

dissolved in it. In previous research it has been shown that a little water helps in particle removal but adding more water makes the removal more difficult. We here show that not only the amount of water in these type of organic solvents plays a crucial role in particle removal, but the surface architecture of surfaces also is very important in the overall process.

3.2 Materials and methods

n-Hexane (Sigma-Aldrich with purity > 99 %) was dried using copper sulphate powder and filtered with a syringe filter of 0.2 μm. Water used in all the experiments was de-ionized and had a resistance of 18.2 MΩ cm. Preparation of wet hexane was done by saturating the hexane with water. The maximum solubility of water in n-hexane is 0.01 % (w/w).[17] Saturation was ensured by adding water until excess water was seen at the bottom of the container as a phase separated layer. Throughout the chapter we follow the terminology of wet hexane for the water-saturated hexane and dry hexane for the hexane dried using CuSO4 crystals.

3.2.1 Preparation and characterization of the cellulose layer

Silicon wafers (WaferNet) with a 3 nm surface oxide layer were cut into small pieces of 0.5 cm $\times$ 2 cm using a diamond craft knife. The wafers were sonicated in water and subsequently in ethanol, each for 15 minutes. After this the wafers were cleaned using a plasma cleaner for 10 minutes. Cellulose layers were spin-coated on the wafers following a standard procedure described elsewhere.[18] After coating, the layers were oven dried at 373 K for 1 hour to remove any water from the surface. After drying the layer thickness was measured using an ellipsometer. The roughness of the layer in air was measured by AFM imaging (Nanoscope V Multimode SPM, Bruker Corp.) using a V-shaped contact mode cantilever with silicon nitride tip (NP, Bruker Corp., nominal spring constant k = 0.06 N m^{-1}).

3.2.2 Measurement of the Young's modulus of the cellulose layer

Quantitative measurement of the Young's modulus of cellulose at nanoscale was performed using QNM (quantitative nanomechanics, Nanoscope V, Bruker Corporation). In this mode, the piezo oscillates in the z-direction at 2 kHz with an amplitude of 150 nm and force curves are recorded at every pixel in the image. These force curves were analyzed to calculate the force due to adhesion and the peak interaction force. To obtain the Young's modulus from the data, the default model used by the software is DMT (Derjagin, Muller, Toropov),[19] which corresponds to low sample deformation (1 to 10 nm). The sample deformations in all measurements were between 2 and 5 nm (Appendix, Figure 3.9*a*). The DMT model was fitted to the constant compliance region of the retracting force curves and the reduced Young's modulus, E^*, which includes the Young's moduli of both the tip and the sample, is calculated from the following relation

$$f_{\text{tip}} = \frac{4}{3} E^* \sqrt{R\delta^3} + f_{\text{adh}} \tag{3.2}$$

where f_{tip} is the force (peak force) on the tip, f_{adh} is the adhesion force, R is the tip end radius and δ is the deformation depth. The sample modulus is related to the measured reduced modulus by

$$E^* = \frac{1}{\left[\frac{1-\nu_t^2}{E_t} + \frac{1-\nu_s^2}{E_s}\right]} \tag{3.3}$$

where E_t and ν_t are the Young's modulus and Poisson's ratio of the tip, respectively, and E_s and ν_s are the Young's modulus and Poissons ratio of the sample. By assuming an infinite Young's modulus for the tip and knowing the sample Poissons ratio (0.3 for our samples), the sample modulus is calculated. The error in the modulus measurement due to the uncertainty in the value of the Poissons ratio would be between 4 and 25 %. The deflection sensitivity of the tip was measured on a hard surface, i.e. fused silica (FSILICA sample, Bruker Corp.). The spring constant was measured using the thermal tune method of Hutter and Bechhoefer.[20] To measure the tip radius, we used

the relative method of calibration using reference samples of known modulus supplied by Bruker Corporation. The relative method was preferred over the direct method in order to minimize the cumulative error in the modulus measurement. As reference sample highly ordered pyro graphite (HOPG-15M, Bruker Corp.) was used for the measurements in air and hexane, and PDMS gel (PDMS-soft-2, TACK 4, Bruker Corp.) was used for the measurements in water.

The choice of the probe is crucial for Young's modulus measurements. For accurate measurements, the selected probe should be able to produce high force sensitivity and large enough deformation. In order to select the right tip, one must have some idea about the sample stiffness. Since in our case the Young's moduli of the cellulose layer in various liquids were not known a priori, the selection of the cantilever involved a trial and error method. Overall, we followed the tip selection guide provided by the manufacturer. For this we used the value of Young's modulus of cellulose reported in literature,[21] which is 25 ± 4 GPa for a microcrystalline cellulose with 70 % crystallinity. The AFM probe chosen for all our measurements was a RTESPA (nominal spring constant 20 - 80 N m^{-1}, phosphorus doped Si, Bruker Corp.), except in water, for which a ScanAsyst-Air probe (nominal spring constant 0.4 N m^{-1}, silicon tip with nitride lever, Bruker Corp.) was used. The measurements were performed in both air and liquids. In case of measurement in liquids, the samples were equilibrated for 10 minutes before the measurements were performed.

3.2.3 Roughness determination of the cellulose layer in n-hexane and water

The height channel data obtained in the QNM mode (see above) was used for roughness determination of the cellulose layer in n-hexane and water. The roughness analysis was performed using WSxM 5.0 Develop 4.1 software. As a check we also analyzed the roughness by employing the section cut feature of the Nanoscope Analysis software (version 1.30, Bruker Corp.) and found comparable values for root mean square (rms) roughness.

3.2.4 Preparation of the mica surface

A molecularly smooth mica surface was prepared by freshly cleaving the surface using scotch tape just prior to force measurements.

3.2.5 Preparation of the colloidal silica probe

A silica particle of 3 μm radius (Phillips Laboratories) was glued to an AFM tip (NP10, Bruker Corp., silicon nitride tip with V-shaped cantilever, nominal spring constant of 0.06 N m^{-1}) using an UV curable glue (Norland 61) following a standard procedure.[22] This glue is particularly suitable for apolar liquids such as n-hexane. After attaching the particle to the tip, the glue was cured for 10 minutes using an OmniCure LX300 LED lamp.

3.2.6 Roughness determination of the silica particle

Silica particles attached to the AFM tips were imaged (Nanoscope V, Bruker Corp., ScanAsyst mode) with a Ti-Roughness sample (RS-15M, Bruker Corp.) as the bottom surface. This particular way of imaging using a substrate with spike-like structures of nm tip radius on its surface, is known as reverse imaging technique and has been described elsewhere.[23] After attachment to the AFM tip, the silica particle was plasma cleaned to remove any organic debris from its surface. At least five different colloidal probes were imaged to see the reproducibility. We checked the effect of length scales on the roughness by scanning different scan areas. For each image, the roughness analysis was performed using the section analysis feature of the Nanoscope analysis software (version 1.30) after flattening.

3.2.7 Measurement of surface forces

Force measurements were performed in a Nanoscope IIIa Multimode SPM with PicoForce extension (Bruker Corp.) using a liquid cell. To get a leak proof system, we used special nitrile rubber O-rings, coated with Teflon. These are particularly suitable for apolar organic solvents. For each measurement 30

curves were recorded and the reproducibility was checked by overlaying these curves. The waiting time of the colloidal probe at the surfaces was varied between 0 and 200 seconds and during the waiting step a constant force was applied. The rate of approach and retract in all the experiments was 2 μm s^{-1}. The deflection sensitivity (nm V^{-1}) was obtained from the slope of the constant compliance region, where the distance between the tip and sample is zero, and the deflection data in Volts were multiplied by the deflection sensitivity and cantilever spring constant (N m^{-1}) to calculate the surface forces following Hooke's law. The spring constants were measured using the thermal tune method as mentioned earlier and were found to be between 0.15 and 0.28 N m^{-1}.

3.3 Results and discussion

3.3.1 Roughness and Young's modulus of the cellulose surface

The model cellulose layer deposited on the silica plate had a thickness of 95 $\pm$ 5 nm in air as measured by ellipsometry. The Young's moduli of this layer in n-hexane and water were measured using quantitative nanomechanical analysis by AFM. As a control the Young's modulus of the cellulose layer was also measured in air and was found to be 40 $\pm$ 12 GPa. The Young's moduli of the cellulose layer in hexane and in water are shown in Figure 3.1a and Figure 3.1b respectively. The histogram data reported here is an average of five trials in water and four trials in hexane. The figures show that the cellulose layer is softer in water as compared to hexane. The mean Young's modulus of cellulose, as obtained from a Gaussian fit to the data, is 7 $\pm$ 4 GPa in hexane and 7 $\pm$ 6 MPa in water. A difference of three orders of magnitude in the Young's modulus can be explained from the plasticization of cellulose by water. The hydroxyl groups in cellulose are able to form H-bonds with water and hence penetration of water leads to a favourable interaction whereas any such interaction is clearly absent in hexane. The height images of cellulose in hexane and water were analyzed for roughness determination. The roughness parameters are shown in Table 3.1. The rms roughness is 7.6 $\pm$ 2.4 nm in

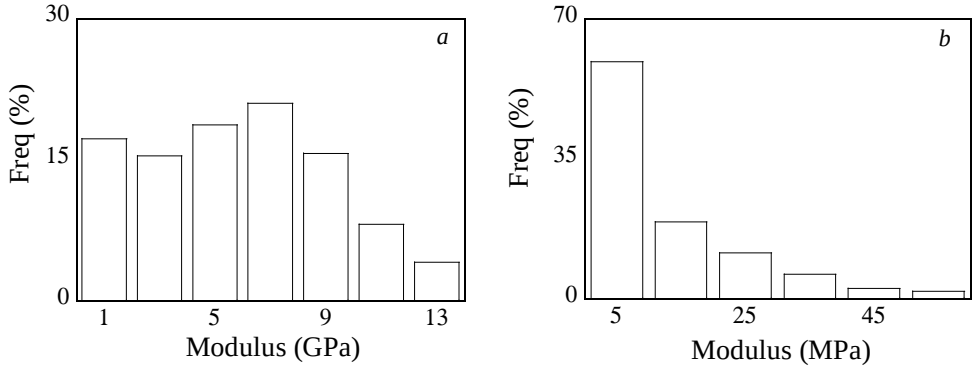

Figure 3.1: *Modulii of cellulose in (a) hexane (b) water.*

hexane with a peak-to-peak distance of 69.9 ± 23.1 nm, whereas the cellulose layer in water has a higher rms roughness of 11.7 ± 5.3 nm with a much higher peak-to-peak distance of 809 ± 417 nm. As a comparison the rms roughness of the cellulose layer in air is much smaller (0.5 ± 0.1 nm with a peak-to-peak distance of 4.1 ± 0.3 nm), see Table 3.2 in the appendix.

Table 3.1: *Roughness parameters of cellulose surface measured by AFM.*

	Roughness (nm)	
	hexane	water
rms roughness	7.6 ± 2.4	11.7 ± 5.3
peak to peak distance	69.9 ± 23.1	809 ± 417

3.3.2 Roughness of the silica probe

The roughness of the silica particle, used as a colloidal probe, was measured using the reverse imaging technique.[23] In this type of imaging a spiked substrate is used and a convolution of the probe and the substrate surface is captured by the AFM image.

Figure 3.2a shows a 2D image obtained by scanning with the silica probe over the spiked Ti-Roughness sample over an area of 10.8 × 5.4 μm^2. Each spherical object in the image represents the colloidal probe particle as imaged

Figure 3.2: *AFM images obtained by scanning with a spherical SiO_2 colloidal probe of radius 3 µm over a sharply spiked Ti roughness sample (RS-15M, Bruker Corp.). (a) 2D image (10.8 ×5.4 μm^2) where the spherical objects all represent the SiO_2 particle imaged by different sharp spikes on the sample surface; the line along which roughness analysis was performed is indicated. (b) 2D image of a smaller area (1 ×0.5 μm^2) showing the local roughness of the SiO_2 particle.*

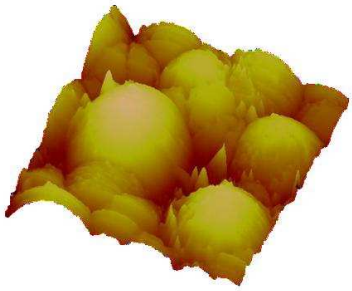

Figure 3.3: *AFM image (3D) obtained by scanning with a spherical SiO_2 colloidal probe of radius 3 µm over a sharply spiked Ti roughness sample (RS-15M, Bruker Corp., scan area 2.5 × 2.5 μm^2.*

by individual sharp spikes on the Ti sample. The rms roughness of the colloidal probe was 6.83 ± 2.06 nm. Figure 3.2b shows a 2D image obtained by scanning over an area of 1 × 0.5 μm^2 and shows a comparable roughness. In Figure 3.3 a 3D image is shown. All features visible in Figures 3.2a, b and 3.3 are resulting from the reverse imaging and not because of any contamination of the colloidal probe.

3.3.3 Force-distance curves

Typical force-distance curves for the interaction between a cellulose surface and a silica particle through wet and dry hexane are shown in Figure 3.4. Only the retraction part of the curves is plotted, i.e. they show the pull-off

force during the detachment of the silica particle from the cellulose surface. In case of interactions through dry hexane (Figure 3.4a), a small attractive force $\sim$ 0.5 to 3 nN is recorded, whereas in case of water-saturated hexane, the adhesion force is significantly larger ($\sim$ 5 times, Figure 3.4b), suggesting a role of water. The origin of the large adhesion force in wet hexane is therefore concluded to be the formation of water capillary bridge between the silica particle and cellulose surface. The driving force for capillary condensation is the difference in chemical potential of water dissolved in the bulk hexane phase and in the condensed water phase. Therefore a net flow takes place from the bulk towards the meniscus. This process continues until the chemical potentials equalize and equilibrium is established. For a sphere-plate geometry the force due to capillary condensation (f_c) can be written in the following form[14]

$$F_c = \pi\gamma R_0 \sin\beta \left[2\sin(\theta_1 + \beta) + R_0 \sin\beta \left(\frac{1}{r} - \frac{1}{l}\right)\right] \tag{3.4}$$

where R_0 is the radius of the sphere, γ is the interfacial tension between the condensed water phase and hexane, β is the filling angle, θ_1 is the three-phase contact angle at the particle surface, and r and l are the two radii of curvature of the liquid meniscus. The first term in Equation 3.4 is due to the vertical component of the surface tension and the second term is due to the Laplace pressure. The geometric parameters used in Equation 3.4 are depicted in Figure 3.5, which also schematically shows the effect of surface roughness.

In the approach curves we observed no or little attractive forces (Appendix, Figure 3.8. The hysteresis between the approach and retract curves could be related to the slow kinetics of nucleation[12] of water molecules from water-hexane mixtures due to the high interfacial tension between water and hexane ($\sim$ 50 mN m^{-1} at 298 K).[24] The maximum adhesion force was independent of the peak force (f_{tip}) applied, which is evident from Figure 3.9b in the appendix.

The small attractive forces seen in case of dry hexane (Figure 3.4a) might be due to the presence of traces of water entering the system during the setting up of the experiment, in absence of a humidity controlled environment. The average ambient RH was 40 - 60 %.

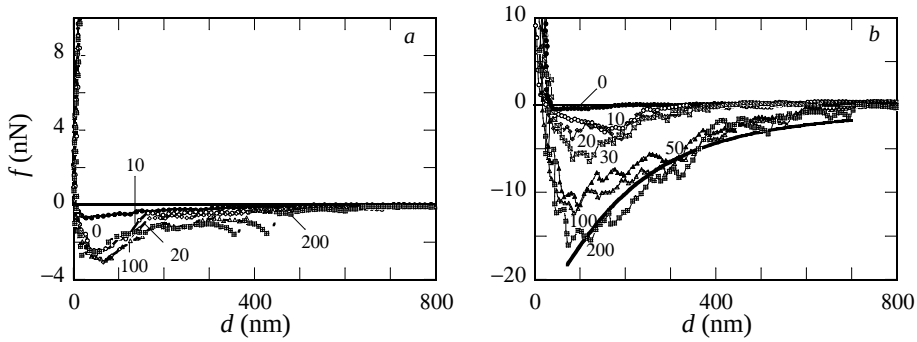

Figure 3.4: *Interaction curves between cellulose and silica through (a) dry hexane (b) wet hexane upon retraction, effect of surface delays.*

Even though the adhesion force in wet hexane is much larger as compared to dry hexane, the magnitude of this attractive force is much smaller than that predicted by the theory of capillary condensation. For example, in case of complete wetting of water on both cellulose and silica, theoretically one would expect an adhesion force of around 1900 nN, assuming $\gamma = 0.05$ N m^{-1} and $R = 3$ μm. Even for partial wetting, assuming an average contact angle of 50 °, the attractive force would be around 1200 nN, which is still two orders of magnitude higher than what is found experimentally. The fact that we record a much smaller force than what is theoretically expected indicates that the capillary bridge may not span the whole particle surface and can be explained either from the roughness of the cellulose and silica surfaces involved in the bridge formation or due to electrostatic repulsive forces acting in the water bridge. The radius of the capillary bridge corresponding to the maximum force that has been measured is only ~ 1 % of the radius of the silica particle. It must be noted here that the total amount of water in the cell is much higher than that required to cover the whole silica particle. The volume of the liquid cell is around 30 μL and the amount of water in that volume is around 0.18 μL, based on the water solubility of 0.01 % (w/w) in hexane.[17] This is much higher than required for the formation of a capillary bridge that spans the entire sphere ($3.3 \times 10^{-7}\mu$L).

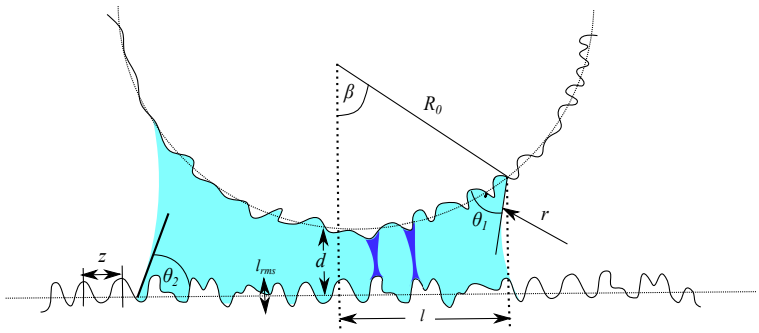

Figure 3.5: *Schematics of capillary condensation of water between a rough spherical silica particle and a rough cellulose layer. The dark shade of grey represent the bridges between the closest asperities on both the surfaces, light shade of grey represents filling of the whole available surface with water. R_0 is the radius of the sphere, l and r are the two radii of curvature of the meniscus, θ_1 and θ_2 are the contact angles of water on the particle and fabric surfaces respectively, β is the filling angle, l_{rms} is the root mean square roughness, z is the peak-to-peak distance and d is the distance of approach between the surfaces.*

Another interesting feature of the force-distance curves is the time-dependent behaviour. Both dry and wet hexane display an increase of the adhesion force with increasing surface delay time, but the increase is much stronger in case of wet hexane (from $\sim$ 0.5 nN to $\sim$ 16 mN m^{-1}) than for dry hexane (from $\sim$ 0.5 nN to $\sim$ 3 nN). Apart from the adhesion force, the range of attraction also increases with increasing waiting time.

3.3.4 Capillary bridge formation

The force-distance curves depicted in Figure 3.4b were analyzed using the capillary condensation model based on a constant volume of the condensate at all separations. In this model the force due to capillary condensation is given by[14]

$$f = 4\pi\gamma\kappa R_0 \left(1 - \frac{d}{\sqrt{\frac{V}{\pi R_0 + d^2}}}\right) \tag{3.5}$$

with

$$\kappa = \frac{\cos(\theta_1 + \beta) + \cos\theta_2}{2} \tag{3.6}$$

where V is the volume of the condensate, d is the distance, and θ_1 and θ_2 are the contact angles of water on the silica particle and cellulose surface respectively. This particular model[14] was chosen over the constant radius one, since at the retraction rate employed (2 μm s^{-1}) the typical break-up distance of around 1000 nm is reached in 0.5 s. Hence, the experimental time scale of retraction is much smaller than the typical experimentally observed capillary condensation time scale of 200 s or more. This situation can be considered as a constant volume condensate being stretched instantaneously. The solid curve in Figure 3.4b is a least square fit of Equation 3.5 to the experimental data using known values for γ and R_0 and κ and V as the fitting parameters. We are aware that this model is not applicable for multiple bridges. Since analysis in case of multiple bridges is complicated, we restrict ourselves to the case of single bridge formation to give an estimate of the condensate volume. The volume of the condensate obtained from fitting to the force curves in Figure 3.4b has been plotted as a function of waiting time in Figure 3.6 (black dots).

If the growth of the capillary bridge during the waiting time at the surface would result purely from diffusion of water molecules from the bulk hexane towards the meniscus, the growth rate of the capillary condensate can be approximated as[6]

$$\frac{dr}{dt} = \frac{DMC_0}{\rho R^*}\left(\frac{C}{C_0} - \exp^{(-\lambda_K/r)}\right) \tag{3.7}$$

where r is the meniscus radius, D is the diffusion coefficient of water through hexane, M is the molar mass of water, C_0 is the saturation concentration of water in hexane, C/C_0 is the degree of saturation, ρ is the density of water, and R^* is the length scale related to the geometry of the system.[14] The Kelvin length, λ_K,[14] is a function of the interfacial tension between water and hexane

(λ_K) and the molecular volume (ν_m) of water and is given by

$$\lambda_K = \frac{\gamma \nu_m}{k_B T} \tag{3.8}$$

where k_B is Boltzmanns constant and T is the absolute temperature. The exact expression for R^* can be found in Reference 6. This length scale can be chosen as effective mean radius of curvature (R^*) given by

$$R^* = \frac{R_0 R_1}{R_0 + R_1} \tag{3.9}$$

where R_0 and R_1 are the radii of curvature of the two interacting surfaces. In case of a sphere and a plate R^* equals R_0, the radius of the sphere. The volume and radius of the bridge are related by[6]

$$V \approx 4\pi r^2 R_0 \tag{3.10}$$

From the growth rate, the volume of the capillary bridge as a function of waiting time can be calculated. The dashed curve in Figure 3.6a represents the numerical integration of Equation 3.7 by using realistic values: $DMC_0/\rho R^* = 161.46$ nm s^{-1}, $C/C_0 = 0.99$ and $\lambda_K = \gamma v_m/kT = 0.291$ nm using $D = 8.9 \times 10^{-9}$ m^2 s^{-1}, $M = 0.018$ kg mol^{-1}, $C_0 = 3$ mole m^{-3}, $\rho = 1000$ kg m^{-3}, $R_0 = 3 \times 10^{-6}$ m, $\gamma = 0.04$ N m^{-1} and $T = 298$ K and Equation 3.10. As can be seen from the plot, the diffusion model strongly underestimates the growth rate of condensate volume. This indicates that there must be an additional contribution to the growth of the capillary bridge.

In the literature, capillary bridge formation by non-volatile liquids has been described by thin film hydrodynamics[14,16] in which liquid transport from the film situated adjacent to the capillary bridge can become a dominant mechanism. For the present system, water can adsorb and form a thin wetting film on both cellulose and silica. This thin film of water can be present even before the surfaces are brought into contact, depending on the wetting characteristics of the surfaces. These thin films can drain into the condensed meniscus due to the pressure differences.

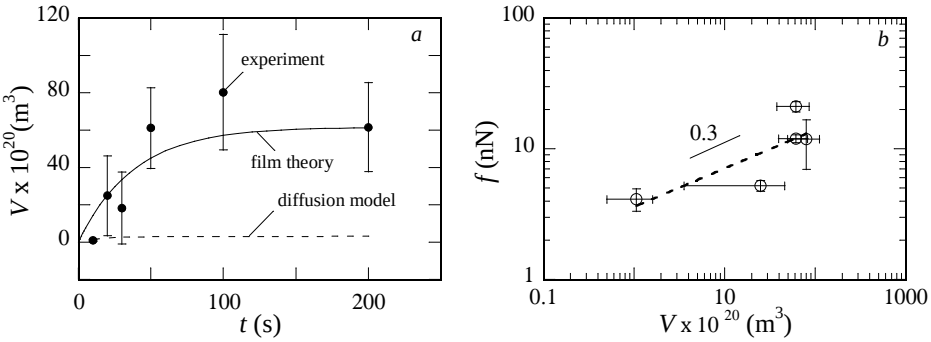

Figure 3.6: *(a) Volume of the condensed liquid as a function of waiting time before retraction. The points (black dots) were obtained by fitting Equation 3.5 to various force distance curves similar to that shown in Figure 3.4a using κ and V as fitting parameters. For the data shown in this curve, κ was found to be always between 0.003 and 0.551. The solid curve is calculated from Equation 3.11 (film drainage model) and the dashed curve is calculated using Equations 3.7 and 3.10 (diffusion model. (b) Maximum adhesion force versus condensed liquid volume. Condensate volumes were obtained by fitting Equation 3.5 to the force-distance curves of Figure 3.4b. The solid line is a power law fit to the data with slope 0.30.*

We have used the thin film hydrodynamics model proposed by Bhushan and Gao[16] to see if this mechanism can explain the estimated condensate volume as a function of waiting time. This model is based on the balance between the disjoining pressure in the liquid film and the Laplace pressure in the meniscus. The volume of the capillary bridge is given by

$$V(t) = V_m \left(1 - \exp^{\left(\frac{-\alpha h^3}{V_m \eta}\right)t}\right) \tag{3.11}$$

where V_m is the maximum condensate volume, h is the film thickness, η is the viscosity and α is a constant with dimension of pressure. The solid curve in Figure 3.6a is the fit of Equation 3.11 with V_m, which is equal to the volume of the condensate corresponding to the waiting time of 200 s, $\eta = 0.001$ Pa s and $\alpha h^3 = 2.7 \times 10^{-5}$ Pa m^3. The film thickness h was estimated from the disjoining pressure (Π) of the adsorbed film,[11] assuming that interactions of the bulk phase and the substrate through the water film are purely of dispersive

origin. The relation between Π and h is given by

$$\Pi = \frac{A}{6\pi h^3} \tag{3.12}$$

where A is the Hamaker constant. Since at equilibrium the Laplace pressure in the meniscus will be equal to the disjoining pressure in the film, we can write

$$\Pi = \frac{2\gamma}{r} \tag{3.13}$$

where r is the effective radius of curvature and γ is the interfacial tension between hexane and water. We calculated r in the same manner as described before, i.e. from Equation (10) corresponding to the volume (V_m) at $t = 200$ s. Using Equation 3.12 with a Hamaker constant of 1×10^{-20} J for water, we got an estimate of $h \approx 7$ nm. Using this value of h in Equation 3.11, α was estimated to be 7.5×10^{19} Pa. From Figure 3.6a we can see that the film drainage model describes the rate of increase of volume of the condensate very well. Hence as soon as the cellulose and silica surfaces come in contact with the wet hexane, thin films of water may be formed at these surfaces. Following this analysis it can be stated that the mechanism of the overall growth of the capillary bridge is mainly due to film drainage with a small contribution of diffusive mass transport from the bulk. The water film surrounding the silica and cellulose surfaces can be stabilized by both van der Waals and H-bonding interactions.

3.3.5 Roughness and capillary condensation: various regimes

Halsey *et al.*[25] have defined three power law regimes for the capillary force as a function of the bridge volume. For very low volumes, an asperity regime[25] is defined, where the capillary force arises due to the condensation of liquid around a single or a few asperities. In this regime the force scales with condensate volume as 1/3. For larger volumes (volume > single asperity), the system is in the roughness regime in which the force varies linearly with the

volume of the condensate. For even higher condensate volumes, the capillary force is independent of the volume and the force is dominated by the macroscopic rather than the microscopic curvature of the interacting bodies. This regime is known as the spherical regime. In order to see if the measured adhesion forces comply with one of these different regimes, we have plotted in Figure 3.6b the maximum adhesion force against the estimated volume of the condensed liquid for different waiting times on a log-log scale. We obtain an exponent of ~ 0.3, which suggests the asperity regime for the present system and applied settings in the force measurements. This seems plausible as the cellulose and silica particles are both rough in water, and hence formation of small (multiple) bridges is likely between asperities on either surface that are close to each other. Due to roughness, the volume of the condensate is small leading to weak adhesion; as shown earlier the adhesion corresponds to a capillary bridge radius that is only ~ 1 % of the radius of the particle (40 nm instead of 3 μm).

3.3.6 Oscillations in the force-distance curve

In Figure 3.4b oscillations in the force-distance curves are clearly visible. Their occurrence could be another consequence of the roughness of the cellulose and silica surfaces, namely, rupture of multiple capillary bridges having a distribution of rupture time scales. In case of two approaching rough surfaces, formation of multiple bridges can take place as the nearest asperities are filled up followed by more distant asperities. This argument was further investigated by measuring the adhesion force between a hard and atomically smooth mica surface and the same silica particle in wet hexane (Figure 3.7a). Indeed, oscillations were found to be much less visible than in the cellulose-silica case, which points out the validity of our hypothesis. The absence of any time dependent increase of the adhesion force furthermore indicates that on the smooth mica surface the activation barrier for condensation is less or absent and hence the adhesion force reaches its maximum value at a shorter time scale than was found for the cellulose-silica system. On a rough surface bridge formation between asperities for which the gap is smaller, occurs more readily

than between asperities that are further apart. The bridges for which the gap is smaller will exhibit a higher resistance towards rupture and will have a longer rupture time scale compared to the ones, which are already far apart. In a recent simulation[26] it was shown that for a sphere and a particle the bridges located at the centre of the contact area break later than the ones which are peripheral. Corresponding to these different time scales there could be different barriers of rupture, and as multiple bridges with a particular barrier break, the tip jumps to the next barrier. The thermodynamic stability of multiple bridges has been described as poor for smooth surfaces; however, their stability is enhanced for surfaces with wetting barriers.[27] For our case these wetting barriers could be the height of the asperities[28] coupled with the fact that the cellulose surface has both hydrophobic and hydrophilic patches.

Another plausible reason for the observed oscillations could be the pinning of the three-phase contact line, which occurs on rough surfaces at finite contact angle. In addition, the oscillations could originate from other dissipative processes, such as H-bond formation between water and silica, water and cellulose, or cellulose and silica. The breakage of H-bonds during the pull-off process could lead to additional energy barriers. Finally, formation of multiple direct contacts between the silica probe and the cellulose polymeric chains cannot be ruled out, especially since hexane is not a good solvent for cellulose: cellulose might be preferably in contact with silica over hexane. Finally, the Young's modulus measurements displayed in Figure 3.1 show that the cellulose is much softer in contact with water than with hexane and this difference in Young's moduli of the cellulose layer can bring in additional complexities during the retraction of the silica particle from the cellulose surface, which also may result in oscillations in the force-distance curves.

3.3.7 Water transport over heterogeneous surface as a thermally activated process

The condensation of liquids on rough surfaces is complex and may lead to unexpectedly slow kinetics.[29] Assuming that capillary condensation is an activated first order process, the time scale of condensation of one capillary

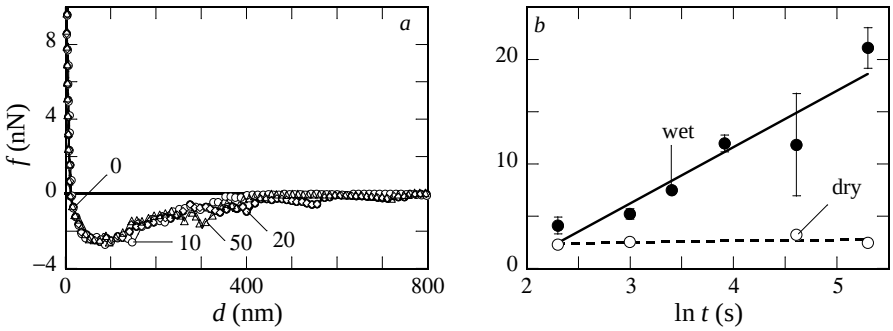

Figure 3.7: *(a) Force-distance curves for the interaction between mica and silica in hexane saturated with water. Mica has an atomically smooth surface resulting in much less oscillations in the force curves than observed for the cellulose-silica system (Figure 3.4b).(b) Maximum adhesion force versus* ln *(time) for the system cellulose and silica through wet and dry hexane as a function of waiting time before retraction*

bridge can be written as[30]

$$\tau_{\text{act}} = \tau_0 \exp^{\frac{\Delta E}{k_B T}} \tag{3.14}$$

where τ_0 is the time needed to condense out one liquid layer and ΔE is the activation energy. Assuming that because of roughness there would be multiple bridge formation between asperities at the two surfaces and that these asperities are separated by distances that have a finite distribution, Bocquet *et al.*[30,31] have arrived at the conclusion that the activation times for these bridges to form, will also have a finite distribution. The larger the distance between asperities, the higher is the resistance to nucleation and growth of a bridge. These topographical elements have been termed as defects that pose an additional energy barrier to the condensation process, leading to a logarithmic dependence of force with time. Following these arguments and realizing that at a particular time only those liquid bridges will have a chance to form that have an activation time $\tau_{\text{act}} < t$, the capillary force will be[30]

$$f(t) \approx \frac{2\pi R_0 \gamma}{\omega \nu_m a_0^2} \frac{1}{\ln \frac{C_0}{C}} \ln \frac{t}{\tau_0} \tag{3.15}$$

where w is the typical width of the distribution of distances between the surfaces and a_0^2 is the nucleation area. Plots of the measured adhesion force with waiting time for wet and dry hexane ($f(t)$ *versus* $\ln(t)$) are shown in Figure 3.7b. The straight lines in this figure show the validity of the model described by Equation 3.15 for our experimental data, i.e. the force depends logarithmically on time. This corroborates the idea of the formation of multiple capillary bridges between the rough cellulose and silica surfaces and underpins the slow kinetics of capillary condensation as a result of roughness alone.

3.4 Conclusions

Capillary condensation of water on soft and rough surfaces is more complex than on hard and smooth surfaces. The effects of roughness on capillary condensation can be manifold. Roughness can lead to formation of multiple bridges and slow kinetics of condensation, which in turn may be responsible for the oscillations seen in the force distance curves between cellulose and silica in water-saturated hexane. The cellulose surface is softer and rougher in hexane or water than in air and these factors could be responsible for the unique features of the force-distance curves seen in this particular system. The slow kinetics of condensation could also be rationalized based on film flow as the dominant mechanism for formation of the capillary condensate.

Bibliography

[1] A. Elkamel and R. D. Noble. Prediction of capillary condensation in small cylindrical pores using the local density approximation and a full lennard-jones 6-12 potential. *J. Phys. Chem.*, 95(24):10076–10080, 1991.

[2] J. Wood and L. F. Gladden. Modelling diffusion and reaction accompanied by capillary condensation using three-dimensional pore networks. Part 1. fickian diffusion and pseudo-first-order reaction kinetics. *Chem. Eng. Sci.*, 57(15):3033–3045, 2002.

[3] H. K. Christenson, D. W. R. Gruen, R. G. Horn, and J. N. Israelachvili. Structuring in liquid alkanes between solid surfaces: Force measurements and mean-field theory. *J. Chem. Phys.*, 87(3):1834–1841, 1987.

[4] H. K. Christenson and C. E. Blom. Solvation forces and phase separation of water in a thin film of nonpolar liquid between mica surfaces. *J. Chem. Phys.*, 86(1):419–424, 1987.

[5] H. K. Christenson, J. Fang, and J. N. Israelachvili. Experimental study of phase separation in films of molecular dimensions. *Phys. Rev. B*, 39:11750–11754, 1989.

[6] M. M. Kohonen, N. Maeda, and H. K. Christenson. Kinetics of capillary condensation in a nanoscale pore. *Phys. Rev. Lett.*, 82:4667–4670, 1999.

[7] P. Petrov, U. Olsson, H. K. Christenson, S. Miklavic, and H. Wennerström. Forces between macroscopic surfaces in a sponge phase. *Langmuir*, 10(4):988–990, 1994.

[8] P. Petrov, S. Miklavcic, U. Olsson, and H. Wennerström. A confined complex liquid. oscillatory forces and lamellae formation from an L3 phase. *Langmuir*, 11(10):3928–3936, 1995.

[9] P. Petrov, U. Olsson, and H. Wennerström. Surface forces in bicontinuous microemulsions: water capillary condensation and lamellae formation. *Langmuir*, 13(13):3331–3337, 1997.

[10] N. Maeda, M. M. Kohonen, and H. K. Christenson. Phase transition of *n*-alkane layers adsorbed on mica. *Phys. Rev. E*, 61:7239–7242, 2000.

[11] N. Maeda, M. M. Kohonen, and H. K. Christenson. Phase behavior of long-chain n-alkanes at one and between two mica surfaces. *J. Phys. Chem. B*, 105(25):5906–5913, 2001.

[12] J. Sprakel, N. A. M. Besseling, F. A. M. Leermakers, and M. A. Cohen Stuart. Equilibrium capillary forces with atomic force microscopy. *Phys. Rev. Lett.*, 99:104504, 2007.

[13] F. M. Orr, L. E. Scriven, and A. P. Rivas. Pendular rings between solids: meniscus properties and capillary force. *J. Fluid Mech.*, 67:723–742, 1975.

[14] H. -J. Butt and M. Kappl. Normal capillary forces. *Adv. Colloid Interface Sci.*, 146:48–60, 2009.

[15] R. J. Stokes and D. F. Evans. *Fundamentals of Interfacial Engineering.* Wiley–VCH Inc., 1997.

[16] C. Gao and B. Bhushan. Tribological performance of magnetic thin-film glass disks: its relation to surface roughness and lubricant structure and its thickness. *Wear*, 190:60–75, 1995.

[17] B. A. Énglin, A. F. Platé, V. M. Tugolukov, and M. A. Pryanishnikova. Solubility of water in individual hydrocarbons. *Chem. Technol. Fuels Oils*, 1(9):722–726, 1965.

[18] E. Kontturi, P. C. Thüne, and J. W. Niemantsverdriet. Cellulose model surfacessimplified preparation by spin coating and characterization by x-ray photoelectron spectroscopy, infrared spectroscopy, and atomic force microscopy. *Langmuir*, 19(14):5735–5741, 2003.

[19] B. V Derjaguin, V. M Muller, and Y. P Toporov. Effect of contact deformations on the adhesion of particles. *J. Colloid Interface Sci.*, 53(2):314 – 326, 1975.

[20] J. L. Hutter and J. Bechhoefer. Calibration of atomic–force microscope tips. *Rev. Sci. Instrum.*, 64(7):1868–1873, 1993.

[21] S.J. Eichhorn and R.J. Young. The Young's modulus of a microcrystalline cellulose. *Cellulose*, 8:197–207, 2001.

[22] W. A. Ducker, T. J. Senden, and R. M. Pashley. Direct measurement of colloidal forces using an atomic force microscope. *Nature*, 353:239–241, 1991.

[23] C. Neto and V. S. J. Craig. Colloid probe characterization: radius and roughness determination. *Langmuir*, 17(7):2097–2099, 2001.

[24] S. Zeppieri, J. Rodríguez, and A. L. López de Ramos. Interfacial tension of alkane + water systems. *J. Chem. Eng. Data*, 46(5):1086–1088, 2001.

[25] T. C. Halsey and A. J. Levine. How sandcastles fall. *Phys. Rev. Lett.*, 80:3141–3144, 1998.

[26] Y. Men, X. Zhang, and W. Wang. Rupture kinetics of liquid bridges during a pulling process: a kinetic density functional theory study. *J. Chem. Phys.*, 134(12):124704–124709, 2011.

[27] E. J. De Souza, M. Brinkmann, C. Mohrdieck, and E. Arzt. Enhancement of capillary forces by multiple liquid bridges. *Langmuir*, 24(16):8813–8820, 2008.

[28] Y. I. Rabinovich, J. J. Adler, M. S. Esayanur, A. Ata, R. K. Singh, and B. M. Moudgil. Capillary forces between surfaces with nanoscale roughness. *Adv. Colloid Interface Sci.*, 96:213–230, 2002.

[29] F. Restagno, L. Bocquet, J. Crassous, and E. Charlaix. Slow kinetics of capillary condensation in confined geometry: experiment and theory. *Colloids Surf A Physicochem Eng Asp*, 206:69–77, 2002.

[30] L. Bocquet, E. Charlaix, S. Ciliberto, and J. Crassous. Moisture-induced ageing in granular media and the kinetics of capillary condensation. *Nature*, 396:735–737, 1998.

[31] F. Restagno, L. Bocquet, and T. Biben. Metastability and nucleation in capillary condensation. *Phys. Rev. Lett.*, 84:2433–2436, 2000.

Appendix

Table 3.2: *Roughness analysis results for cellulose in air measured by AFM.*

Sample	rms roughness	peak to peak distance
cellulose in air	0.5 ± 0.1	4.1 ± 0.3

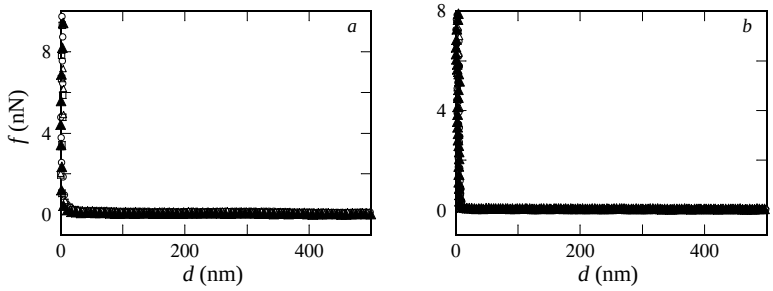

Figure 3.8: *Approach curves for the system silica-cellulose through (a) dry and (b) wet hexane.*

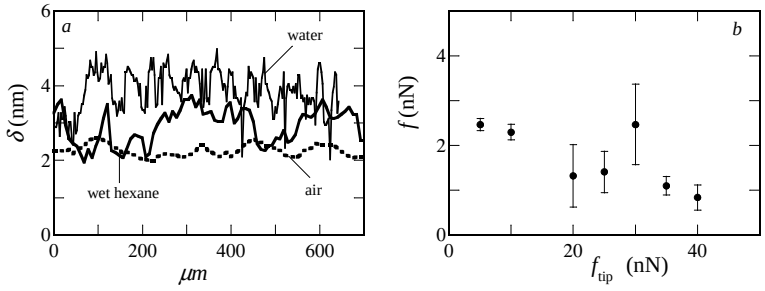

Figure 3.9: *(a) Deformation of cellulose during modulus measurement in three fluids. (b) Maximum adhesion force as a function of peak force (f_{tip}).*

Chapter 4

Towards Detergency in Liquid CO_2 - A Surfactant Formulation for Particle Release in an Apolar Medium [a]

In this chapter we propose, characterize and test a surfactant formulation, consisting of a branched polyoxyethylene type commercial non-ionic surfactant (Igepal CA520), n-hexane and water, for use in CO_2 dry-cleaning to enhance the removal of particulate soil. In the formulation lamellar mesophases L_α coexist in an L_2 microemulsion (reverse micellar) phase. We hypothesize that enhanced soil removal would be possible due to the adsorption of lamellar liquid crystalline phases at the fabric-soil interface, the presence of water pools, the improvement of the solvent quality of liquid CO_2 by the presence of n-hexane, and the enhanced viscosity due to the presence of the lamellar mesophases. We have characterized the formulation by optical microscopy with crossed polarizers, confocal microscopy, dynamic light scattering and shear viscometry to determine the phase behaviour, the size of the reverse

[a]This chapter is published as: Soumi Banerjee, Stevia Sutanto, J. Mieke Kleijn and Martien A. Cohen Stuart, Colloids Surf. A Physicochem. Eng. Asp., 415, 2012, 1-9.

micelles and the flow behaviour. AFM force measurements in n-hexane show that large adhesion forces between a model soil particle (silica) and fabric surface (cellulose) in water-saturated hexane can be reduced by the action of the surfactant mesophases. In the presence of the surfactant formulation the interaction forces were found to be decreased from $\sim$ 15 nN to 0.5 nN. The formulation, applied as a pre-treatment on standard soil test monitors and followed by washing in liquid CO_2, showed a five times better soil removal ability than the control.

4.1 Introduction

Traditional dry cleaning is carried out with perchloroethylene (PERC) which is toxic, harmful, carcinogenic and a depletant of the ozone layer. Therefore a more sustainable alternative is needed. Liquid CO_2 has been identified as a promising replacement for PERC in dry cleaning, as it is environmentally benign, non-toxic, and cheap.[1] Tests with liquid CO_2 as a medium for textile cleaning have shown that it indeed is capable of removing fatty and greasy substances, which are sufficiently soluble. Moreover, polar compounds are also fairly well removed, in particular when a little water (1 - 2 %) is added.[1] However, particulate dirt (soil) is poorly removed by liquid CO_2. This is to some extent expected, as the physical properties of liquid CO_2 make it a rather unfavourable medium for particle detachment and dispersion.[1,2] At industrially relevant pressures and temperatures (45 - 60 bar, 5 - 10 °C) liquid CO_2 has a very low dielectric constant.[1] This implies that particle-textile interactions (van der Waals forces) are likely to be much stronger than that in PERC. Moreover, the viscosity of liquid CO_2 is low, so that hydrodynamic forces exerted on attached particles are also expected to be weak.[1] Finally, the search for additives that might take the role of detergent in the cleaning process has so far had little success, mainly because the low cohesive energy density of liquid CO_2 prohibits dissolution of many candidate surfactants.[1] As a consequence, particle detachment, if successful at all, is prone to be followed by redeposition because there is no stabilizing dispersant.

The shift from the traditionally employed toxic, harmful chemical PERC to the environmentally friendly liquid CO_2 is urgent, but unless a suitable surfactant or surfactant formulation is developed, the numbers of dry-cleaners using liquid CO_2 as the cleaning medium will remain limited. Previous research shows that there are possibilities to improve the cleaning results for particulate soil in CO_2.[2] However, far too many parameters play a role to allow for a trial-and-error method to optimize the process. Instead a combination of fundamental and practical research is needed.

In this chapter we propose a new surfactant formulation to solve the problem of insufficient particle detachment and stabilization in liquid CO_2, based on the above presented analysis of that problem and on the existing knowledge on surfactants used in liquid and supercritical CO_2. Therefore, we start with a short overview of what is known about surfactants for CO_2, and then rationalize our choices for the new surfactant formulation in terms of the desired properties. The proposed formulation consists of a commercial surfactant (Igepal CA520, see Figure 4.1), n-hexane and water. We hypothesize that the most important aspect for its detergency action would be the formation of mesophases such as reverse micelles and lamellar phases. Thus, we explore the three-component phase diagram of the Igepal CA520/hexane/water system and assess the nature, size and composition of the mesophases. Furthermore, we present the viscosity as a function of total water and surfactant concentration to investigate the potential use of the formulation as a viscosity modifier for liquid CO_2. Finally, we test the detergency action of the new surfactant formulation in two different ways: firstly, by directly measuring the effect on the adhesion force between a model soil (silica) particle and a cellulose surface, and, secondly, by a practical test using the Igepal CA520/hexane/water system as a pre-treatment formulation in pilot-scale CO_2 dry-cleaning experiments. With respect to the first method, atomic force microscopy seems very appropriate to study the adhesive force profile between silica and cellulose. Unfortunately, it is still not possible to perform AFM force measurements under high pressure such as needed for liquid CO_2. Hence, we decided to first explore the forces in hexane. Although there are differences, this might give

some hints as to the strength and range of the forces operating in CO_2. We compare the adhesion forces between silica and cellulose in (wet) hexane in the absence and presence of the Igepal CA520, and discuss these data in the context of the phase behaviour.

4.2 Surfactants for liquid CO_2 - state-of-the-art

Research on surfactants for liquid CO_2 was started by trying out various commercially available surfactants. Consani and Smith[3] tried 130 commercially available surfactants and found that none of them was promising to be employed as a cleaning aid in liquid CO_2. In general, overcoming the surfactant tail-tail attraction in liquid CO_2 was one of the main challenges. To achieve solubility of surfactants in liquid or supercritical CO_2 design of novel molecules gained momentum. In synthesizing novel surfactants two approaches were taken: introduction of fluorine in the apolar tail of the surfactant replacing hydrogen[4–6] and introduction of hydrocarbon branching in the apolar tail.[7] The incorporation of fluorine in the tail was motivated by fluorine and CO_2 having similar cohesive energy densities.[4] However, fluorination did not solve the problem for CO_2 dry-cleaning, firstly because one has to increase the pressure above 150 bar to solubilize these surfactants[4–6] and secondly because the fluorinated surfactants themselves are not environmentally friendly. The second route, i.e., methyl branching of the tail tip was motivated by the prediction (using fractional free volume (FFV) theory[7]) that such branching leads to low density structures which should dissolve more easily in liquid CO_2. Ryoo *et al.* used a surfactant called polyoxyethylene 2, 6, 8-trimethyl-4-nonyl ether (Tergitol TMN) having methyl branching at 2, 6 and 8 positions of the apolar tail, and compared its solubility with a surfactant having a linear alkane chain as the tail.[7] The surfactant showed a cloud point at $\sim$ 100 bar, which is quite good but still higher than the pressure employed by the dry-cleaning industry.[7]

Thus, the search for suitable surfactants to enhance particle release in CO_2 dry-cleaning is still going on. In the next section we will describe a

novel surfactant formulation based on a commercially available surfactant, and explain step by step the rationale of the design.

4.3 Rationale of the design of the surfactant formulation

Our target properties in designing a surfactant formulation for liquid CO_2 were (i) a strong adsorption or wetting by the surfactant at the fabric-soil interface, (ii) enhancement of liquid CO_2 viscosity, (iii) deployment of a water pool to improve the removal of polar soils, and (iv) improvement of solvency power of liquid CO_2 by n-alkanes. We hypothesized that a lyotropic lamellar liquid crystalline phase of a surfactant should have a good adsorption/wetting capability at the fabric-soil interface: due to its flat structure (packing parameter ≈ 1) it has a strong tendency to adsorb in multilayers.[8] Based on the idea of branching to enhance solubility in liquid CO_2, supported by FFV theory, we looked for a surfactant with branched tail, with a molecular weight restricted to $\sim$ 400 - 500 g mol^{-1}. A higher molecular weight would result in low or no solubility in liquid CO_2. Thus, a non-ionic surfactant, polyoxyethylene (5) iso-octylphenyl ether (M_w = 427 g mol^{-1}, Figure 4.1), which is commercially available under the name Igepal CA520, was selected.

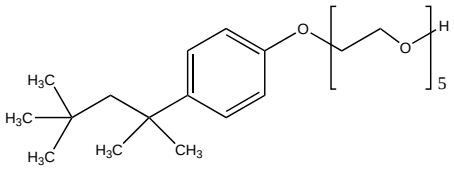

Figure 4.1: *Chemical structure of Igepal CA520, branched polyoxyethylene (5) isooctylphenyl ether.*

The second idea was to use n-hexane as a solvent in the surfactant formulation. The use of short chain alkanes such as heptane as a co-solvent (30 % v/v) in CO_2 to improve the solvent quality had already been reported by Hollamby *et al.*[9,10] They showed by SANS measurements that it is possible to use a CO_2-heptane blend to drive the self-assembly of AOT in the solvent mixture

when CO_2 is in the supercritical state. The dependence of the aggregation behaviour on solvent quality for surfactants such as AOT and $C_{12}EO_5$ has been rationalized by the Snyder polarity parameter, dielectric constant and Hildebrand solubility parameter.[9,10] In our formulation, n-hexane was chosen since its dielectric constant is close to that of liquid CO_2 (1.5 at 60 bar and 283 K),[11] so that it is likely to be miscible with that liquid.

Finally, the use of water in the formulation is necessary to drive the formation of lamellar liquid crystalline phases. The hydrophilic ethylene oxide (EO) groups of the ethoxylated non-ionic surfactant would drive association in n-hexane, and water would promote the formation of the liquid crystal.[12,13] This is schematically presented in Figure 4.2. The addition of water as a minor component in CO_2 dry-cleaning is not unheard of. In dry-cleaning industry water is deliberately added to improve the removal of polar soil.[1,14] Hence, we propose that the presence of water in our formulation could serve two purposes: it would drive the lamellar phase formation[12,13] and in addition enhance the polar soil removal.[14]

The effectiveness of the lamellar phase in improving soil removal could also be conceived from the viscosity modification of liquid CO_2 due to the high viscosity of the former, if these mesophases could be formed in liquid CO_2 also. Previous research[15] has shown that rod like micelles of fluorinated surfactants can increase the viscosity of CO_2 by ~ 40 %. As we will show in this chapter, in our formulation the lamellar phase is dispersed in a reverse micellar phase which may have aggregate shapes ranging from spheres to rods. Hence, it is possible that adding the formulation to liquid CO_2 leads to an increase in viscosity and to stronger hydrodynamic drag on the particles, thereby enhancing particle detachment.

4.4 Materials and methods

The surfactant chosen for our study is a branched non-ionic surfactant, Igepal CA520 (Sigma-Aldrich). The chemical structure is given in Figure 4.1. The mean number of oxyethylene groups $n = 5$, and the average molecular

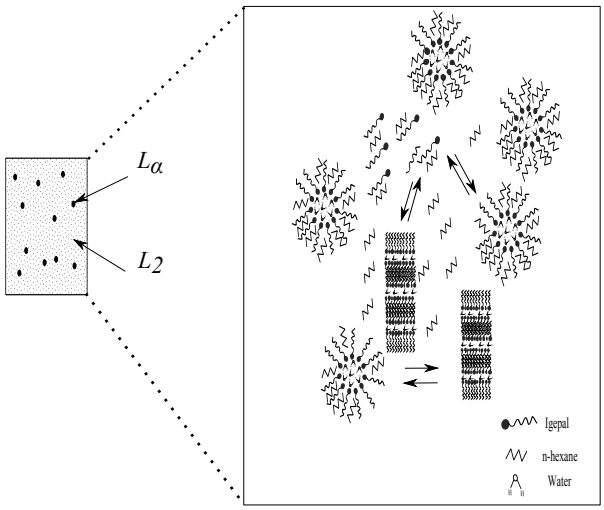

Figure 4.2: *Schematics of the surfactant formulation: a biphasic system consisting of lamellar (L_α) phase dispersed in the continuous medium of reverse micelles (L_2).*

weight 427 g mol^{-1}. n-Hexane (purity > 99 %, Sigma-Aldrich) was used as a solvent. Prior to use, n-hexane was dried by adding copper sulphate powder and filtered by using a syringe filter of 0.2 μm for all experiments except for the measurements with water saturated hexane. Water used in all the experiments was de-ionized with a resistance of 18.2 MΩ cm.

Carbon dioxide (grade 2.7, Linde Gas Benelux B.V.) at a pressure of $\sim$ 50 bar and 283 K was used for the dry-cleaning trial. The standard test monitor used was clay on polyester (Center for Testmaterials B.V.).

4.4.1 Polarising optical microscopy: phase analysis

Different mesophase compositions were prepared by mixing surfactant and n-hexane in various weight ratios (70/30, 60/40, 50/50, 40/60, 30/70, 20/80 and 10/90). The amount of water added to these surfactant-n-hexane mixtures was varied from 0 to 40 % (w/w). Weighed amounts of surfactant and n-hexane were added to glass containers and mixed by stirring for 10 minutes on a magnetic stirrer. Weighed amounts of deionized water were added to these mixtures and stirred for 15 minutes. For equilibration the mixtures were

kept in a shaker bath for two days at a constant temperature of 298 K. Glass containers were sealed with Teflon tape to prevent evaporation of the volatile n-hexane.

A polarising optical microscope (Olympus BX60) was used to study the phase behaviour of the ternary system. The images were collected using a camera (Olympus DP70) and processed with AnalySIS image processing software. For all samples, an aliquot was withdrawn by a Pasteurized pipette, put in between a glass slide and a cover slip, and viewed under the microscope. All the four sides of the cover slip were sealed to prevent evaporation of n-hexane. Liquid crystals are birefringent and have optical textures that can be used for their identification under cross polarizers.[16] In polarized white light lamellar phases appear as Maltese cross textures, and the hexagonal liquid crystals appear as coloured mosaics. The isotropic reverse micelles are non-birefringent and appear as black.

4.4.2 Rheometry: viscosity as a function of water content

An Anton Paar MCR 300 rotational rheometer with double gap concentric cylinder geometry was used to measure the bulk viscosities of the samples, having a fixed surfactant-to-hexane weight ratio of 50/50 and a water content varying between 0 and 30 % (w/w). A pre-shear was applied for 60 seconds to eliminate any shear history in the samples. The samples were then allowed to rest for 10 minutes for equilibration. After equilibration, viscosities were measured at shear rates from 0.01 to 100 s^{-1}. All measurements were performed at a constant temperature of 298 K.

4.4.3 Dynamic Light Scattering: size of reverse micelles

Dynamic light scattering (ALV 5000/60X0) with a Cobolt Samba-300 DPSS laser was used to analyse the Brownian motion of the mesophases with increasing water content, and from that their effective hydrodynamic radius. The wavelength of the laser was 532 nm and the data were collected at an angle of 90 °. The temperature was fixed at 298 K with an accuracy of ± 0.1

K using a Haake F8-C35 thermostatic bath. We considered the bulk of the sample to be continuous in n-hexane with dissolved surfactant monomers and approximated the viscosity and refractive index of this mixture to be the same as that of n-hexane. The refractive index of n-hexane was measured using an Abbe refractometer (Atago Co. Ltd) and was found to be 1.375.

4.4.4 Preparation and characterization of cellulose coated silicon wafers

Silicon wafers with spin-coated cellulose layers were prepared and used to study the interactions between a cellulose layer and a model particle (silica, 3 μm radius) by AFM force measurements. The silicon wafers were cut into small pieces of 0.5 cm $\times$ 2 cm using a diamond craft knife and were cleaned by sonicating in water and subsequently in ethanol, each for 15 minutes, and dried using N_2 gas. After this the wafers were cleaned using a plasma cleaner (Harrick Scientific Corp., model PDC-32G) for 10 minutes. To ensure a good anchorage between the silicon wafer and the cellulose layer, a di-block copolymer layer of polystyrene-poly (4-vinylpyridine) (PS-P4VP, 100 ppm in chloroform) was deposited on the silicon wafer. The PVP blocks (hydrophilic) are bound to the wafer and free PS blocks (hydrophobic) remain free for attachment with the cellulose. The cleaned wafers were dipped inside the polymer solution for 30 minutes and then rinsed with fresh chloroform to exclude any free polymer at the surface of the wafer, and dried with N_2. The spin-coating of the cellulose layer was done by following a standard procedure described elsewhere.[17] The thickness of the cellulose layers was measured using an ellipsometer (Multiskop, Optel GBR) with an angle of incidence of 70 ° and a laser wavelength of 632.8 nm. The optical model used for the measurement consisted of four layers: silicon, SiO_2, block copolymer (PS-P4VP), and cellulose. The thickness of the cellulose layer was found to be 97.5 $\pm$ 5.8 nm, averaged over 11 different strips, measured at three different locations and taking the literature value of 1.51 as the refractive index of cellulose.

4.4.5 Adhesion force measurements

Force measurements between a model cellulose surface ("fabric") and a silica particle ("soil") were performed in a Nanoscope IIIa Multimode atomic force microscope provided with a PicoForce module (Bruker Corporation) and using a liquid cell. A silica particle of 3 μm radius was glued to the AFM tip (NP, Bruker Corporation) using a UV curable glue (Norland 61, Norland products). This glue is stable (unsolvable) in low dielectric constant liquids such as n-hexane. After attaching the particle to the tip, the glue was cured for 10 minutes using an OmniCure LX300 LED lamp. The nominal spring constant of the cantilevers for all the experiments was 0.06 N m^{-1}, the velocity of approach and retract was 2 μm s^{-1} and the force curves reported here correspond to a waiting time of 200 s at the surface. More detail about the force measurements can be found elsewhere.[18]

4.4.6 Pilot scale CO_2 dry-cleaning trial

For the dry-cleaning trial, formulations containing Igepal CA520 n-hexane and water were used as a pre-treatment. Two different formulations were tested with the same surfactant-to-hexane ratio of 50/50 (w/w) and with 10 or 20 % water (w/w). Soil removal efficacy was tested in a high pressure pilot scale washing machine using liquid CO_2 as the cleaning medium. The schematic representation of the set-up is given in Figure 4.3. It has a capacity of 25 L with a rotating inner drum to provide mechanical action.

CO_2 from storage is circulated through the closed system by a pump. During each washing or rinsing cycle, it passes through a heat exchanger which serves to cool and/or to heat the CO_2, and thus regulates the pressure. Before the fluid from the vessel enters the pump, it passes through a filter with a pore size of 11 μm in order to remove unwanted particles. The temperature, pressure, density, and mass flow are monitored. When a washing cycle is finished, the used CO_2 is replaced by fresh CO_2 to rinse the fabrics. A detailed description of the procedure and apparatus is given elsewhere.[14] The process conditions used in the CO_2 dry-cleaning experiments are given in Table 4.1.

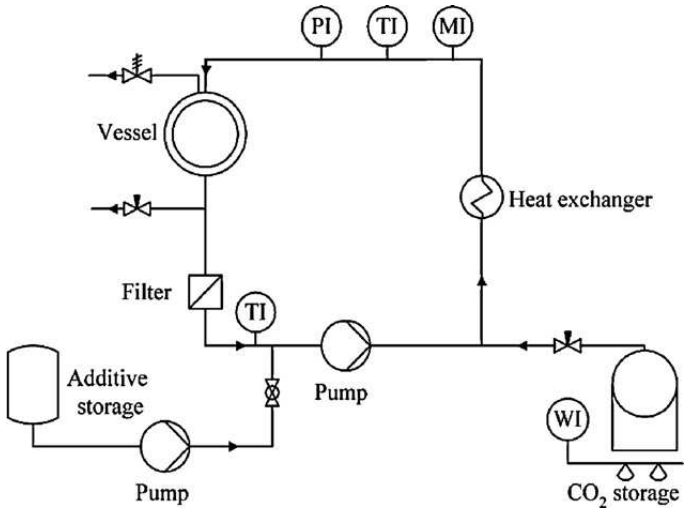

Figure 4.3: *Schematic diagram of* CO_2 *dry-cleaning set up*

Clay on polyester[2] (standard soiled fabrics) were used for liquid CO_2 dry-cleaning trials. The soiled monitors made up 20 g of the total 400 g wash load; the rest was filling material (several sheets of a cotton fabric of 25 cm $\times$25 cm) to reach the desirable washing load.

The color differences of the monitors were measured before and after the wash with a spectrophotometer (Data Color 110) using Standard Illuminant C as light source (average daylight, excluding ultraviolet light). The viewing angle used was the CIE 10 ° Supplementary Standard Observer. The test

Table 4.1: *Process conditions of* CO_2 *dry-cleaning*

Process condition	value	Unit
Amount of CO_2/cycle	6	kg
Wash load	400	g
Temperature	283	K
Pressure	50	bar
Washing time	20	min
Rinsing time	10	min
Rotational speed of inner drum	75	rpm

fabrics were measured using the $L^*a^*b^*$ color space, where L^* indicates the lightness, and a^* and b^* are the chromaticity coordinates; $+a^*$ is the red direction, $-a^*$ the green direction, $+b^*$ the yellow direction, and $-b^*$ the blue direction. In this color space, the color difference (ΔE) is defined by Equation 4.1:[14]

$$\Delta E_{1-2} = \left((L_1^* - L_2^*)^2 + (a_1^* - a_2^*)^2 + (b_1^* - b_2^*)^2\right)^{0.5} \tag{4.1}$$

The soil removal is represented by the Cleaning Performance Index (CPI), which is defined by

$$CPI = \left[1 - \frac{\Delta E_{washed-unsolied}}{\Delta E_{soiled-unsolied}}\right].100 \tag{4.2}$$

The test monitors were presoaked for 5 or 15 minutes in the surfactant formulation and then put inside the washing machine and cleaned in liquid CO_2. The results obtained using the Igepal formulations as pretreatment were compared with results obtained in CO_2 without any additive.

4.5 Results and Discussion

Part of the phase behaviour of the surfactant/n-hexane/water mixtures is shown in the phase diagram in Figure 4.4. In n-heptane the surfactant Igepal CA520 forms lamellar liquid crystalline phases with the addition of water.[19] Since n-hexane has only one CH_2 group less than heptane, phase diagram of Igepal CA520/n-hexane/water was expected to be similar. Several mixtures of n-hexane and Igepal CA520 of various weight ratios were prepared to which different amounts of water were added. Subsequently, the mixtures were well stirred and equilibrated.

From Figure 4.4 it is apparent that the phase behaviour is sensitive to the water content. At high surfactant-to-hexane weight ratios (30/70 to 70/30) and at 10 - 15 % (w/w) water, the phase is isotropic and oil continuous, denoted usually by L_2 or sometimes also as μE_2 (microemulsion of type 2),[19] and remains in equilibrium with the free surfactant monomer in n-hexane.

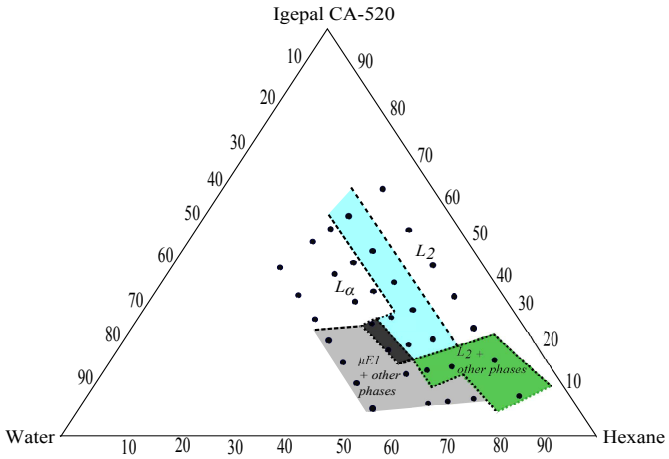

Figure 4.4: *Ternary phase diagram of Igepal CA520, n-hexane and water at 298 K as partially explored by polarised optical microscopy. Points represent the investigated compositions. The blue region indicates the co-existence of L_α and L_2 phases, green indicates phase separated compositions of L_2 and some phase of undetermined structure, grey indicates phase separated compositions of $\mu E1$ and some other unidentified phase, and black refers to a viscous isotropic monophasic composition of undetermined structure. The dashed lines indicate approximate phase boundaries.*

The Igepal CA520 headgroup consists of five EO groups and has an approximate area[20] of 0.43 nm^2. The length of the hydrophobic tail is $\sim$ 0.8 nm, as estimated from a molecular mechanics simulation. This corresponds to a tail volume of $\sim$ 0.51 nm^3, leading to a packing parameter of $\sim$ 1.5. A packing parameter > 1 indicates that the surfactants promote the formation of reversed water-in-oil systems. The oxyethylene chains of the surfactants can form hydrogen bonds with water and remain hydrated.[21] Hence, the formation of reverse surfactant aggregates in an oil continuous phase is enthalpy driven.[22] In the present system, the L_2 phase is a W/O microemulsion but since the structure of reverse micelles is not as well characterized as for normal micelles, it is better to denote this phase as oil continuous isotropic phase. Once the water uptake capacity inside the reverse micelles is exceeded, addition of more water causes the isotropic phase to rearrange into liquid crystalline mesophases. This transition gives rise to a coexistence region of liquid-crystalline phase with the oil-continuous isotropic phase. Upon passing

through the co-existence region, more liquid crystals are formed as the water fraction in the samples is increased. In our system we have observed optical textures under cross-polarized light, typical of lamellar liquid crystals (see Appendix Figure 4.10a). It must be noted that the identification of a particular kind of liquid crystalline phase in our samples is solely based on the visualization by polarised optical microscopy of its typical optical texture reported in literature. For surfactant-to-oil ratios between 10/90 and 40/60 and water contents between 20 and 40 %, a different microemulsion phase ($\mu E1$) in equilibrium with some unidentified phase is seen. The former is a bicontinuous microemulsion (see Appendix Figure 4.10b)), unlike the L_2, as confirmed by confocal microscopy (see Appendix, Figure 4.11c). In Figure 4.10b, the red regions are oil continuous, while the black regions are continuous in water. In contrast, the L_2 (Appendix, Figure 4.10c) has smaller oil and water domains (typical correlation length scales of $\sim$ 8 nm as seen by DLS). This clearly shows that two different microemulsions are formed depending on the oil to water ratios.

4.5.1 Reverse micelle size

The size of the reverse micelles was determined using dynamic light scattering. We used a composition having a surfactant-to-hexane ratio of 50/50 (w/w) and followed the increase of the size of the oil continuous surfactant mesophases with increasing amount of water, which is shown in Figure 4.5.

At 0 % (w/w) water we observe a hydrodynamic radius of 7.8 nm and this stays the same with the addition of water. It has been reported earlier that with the addition of water, the cores of the reverse micelles swell with water.[23] However, we did not observe any increase in the typical dimension (size) of the mesophases upon adding water up to 20 % (w/w) water. This probably implies that with the addition of water, the volume fraction of the reverse micelles increases keeping the size of the individual mesophases constant. Lemyre *et al.*[24] found similar results for the Igepal CO520/cyclohexane/water system up to 8 % (w/w) water concentration and with a surfactant concentration of 20 or 26 %. From the phase diagram (Figure 4.4) it can be seen that above $\sim$ 16%

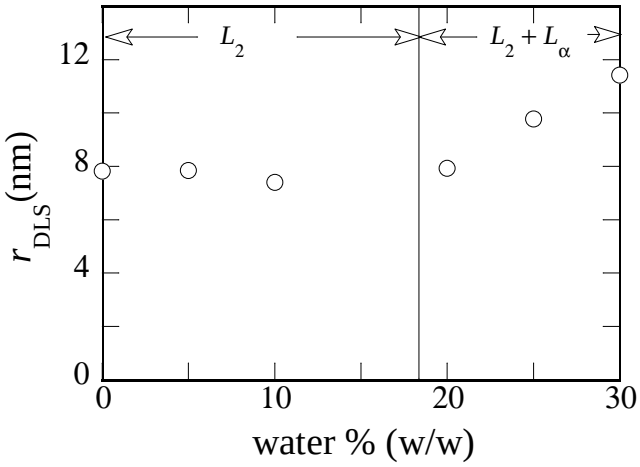

Figure 4.5: *Hydrodynamic radius of the reverse micelles measured by DLS as a function of water content at 298 K; surfactant-to-hexane ratio 50/50 (w/w), data calculated using the refractive index and viscosity of n-hexane*

.

water (w/w), the system undergoes a phase transition and a coexistence region appears featuring lamellar phases and L_2. Between 25 % and 30 % water the system forms liquid crystal phases (Figure 4.4) and the size increase is due to the formation of the larger aggregates with higher water content.

The state of the water inside the core of the reverse micelles is a subject of argument as it can change depending on the amount of water inside the micelles.[25] The polar core can consist of swollen (hydrated by water) headgroups or can have a separate water pool with or without impregnated hydrophilic chains, as indicated by recent molecular dynamics simulations.[21,25] Water would form a separate (free) water pool if the radius of the core is larger than twice the length of the oxyethylene chain.[25]

For Igepal CA520, the length of the hydrophilic chain is ~ 0.9 nm, calculated from the length of one oxyethylene group, 0.18 nm.[26] The hydrodynamic radius (r_{DLS}) of the reverse micelles as measured by DLS is ~ 8 nm (Figure 4.5). Since the length of the hydrophobic tail (l_{hphobe}) is ~ 0.8 nm, the estim-

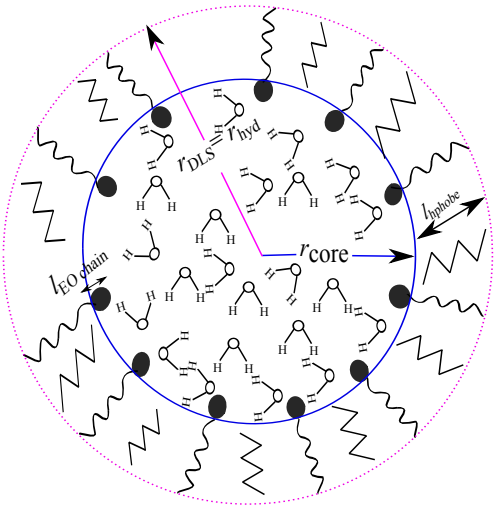

Figure 4.6: *Schematics of a spherical reverse micelle with various length scales. The polar core contains surfactant headgroups and water molecules. Representations of surfactant molecule, hexane and water are similar as in Figure 4.2.*

ated radius of the core is ~ 7.2 nm. This much larger radius than the length of the oxyethylene chain implies that a large fraction of the water inside the surfactant aggregates is free water, i.e. not associated with the EO headgroups of the surfactants. A schematic representation of the reverse micelle is given in Figure 4.6.

The existence of free water pools has also been proved using NMR.[25,27] Lemyre *et al.*[24] reported for the Igepal CO520/cyclohexane/water system that the reverse micelles, which have a diameter of about 4 nm, contain more than 20 water molecules per surfactant molecule.

As mentioned earlier, the structure of the reverse micelles is not as well understood as that of normal micelles. There has been speculation about the configuration of the oxyethylene chains inside the core.[21,24] Lemyre *et al.*[24] have argued that the configurations of the polar chains are very much dependent on the size of the aggregates: for small surfactant aggregates (at low water content) the oxyethylene chains would be confined and not fully extended, but as the water content is increased, the micelle size would increase and the

surfactant headgroups would extend inside the hydrophilic core.[24] Further investigation is needed before we can conclude whether any such transition from a confined to a fully extended configuration of the oxyethylene chain occurs. From the size of the reverse micelles, the aggregation number can be estimated by a simple area-to-volume argument,[24]

$$N = \frac{4\pi}{3} \frac{(r_{\mathrm{DLS}} - l_{\mathrm{hphobe}})^3}{\left(V_{\mathrm{H_2O,total}/\mathrm{n_{surf,inmicelles}}}\right) + V_{\mathrm{surf,hphile}}} \tag{4.3}$$

where N is the aggregation number, r_{DLS} is the hydrodynamic radius of the micelles obtained by DLS, l_{hphobe} is the effective length of the hydrophobic tail of the surfactant, $V_{\mathrm{H_2O,\ total}}$ is the total volume of water, $n_{\mathrm{surf,in\ micelles}}$ is the total number of surfactant molecules, and $V_{\mathrm{surf,hphile}}$ is the volume of the hydrophilic part of the surfactant molecule (Figure 4.6). The effective length of the hydrophobic tail, l_{hphobe}, depends on its conformation. For example, for the case of polyoxyethylene(5)nonylphenyl ether (Igepal CO520), the maximum length of a fully extended hydrophobic chain of the surfactant[24] has been reported to be 1.4 nm, whereas the effective length used for the calculation of the micelle aggregation number was 1.35 nm, considering the conformation possibilities at room temperature. In our case *lhphobe* is ~ 0.84 nm which is the end-to-end distance of the hydrophobic tail calculated by a molecular mechanics simulation. The value of the parameter $V_{\mathrm{surf,hphile}}$ of 0.35 nm^3/molecule, has been taken from the literature for polyoxyethylene (5) nonylphenyl ether (Igepal CO520) which also has 5 EO groups.[24] The aggregation number calculated using Equation (3) is around ~ 4000 for compositions having 0 to 10 % water (w/w). An aggregation number of the order of 100 has been reported for polyoxyethylene(5)nonylphenyl ether (Igepal CO520)[24] in cyclohexane/water. The fact that we find a considerably larger aggregation number indicates that formation of rod-like micelles might be favoured in concentrated systems such as ours, in which the surfactant concentration varies between 28.5 and 38.6 % (v/v). An even simpler, rough estimation based on a surfactant molecular area of 1 nm^2 at the hexane-water interface shows that the lowest estimate of the aggregation number would be 800-1000 for aggreg-

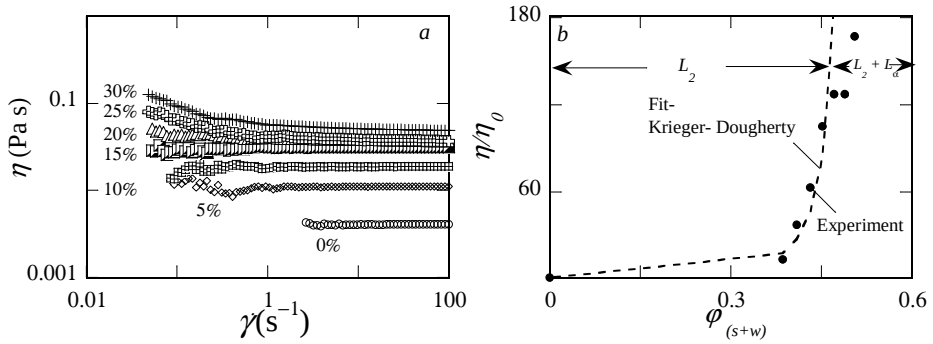

Figure 4.7: *(a) Bulk viscosities as a function of shear rate at 298 K, showing shear thinning behaviour at low shear rates. Surfactant-to-hexane ration 50/50 (w/w), water content as indicated.(b) Increase of bulk viscosities as a function of water volume fraction at 298 K, surfactant–to–hexane ratio was 50/50 (w/w). The fitting parameters used in the Krieger-Dougherty equation are the maximum packing volume fraction*= 0.51 *and the intrinsic viscosity* $[\eta] = 4$. *The dashed line represents phase transition composition.*

ates of 8 nm size. In literature, molecular areas between 0.45 and 0.84 nm^2 have been previously reported for linear surfactants. We assume a slightly higher value than reported in literature, as our surfactant tail is branched and therefore the molecule is likely to occupy a larger area at the oil-water interface due to higher excluded volume interactions. In both cases the numbers of surfactant molecules per reverse micelles are on the order of ~ 1000. With the addition of water the aggregates keep the same hydrodynamic radius (Figure 4.5), implying that the addition of water leads to an increase in the volume fraction of the aggregates in the constant size zone. Addition of more water beyond the constant size zone leads to a phase change forming larger liquid crystal mesophases.

4.5.2 Viscosity as a function of water content

Figure 4.7a shows the effect of water on the viscosity of the composition having a surfactant-to-hexane ratio of 50/50. An increase of bulk viscosity with increasing water content is observed for all the samples. An interesting feature

is that the samples mostly exhibit Newtonian behavior beyond shear rates 0.1 s^{-1}, while below this value their behavior is slightly non-Newtonian. This could be due to the presence of very weak aggregates which are broken down as the shear rate is increased. Newtonian behavior has been reported in literature[26] for reverse micelles in the shear rate range of 0.1 to 100 s^{-1}.

From Figure 4.7a, we got the Newtonian viscosities by taking the average of the last 20 - 30 data points. The Newtonian viscosities (η) were divided by the viscosity of pure hexane (η_0) to get the relative viscosity (η_r) of the samples. From the plot of the relative viscosity against the volume fraction of surfactant and water (Figure 4.7b), it is evident that as the combined volume fraction is increased from 0.39 to 0.51, the increase of viscosity is $\sim$ 13 times. The increase of viscosity with increasing volume fraction of water and surfactant correlates well with the phase diagram. At low water content, i.e. at 0 to 15 % (w/w) water ($\varphi_{(s+w)}$ = 0.38 to 0.45), reverse micelles (L_2) are present, while above 15 % water ($\varphi_{(s+w)} > 0.45$) lamellar phases (L_α) start to form. L_α phases are more viscous than the L_2 phases and hence the curve is drifting upwards (Figure 4.7b). We compared the experimental viscosity data with the curve predicted by the Krieger-Dougherty equation[28] with the maximum packing volume fraction $\varphi_m = 0.51$ and the intrinsic viscosity $[\eta] = 4$ as fitting parameters. This maximum packing volume fraction is much smaller than the random close packing volume fraction for hard spheres (i.e. 0.64). This may have various causes, such as long range interactions, polydispersity, deviation from spherical shape etc. For this system $[\eta]\varphi_m \approx 2$, implies a quadratic dependence[28,29] of the suspension viscosity with the dispersed phase volume fraction ($\eta \sim \varphi^2_{(s+w)}$).

The strong increase in viscosity with increasing amount of water is promising for the use of our formulation as a viscosity modifier for liquid CO_2. As mentioned in the introduction section, a viscosity enhancer is highly sought-after for enhancing the mechanical action in liquid CO_2 dry-cleaning. One order of magnitude increase of viscosity by driving the system towards the formation of lamellar liquid crystalline mesophases could turn out to be very beneficial.

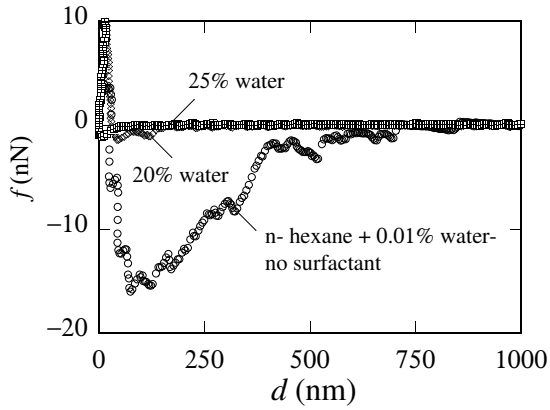

Figure 4.8: *Reduction of the adhesion force between cellulose and silica by the lamellar phase formulation.*

4.5.3 Effect of the surfactant formulation on the adhesion force

The interaction forces between a model cellulose surface and a model soil particle, silica, with or without surfactant, were quantified using colloidal probe atomic force microscopy. The control for this experiment was n-hexane saturated with water ($\sim$ 0.01 %, w/w). The formulation chosen for this study has a surfactant-to-hexane weight ratio of 40/60 and the water content was varied between 20 and 25 % (w/w). These formulations have a lower viscosity compared to the formulations with a surfactant-to-hexane ratio of 50/50 and hence it was easy to fill the liquid cell of the AFM. This should however not influence our results, since for both surfactant–to–hexane ratios L_α and L_2 are found at 20 or 25 % (w/w) water.

In case of the control, n-hexane plus water, the interaction force between cellulose and silica is approximately 15 nN (Figure 4.8). In the presence of the surfactant formulations, the force of adhesion was significantly reduced (to about 0.5 nN). In case of the saturated n-hexane, the adhesion force may originate from capillary bridge formation by water between cellulose and silica.[18] When the two surfaces come at close distance, water may phase separate between the surfaces and then the condensate grows in volume, resulting in a large adhesion force.[18] This effect is obviously not beneficial in dry-cleaning.

In dry-cleaning industry water is often added to improve the ability to solubilize polar soils.[1] However, it has been reported by Roosmalen *et al.*[14] that above a certain amount, the presence of water is actually detrimental to the detergency in liquid CO_2. Our results show that the amount of water can be increased to as high as 25 % (w/w) without increasing the force of adhesion: if the water is trapped inside the mesophases, either inside the L_2 or between the head-groups of L_α (Figure 4.2 and Figure 4.6), it would have less probability to form capillary bridges or result in weak capillary forces, yet this water can be utilized to solubilize polar soils.

4.5.4 Dry-cleaning in liquid CO_2 using the Igepal CA520/n-hexane/water formulations

The cleaning performance using the surfactant formulations containing Igepal, hexane and water as pretreatment agents is summarized in Figure 4.9. All the compositions contain Igepal to n-hexane ratio of 50/50 (w/w) with 10 or 20 % (w/w) water. The cleaning performance index (CPI) using the Igepal formulations is better irrespective of their water content than the control, which was CO_2 without the surfactant formulation (CPI 2.5 %). The best cleaning performance of Igepal as a pre-treatment agent is 12 % (Figure 4.9).

Moreover, the cleaning performance index displays (pretreatment) time dependence. For the 10 % water formulation we see that the higher the pretreatment time, the higher the CPI. However, for the formulation having a dispersion of L_α in L_2, the CPI of textiles treated for 5 minutes is higher than those treated for 15 minutes. In addition, the CPI pertaining to the formulation containing 10 % water and treated for 5 minutes is the same as that of the formulation containing 20 % water and treated for 15 minutes. There is no clear pattern emerging from these results indicating that the overall cleaning is a complex subject, and the parameter cleaning performance index is an average of the effect of removal and redeposition involved in the process. The maximum CPI obtained with PERC, which is the benchmark for dry-cleaning industry, is 15 % for a particular soil and fabric combination. However, the trial with PERC was conducted by a commercial dry-cleaner with Clip Com-

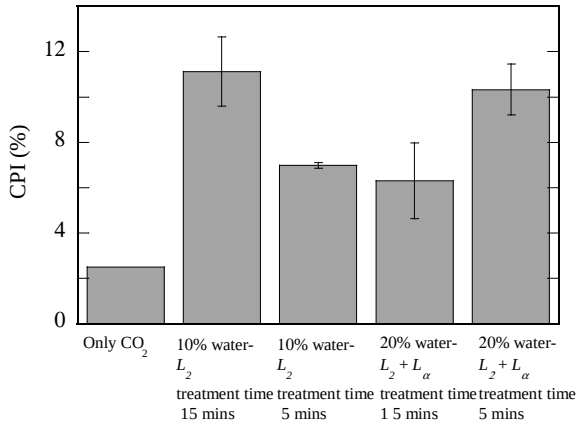

Figure 4.9: *Detergency results for the Igepal CA520/n-hexane/water formulation(used as a pretreatment)in the pilot scale liquid* CO_2 *setup. The surfactant-to-hexane ratio was 50/50 (w/w). Soiled monitor: clay on polyester.*

fort surfactant from Kreussler in a real dry-cleaning machine using different hydrodynamic conditions. Hence such a comparison would always be crude and highly approximate.

Here we mention that in observation cell experiments no enhancement of turbidity was observed (data not shown) which means that the surfactant formulation remains soluble in liquid CO_2, even at a pressure as low as 45 - 60 bar.

4.6 Conclusions

In this chapter we proposed to exploit lamellar liquid crystalline phases of a commercially available branched tail surfactant using n-hexane and water for application in liquid CO_2 dry-cleaning, to promote the release of particulate soil. The approach adopted by us is unique as we have combined four different concepts in one single formulation and have given the first proof of successful deployment of a commercially available non-ionic surfactant in liquid CO_2 dry-cleaning at a pressure as low as 45-60 bar.

It was shown that an Igepal CA520/n-hexane/water formulation in which

lamellar mesophases L_α coexist in an L_2 microemulsion phase, can bring a detergency benefit for CO_2 dry-cleaning. We adopted the route of forming a lamellar liquid crystalline dispersion in n-hexane by using water as a liquid crystal promoter. Lamellar liquid crystals have negligible curvature (packing parameter ≈ 1) and hence their adsorption on a flat surface such as a fabric should be more effective than that of reverse micelles. Our AFM force measurements confirm the hypothesis that adsorption of surfactant mesophases on fabric and soil decrease adhesion forces considerably, making soil removal much easier.

In addition, the water in the Igepal formulation is mostly present as pools in the surfactant aggregates, which can help removal of polar soil types. Furthermore, the presence of n–hexane could be beneficial, as claimed in literature for heptanes. Addition of heptane has been shown to improve the solvent quality of supercritical CO_2 resulting in the formation of surfactant aggregates which was otherwise impossible in only CO_2 as a solvent.

Finally, the viscosity of the formulation is considerably higher (~ 12 times) compared to systems containing only the reverse micellar phase and hence it may be used as a viscosity modifier for liquid CO_2. A higher viscosity would result in higher mechanical action which in turn can benefit the soil removal process.

From observation cell experiments in which the formulation was mixed with liquid CO_2, it was found that the surfactant remains soluble under dry-cleaning conditions. Our next step is to study the solubility of Igepal CA520 in liquid CO_2 and the formation of mesophases in this solvent with the addition of water and n-hexane.

Bibliography

[1] S. Banerjee, S. Sutanto, J. M. Kleijn, M. J. E. van Roosmalen, G. J. Witkamp, and M. A. Cohen Stuart. Colloidal interactions in liquid CO_2 – a dry-cleaning perspective. *Adv. Colloid Interface Sci.*, 175:11–24, 2012.

[2] M. J. E. van Roosmalen, M. van Diggelen, G. F. Woerlee, and G. J. Witkamp. Dry-cleaning with high-pressure carbon dioxide-the influence of mechanical action on washing-results. *J. Supercrit. Fluids*, 27:97–108, 2003.

[3] K. A. Consan and R. D. Smith. Observations on the solubility of surfactants and related molecules in carbon dioxide at 50°C. *J. Supercrit. Fluids*, 3(2):51–65, 1990.

[4] J. Eastoe, A. Dupont, A. Paul, Steytler D. C., and E. Rumsey. Design and performance of surfactants for carbon dioxide. In *Supercritical Carbon Dioxide*, volume 860 of *ACS Symposium Series*, pages 285–308. American Chemical Society, 2003.

[5] T. Hoefling, D. Stofesky, M. Reid, E. Beckman, and R. M. Enick. The incorporation of a fluorinated ether functionality into a polymer or surfactant to enhance CO_2-solubility. *J. Supercrit. Fluids*, 5(4):237–241, 1992.

[6] C. T. Lee, K. P. Johnston, H. J. Dai, H. D. Cochran, Y. B. Melnichenko, and G. D. Wignall. Droplet interactions in water–in–carbon dioxide microemulsions near the critical point: a small-angle neutron scattering study. *J. Phys. Chem. B*, 105(17):3540–3548, 2001.

[7] W. Ryoo, S. E. Webber, and K. P. Johnston. Water–in–carbon dioxide microemulsions with methylated branched hydrocarbon surfactants. *Ind. Eng. Chem. Res.*, 42(25):6348–6358, 2003.

[8] J. N. Israelachvili. *Intermolecular and surface forces.* Academic Press, London; San Diego, 1991.

[9] M. J. Hollamby, K. Trickett, A. Mohamed, J. Eastoe, S. E. Rogers, and R. K. Heenan. Surfactant aggregation in CO_2/Heptane solvent mixtures. *Langmuir*, 25:12909–12913, 2009.

[10] Martin J. Hollamby, Rico Tabor, Kevin J. Mutch, Kieran Trickett, Julian Eastoe, Richard K. Heenan, and Isabelle Grillo. Effect of solvent quality on aggregate structures of common surfactants. *Langmuir*, 24(21):12235–12240, 2008.

[11] D. R. Lide. *Handbook of Chemistry and Physics*. CRC Press, Boca Raton, FL, USA, 2004.

[12] H. Kunieda, C. Solans, N. Shida, and J. L. Parra. The formation of gel-emulsions in a water/nonionic surfactant/oil system. *Colloids and Surfaces*, 24:225–237, 1987.

[13] K. Shinoda and H. Saito. The effect of temperature on the phase equilibria and the types of dispersions of the ternary system composed of water, cyclohexane, and nonionic surfactant. *J. Colloid Interface Sci.*, 26:70–74, 1968.

[14] M. J. E. van Roosmalen, G. F. Woerlee, and G. J. Witkamp. Dry-cleaning with high-pressure carbon dioxide–the influence of process conditions and various co-solvents (alcohols) on cleaning-results. *J. Supercrit. Fluids*, 27(3):337–344, 2003.

[15] K. Trickett, D. Xing, R. Enick, J. Eastoe, M. J. Hollamby, K. J. Mutch, S. E. Rogers, R. K. Heenan, and D. C. Steytler. Rod–like micelles thicken CO_2. *Langmuir*, 26:83–88, 2010.

[16] G. J. T. Tiddy. Surfactant-water liquid crystal phases. *Phys. Rep.*, 57:1–46, 1980.

[17] E. Kontturi and Th˙Novel method for preparing cellulose model surfaces by spin coating. *Polymer*, 44:3621–3625, 2003.

[18] S. Banerjee, P. Mulder, J. M. Kleijn, and M. A. Cohen Stuart. Effect of surface roughness and softness on water capillary adhesion in apolar media. . *Phys. Chem. A*, 116:6481–6488, 2012.

[19] K. Grätz, M. Helmstedt, H. W. Meyer, and K. Quitzsch. Structure and phase behaviour of the ternary system water, n–heptane and the nonionic surfactant Igepal CA520. *Colloid. Polym. Sci*, 276:131–137, 1998.

[20] M. S. Celik and R. H. Yoon. Adsorption of poly(oxyethylene)nonylphenol homologs on a low–ash coal. *Langmuir*, 7:1770–1774, 1991.

[21] A. Allen, Rosalind, S. Bandyopadhyay, and M. L. Klein. $C_{12}E_2$ reverse micelle: a molecular dynamics study. *Langmuir*, 16:10547–10552, 2000.

[22] K. Mukherjee, S. P. Moulik, and D. C. Mukherjee. Thermodynamics of micellization of Aerosol OT in polar and nonpolar solvents. a calorimetric study. *Langmuir*, 9:1727–1730, 1993.

[23] L. K. Shrestha, R. G. Shrestha, D. Varade, and K. Aramaki. Tunable parameters for the structural control of reverse micelles in glycerol monoisostearate/oil systems: A SAXS study. *Langmuir*, 25:4435–4442, 2009.

[24] J.-L. Lemyre, S. Lamarre, A. Beaupré, and A. M. Ritcey. A new approach for the characterization of reverse micellar systems by dynamic light scattering. *Langmuir*, 26:10524–10531, 2010.

[25] J.-L. Lemyre and A. M. Ritcey. Characterization of a reverse micellar system by 1H NMR. *Langmuir*, 26:6250–6255, 2010.

[26] L. K. Shrestha, R. G. Shrestha, and K. Aramaki. Intrinsic parameters for the structure control of nonionic reverse micelles in styrene: SAXS and rheometry studies. *Langmuir*, 27:5862–5873, 2011.

[27] M. A. Sedgwick, D. C. Crans, and N. E. Levinger. What is inside a nonionic reverse micelle? Probing the interior of Igepal reverse micelles using Decavanadate. *Langmuir*, 25:5496–5503, 2009.

[28] S. P. Meeker, W. C. K. Poon, and P. N. Pusey. Concentration dependence of the low–shear viscosity of suspensions of hard–sphere colloids. *Phys. Rev. E*, 55:5718–5722, 1997.

[29] L. Bergström. Rheological properties of concentrated, nonaqueous silicon nitride suspensions. *J. Am. Chem. Soc.*, 79:3033–3040, 1996.

[30] R. W. Greiner and D. F. Evans. Spontaneous Formation of a Water-continuous Emulsion from a W/O Microemulsion. *Langmuir*, 6(12):1793–1796, 1990.

[31] N. Shahidzadeh, D. Bonn, J. Meunier, M. Nabavi, M. Airiau, and M. Morvan. Dynamics of Spontaneous Emulsification for Fabrication of Oil in Water Emulsions. *Langmuir*, 16(25):9703–9708, 2000.

[32] N Shahidzadeh, D. Bonn, O. Aguerre-Chariol, and J. Meunier. Spontaneous Emulsification: Relation to Microemulsion Phase Behaviour. *Colloids Surf. A Physicochem. Eng. Asp.*, 147(3):375–380, 1999.

[33] W. J. Benton, K. H. Raney, and C. A. Miller. Enhanced Videomicroscopy of Phase Transitions and Diffusional Phenomena in Oil-Water-Nonionic Surfactant Systems. *J. Colloid Interface Sci.*, 110(2):363–388, 1986.

[34] C. V. Sternling and L. E. Scriven. Interfacial Turbulence: Hydrodynamic Instability and the Marangoni Effect. *AIChE Journal*, 5(4):514–523, 1959.

[35] M. J. Rosen. *Surfactant and Interfacial Phenomena*. Wiley-Interscience, John Wiley & Sons, NJ, 2004.

Appendix

Confocal microscopy: Phase analysis

Apart from using optical microscopy with cross polarizers, the phase behaviour of the Igepal CA520/n-hexane/water system was investigated by confocal microscopy. The confocal microscope (Zeiss 200M Axiovert, LSMS exciter) had an oil objective of magnification 100x and a laser of wavelength 633 nm. The images and videos were analyzed by the software ZEN 2008. We used confocal microscopy for two purposes: (i) to distinguish between the two different types of microemulsions that we observed in the phase behaviour, namely a bicontinuous microemulsion ($\mu E1$) and a W/O microemulsion (L_2) and (ii) to confirm the formation of microemulsion phases by investigating their ability to spontaneously phase invert or emulsify in contact with a large volume of water.[30] The samples were dyed with the oil soluble fluorescent dye Nile red. To observe the phase inversion a Teflon ring of 1.6 cm internal diameter, fixed on a glass slide, was filled with water. A tiny drop of the microemulsion was carefully added to the water, and the subsequent process was observed using the confocal microscope. The interfacial instability[31] at the water-air interface was monitored by taking a three minute long video.

Spontaneous emulsification

It is known that W/O microemulsions undergo spontaneous emulsification to produce an O/W emulsion after the addition of an excess of water. This inversion process is very often associated with convective instabilities at the air-water interface due to the surface tension gradients (Marangoni effect) and/or gravitational forces due to density differences.[31–34] During the process, many intermediate phases may be formed such as bicontinuous microemulsions, lamellar mesophases, and vesicles. Many such examples are reported in literature mentioning the importance of the surfactant-to-co-surfactant ratio and oil type.[31] In our experiment, the sample having surfactant-to-hexane ra-

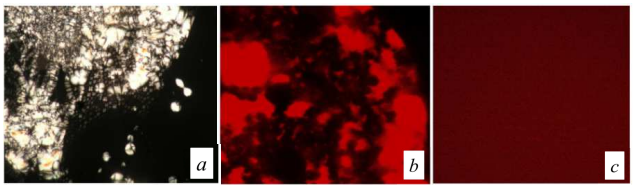

Figure 4.10: *(a) Lamellar L_α phase textures as seen in the composition of surfactant-to-oil 50/50 (w/w) and 20% (w/w) water; crossed polarisers, magnification 100 x. (b) Confocal microscope image of the microemulsion $\mu E1$, possible a bicontinuous phase. The oil phase is dyed with Nile Red, the water continuous domains are black. Magnification 20 x, aperture time 1.8 seconds. (c) Confocal microscope image of the microemulsion L_2, with smaller oil and water domains. The oil phase is dyed with Nile Red, magnification 20x, aperture time 1.8 seconds.*

tio 50/50 and 10 % (w/w) water (L_2, Figure 4.10c) was brought into contact with an excess water phase, and the subsequent process of phase transitions was observed by confocal microscopy using an oil soluble dye, Nile red. We observed a rapid mass transport through the interface, following a very dynamic process of formation and breakdown of oil droplets. In our case the surfactant has considerable solubility in both oil and water (HLB, hydrophilic lyophilic balance,[35] $\approx$ 10) and hence, when a phase rich in surfactant and oil comes in contact with water, surfactant transport is bound to take place through the oil-water interface causing a rapid motion in the underlying liquid. This hydrodynamic instability (see Figure 4.11), possibly stems from the formation of a surface tension gradient across the interface as the microemulsion, having ultralow oil-water interfacial tension, comes in contact with a pristine water surface having a surface tension of $\sim$ 72.8 mN m^{-1}. We also probed the spontaneous phase inversion of the bicontinuous microemulsion ($\mu E1$), and this showed similar phase transitions and hydrodynamic instability when brought in contact with a large reservoir of water (data not shown). As a control, we checked the spontaneous emulsifying ability of the liquid crystal mesophase composition having a surfactant-to-hexane weight ratio of 70/30 and 40 % (w/w) water. This composition did not show interfacial instability and hence it is concluded that the compositions that spontaneously emulsified were indeed microemulsions.

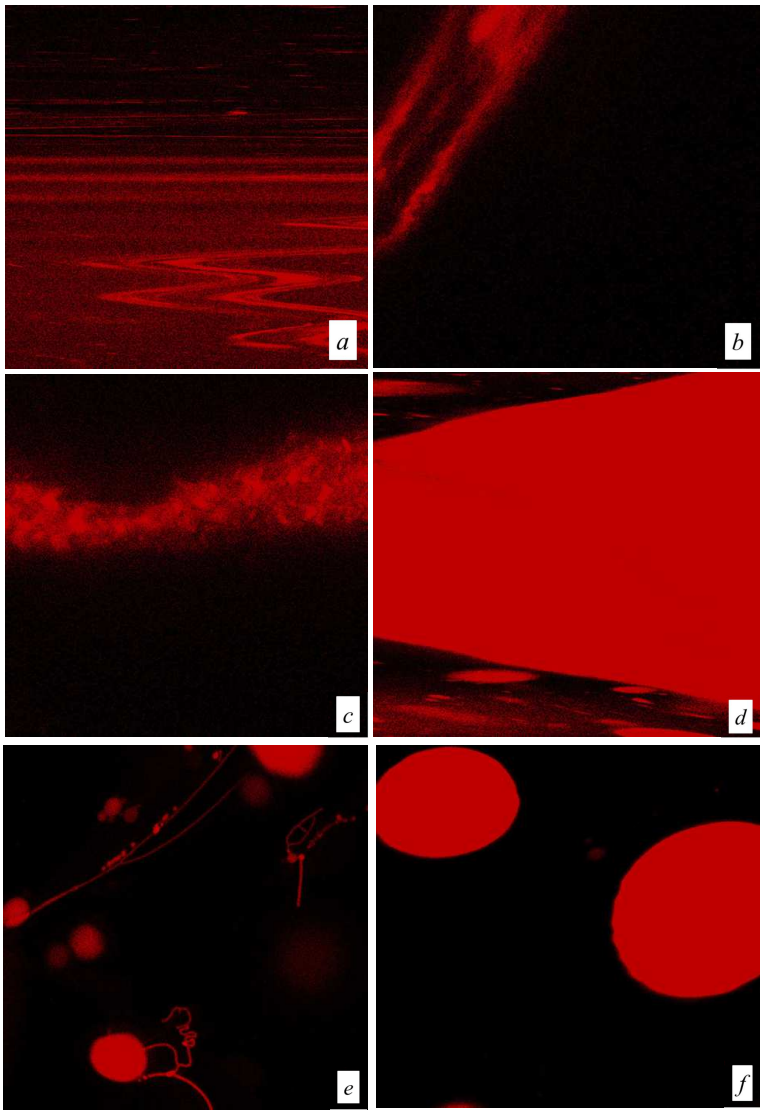

Figure 4.11: *Confocal microscope images showing interfacial instability of the W/O microemulsion immediately after coming into contact with an excess of water; the oil and water phases have red and black colour respectively (a)* $t = 3.13$ *s. (b)* $t = 8.85$ *s: the initial drop gets broken down into many tiny droplets. (c)* $t = 21$ *s. (d)* $t = 33.63$ *s: the small droplets come in contact due to the turbulence and coalesce to form very large droplets. (e)* $t = 92$ *s: the droplets break down again and get interconnected by strings of oil droplets. (f)* $t = 187$ *s: the process continues till the formation of the oil in water emulsion.*

Chapter 5

Ternary Fluid Mixture Confined Between Surfaces: Surface-Induced Phase Transition and Long-Range Oscillatory Forces [a]

Surface forces between a soft cellulose surface and a hard silica particle were measured in wet hexane with or without the addition of a surfactant. In the absence of a surfactant, the adhesion force was enhanced as a result of capillary condensation of water. The effect of the surfactant in reducing the adhesion force with increasing water content in a ternary fluid mixture of a surfactant, hexane, and water was systematically studied. Long-range oscillations of the force-distance curves are discussed in the light of various mesophase compositions in the bulk.

[a]This chapter is based on: Soumi Banerjee, Pieter Mulder, J. Mieke Kleijn, and Martien. A. Cohen Stuart, Chem. Lett., 2012, 41, 1113-1115.

5.1 Introduction

Water is often used as an additive to enhance detergency for polar soils in liquid-CO_2 dry-cleaning. However, above a certain amount, the presence of water is actually detrimental[1,2] to detergency in liquid CO_2. This is probably a result of the formation of water capillary bridges,[3] resulting in enhanced adhesion forces between the fabric and soil surfaces. In one of our recent papers on capillary condensation of water,[3] we measured the adhesion force between a hard silica particle (3 μm radius) and a soft cellulose layer (spin coated, $\sim$ 100 nm thickness) in water-saturated hexane, using colloidal probe atomic force microscopy (AFM). Hexane has a dielectric constant similar to that of liquid CO_2 and appears to be a suitable model solvent.

In this chapter, we show that surfactants can prevent water capillary bridge formation and reduce the force to almost zero in a model apolar solvent. In addition, we also show that depending on the mesophase composition, the force-distance curves contain alternating attractive and repulsive domains, probably originating from long- and short-range orientations of the surfactant mesophases.

5.2 Materials and methods

A branched polyethoxylated nonionic surfactant (polyoxyethylene (5) isooctylphenyl ether, average molecular weight 427 g mol^{-1}), average number of oxyethylene groups $n = 5$, Igepal CA520 (Sigma-Aldrich), was tested for its effectiveness in reducing enhanced adhesion in hexane/water systems. n-Hexane (purity $>$ 99 %, Sigma-Aldrich) was used as a solvent. Water used in all the experiments was de-ionized with a resistance of 18.2 MΩ cm.

5.2.1 Polarising optical microscopy: phase analysis

The surfactant-to hexane ratio was kept constant at 40/60 (w/w), and varying amounts of water were added to this mixture, i.e., 0, 20, and 25 % (w/w). Weighed amounts of surfactant and n-hexane were added to glass containers

and mixed by stirring for 10 minutes on a magnetic stirrer. Deionized water were added to these mixtures and stirred for 15 minutes. For equilibration the mixtures were kept in a shaker bath for two days at a constant temperature of 298 K. Glass containers were sealed with Teflon tape to prevent evaporation of the volatile n-hexane. A polarising optical microscope (Olympus BX60) was used to study the phase behaviour of the ternary system. The images were collected using a camera (Olympus DP70) and processed with AnalySIS image processing software. Liquid crystals are birefringent and have optical textures that can be used for their identification under cross polarizers.[4] In polarized white light lamellar phases are birefringent and display Maltese cross textures. The isotropic reverse micelles are non-birefringent and appear as black.

5.2.2 Preparation and characterization of cellulose coated silicon wafers

Interaction force between a spin-coated cellulose layer on a silicon wafer and a model particle (silica, 3 μm radius) was studied by AFM force measurements. The silicon wafers were cut into small pieces of 0.5 cm $\times$ 2 cm and were cleaned by sonicating in water and subsequently in ethanol, each for 15 minutes, and dried using N_2 gas. The wafers were cleaned using a plasma cleaner (Harrick Scientific Corp., model PDC-32G) for 10 minutes. To ensure a good anchorage between the silicon wafer and the cellulose layer, a di-block copolymer layer of polystyrene-poly (4-vinylpyridine) (PS-P4VP, 100 ppm in chloroform) was deposited on the silicon wafer. The PVP blocks (hydrophilic) are bound to the wafer and free PS blocks (hydrophobic) remain free for attachment with the cellulose. The cleaned wafers were dipped inside the polymer solution for 30 minutes and then rinsed with fresh chloroform to exclude any free polymer at the surface of the wafer, and dried with N_2. The spin-coating of the cellulose layer was done by following a standard procedure described elsewhere.[5] The thickness of the cellulose layers was measured using an ellipsometer (Multiskop, Optel GBR) with an angle of incidence of 70 $^\circ$ and a laser wavelength of 632.8 nm. The optical model used for the measurement consisted of four layers: silicon, SiO_2, block copolymer (PS-P4VP), and cel-

lulose. The thickness of the cellulose layer was found to be 97.5 ± 5.8 nm, averaged over 11 different strips, measured at three different locations and taking the literature value of 1.51 as the refractive index of cellulose.

5.2.3 Adhesion force measurements

Nanoscope IIIa Multimode atomic force microscope provided with a PicoForce module (Bruker Corporation) and using a liquid cell was used to measure interaction forces between a model cellulose surface ("fabric") and a silica particle ("soil"). A silica particle of 3 μm radius was glued to the AFM tip (NP, Bruker Corporation) using a UV curable glue (Norland 61, Norland products). After attaching the particle to the tip, the glue was cured for 10 minutes using an OmniCure LX300 LED lamp. The nominal spring constant of the cantilevers for all the experiments was 0.06 N m^{-1}, the velocity of approach and retract was 2 μm s^{-1}. More detail about the force measurements can be found elsewhere.[3] Prior to AFM force measurements between the cellulose surface and the silica particle, the liquid cell was filled with the surfactant formulation and the system was left to equilibrate for 30 min. The force curves reported here correspond to a waiting time of 200 s at the surface.

5.3 Results and discussion

A typical example of the force-distance curve is shown in Figure 5.1 (represented by black circles). A surface waiting time of 200 s was applied, since previously we found that the adhesion force increases over this time interval.[3] The surfactant formulation without any water was isotropic oil continuous (L_2) and all the other formulations were lamellar phase (L_α) dispersions in an L_2 micellar phase[6](Figure 5.2).

In the next section, we focus on the individual force-distance curves in the presence of a surfactant (Figure 5.3). Although the adhesion force is signficantly reduced in the presence of the surfactant mixtures, the force-distance profiles still show a very weak attraction of ca. 1 nN at a distance between 30 and 160 nm. We think that this small attraction could be either caused

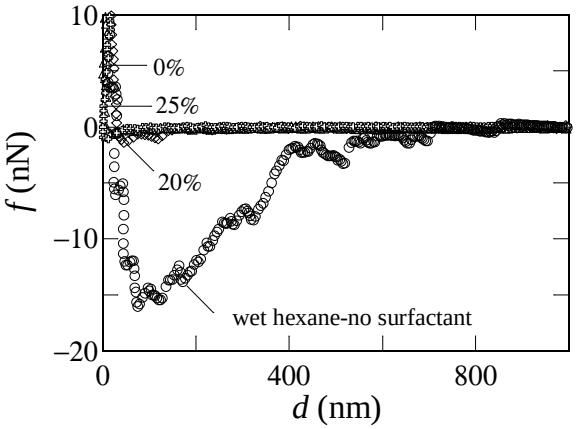

Figure 5.1: *Effect of L_2 and L_α dispersion in L_2 on the adhesion force between a cellulose surface and a silica particle (retract curves after 200 s waiting time at the surface). The curve with the filled symbols is for the case that no surfactant is present and water only to the saturation limit in hexane. For the other curves the surfactant-to-hexane ratio is 40/60 (w/w) and the amount of water was varied as indicated.*

by wetting of the surfaces by the lamellar phases, followed by condensation of water from the bulk[7] (in addition to the water already present in L_α phases), or the result of confinement induced transition of micelles (L_2) to lamellar (L_α) structures, followed by water condensation.

In either case, the process should give rise to a small attraction as a result of wetting of the surfaces and the low interfacial tension between water and hexane in the presence of the surfactant. Wetting of the surfaces by the lamellar phases is expected to be favourable as the packing of lamellar mesophases would be better at any planar surface[8] (Figure 5.4) compared to mesophases for which the packing parameter differs from unity. A transition of the condensed L_3 phase, confined between two mica surfaces, to lamella-like phases has been reported by Petrov *et al.* for AOT/brine/water and $C_{12}E_5$/hexanol/water systems.[8]

In the case of the control, water-saturated n-hexane, the adhesion force between cellulose and silica was ca. 15 nN (Figure 5.1). In the presence of the

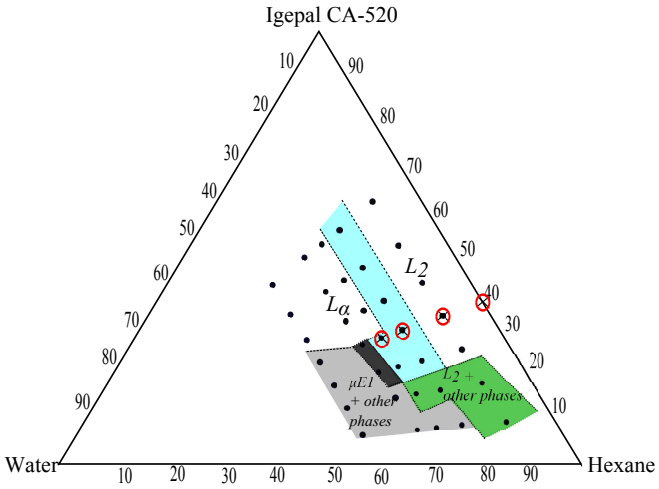

Figure 5.2: *Ternary phase diagram of Igepal CA520, hexane and water at 25 ∘C as partially explored by polarized optical microscopy. Points represent the investigated compositions. The points with red crosses are the compositions for which force-distance curves were recorded. The blue region indicates the coexistence of L_α and L_2 phases, green indicates phase separated compositions of L_2 and some phase of undetermined structure, gray indicates phase separated compositions of $\mu E1$ and some other unidentified phase, and black refers to a viscous isotropic monophasic composition of undetermined structure. The dashed lines indicate approximate phase boundaries based on optical microscopy observations alone. Reproduced from 6.*

surfactant formulations, the force of adhesion was significantly reduced (ca. 0.5 nN). Figure 5.1 shows that the amount of water can be increased to as high as 25 % (w/w) without increasing the adhesion force.

Petrov *et al* have argued that the interfacial tension between L_α and mica is lower than that between L_3 and mica, and it is the difference in surface free energies that drives the L_3 to L_α transition.[8] Apart from the small attractive force, the force-distance curves in Figure 5.3a (retract cycle) show oscillations over an extremely long range (800 nm and beyond) for all samples containing the surfactant, irrespective of the water content. Oscillations seen in the force-distance curves during the approach cycle is shown in Figure 5.3b.

The oscillations might originate from the orientation and structuring of the mesophases, not only at or near the surface, but also extending into the bulk. Similar long-range structuring up to 800 nm in the bulk has been observed for

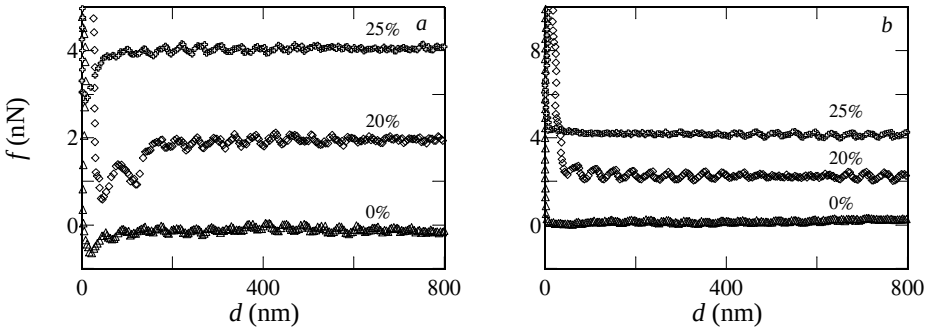

Figure 5.3: *(a)Effect of L_2 and L_α dispersion in L_2 on the adhesion force between cellulose and silica. The numbers indicate the water content of the formulations (% w/w), all with a surfactant-to-hexane ratio of 40/60 (w/w). For clarity the curves for 20% and 25% water are shifted on the vertical axis by an offset of 2 nN and 4 nN, respectively. Waiting time at the surface was 200 s. (b) Force-distance curves between a cellulose surface and silica particle recorded during the approach cycle. All the compositions show oscillations over an extremely long range, irrespective of the water content. The surfactant-to-hexane weight ratio is 40/60. The numbers indicate the water content of the formulations. The curves for 20 % and 25 % water are shifted on the vertical axis by an offset of 2 and 4 nN, respectively.*

lamellar phases of the anionic surfactant AOT[9] and for capillary condensation of nematic liquid crystals.[10] Since we also see such oscillations in the case of the formulation containing only surfactant and hexane, i.e., with no water (L_2 phase), albeit of low amplitude, we hypothesize that confinement-induced ordering in the bulk is also possible for L_2 phases. Such ordering for phases other than L_α, has been observed before for systems containing micelles of nonionic surfactants.[11]

Another interesting feature of the force curves is that the adhesion force is only visible during retraction of the sample, indicating that the process is kinetically controlled,[3] even though the interfacial tension is expected to be low. In contrast to most of the existing literature, where the amplitudes of oscillations have been found to decay exponentially,[12] we do not observe any such decay.

Moreover, with increasing water concentration, the amplitudes of oscil-

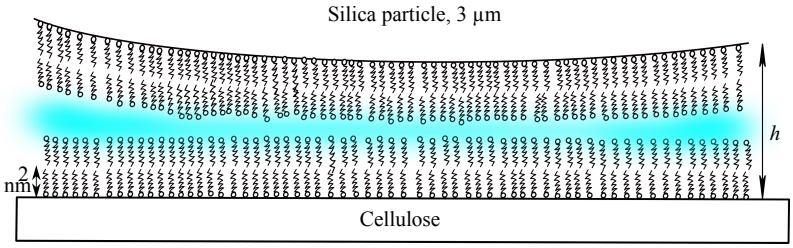

Figure 5.4: *Schematics of interactions between cellulose and silica through hexane, each having an adsorbed lamellar phase of surfactant.*

lations and wavelengths remain approximately the same. The oscillation wavelengths have been correlated to the mesophase or particle number densities or to dimensions in the bulk.[12,13] Moreover, the range of interactions was found to increase with the volume fraction,[12] whereas the wavelength decreased with a scaling exponent of -0.33. In our case, the volume fraction of the mesophases is expected to increase with increasing water concentration,[6,14] but any effect of the increasing volume fraction of the mesophases was not apparent either in the wavelength or amplitude of the force-distance curves. These differences show that there could be some other effect occurring on top of the surface-induced structuring occurring in our system.

Our hypothesis is that as a result of the high amount of surfactant in the system (30 - 40 %, w/w), during the motion of the sample to the tip, the mesophases in the bulk are also compressed and pose resistance. This phenomenon is manifested as oscillations during both the retraction (Figure 5.3a) and approach cycles (Figure 5.3b). These types of oscillations have been theorized to originate from interaction forces between surfaces containing lamellar phases in homeotropic alignment.[9] During the approach cycle, the system becomes strained and ejects solvent molecules, which are between the confined spaces formed by the two approaching surfaces, to keep the layer thickness constant. During the retraction cycle, solvent molecules are drawn toward the expanding space.[9]

We believe that the small attractive force observed during retraction (shown in more detail in Figure 5.5) could be caused by capillary condensation of a

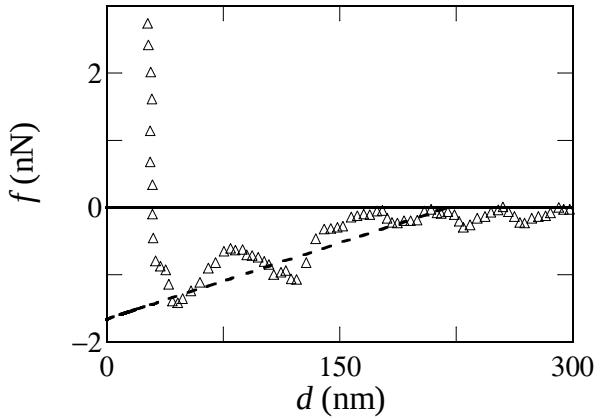

Figure 5.5: *Detail of the force-distance profile for the composition containing a dispersion of lamellar phase in L_2 corresponding to surfactant-to-oil ratio of 40/60 and 20 % water (w/w) as shown in Figures 5.2. Experimental data are shown as unfilled triangles and the dashed line line is the fit according to Equation 5.1.*

lamellar phase containing water from the L_α in L_2 dispersion. The variation in the capillary force with distance can be described by[8]

$$F = -4\pi R\gamma \cos\theta \left(1 - \frac{d}{2R_K}\right) \tag{5.1}$$

where γ is the interfacial tension, R is the radius of the sphere, θ is the three-phase contact angle, and R_K is the Kelvin radius. The plot of Equation 5.1, assuming complete wetting and with fitted parameters $\gamma = 44$ μN m^{-1} and $R_K = 110$ nm, is shown in Figure 5.5 (dashed line).

The fit describes the overall decrease in the attraction force with distance quite well, and the fitted parameters seem reasonable. For example, the interfacial tension must be low between the lamellar and the surrounding dispersion containing a mixture of reverse micelles, surfactant monomers, and L_2 phase. Hence, a value for γ of the order of 50 μN m^{-1} seems quite a reasonable value. The value of 110 nm for R_K corresponds to a saturated system (saturation of the condensing phase in the continuous medium) with the fitted value for γ.

We must point out here that at short distances such as lower than 50 nm, the contribution of van der Waals forces cannot be ignored. However, to give an estimate of the van der Waals forces between cellulose and silica coated with a layer of surfactant mesophases, one would need exact values of several Hamaker constants[15] involved in the multibody interactions between a sphere and a plate through a mixture of surfactant, hexane, and water. This situation is quite complicated and no such attempt has been made here.

An estimate of the thickness of the surfactant layer (h, Figure 5.4) adsorbed between the surfaces can be obtained from the approach curves (Figure 5.3b). The repulsive force starts from a distance of 4 to 40 nm, so on each surface, the thickness of the surfactant layer would be between 2 and 20 nm. This thickness must correspond to a multilayer adsorption of the surfactant at the silica-cellulose interface, considering the length of one surfactant molecule (1-2 nm).[6] Such a thick layer should correspond to an adsorbed multilayer structure like a lamellar phase, and cannot be the result of an adsorbed monolayer of the surfactant monomer.

5.4 Conclusion

To conclude, we have shown that the force caused by capillary condensation of water between solid surfaces in hexane can be minimized by using surfactants. Long-range oscillatory forces extending up to 800 nm in the bulk are most probably related to confinement-induced ordering of surfactant mesophases. However, some additional mechanism could also be operational in an essentially apolar system like ours, where the amplitudes of the oscillations were not observed to decay as expected, and the wavelengths of the oscillations did not seem to scale with the mesophase volume fraction in the bulk.

Bibliography

[1] S. Banerjee, S. Sutanto, J. M. Kleijn, M. J. E. van Roosmalen, G. J. Witkamp, and M. A. Cohen Stuart. Colloidal Interactions in Liquid CO_2 – a Dry-cleaning Perspective. *Adv. Colloid Interface Sci.*, 175:11–24, 2012.

[2] M. J. E. van Roosmalen, G. F. Woerlee, and G. J. Witkamp. Dry-cleaning with High-pressure Carbon Dioxide–the Influence of Process Conditions and Various Co-solvents (Alcohols) on Cleaning-results. *J. Supercrit. Fluids.*

[3] S. Banerjee, P. Mulder, J. M. Kleijn, and M. A. Cohen Stuart. Effect of Surface Roughness and Softness on Water Capillary Adhesion in Apolar Media. *J. Phys. Chem. A*, 116:6481–6488, 2012.

[4] G. J. T. Tiddy. Surfactant-water Liquid Crystal Phases. *Phys. Rep.*, 57:1–46, 1980.

[5] E. Kontturi, P. C. Thüne, and J. W. Niemantsverdriet. Cellulose Model Surfaces- Simplified Preparation by Spin Coating and Characterization by X-ray Photoelectron Spectroscopy, Infrared Spectroscopy, and Atomic Force Microscopy. *Langmuir*, 19(14):5735–5741, 2003.

[6] S. Banerjee, S. Sutanto, J. M. Kleijn, and M. A. Cohen Stuart. Towards Detergency in Liquid CO_2 A Surfactant Formulation for Particle Release in an Apolar Medium. *Colloids Surf. A Physicochem. Eng. Asp.*, 415:1–9, 2012.

[7] P. Petrov, U. Olsson, and H. Wennerström. Surface Forces in Bicontinuous Microemulsions: Water Capillary Condensation and Lamellae Formation. *Langmuir*, 13:3331–3337, 1997.

[8] P. Petrov, S. Miklavcic, U. Olsson, and H. Wennerström. A Confined Complex Liquid. Oscillatory Forces and Lamellae Formation from an L3 Phase. *Langmuir*, 11:3928–3936, 1995.

[9] D. A. Antelmi and P. Kèkicheff. Measurement of the Compressibility Modulus in a Lyotropic Lamellar Phase Stabilized by Undulation Forces. *J. Phys. Chem. B*, 101:8169–8179, 1997.

[10] K. Kočevar, A. Borštnik, I. Muševič, and S. Žumer. Capillary Condensation of a Nematic Liquid Crystal Observed by Force Spectroscopy. *Phys. Rev. Lett.*, 86:5914–5917, 2001.

[11] N. C. Christov, K. D. Danov, Y. Zeng, P. A. Kralchevsky, and R. von Klitzing. Oscillatory Structural Forces Due to Nonionic Surfactant Micelles: Data by Colloidal–Probe AFM vs Theory. *Langmuir*, 26:915–923, 2010.

[12] A. Tulpar, P. R. Van Tassel, and J. Y. Walz. Structuring of Macroions Confined between Like-Charged Surfaces. *Langmuir*, 22:2876–2883, 2006.

[13] C. E. McNamee, Y. Tsujii, H. Ohshima, and M. Matsumoto. Interaction Forces between Two Hard Surfaces in Particle-Containing Aqueous Systems. *Langmuir*, 20:1953–1962, 2004.

[14] J.-L. Lemyre, S. Lamarre, A. Beaupré, and A. M. Ritcey. A New Approach for the Characterization of Reverse Micellar Systems by Dynamic Light Scattering. *Langmuir*, 26:10524–10531, 2010.

[15] J. N. Israelachvili. *Intermolecular and surface forces.* Academic Press, London; San Diego, 1991.

Chapter 6

Interfacial Tension and Wettability in Water - CO_2 Systems: Experiments and Self-Consistent Field Modeling [a]

The chapter presents experimental and modelling results on water - CO_2 interfacial tension (IFT) together with wettability studies of water on both hydrophilic and hydrophobic surfaces immersed in CO_2. CO_2 - water interfacial tension (IFT) measurements showed that the IFT decreased with increasing pressure and the negative slopes of IFT - pressure isotherms decreased with increasing temperature. Water contact angle on a cellulose surface (hydrophilic) immersed in CO_2 increased with pressure, whereas the water contact angle on a hydrophobic surface such as hexamethyl disilazane (HMDS) coated silicon surface was almost independent of pressure. These experimental findings were augmented by modelling using the self-consistent field theory. The theory applies the lattice discretization scheme of Scheutjens and Fleer, with

[a]This chapter is published as: Soumi Banerjee,Eveline Hassenklöver, J. Mieke Kleijn, Martien A. Cohen Stuart and Frans A. M. Leermakers, J. Phys. Chem. B 2013, 117, 8524-8535.

a discretisation length close to the size of the molecules. In line with this we have implemented a primitive molecular model, with just small variations in the molar volume. The theory makes use of the Bragg-Williams approximation and has binary Flory-Huggins interaction parameters (FH) between CO_2, water and free volume. Using this model we generated the complete IFT - pressure isotherms at various temperatures, which coincided well with the trends reported in literature, that is, the water - CO_2 interfacial tension decreased with increasing pressure for pressures $\leq$ 100 bar and became independent of pressure $>$ 100 bar. The transition point occurred at higher pressures with increasing temperature. At three-phase coexistence (water - CO_2 - free volume) and at the water - vapour interface (water - free volume) we always found the CO_2-phase in between the water-rich and free volume-rich phases. This means that for the conditions studied, the water - vapour interface is always wet by CO_2 and there are no signs of a nearby wetting transition. Calculation of the water contact angle on a solid surface was based on the computed adsorption isotherms of water from a vapour or from a pressurised CO_2-rich phase and analysis of surface pressures at water - vapour or water - CO_2 coexistence. The results matched reasonably well with the experimental contact angle data. Besides, we also computed the volume fraction profiles of the CO_2, H_2O and the V phase, from which the preferential adsorption of CO_2 near the hydrophilic surface was deduced.

6.1 Introduction

Interfacial tension and wettability of water - CO_2 (gaseous, liquid or supercritical) systems are important for many industrial processes, such as Geological storage,[1–3] dry-cleaning,[4] oil recovery[5] and fluid extractions.[6] Hence it is necessary to understand the molecular origin of CO_2 - water interfacial tension (IFT), influence of pressure and temperature on IFT and contact angles. Subject to the temperature and pressure range, several interfaces such as gaseous CO_2 - liquid water, liquid CO_2 - liquid water and supercritical CO_2 - liquid water come into play at the various stages of the above mentioned processes.

Experimental CO_2 - water IFT data, measured by various research groups[1,7–13] and including the present study, show a decrease of IFT with pressure. Contact angle measurements under similar conditions are rare,[14] probably because of the difficulty involved in the measurement, even though wetting plays a significant role in all those above mentioned processes. This brings us to the development of a molecular model for water - CO_2 system to gain molecular insight into the physics of the processes at one hand and on the other hand deepen the insight about the interfacial properties of CO_2/water systems covering the relevant pressure range.

To date there have been only a few attempts[11,15–19] to predict the IFT and thermodynamic properties of the CO_2 - water interface and these are mainly based on (n, P, T) and (n, V, T) molecular dynamics and Monte Carlo simulations, in which the IFT is computed from integrating the difference between the normal and tangential pressure components across the interface. These simulations are still reasonably inexpensive (involving reasonable CPU time) to compute a particular interfacial tension corresponding to a specific pressure and temperature condition. However, prediction of IFT subject to a large pressure range imposes long CPU time for a sufficiently large system size (for a reasonable accuracy of the calculated IFT, a good system size would consist of $\geq 10^6$ molecules). One issue is that the interface will fluctuate in shape and in simulations it is expensive to allow for this. The interfacial tension should incorporate these fluctuations. This feature of MD simulation makes it even more unattractive to study systems consisting of more than one interface such as the present system. This problem becomes more severe for multicomponent systems, that is, systems that feature amphiphiles that may self-assemble in CO_2. In this study, we develop an alternative type of modelling of such systems.

Following the work of van der Waals and Cahn and Hilliard,[20] an equation of state based model in combination with density gradient theory has been employed recently to model CO_2 - water[2] and alkane systems.[21] In this approach, the equation of state was employed to calculate the Helmholtz energy of water - CO_2 mixtures and using a so-called influence parameters coupled

with the density gradients of the two components led to a reasonable fit of the IFT data.[2] However, it should be noted that since the influence parameters were used as fitting parameters to match the experimental and the theoretical IFT - P isotherms, this method potentially hides problems that should be traced to the mean field approximation or the approximate models used. The density gradient theory may be extended to account for more complicated situations, but then this approach becomes definitely more involved.

In this chapter we focus on an even more primitive mean field model with a regular solution based equation of state. More specifically we follow the self-consistent field (SCF) theory making use of the lattice discretization scheme of Scheutjens and Fleer (SF).[22,23] In the model the molecules occupy an integer number of lattice sites. The segments are freely jointed, which allows for an efficient way of computing entropic contributions resulting from the many possible configurations of the molecules on the lattice. We chose this approach because it had been applied before to describe self-assembly of amphiphiles, so it naturally fits in with our ambition to model, in a follow-up study, amphiphiles in water - CO_2 systems. Here we focus on systems that do not yet feature such amphiphiles. We haste to mention that our mean field approach is subject to the same criticism as for the gradient theory mentioned above. That is why we have not pushed the fitting to its limits.

Here we will show that the SF-SCF theory can be applied to systems that have small molecules such as CO_2 and water. Again, the lattice approximation prevents an accurate account for the molecular details, which unavoidably leads to a qualitative rather than quantitative description. Interfacial tensions (captured in the grand potential per unit area of an interface) can be computed in SCF by knowing the volume fractions, the complementary segment potential profiles and all binary (Flory-Huggins) interaction parameters.[24] The water contact angle on a solid substrate can be extracted from the analysis of the computed adsorption isotherms of water either from a CO_2 - vapour phase, or from a pressurized CO_2 fluid, as explained in more detail below. One of the goals of this paper is to find a set of interaction parameters, which for the CO_2 - water - free volume system reproduces approximately the phase behaviour

and the interfacial tensions. The same model is then carried further to study the water contact angle in liquid CO_2 (and in future will be used to study surfactant self-assembly in these systems). Comparison with experimental data will be informative about the physico-chemical behaviour of the mimicked surfaces.

The chapter is organized in the following way: we first present the experimental data of water - CO_2 IFT and water contact angles on hydrophilic and hydrophobic surfaces with respect to CO_2 activity at pressures and temperatures relevant for the dry-cleaning process. This is followed by a description of the SF-SCF theory, focussing on the (primitive) molecular model that is used. The experimental and modeling results are presented together in such a way that we consider systems with increasing complexity. Correspondence to the experimental data has directed us to particular choices for the various interaction parameters which we mostly motivate *a postiori*. As usual, at the end of the paper we will summarise our conclusions.

6.2 Materials and methods

6.2.1 Preparation of cellulose and HMDS-modified silica surfaces

Silicon wafers (WaferNet) with a 3 nm surface oxide layer were cut into small pieces of 0.5 cm $\times$ 2 cm using a diamond craft knife. The wafers were sonicated in water and subsequently in ethanol, each for 15 minutes. After this the wafers were cleaned using a plasma cleaner for 10 minutes and the cellulose layers were spin-coated on the wafers and hydrolysed.[25,26] After coating, the layers were oven dried at 373 K for 1 hour and their thickness was measured using an ellipsometer. The hydrophobic silica surfaces were prepared by exposing silica surfaces to hexamethyldisilazane (HMDS) vapour in a desiccator for at least 24 hours. Before closing the desiccator, nitrogen was purged to prevent HMDS to react with the moisture present in the air. The modified strips were washed with toluene, ethanol and acetone. The strips were finally dried using nitrogen flow. The IRRAS spectrum of the modified and un-modified surfaces are given in Figure 6.14 in the Appendix. The modified HMDS surface clearly

contains methyl rich domains compared to the un-modified surface.

6.2.2 Measurement of Interfacial properties in liquid CO_2

Water (deionized) - liquid CO_2 (Westfalen Gas, purity 99.5 %) interfacial tension and contact angle measurements were done using a high pressure view cell having two transparent windows. A schematic of the instrument can be found in reference.[13] The interfacial tension and contact angles were measured using the pendant drop and sessile drop methods respectively, where in the former case a water drop was generated at the end of a steel capillary and in the latter a water drop was placed on a solid surface of interest. In both cases a CCD camera recorded the image of these drops and the analyses of drop shapes were done using the DSA software (Kruss, GmbH). A description of the pendant drop technique can be found in references.[1,10]

6.3 Theory

As mentioned in the introduction we used a mean field approach implementing the lattice discretization scheme as proposed by Scheutjens and Fleer.[22,23] More precisely we implemented a so-called lattice gas model, similar to regular solution theory.[27] On this lattice molecules are placed, which are composed of (an integer number of) monomeric units called segments. A segment exactly fits on one lattice site. Hence, both are characterised by a linear length a. Degrees of freedom at length scale smaller than a are not taken into consideration. In the lattice we recognise layers, numbered $z = 1 \cdots M$ and each layer has L sites. Formally $L \to \infty$, and fluctuations in composition within a lattice layer are ignored (mean-field approximation). This allows us to normalize, e.g. the free energy, by L and thus to focus on the free energy per unit area (that is per a^2) as the leading thermodynamic quantity. On the lattice there are two molecular species: water ($i = 1$) and CO_2 ($i = 2$) and there are unoccupied lattice sites. Such a model may be referred to as a two-component compressible model. It features chemical potentials μ_i for the molecular components and a pressure P as the intensive parameters (on top of the entropy). It is possible

to map this model onto a three-component incompressible model, wherein the 'free volume' sites are interpreted as being composed of a new (monomeric) species. In such a three component model the system is incompressible: all lattice sites are occupied by either water ($i = 1$), CO_2 ($i = 2$) or free volume ($j = 3$). In this system we have three chemical potentials $\tilde{\mu}_j$, and the system is incompressible as the volume is not a free variable. The calculations and the presentation of the SF-SCF theory typically is done in the context of the incompressible model, but below we will report the results in terms of the compressible model. The mapping rules are:

$$\mu_1 \leftrightarrow \tilde{\mu_1} - N_1\tilde{\mu_3} \tag{6.1}$$

$$\mu_2 \leftrightarrow \tilde{\mu_2} - N_2\tilde{\mu_3} \tag{6.2}$$

$$Pa^3 \leftrightarrow -\tilde{\mu_3} \tag{6.3}$$

where N_1 is the number of lattice sites occupied by a single molecule water, and N_2 represents the molar volume (in lattice sites) for CO_2, as will be elaborated below.

Volume fractions, $\varphi_i(z)$, are the natural concentration units of species i in layer z. These are related to the actual number concentrations, c

$$\varphi_i(z) = c_i(z)a^3 = \frac{n_i(z)}{L} \tag{6.4}$$

where $n_i(z)$ represents the number of monomers of type i in layer z. Typically we use volume fractions and reserve the number of molecules of molecule i to refer to the system, that is, $n_i \equiv \sum_z \varphi_i(z)/N_i$ from which it is understood that the number of molecules is normalised by L.

For bulk-phase behaviour we have implemented mirror-like boundary conditions. This means that we impose

$$\varphi_i(0) = \varphi_i(1) \tag{6.5}$$

$$\varphi_i(M+1) = \varphi_i(M) \tag{6.6}$$

or in other words, we assume that there are no gradients in density across the boundaries of the system.

In some of our calculations we are interested in the interaction of the molecular species with a substrate. In this case we replace the boundary condition at the lower bound by setting the volume fractions of all molecular species equal to zero at layer $z = 0$. The substrate on the other hand will have the volume fraction unity in layer $z = 0$.

6.4 Molecular detail

The molecular description of the three types of molecules is explained in Figure 6.1. Water is represented as a cluster of 5 segments,[28] W_5, with $N_1 = 5$ to take into account (admittedly very approximate) H-bonded interactions. The architecture is such that one central W segment is (permanently) surrounded by four neighbours. CO_2 is represented as a dimer, D_2, with $N_2 = 2$ and the free volume as a single entity, V_1, with $N_3 = 1$.

In our adsorption study, we impose the volume fraction of the solid phase S as follows:

$$\varphi_S(z) = \begin{cases} 1 & z = 0 \\ 0 & z > 0 \end{cases} \tag{6.7}$$

At this stage it is good to mention that this molecular representation inherently brings in asymmetry in the system as the overall interactions are determined by the individual and cross-interactions among three different types of species, differing in segment numbers N_i as well as in architecture. The conformational degrees of freedom are evaluated by the freely jointed chain (FJC) model[29–31] as will be elaborated below, that is, where the SCF machinery is outlined.

6.5 Interaction parameters

Interactions between CO_2, water and free volume give rise to thermodynamic properties of the system. These interactions are, for incompressible systems,

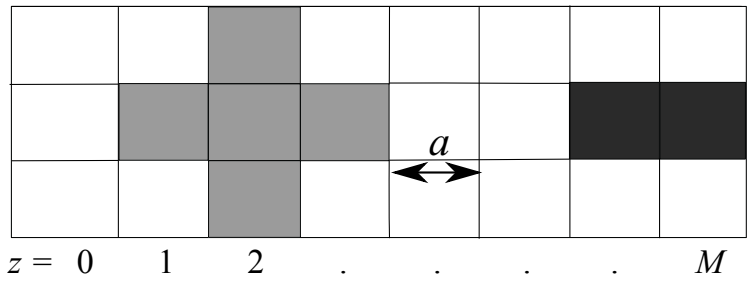

Figure 6.1: *Two-dimensional representation of a lattice filled with three species: (i = 1) water, (filled grey □) represented as clustered pentamers, (i = 2) CO_2 as dimer (filled black □) and (i = 3), free volume as a monomeric unit (unfilled □). The lattice parameter a is indicated.*

conveniently specified by Flory-Huggins (FH) interaction parameters specified on the segment level. More specifically for segments A and B by

$$\chi_{AB} = \chi_{BA} = \frac{Z}{2k_BT}\left[2U_{AB} - U_{AA} - U_{BB}\right] \tag{6.8}$$

where Z is the lattice coordination number ($Z = 6$ for a cubic lattice), and k_BT the thermal energy. It is easily seen that the χ parameter is zero for like contacts, that is $\chi_{AA} = 0$. For J species in the incompressible system, we need $J \times (J-1)/2$ different χ values to fully specify the interaction set. Note that there are J reference values in this case.

In a compressible lattice gas model it is, arguably, more intuitive to choose the interactions U_{AB} as the natural parameters and take the interactions with the free volume component to be zero. Then there are $J-1$ molecular components and thus it suffices again to specify $((J-1)^2 + (J-1))/2 = J(J-1)$ different parameters. Indeed, we can 'translate' the set of χ parameters (one-to-one) into the set which takes the interactions with free volume to be zero. As the SCF theory is most easily elaborated in the incompressible system, we choose to report the corresponding FH-parameters.

In Table 6.1 we have summarized the parameters assigned to each unlike (and like) interaction between the segments. We would like to stress that with our model we focus more on understanding qualitative trends and mo-

Table 6.1: *Interaction parameters χ between various pairs at 313 K. Here D is the monomer in CO_2, W is the monomer in water, V is the empty site, S_c is the cellulose and S_m is the HMDS-modified silica.*

χ	D	W	V	S_c	S_m
D	0	1.5	1.5	-3.6	-1.91
W	1.5	0	3.5	-4.5	-0.91
V	1.5	3.5	0	0	0
S_c	-3.6	-4.5	0	0	-
S_m	-1.91	-0.91	0	-	0

lecular mechanisms rather than exactly matching the experimental data. The rationale behind the chosen values will be briefly elaborated.

From the Flory-Huggins theory one can find a critical χ^{cr} above which in a system with two molecular components A and B, having a molar volume $N_A a^3$ and $N_B a^3$, a solubility gap exists:

$$\chi_{AB}^{\mathrm{cr}} = \frac{1}{2}\left(\frac{1}{\sqrt{N_A}} + \frac{1}{\sqrt{N_B}}\right)^2 \tag{6.9}$$

Focussing on the parameters for D, W and V, we have to choose χ_{DW}, χ_{DV} and χ_{VW} above their critical values, being 0.67, 1.46 and 1.05, respectively. Even then, the question remains how far the chosen χ should be above the χ^{cr}. We can make educated guesses. For example we know that water - free volume is very far from critical and therefore we used a value of $\chi_{VW} = 3.5$. This value leads to a value of the water - vapour interfacial tension which is close to the experimental one. Similar considerations apply for the other two binary parameters. The CO_2 - vapour is much closer, indeed relatively close to critical and we settled for $\chi_{DV} = 1.5$ accordingly. The value of χ_{DW} was selected to reproduce the value of the interfacial tension between liquid CO_2 and water. Interestingly this gave a value of 1.5. Inspection shows that this value, even though numerically the same as for CO_2 and V, it is reasonably far from critical.

So far we have discussed the selection of χ parameters for the CO_2 - water system. To describe the wetting phenomena on hydrophilic and hydrophobic surfaces we need additional FH parameters. Our choices are also listed in Table 6.1. Basically because the surface component has a fixed and specified volume fraction profile, one can select one species for which the surface interactions can be set to zero. Other interactions are then counted with respect to this reference. For obvious reasons we have chosen to assign the surface - free volume interaction parameter to zero, leaving two χ parameters, i.e. surface - CO_2 and surface - water, to be specified.

Although data fitting was not intended, we succeeded in reproducing the correct trends of the CO_2 - water interfacial tension and water contact angles as a function of pressure. We also attempted to understand the effect of temperature on interfacial tension or contact angle. From comparison with experimentally found trends, it was decided that parameters in Table 6.1 correspond to $T = 313$ K. Unless mentioned otherwise, we use Eqn 6.8 to compute the interactions parameters for other temperatures, implying that we have interpreted the FH parameters as purely enthalpic in nature. This means that with increasing temperature the interactions become less repulsive.

6.6 SCF equations

Formally, the SCF theory can be introduced by starting with an appropriate free energy expression that can be written in terms of the volume fraction profiles $\varphi_i(z)$ and the complementary segment potential profiles $u_i(z)$. The segment potential may be interpreted as the work needed (in units of k_BT) to bring a segment form the bulk (where the potential is zero) to the coordinate z. Optimising the free energy both with respect to the volume fractions and the segment potentials leads to the mutually dependence of these two profiles: the volume fractions can be computed from the potentials and vice versa. Clearly, these two profiles should be consistent with each other and the self-consistent field solution is found numerically by an iterative procedure. Here we do not go into these details. Instead we state the resulting equations.

The segment potentials u_A, with $A = D, W, V$ are given by

$$u_A(z) = \alpha(z) + \sum_B \chi_{AB} \left(\langle \varphi_B(z) \rangle - \varphi_B^b \right) \tag{6.10}$$

Here the summation over the segments B include the surface component (if present). The volume fraction in the bulk is denoted by the super index b. The angular brackets implement a three-layer average:

$$\langle \Xi(z) \rangle = (\Xi(z-1) + \Xi(z) + \Xi(z+1))/3 \tag{6.11}$$

for some spatially dependent quantity $\Xi(z)$.

Finally, the contribution $\alpha(z)$ originates from the incompressibility constraint

$$\sum_i \varphi_i(z) = 1 \tag{6.12}$$

Physically, the value of $\alpha(z)$ specifies how much work it takes to generate space for the segment to be located at coordinate z (again with respect to that in the bulk). In practise, α was made more negative or less positive in an iterative way when the sum of the volume fractions was less than unity and the opposite when the volume fractions exceed unity.

The segment potentials are used in Boltzmann-like equations: defining the weighting factor $G_A(z) = \exp(-u_A(z))$, again for $A = D, W, V$. Physically these weights specify the distribution of segments A if these are not connected to other segments. Therefore, we name these weights 'free segment distribution functions'. Accordingly, the distribution of free volume is found from

$$\varphi_V(z) = \varphi_V^b G_V(z) \tag{6.13}$$

When the φ_V^b is not known, it should be computed from the incompressibility relation in the bulk $\varphi_V^b = 1 - \varphi_W^b - \varphi_D^b$.

The CO_2 molecules are composed of two monomers that occupy neighbouring lattice sites on the lattice. This correlation should be accounted for in the evaluation of the volume fraction profile. The target is to compute the

end-point distribution function $G_D(z,2|1)$ as the statistical weight of finding segment $s=2$ in coordinate z provided that it is connected to segment $s=1$. We can compute this quantity by realising that the first segment can be either in layer $z-1$, z or $z+1$. Averaging over these "starting" positions we find

$$G_D(z,2|1) = G_D(z)\langle G_D(z,1|1)\rangle \tag{6.14}$$

$$G_D(z,1|1) = G_D(z) \tag{6.15}$$

where $G_D(z,1|1)$ is the statistical weight of a "walk" starting with segment $s=1$ and ending with segment $s=1$. As no steps are taken, we can substitute the free segment distribution function $G_D(z,1|1) = G_D(z)$ as specified. We further realise that the volume fraction distribution of segment $s=2$ is proportional to $G_D(z,2|1)$

$$\varphi_D(z,2) = C_D G_D(z,2|1) \tag{6.16}$$

The total volume fraction of D should result from the sum of the distribution of the first and second segment. Realising that for symmetry reasons the two segments must have the same profile we find

$$\varphi_D(z) = 2\varphi_D(z,2) = \varphi_D^b \varphi_D(z,2) \tag{6.17}$$

where we have used $C_A = \varphi_A^b/N_A$ which follows from the fact that the potentials are normalised to zero in the bulk. When the bulk volume fraction φ_D^b is not known, we should know the $\theta_D = \sum_z \varphi_D(z)$ as an input quantity. We can find a value for C_D so that the summation over the profile gives θ_D.

The water molecules are seen as a star-like cluster of five W segments: one central segments and four neighbours. Let us denote one of the exterior segments as $s=1$, the central segment as $s=2$ and one other exterior segment as $s=3$. Now we have three end-point distribution functions which depend

recursively on each other

$$G_W(z,3|1) = G_W(z)\langle G_W(z,2|1)^3\rangle / G_W(z)^2 \tag{6.18}$$

$$G_W(z,2|1) = G_W(z)\langle G_W(z,1|1)\rangle \tag{6.19}$$

$$G_W(z,1|1) = G_W(z) \tag{6.20}$$

The top equation implements the situation that one has to combine three arms in the center in order to proceed to segment number 3. The division by $G_W(z)^2$ corrects for double counting of the statistical weight for the middle segment.

It is easily checked that for the star-like architecture the volume fraction of W follow from

$$\varphi_W(z) = C_W \left(4G_W(z,3|1) + \frac{G_W(z,2|1)^4}{G_W(z)^3} \right) \tag{6.21}$$

where the first term within the brackets gives the combined contribution of the four exterior segments and the second term is the one for the central segment. Again $C_W = \varphi_W^b/5$, and when φ_W^b is unknown, we do know the θ_W value and find the value C_W such that the profiles obeys to this.

6.7 Thermodynamic output parameters

6.7.1 Interfacial tension

The primary results of the SCF equations are the volume fraction profiles. Then there are also the segment potentials. Using these we can accurately evaluate the Helmholtz energy F of the system. Here our interest is in the chemical potentials $\tilde{\mu}_i$ of the molecules and the grand potential $\Omega = F - \sum_i \tilde{\mu}_i n_i$ of the system, which uniquely follow from the Helmholtz energy. Note that all these quantities are normalised by L, the number of lattice sites in each layer.

The chemical potentials can conveniently be expressed using the volume fractions in the bulk $\Phi_i \equiv \varphi_i^b$ and the relation is known from the Flory-Huggins

theory:

$$\frac{\tilde{\mu}_i - \tilde{\mu}_i^*}{k_B T} = \ln \Phi_i + 1 - N_i \sum_j \frac{\Phi_j}{N_j} - \frac{N_i}{2} \sum_A \sum_B (\Phi_A - \Phi_{Ai}^*) \chi_{AB} (\Phi_B - \Phi_B i^*) \tag{6.22}$$

In this equation Φ_{Ai}^* is the fraction of segments A of molecule i. As we only have segments of one type in each molecule, this value is either unity (when molecule i is composed of segments of type A) or zero (otherwise). Note that the chemical potentials are defined with respect to a reference phase, for which the pure phases (phases that are composed of only molecule i) are used. It is customary to make the chemical potentials dimensionless, and thus we implement $\tilde{\mu}_i \equiv \frac{\tilde{\mu}_i - \tilde{\mu}_i^*}{k_B T}$. We will do the same, that is normalise by $k_B T$, with the grand potential.

The grand potential can be written as $\Omega \equiv \frac{\Omega}{k_B T} = \sum_z \omega(z)$, with $\omega(z)$ the dimensionless grand potential density (ω is equivalent with the difference between (dimensionless) tangential and normal pressures):

$$\omega(z) = -\sum_i \frac{\varphi_i(z) - \Phi_i}{N_i} - \alpha(z) - \frac{1}{2} \sum_A{}' \sum_B{}' \chi_{AB} (\varphi_A(z) \langle \varphi_B(z) \rangle - \Phi_A \Phi_B) \tag{6.23}$$

where the prime indicates that in the sum only the mobile species CO_2, water and V are included.

To obtain the interfacial tension γ from the dimensionless Ω, we use,

$$\gamma = \frac{\Omega k_B T}{a^2} \tag{6.24}$$

and the pressure is related, as mentioned already, from the dimensionless chemical potential of the free volume component

$$P = -\frac{\tilde{\mu}_V k_B T}{a^3} \tag{6.25}$$

In order to calculate the IFT - pressure isotherm for a wide pressure range covering both the gas and liquid, it is necessary to treat the two phases of CO_2

(gas and liquid) separately. For the lower pressure region of the isotherm we started with a water - free volume interface and we varied the amount of CO_2 in the system, thereby changing the chemical potential of free volume, and hence the pressure. To generate the liquid branch of the isotherm, $P > P_{\text{sat}}$, we considered the water - CO_2 interface and varied the amount of free volume in the system (and hence the pressure). The effect of temperature was captured by varying the χ parameter of the system, as explained before (using Eqn 6.8).

6.7.2 Bulk phase behaviour

In the case of three components, water, CO_2 and free volume (V), we can have either one homogeneous phase, three two-phase regions, or one three-phase coexistence region. For a given set of interaction parameters one can easily map out the phase diagram using the Flory-Huggins (dimensionless) Helmholtz energy density:

$$f(\{\Phi\}) = \sum_i \frac{\Phi_i \ln \Phi_i}{N_i} + \frac{1}{2} \sum_A \sum_B \Phi_A \chi_{AB} \Phi_B \tag{6.26}$$

For phase coexistence, we require that the chemical potentials should not depend on the spatial coordinate. This means that for a given component the chemical potential is the same in each phase. This criterion is typically used to find the phase diagram. The compositions of coexisting phases fully specify all the so-called binodal values, that is, the (homogeneous) concentrations (we will use the notation $\varphi_i^{\#}$ for this) of all components in all coexisting phases. Our interest concerns interfacial tensions of the three interfaces, which correspond to the three possible pairs of coexisting phases. These quantities do not follow from the Flory-Huggins theory, so that we have to solve the SCF equations to find them. Interestingly, we obtain as a bonus the bulk binodals, both for any of the two-phase coexistences as well as for the three-phase coexistence situation.

6.7.3 Contact angle

When a macroscopic drop of one phase (liquid), surrounded by a bulk phase (gas) is placed at a substrate (solid), we may consider two situations. Either the liquid spreads along the surface and we have just two interfaces, namely solid-liquid and liquid-gas, or the liquid remains as a drop and we have three interfaces, a solid-gas, solid-liquid and liquid-gas. To maintain mechanical equilibrium there is a finite contact angle of the drop, the value of which is found from the Young equation. In the SCF theory we may study wetting phenomena, and these are most easily studied using adsorption isotherms.

SF-SCF theory of adsorption

In this case we consider systems that have a substrate placed at $z = 0$ as explained above. Here we focus on the adsorption of water onto the substrate. The bulk phase is either a free volume rich phase or a CO_2-rich phase. For a given amount of water in the system we first generate the volume fraction profiles ($\varphi(z)$) and from this compute the excess amount of molecules (Θ_i^{exc}):

$$\Theta_i^{\text{exc}} = \sum_{z=1}^{M} \left(\varphi_i(z) - \varphi_i^b \right) \tag{6.27}$$

The excess number of molecules, n_i^{exc}, can then be computed by,

$$n_i^{\text{exc}} = \frac{\Theta_i^{\text{exc}}}{N_i} \tag{6.28}$$

Water adsorption isotherms are defined as adsorbed amounts Θ_i^{exc} as a function of the bulk volume fraction of water φ_W^b. Of course, the bulk volume fraction (bulk concentration) is limited by the bulk binodal. For water, we denote the bulk binodal by $\varphi_W^{\#}$, where in the context it should be clear whether this is the saturation value in the free-volume rich phase or in the CO_2 rich phase.

To generate the adsorption isotherms of CO_2 at the interface between the water and free volume rich phase, a similar approach was applied. In this

context we are interested in the quantity $\Theta^{\text{exc}}_{\text{CO}_2}$. From $\Theta^{\text{exc}}_{\text{CO}_2}$ it is possible to calculate the surface excess concentration of CO_2 by imagining a mathematical plane of zero thickness, known as the Gibbs plane (z^{Gibbs}) having a zero solvent (in the present case W) excess concentration.

$$z^{\text{Gibbs}} = \frac{\Theta^{\text{exc}}_{W}}{\varphi_W(1) - \varphi_W(M)} \tag{6.29}$$

The excess concentration of any solute (i) can then be found by,

$$\Gamma_i = \frac{\Theta^{\text{exc}}_{i} - z^{\text{Gibbs}}\left(\varphi_i(1) - \varphi_i(M)\right)}{N_i} \tag{6.30}$$

6.7.4 Thermodynamics: Wetting and adsorption

It should be understood that for each value of the excess adsorbed amount we also have an accurate value for the grand potential in the system. This applies to all points of the adsorption isotherm of water on a solid substrate. Informative for wetting studies is the dependence of Ω on φ^b_W, or even better $\tilde{\mu}_W$. Let us first consider $\Omega(\varphi^{\#}_W)$, that is the grand potential for the situation that the water component is at bulk coexistence. It turns out that when there is just one value for $\Omega(\varphi^{\#}_W)$, the surface is wet by water (a macroscopic layer of the adsorbing compound is present on the surface) and when there are two distinct values, we are dealing with partial wetting. We will refer to the value of $\Omega(\varphi^{\#}_W)$ for the case that Θ^{exc}_W is small with Ω(thin) and for the value of $\Omega(\varphi^{\#}_W)$ in the limit of $\Theta^{\text{exc}}_W \to \infty$ by Ω(thick).

Following Young's equation one can write for a solid (S) - water (L) - vapour (V) system,

$$\cos\theta = \frac{\gamma^{SV} - \gamma^{SL}}{\gamma^{LV}} \tag{6.31}$$

where, θ is the contact angle and γ^{SV} is the interfacial tension of the solid with a thinly adsorbed water film formed at the water saturated vapour pressure, and (γ^{SL} is the interfacial tension for the solid-water interface under the same conditions. Finally, γ^{LV} is the interfacial tension between water and vapour (which contains CO_2). Realising that Ω(thin) $= \gamma^{SV}$ and Ω(thick) $= \gamma^{SL} +$

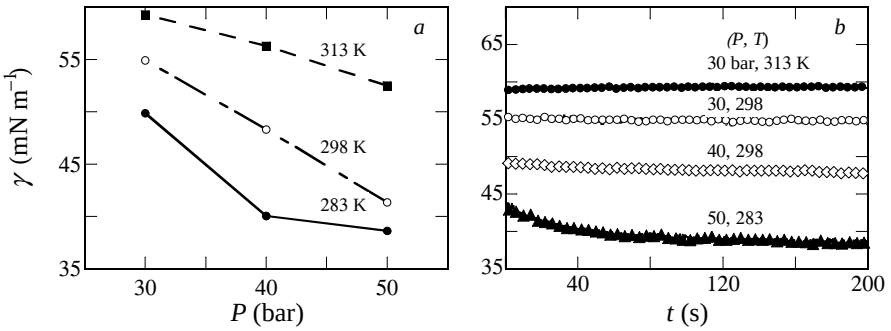

Figure 6.2: *(a) Experimental Water - CO_2 interfacial tension as a function of pressure at three different temperatures. The lines are guides to the eyes. (b) time dependence of interfacial tension at different combinations of pressure and temperature, showing equilibration is reached within 200 s.*

γ^{LV}, we can write

$$\cos\theta = \frac{\Omega(\text{thin}) - \Omega(\text{thick})}{\gamma^{LV}} + 1 \tag{6.32}$$

The difference between the grand potential values of the thin and thick layer divided by the dimensionless interfacial tension of the water - CO_2 yields ($\cos\theta$ - 1). From this it is trivial to extract a value for the contact angle. In this particular case the solid surface corresponds to either cellulose (hydrophilic) or HMDS (hydrophobic) modified silica surface.

6.8 Results and discussion

6.8.1 Interfacial tension

Experimental interfacial tension (γ) as a function of pressure (P) for water - free volume (V) systems in which CO_2 molecules are dispersed at 283 K, 298 K and 313 K are shown in Figure 6.2a. The interfacial tension (γ) decreases with increasing P for all temperatures. The slope of the γ versus P isotherms increases with decreasing temperature. The temperature and pressure ranges

are selected as per the requirements of dry-cleaning and to the best of our knowledge data in the literature pertaining to these conditions are either not available or sparse. Here we corrected our data by taking into account the pure CO_2 and CO_2 saturated water densities. The densities of the CO_2 rich and CO_2 saturated water rich phases at the experimental pressures and temperatures were calculated using the equation of state of Span and Wagner[32] and equations (3) and (4) in reference.[33] The use of pure density instead of the water saturated one for the CO_2 rich phase is justified because of the extremely low solubility of water in CO_2.[33,34] On the contrary the solubility of CO_2 in the water phase is significant, $\sim$ 3 - 5.5 % at our measurement conditions,[35] the density of the water phase is higher in the presence of CO_2. Moreover, the increase in water density was found to be higher in contact with gaseous CO_2 as opposed to the liquid CO_2.[33] There are many research papers dedicated to the effect of density corrections (pure phase densities *versus* saturated phase densities) on the IFT values of water - CO_2 mixtures. Recently it has been concluded that the use of pure phase densities leads to $>$ 10 % error in the measured IFT values above 200 bar and below 343 K.[3] Although we measured water - CO_2 IFT at pressures well below 200 bar we still corrected our data with the saturated phase densities of the water rich phase. The time required for the water drop to saturate with CO_2 is a subject of debate in literature.[3] The effect of equilibration time on the water - CO_2 IFT values has been addressed by Bikkina *et al.*,[7] who had equilibrated a water drop in CO_2 for $\sim$ 24 hours. However, the IFT reached its equilibrium value within 200 s,[7,9] similar to our findings as shown in Figure 6.2b. Coming back to the results of Figure 6.2a, we will, in this section, delineate the molecular phenomena responsible for the decrease with γ in P. In order to do that we first look at the volume fraction profiles of W, V or/ and D over the interfaces in the WV, DV and WVD systems. These are shown in Figure 6.3a, 6.3b and 6.3c respectively. We see from Figure 6.3a and 6.3b that the $W-V$ interface is sharper as opposed to the $D-V$ interface, consistent with $\gamma_{H_2O-V} \gg \gamma_{CO_2-V}$. The volume fraction profiles of the phases at three phase co-existence is shown in Figure 6.3c. In this figure we see three phases and two interfaces. On the left there

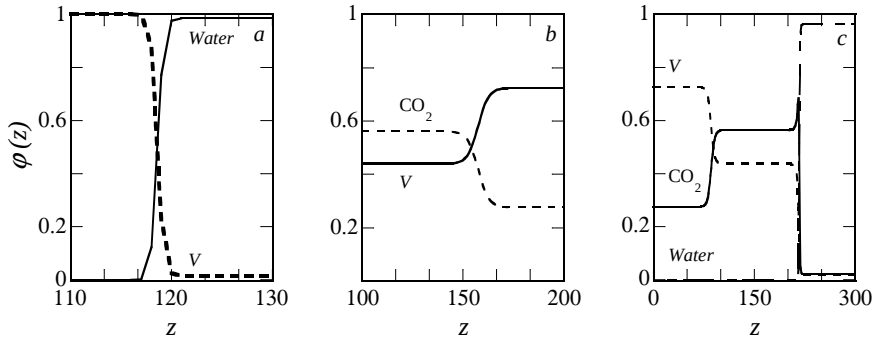

Figure 6.3: *(a) Volume fractions of water and free volume across the binary water - free volume interface. (b) Volume fraction of* CO_2 *and free volume across the binary* CO_2 *- free volume interface. (c) Volume fraction profiles of water, free volume and* CO_2 *at three phase co-existence. The free-volume (V)-rich phase is on the left, the* CO_2 *rich phase is around* $z \approx 100$ *and the water-rich phase is on the right. The z-values on the x-axis are arbitrary.*

is the V-rich phase, on the right there is the water-rich phase and in between there is the CO_2 phase. We would like to draw the attention to the excess CO_2 adsorption, which shows up at the interface between water and CO_2. The bulk binodal values of the respective components can be read from the $\varphi(z)$ profiles, in particular, sufficiently far away from the interfaces, e.g. at layers $z = 0$, 150 and 300 (Figure 6.3c). These densities are summarised in Table 6.2. As can be seen from Table 6.2 the amount of free volume in the CO_2-rich phase is 0.436, which is much higher than that in H_2O (0.016). Moreover,

Table 6.2: *Bulk binodal values of* CO_2*, water and free volume vapour in each phase at 313 K for the system in three-phase coexistence. The phases rich in* CO_2*, water and* V *are labelled as* CO_2*,* H_2O *and* V*, respectively.*

	$\varphi^{\#}_{CO_2}$	$\varphi^{\#}_{\mathrm{H_2O}}$	$\varphi^{\#}_{V}$
CO_2	0.563	0.0005	0.436
H_2O	0.023	0.961	0.016
V	0.274	4.26×10^{-5}	0.725

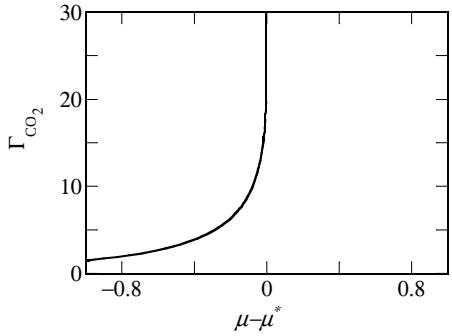

Figure 6.4: *Gibbs excess of CO_2 at the water - V interface for the default χ parameters, i.e. $\chi_{DV} = 1.5$, $\chi_{WD} = 1.5$ and $\chi_{WV} = 3.5$, showing a macroscopic thick layer of CO_2 between water - vapour interface consistent with complete wetting of the water - vapour interface by CO_2.*

the amount of CO_2 in H_2O is 0.023, which is two orders of magnitude higher than the amount of H_2O in CO_2 (0.0005). Qualitatively these results were anticipated.

The CO_2 - water interfacial tension is high and this triggers adsorption of CO_2 (reduction of free volume) as can be seen from Figure 6.3c. The much lower interfacial tension of the CO_2 - vapour interface leads to no clear excess of CO_2 (Figure 6.3a). As long as $\gamma_{H_2O-V} < \gamma_{H_2O-CO_2} + \gamma_{CO_2-V}$ the excess of CO_2 remains finite and macroscopically one can have three interfaces in the system (namely between water and V, water and CO_2, and CO_2 and V. However, in the limit of $\gamma_{H_2O-V} \to \gamma_{H_2O-CO_2} + \gamma_{CO_2-V}$ a wetting transition occurs from whereon a macroscopically thick wetting layer of CO_2 appears between the water and vapour. In this case it is impossible to find a water-vapour interface. In our model we can easily find a CO_2 film in between the water and vapour as is shown in Figure 6.3c. To judge the thermodynamic stability of such a CO_2 film we need to inspect adsorption isotherms of CO_2 at the water - vapour interface corresponding to the χ parameter set described in Table 6.1. The adsorption isotherm shown in Figure 6.4 indicates that at coexistence there is indeed a macroscopic (thick) wetting layer of CO_2 at the water - vapour interface. The shape of the adsorption isotherm corresponds

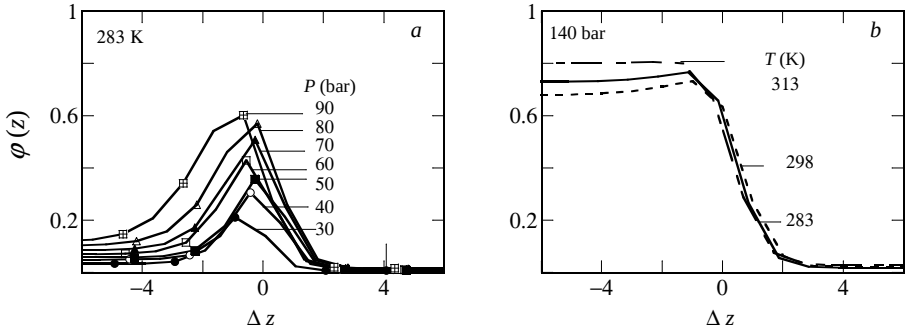

Figure 6.5: *(a) Volume fraction profile of CO_2 across the water - V interface at 283 K and different pressures as indicated showing a Gibbs excess of* CO_2 *at the interface (b) Volume fraction of* CO_2 *at 283, 298 and 313 K at a fixed pressure of 140 bar at the water -* CO_2 *interface. The excess is calculated with respect to the Gibbs dividing plane, which is at $\Delta z = 0$, Δz being $z - z^{Gibbs}$.*

to the complete wetting regime.[36] This indicates that there are no nearby wetting transitions, consistent with the fact that the CO_2 - V system is not too far from the critical point.[36]

It is of interest to focus briefly on the surface excess of CO_2 (D) at the $W - V$ or $W - D - V$ interfaces shown in Figures 6.5a and 6.5b. Figure 6.5a was computed by starting with the $W - V$ system and fixing the $\varphi^b_{CO_2}$ in the water phase corresponding to the pressure and temperature conditions stated in the figure. To generate Figure 6.5b we started with a $W - D$ interface and fixed the φ^b_V in water at values corresponding to 140 bar and 283 K, 298 K and 313 K. We see from Figure 6.5a that with increasing pressure, the Gibbs excess of CO_2 increases, even for $\varphi_{CO_2} \ll \varphi^b_{CO_2}$. Upon reaching the saturation condition and thereby having a three-phase coexistence, CO_2 continues to accumulate at the H_2O - V interface at all the three temperatures as indicated in Figure 6.5.

The accumulation of CO_2 at the water - vapour interface is responsible for the decrease of γ_{H_2O-V} with increasing pressure. The calculated interfacial tension between CO_2 and W with increasing CO_2 activity or P is shown in Figure 6.6. The value of "a", the lattice parameter, as explained in Figure

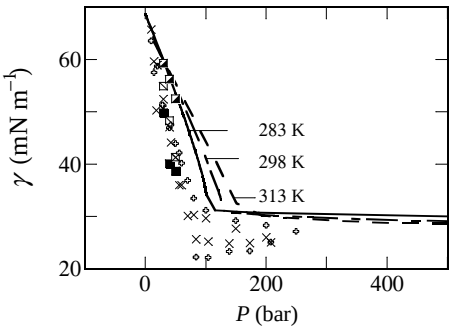

Figure 6.6: *Comparison between experimental $\gamma_{water-CO_2}$ data and theory at 283, 298 and 313 K. The squares represent the present experimental works at 283 K (filled), 298 K (unfilled) and 313 K (half filled) respectively. The cross and plus legends represent data from literatures at 298 K and 313 K respectively.[1] The curves are the interfacial tension obtained from SF-SCF modeling.*

6.1, has been chosen as 2.7 Å, to convert the grand potential (Ω) and chemical potential (μ) to interfacial tension (γ) and pressure (P) respectively (see equations 6.24 and 6.25. For comparison, we overlay in Figure 6.6 the experimental γ values from our work and those obtained by other groups.[1] Not all our measured data points can be compared with literature (as the pressure and temperature ranges at which the experiments were performed were quite different), nevertheless, for some of the data points (e.g., for 298 K and 313 K), there is reasonable agreement between our measurements and results of Georgiadis *et al.*

Figure 6.6 illustrates reasonable semi-quantitative match between experimental and theoretical water - CO_2 interfacial tensions at three different temperatures. Although we can predict γ values for the whole pressure range we only show results up to 500 bar as the γ - P isotherms do not change much above 500 bar. With our simple mean field model all the established trends, such as the increasing slope of the γ - P isotherms with decreasing temperature and the shifting of the gas-liquid transition point (vapour pressure of CO_2) to higher pressures with increasing temperature, could be reproduced quite well even though no detailed data fitting regarding the χ parameters has

been attempted.

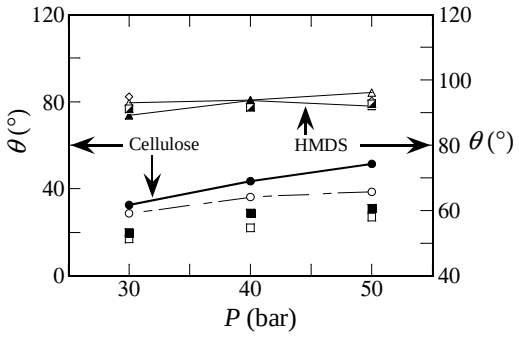

Figure 6.7: *Comparison between experiment and modelling for water contact angle variation with pressure on cellulose (hydrophilic) and HMDS (hydrophobic) surfaces immersed in* CO_2*. The lines represent experimental contact angles. The filled black circles represent experimental data for cellulose at 283 K, the unfilled circles indicate experiments at 298 K, the filled and unfilled squares represent theoretical water contact angle calculated by SF-SCF theory for cellulose at 283 and 298 K respectively. Filled and unfilled triangles correspond to experimental water contact angle on HMDS surface at 283 and 298 K respectively. Unfilled diamond and half filled squares indicate theoretical water contact angle values on HMDS surface calculated using SF-SCF theory at 283 and 298 K respectively.*

6.8.2 Contact angle

Water contact angles on a hydrophilic cellulose surface immersed in CO_2 were experimentally determined as a function of pressure at 283 and 298 K (Figure (6.7). With increasing pressure, the contact angle increases at both temperatures indicating partial wetting of the water drop on cellulose.

The reason for the partial wetting could be related to the adsorption of CO_2 onto the surface-OH (hydroxyl) groups of cellulose, thereby making the surface more hydrophobic. Similar partial wetting by water was observed on glass surfaces immersed in CO_2.[14] If this is indeed the reason, then pre-capping of the -OH groups of hydrophilic surfaces by some alkylsilane group should result in a constant contact angle as a function of CO_2 pressure. This hypothesis was tested by measuring the water contact angle on an HMDS modified silica

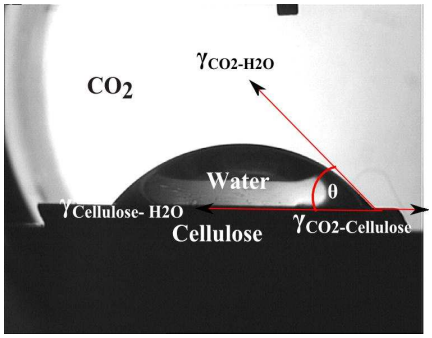

Figure 6.8: *Water drop on a cellulose surface surrounded by CO_2. Arrows show Young's construction of energy balance at the three-phase contact point.*

surface surrounded by CO_2. The results are also shown in Figure 6.7. Indeed no change in contact angle was noted with increasing pressure, thus verifying our hypothesis.

It is well-known that Young's equation relates the contact angle to the respective interfacial free energies (see Figure 6.8), as given in Eqn 6.31 : From Figure 6.2 it can be seen that $\gamma_{CO_2-\mathrm{H_2O}}$ decreases with pressure, and provided the difference $\gamma_{cellulose-CO_2} - \gamma_{cellulose-\mathrm{H_2O}}$ remains constant, θ should decrease. From our data in Figure 6.7 we see the opposite trend, that is, with increasing pressure, θ increases. So, the difference $\gamma_{cellulose-CO_2} - \gamma_{cellulose-\mathrm{H_2O}}$ should also be pressure dependent and this we investigated by the SF-SCF theory again as presented below.

To understand the wetting characteristics of a water drop on a solid surface in CO_2 we resort to SF-SCF theory again. Modelling of contact angles requires three additional FH parameters and these are also documented in Table 6.1. In this case the short range interactions with respect to the surface are attractive and defined with respect to the surface - V interaction, which was set (without loss of generality) to zero. Again we apply a flat geometry and perform a one-

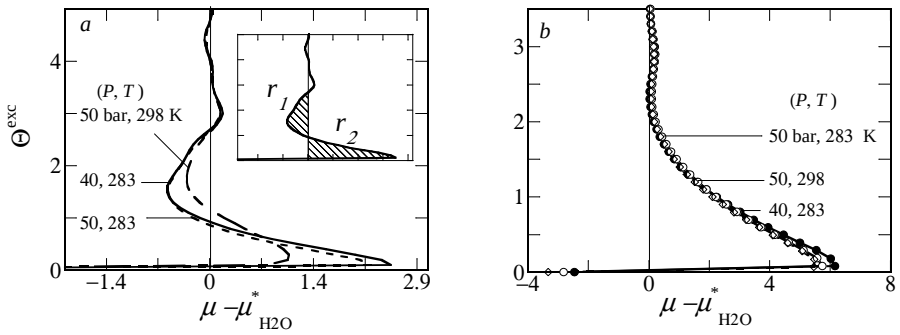

Figure 6.9: *Calculated adsorption isotherms of water molecules on (a) cellulose and (b) HMDS surfaces immersed in CO_2 containing vapour phase at different pressures and temperatures as a function of its relative chemical potential. The shaded regions indicate partial wetting of cellulose surface by the water drop as the area $r_1 < r_2$*[37] *(inset, 40 bar 283 K).*

gradient calculation to generate the adsorption isotherms (Figures 6.9a and 6.9b), plotting the excess amount of water on the cellulose surface as a function of the chemical potential of water. The small oscillations in the isotherms are due to lattice artefacts.[38] Fortunately the oscillations are small and do not obstruct a systematic analysis.

From the adsorption isotherms it is clear that we are dealing with partial wetting, as the isotherm crosses the saturation axis at a finite (intersection between the isotherm and the saturation axis, solid black line in Figure 6.9) adsorbed amount, corresponding to a thin film in equilibrium with a macroscopically thick adsorbed film.[37] Moreover, the shaded areas r_1 and r_2 satisfy $r_1 < r_2$, Figure 6.9a (inset), which also indicates that we are dealing with partial wetting of the cellulose surface by the water drop.[37] Inspection of Figure 6.9 reveals that a thin (corresponding to Ω(thin)) and a thick film (corresponding to Ω(thick)) co-exist at equilibrium owing to the same chemical potential (μ_{H_2O}). This makes it imperative that the interface is curved, implying that it exists at the three- phase contact. To extract the contact angle from these isotherms we re-plot the graph as grand potential (Ω, normalised interfacial tension) versus chemical potential. The contact angle can be calculated as

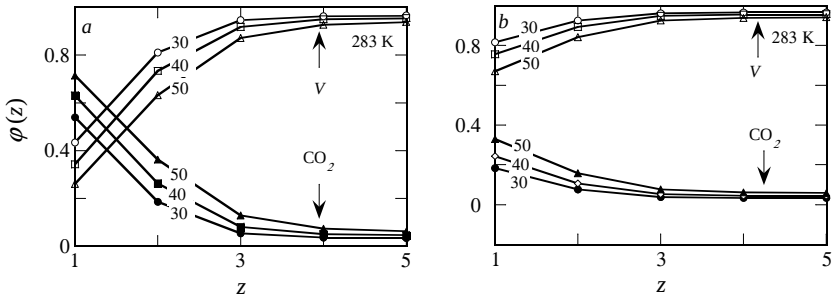

Figure 6.10: *Calculated volume fraction profiles of* CO_2 *and* V *near (a) cellulose and (b) HMDS surfaces corresponding to a microscopic water film (*$\Theta_{H_2O} = 1.0 \times 10^{-5}$*). The numbers in the graphs indicate pressures.*

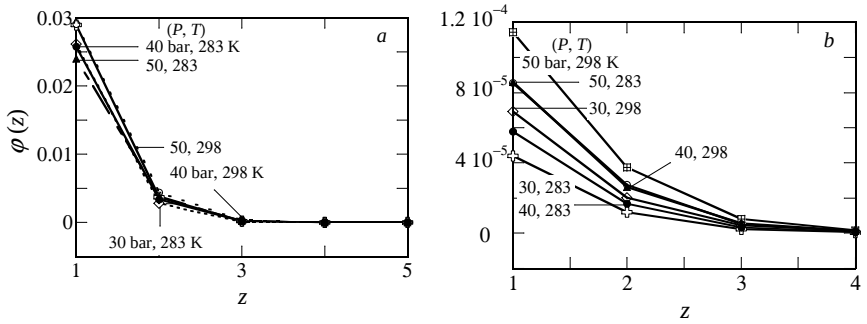

Figure 6.11: *Calculated volume fraction profiles of* H_2O *near (a) cellulose and (b) HMDS surfaces corresponding to a microscopic water film (*$\Theta_{H_2O} = 1.0 \times 10^{-5}$*).*

according to Eqn 6.32.

To model the effect of temperature on contact angle, the χ parameters can be changed as explained before. Assuming that the FH parameters are enthalpic in nature, their absolute values would decrease with temperature (Eqn 6.8). Such a scaling could explain the experimental trends of higher contact angles at lower temperature and the pressure dependence of θ for both surfaces. The modelling data are shown in Figure 6.7. Again we could reproduce the qualitative trends of increase of θ with pressure for the hydrophilic cellulose surface and the invariance of θ with increasing pressure for the hydrophobic

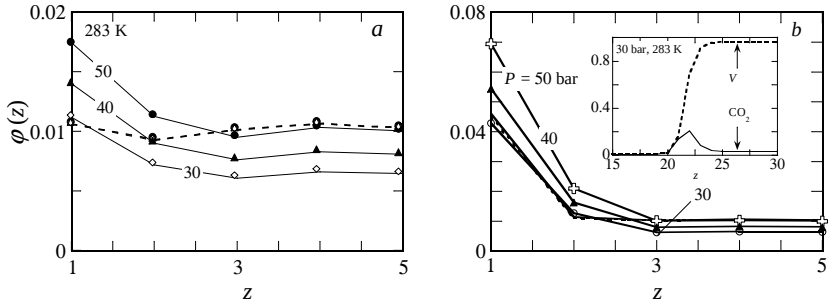

Figure 6.12: *Calculated volume fraction profiles of* CO_2 *and* V *near (a) cellulose and (b) HMDS surfaces corresponding to a macroscopic water film (*$\Theta_{H_2O} = 20$*). The solid and dashed lines indicate the volume fraction profiles of* CO_2 *and* V *respectively.*

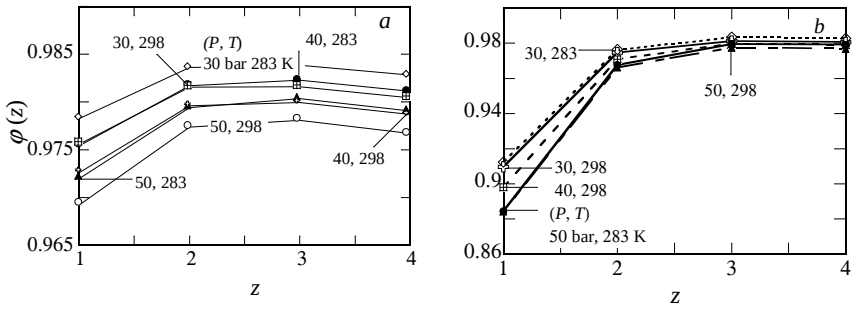

Figure 6.13: *Calculated volume fraction profiles of* H_2O *near (a) cellulose and (b) HMDS surfaces corresponding to a macroscopic water film (*$\Theta_{H_2O} = 20$*).*

HMDS surface.

Molecular-level information on how the molecules accumulate at the interface is available in the form of density (volume fraction) profiles of CO_2, H_2O and V for various amounts of water in the system. A selection of these profiles is depicted in Figures 6.10, 6.11, 6.12 and 6.13.

From each of the adsorption isotherms shown in Figure 6.9, two Θ_{H_2O} values were selected namely corresponding to the thin ($\Theta_{H_2O} = 1.0 \times 10^{-5}$, Figures 6.10 and 6.11) and thick film ($\Theta_{H_2O} = 20$, Figures 6.12 and 6.13) conditions. In these figures the volume fraction profiles of the three components

are given as a function of the distance from the surfaces.

Cellulose shows a stronger affinity for CO_2 (Figure 6.10a) as opposed to the HMDS surface (Figure 6.10b), whereas the opposite is noticed for the V phase. This can be explained from the difference in surface energies between cellulose and HMDS modified silica surfaces. HMDS being much more hydrophobic (water contact angle on HMDS modified silica is $\sim 90^\circ$ compared to $\sim 30-40^\circ$ on the cellulose surface) has a stronger affinity for the V phase, whereas, cellulose having free-OH groups on the surface is capable of capturing CO_2 and thereby minimizing the free energy of the system for not having to expose its hydrophilic-OH groups to the V phase. Note that in the SCF model the presence of -OH groups is not directly modelled but is effectively incorporated by the FH interaction parameters.

The affinity of the cellulose surface for the CO_2 phase arguably also explains the increase of contact angle with increasing pressure. As the concentration of CO_2 in the V phase increases, the surface becomes even more covered with CO_2, making the water drop to retract from the surface (dewetting). Water volume fraction profiles for the cellulose and HMDS surfaces are shown in Figure 6.11a and 6.11b respectively at $\Theta_{H_2O} = 1.0 \times 10^{-5}$. Even at such a low water amount, the volume fraction of water near the cellulose surface is three orders of magnitude higher than that of the HMDS surface.

With an increased amount of water in the system ($\Theta_{H_2O} = 20$, which corresponds to $\varphi_W^b \approx \varphi_W^\#$), condensation of the water film has taken place on the surface, which is evident from the volume fraction profiles of water on both cellulose and HMDS surfaces as displayed in Figure 6.13. Here we focus on the profile near the solid phase, (small values of z), because the fluid - fluid interface (between $z = 20$ & 25 (see Figure 6.12b) far from the surface is identical to the free water - CO_2 interface discussed before (see Figure 6.5a). Interestingly we see that the volume fraction of water decreases somewhat near the surface in favour of an increase of the free volume and CO_2 densities. This is completely in line with the finite contact angles. The higher the contact angle, the more the depletion of water and the enrichment of V and CO_2.

6.9 Conclusions

Measurement of water - vapour interfacial tension with dispersed CO_2 in the vapour phase show that the IFT decreases with increasing pressure. Moreover, the negative slope of the IFT - P isotherm decreases with increasing temperature. These experimental findings stimulated us to model such a three-phase system to improve our molecular insight in the processes involved. We invoked a simple mean-field based approach and showed that a molecular coarse grained model based on SCF theory is sufficient for in-depth understanding of such a complex system. The SCF approach is simpler and arguably preferable over equation-of-state based models, and computationally orders of magnitude less expensive than molecular dynamics simulations.

We could semi-quantitatively reproduce the experimental water - V interfacial tension at 283 K, 298 K and 313 K with dispersed CO_2 phase by incorporating suitable FH parameters into the model. Our modelling results point towards the presence of a surface excess of CO_2 at both the H_2O - V interface and at the three phase co-existence region. The adsorption isotherms of CO_2 point towards the existence of a wetting film of CO_2 at the W - V interface for all the conditions. The trends in the water contact angle on cellulose and HMDS surfaces were also successfully modelled and the volume fraction profiles of all the three phases near the surfaces and at bulk were constructed, which show that the hydrophilic cellulose surface irrespective of the water amount in the system, prefers to have CO_2 molecule on its surface over the free volume phase. This phenomenon could be responsible for the increase of contact angle of water with increasing pressure on the cellulose surface.

In the next chapter we will extend this type of mean field model towards the understanding of phase behaviour of CO_2 soluble surfactants in multi component systems.

Bibliography

[1] A. Georgiadis, G. Maitland, J. P. M. Trusler, and A. Bismarck. Interfacial Tension Measurements of the H_2O +CO_2 System at Elevated Pressures and Temperatures. *J. Chem. Eng. Data*, 5(10):4168–4175, 2010.

[2] T. Lafitte, B. Mendiboure, Manuel M. Piñeiro, D. Bessières, and C. Miqueu. Interfacial Properties of Water/CO_2: A Comprehensive Description through a Gradient Theory- SAFT-VR Mie Approach. *J. Phys. Chem. B*, 114(34):11110–11116, 2010.

[3] L. C. Nielsen, I. C. Bourg, and G. Sposito. Predicting CO_2-Water Interfacial Tension Under Pressure and Temperature Conditions of Geologic CO_2 Storage. *Geochim. Cosmochim. Ac.*, 81(0):28–38, 2011.

[4] S. Banerjee, S. Sutanto, J. M. Kleijn, M. J. E. van Roosmalen, G. J. Witkamp, and M. A. Cohen Stuart. Colloidal Interactions in Liquid CO_2 - A Dry-cleaning Perspective. *Adv. Colloid Interface Sci.*, 175:11–24, 2012.

[5] M. Blunt, F. John Fayers, and F. M. Orr. Carbon Dioxide in Enhanced Oil Recovery. *Energ Convers and Manage*, 34:1197–1204, 1993.

[6] M. A. McHugh and V. J. Krukonis. *Supercritical Fluid Extraction. Principles and Practice*. Butterworth Publishers, Stoneham, MA, 1986.

[7] P. K. Bikkina, O. Shoham, and R. Uppaluri. Equilibrated Interfacial Tension Data of the CO_2-Water System at High Pressures and Moderate Temperatures. *J. Chem. Eng. Data*, (10):3725–3733, 2012.

[8] B.-S. Chun and G. T. Wilkinson. Interfacial Tension in High-Pressure Carbon Dioxide Mixtures. *Ind. Eng. Chem. Res.*, 34:4371–4377, 1995.

[9] A. Hebach, A. Oberhof, N. Dahmen, A. Kogel, H. Ederer, and E. Dinjus. Interfacial Tension at Elevated Pressures Measurements and Correlations in the Water + Carbon Dioxide System. *J. Chem. Eng. Data*, 47:1540–1546, 2002.

[10] P. Chiquet, J. L. Daridon, D. Broseta, and S. Thibeau. CO2/water Interfacial Tensions under Pressure and Temperature Conditions of CO2 Geological Storage. *Energ. Convers. and Manage.*, 48:736–744, 2007.

[11] B. Kvamme, T. Kuznetsova, A. Hebach, A. Oberhof, and E. Lunde. Measurements and Modelling of Interfacial tension for Water+ Carbon Dioxide Systems at Elevated Pressures. *Comput. Mater. Sci.*, 38:506–513, 2007.

[12] S. Bachu and D. B. Bennion. Interfacial Tension between CO_2, Freshwater, and Brine in the Range of Pressure from (2 to 27) MPa, Temperature from (20 to 125) °C, and Water Salinity from (0 to 334000) mg/l. *J. Chem. Eng. Data*, 54:765–775, 2009.

[13] Y. Sutjiadi-Sia, P. Jaeger, and R. Eggers. Interfacial Phenomena of Aqueous Systems in Dense Carbon Dioxide. *J. Supercrit. Fluids*, 46:272–279, 2008.

[14] J. L. Dickson, G. Gupta, T. S. Horozov, B. P. Binks, and K. P. Johnston. Wetting Phenomena at the CO_2/Water/Glass Interface. *Langmuir*, 22:216–2170, 2006.

[15] Monte Carlo Simulation of H_2O- CO_2 Mixtures to 1073.15 K and 30 kbar. *Chem. Geol.*, 133:53–65, 1996.

[16] Patterson C. H. Panhuis, M. H and R. M. Lynden-Bell. A Molecular Dynamics Study of Carbon Dioxide in Water: Diffusion, Structure and Thermodynamics. *Mol. Phys*, 94:963–972, 1998.

[17] Z. Zhang and D. Zhenhao. An Optimized Molecular Potential for Carbon Dioxide. *J. Chem. Phys.*, 122:214507–214522, 2005.

[18] T. Kuznetsova and B. Kvamme. Thermodynamic Properties and Interfacial Tension of a Model Water-Carbon Dioxide System. *Phys. Chem. Chem. Phys.*, 4:937–941, 2002.

[19] L. Zhao, S. Lin, J. D. Mendenhall, P. K. Yuet, and D. Blankschtein. Molecular Dynamics Investigation of the Various Atomic Force Contributions to the Interfacial Tension at the Supercritical CO_2-Water Interface. *J. Phys. Chem. B*, 115:6076–6087, 2011.

[20] J. W. Cahn and J. E. Hilliard. Free Energy of a Nonuniform System. I. Interfacial Free Energy. *J. Chem. Phys.*, 28:258–267, 1958.

[21] O. G. Nino-Amezquita, S. Enders, P. T. Jaeger, and R. Eggers. Measurement and Prediction of Interfacial Tension of Binary Mixtures. *Ind. Eng. Chem. Res.*, 49:592–601, 2010.

[22] O. A. Evers, J. M. H. M. Scheutjens, and G. J. Fleer. Statistical Thermodynamics of Block Copolymer Adsorption. 1. Formulation of the Model and Results for the Adsorbed Layer Structure. *Macromolecules*, 23:5221–5233, 1990.

[23] O. A. Evers, J. M. H. M. Scheutjens, and G. J. Fleer. Statistical Thermodynamics of Block Copolymer Adsorption. Part 2.-Effect of Chain Composition on the Adsorbed Amount and Layer Thickness. *J. Chem. Soc., Faraday Trans.*, 86:1333–1340, 1990.

[24] P. J. Flory. Thermodynamics of High Polymer Solutions. *J. Chem. Phys.*, 9:660–660, 1941.

[25] S. Banerjee, P. Mulder, J. M. Kleijn, and M. A. Cohen Stuart. Effect of Surface Roughness and Softness on Water Capillary Adhesion in Apolar Media. *J. Phys. Chem. A*, 116:6481–6488, 2012.

[26] E. Kontturi, P. C. Thüne, and J. W. Niemantsverdriet. Cellulose Model Surfaces: Simplified Preparation by Spin Coating and Characterization by X-ray Photoelectron Spectroscopy, Infrared Spectroscopy, and Atomic Force Microscopy. *Langmuir*, 19:5735–5741, 2003.

[27] T. L. Hill. *An Introduction to Statistical Thermodynamics.* Addison-Wesley, third edition, 1960.

[28] B. R. Postmus, F. A. M. Leermakers, and M. A. Cohen Stuart. Self-Consistent Field Modeling of Poly(ethylene oxide) Adsorption onto Silica: The Multiple Roles of Electrolytes. *Langmuir*, 24:1930–1942, 2008.

[29] F. A. M. Leermakers and J. M. H. M. Scheutjens. Statistical Thermodynamics of Association Colloids: V. Critical Micelle Concentration, Micellar Size and Shape. *J. Colloid Interface Sci.*, 136:231–241, 1990.

[30] A. B. Jòdar-Reyes, J. L. Ortega-Vinuesa, A. Martìn-Rodrìguez, and F. A. M. Leermakers. Modeling the Effect of Structural Details of Nonionic Surfactants on Micellization in Solution and Adsorption onto Hydrophobic Surfaces. *Langmuir*, 18:8706–8713, 2002.

[31] J. M. H. M. Scheutjens and G. J. Fleer. Statistical Theory of the Adsorption of Interacting Chain Molecules. 1. Partition Function, Segment Density Distribution, and Adsorption Isotherms. *J. Phys. Chem.*, 83:1619–1635, 1979.

[32] R. Span and W. Wagner. A New Equation of State for Carbon Dioxide Covering the Fluid Region from the Triple-Point Temperature to 1100 K at Pressures up to 800 MPa. *J. Phys. Chem. Ref. Data*, 25:1509–1596, 1996.

[33] A. Hebach, A. Oberhof, and N. Dahmen. Density of Water + Carbon Dioxide at Elevated Pressures: Measurements and Correlation. *J. Chem. Eng. Data*, 49:950–953, 2004.

[34] M. B. King, A. Mubarak, J. D. Kim, and T. R. Bott. The Mutual Solubilities of Water with Supercritical and Liquid Carbon Dioxides. *J. Supercrit. Fluids*, 5:296–302, 1992.

[35] Z. Duan and R. Sun. An Improved Model Calculating CO_2 Solubility in Pure Water and Aqueous NaCl Solutions from 273 to 533 K and from 0 to 2000 bar. *Chem. Geol.*, 193:257–271, 2003.

[36] J. W. Cahn. Critical Point Wetting. *J. Chem. Phys.*, 66(8):3667–3672, 1977.

[37] B. V Derjaguin, N. V. Churaev, and V. M Muller. *Surface Forces*. New York: Plenum Press, 1960.

[38] L. Schlangen, F. A. M. Leermakers, and L. K. Koopal. Self-Consistent Field Theory for Wetting of Binary Polymer-Solvent Mixtures on Rigid and Soft Interfaces. *J. Chem. Soc., Faraday Trans.*, 92:579–587, 1996.

Appendix

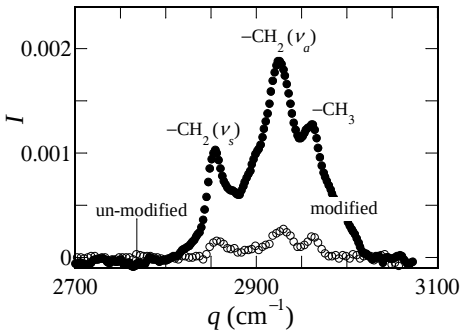

Figure 6.14: *IRRAS spectrum of the HMDS-modified and unmodified Si surfaces.*

Apart from the water contact angle measurements on the modified and unmodified surfaces, we have verified spectroscopically the modification of the Si wafer by HMDS. The technique employed is Infra-red reflection absorption spectroscopy (IRRAS). We measured the intensity of the reflected infra-red light on the modified and unmodified surface using IRRAS (Bruker TENSOR 27) equipped with a Harrick Auto SeaguIITM sample holder and a MCT (mercury, cadmium, telluride) detector. The software used was Auto SeaguII Pro v1.50. The p-polarized spectra were recorded at a mirror angle of 68 °. We collected 2048 scans at a resolution of 4 cm^{-1}. The spectra were analyzed using the Opus 6.5 software. The final spectra were background subtracted using the IRRAS spectrum of a HF (2 % for 5 min) etched reference surface. All spectra were recorded at room temperature in a dry, nitrogen atmosphere. The spectra were subjected to linear baseline correction.

The HMDS modified surface displays clear stretching peaks assigned to CH_2, anti-symmetric (2925.9 cm^{-1}) and symmetric (2856.5 cm^{-1}), and CH_3 (2962.5 cm^{-1}). Similar peaks in the spectrum of the un-modified Si wafer are much weaker in intensities. These results corroborate that after the modfication, the HMDS surface is methyl rich due to the formation of $OSi(CH_3)_3$ from SiOH.

Chapter 7

A Liquid CO_2-Compatible Hydrocarbon Surfactant: Experiment and Modeling [a]

Surfactants soluble in liquid CO_2 are rare and knowledge on interfacial and self-assembly behaviour is fragmented. We found that polyoxyethylene (5) isooctylphenyl ether is interfacially active at the water - liquid CO_2 interface. Water - liquid CO_2 interfacial tension was measured at various surfactant concentrations at 50 bar and 283 K using the pendant drop method, and a CMC like cusp was observed at a surfactant concentration of $\sim$ 50 mM in the bulk liquid CO_2. This system was modelled applying the self-consistent field theory of Scheutjens and Fleer (SF-SCF). We use a free-volume approach, wherein the chemical potential of the vacancies was linked to the pressure and the molecules were described using a freely-jointed chain model on a united atom level. The model indicates that typically the water - vapour interface is wet by CO_2. Interestingly, a window of partial wetting was identified at the water - vapour interface as a function of the chemical potential of the surfactant. The second-order nature of both wetting transitions is attributed to the close proximity to the critical point of the CO_2 - vapour system. Furthermore, the

[a] This chapter is accepted as a manuscript in J. Phys. Chem. Chem. Phys.

SF-SCF theory was used to study the self-assembly of the surfactant in bulk CO_2 or water, focusing on the three-phase coexistence, that is at $P/P_{\text{sat}} = 1$. Above $\sim$ 40 mM in the CO_2-rich phase, the theory indicates stable water swollen reverse micelles with an aggregation number of $\sim$ 100. The analysis further shows the stability of compressible CO_2-swollen surfactant bilayers in the bulk water phase at elevated surfactant concentrations. Finally it was found that the critical reverse micellar concentration (in liquid CO_2) increases and the aggregation number decreases with increasing pressure.

7.1 Introduction

The phase behaviour of surfactants in biphasic solvent systems is of interest for both academia and industry. For example, in oil/water systems surfactants, which are inherently both lyophilic and lyophobic (HLB $\sim$ 10), can partition in both solvents and then form a rich variety of mesophases, which pose challenging modelling problems. Although oil-water systems containing amphiphiles are often encountered in practice in the form of emulsions and microemulsions, systematic theoretical investigation of these systems are scarce.[1,2] Compared to the formation of micelles in water, the reverse micellization of surfactants in apolar media has been relatively less studied in particular when water is also present in such systems as a second phase.

In this chapter, we consider biphasic liquid CO_2/ water systems in the presence of a CO_2 soluble surfactant. Hydrocarbon surfactants, soluble in liquid CO_2, are encountered rarely. For those that exist, understanding their phase behaviour in liquid CO_2 is either lacking or superficial. The ongoing challenge to find soluble amphiphiles for liquid CO_2 is hampered by the lack of specialised high pressure equipment needed for this search. Liquid CO_2 appears to be a poor solvent for most hydrocarbon surfactants, as it is unable to screen the tail-tail attractions between the surfactants. These aspects have been discussed in detail in references.[3,4]

Computer simulations have been used to model surfactant phase behaviour in supercritcal (sc) CO_2, sc CO_2 - water or sc CO_2 - water - alcohol

mixtures using the coarse grain lattice Monte Carlo approach of Larson[5] or a slightly modified version[6] thereof. In some cases models covering atomistic details were also employed, e.g., for the self-assembly in double chain surfactant/sc CO_2/water ternary systems.[7–9] In our study we focus on a hydrocarbon amphiphile with methyl branching in the apolar tail. Such surfactants have previously been identified as suitable for liquid CO_2, following the argument of fractional free volume.[3,4] In our previous publication we have introduced polyoxyethylene (5) isooctylphenyl ether (Igepal CA 520) as a potential surfactant for liquid CO_2 from the perspective of dry-cleaning.[4] In the present chapter we first present the experimental interfacial tension of this hydrocarbon surfactant at the water - liquid CO_2 interface. We then employ the lattice based self-consistent field of Scheutjens and Fleer (SF-SCF) model targeted to enhance our molecular understanding (surface phase behaviour of liquid CO_2 in presence of the surfactant, micellar shape, size, aggregation number, bilayer formation) of the various self-assembled structures formed by this surfactant in the biphasic system, water/liquid CO_2. This may seem a gigantic effort, but the SF-SCF is so efficient that it turned out possible to scan a large phase and parameter space in very short time allowing us to develop an appropriate model and parameter set to first order.

This chapter is a follow up of two of our previous studies, namely reference 10 where we introduced self-consistent field modelling to predict the properties of the CO_2/water interface and reference 4 where we have shown experimentally the effectiveness of Igepal CA520 towards particle release in liquid CO_2. In this chapter, we build upon the SF-SCF model that we have used in[10] by incorporating the surfactant as an additional molecular component. The chapter is organized as follows: we first briefly discuss experimental and theoretical aspects. This is followed by a more extensive discussion of parameter values in the model. While discussing the self-consistent field theory we refer to our previous publication,[10] where we already discussed the scheme in general. Moreover, the interaction parameters between the segments of water, free volume and CO_2 were already introduced in.[10] Hence, in the present chapter we focus on the self-consistent field treatment of chain like molecules.

Most of the extra modelling parameters we deduce from previous studies.[11] However, some of the parameters, typically those involving the CO_2 molecule are unknown and we here will give a suggestion for appropriate values. In the results section we perform a short parameter survey. From this study we obtain insights in why the micellisation of surfactants in liquid CO_2 is so difficult.

We then characterize the adsorption of surfactant at the water - vapour interface by measuring the corresponding interfacial tension. The modelling of this leads us to consider the wetting behaviour of CO_2 at this surfactant-decorated interface. More specifically, we show how the presence of surfactant at the water - vapour interface may influence the wetting of this interface by liquid CO_2 .

Next we employ the self-consistent field theory to study the self-assembly of the surfactant in the bulk CO_2 or water phase. We explore the nature of the assemblies, and the sequence in which they occur as the chemical potential of the surfactant is gradually increased.

7.2 Materials and methods

The interfacial tension between deionized water and liquid CO_2 (Westfalen Gas, purity 99.5 %) in the presence of Igepal CA520 (Sigma Aldrich, purity $>$ 99 %, molecular weight 427 g mol^{-1}) was measured using the pendant drop technique in a high pressure view cell equipped with two transparent windows.[12] The surfactant concentration in liquid CO_2 was varied between 0 and 12 % (v/v). The cell volume was $\sim$ 30 ml.

The cell was filled with liquid CO_2 and a water drop was generated at the end of a steel capillary. A CCD camera recorded the image of the drop, the shape of which was then analyzed using the DSA software (Kruss, GmbH). Details on the pendant drop technique can be found in references.[13,14]

The experimental and modelling results were presented as a function of P/P_{sat}. The interfacial tensions (IFTs) were measured at 50 bar and 283 K and $P/P_{\mathrm{sat}} \approx 1.2$ ($P_{\mathrm{sat}} = 44.5$ bar at 283 K). The IFT calculations in the

model correspond to P/P_{sat} of ~ 1.2. For the study of self-assembly in CO_2 and/or water we focused on the three phase co-existence, i.e at $P/P_{\text{sat}} = 1$. We also predicted the effect of pressure on the thermodynamics of reverse micellization using the SF-SCF theory and for that we varied P/P_{sat} between 1 and 1.3.

7.3 Theory

7.3.1 Pressure in lattice models

The SF-SCF method is lattice based. As the lattice has a fixed volume, this implies an incompressibility constraint. In such a system the pressure is not defined. In order to deal with pressure variations, in Chapter 6, we implemented a lattice-gas variant in which the "chemical potential" of the vacancy, species V, referring to unoccupied lattice sites, is interpreted as (minus) the pressure times the volume of a lattice site. Besides these vacancies, the lattice is filled with CO_2 and water molecules. The details of the molecular model is further specified below. In this chapter we extend this model and elaborate the same (validated) parameter set.

The SF-SCF method is based on similar pre-averaging approximations as the regular solution theory of Flory. This implies that it uses the Bragg-Williams mean-field approximation to evaluate the number of unlike contacts between the monomeric species in the system. The Flory-Huggins interaction parameters were adopted, which take the "like" contacts as the reference. For lattice-gas systems it may be more intuitive to take the interactions with the free volume component as the reference. We follow the choices made in Chapter 6 but note that the reference state is inconsequential for the final results. We specified the conversion rules in Chapter 6 .

7.3.2 Chain model

Scheutjens and Fleer originally developed their variant of the SCF theory to model polymer adsorption from solutions.[15] Later, the SF scheme was mod-

ified by Leermakers *et al.*[16] to apply the theory to amphiphilic molecules. The conformations of the polymer/amphiphilic chains are evaluated using the freely-jointed chain model (FJC).[15] An obvious concern for FJC models is that a chain can fold back on previously occupied sites. A self-avoiding chain does not have this problem. However, within the SCF approach inter-molecular excluded volume interactions are not rigorously accounted for either. The FJC model accounts for the inter and intra-molecular excluded volume interactions on the same footing. However, a significant advantage of selecting the FJC model is that the single chain partition function is extremely efficiently computed using the propagator formalism, which gives a huge gain in computation time compared to the algorithm for self-avoiding chains. Moreover, self-avoiding effects are not important for short chains, which are our focus here. We therefore adopt the FJC model. Some details of the lattice used and the propagator formalisms for the surfactant chains are given in the appendix. Below we pay attention to the thermodynamics of self-assembly.

7.4 Molecular detail

As motivated in the previous chapter, we chose to model water as a small cluster consisting of five segments (W), in which a central W was surrounded by four neighbours and was represented as W_5. CO_2 was modelled as a dimer (D_2), while the vacancies V occupy just one lattice site. Igepal surfactant molecules are represented by a string of 30 segments as given in Figure 7.1a. For comparison the chemical structure of the Igepal CA520 is also shown in Figure 7.1b.

In this way we implement that the alkyl-terminus of the surfactant is rich in CH_3 ($C3$), the central part is rich in CH_2 (C) and the hydrophilic head group is rich in O. The architecture of the surfactant mimics that of the real Igepal, though it is not an exact match e.g. the aromatic ring carbons could not fit in the FJC model and therefore we rearrange these segments by putting two of them in the main chain both having two branched segments side by side (Figure 7.1a).

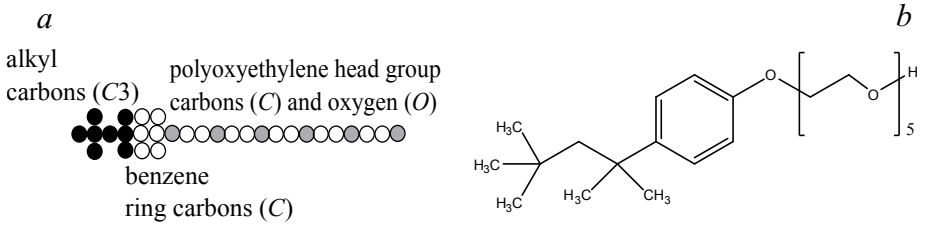

Figure 7.1: *(a) Schematic of the surfactant molecule containing 30 segments each with volume a^3 where a is the length of a lattice site. The black circles, labelled C3, and the white circles, labelled C represent CH_3 and CH_2 groups, respectively. The grey circles represent oxygen or OH (O). (b) Chemical structure of Igepal CA520, branched polyoxyethylene (5) isooctylphenyl ether.*

7.5 Interaction parameters

In the self-consistent field theory there are segment potential profiles $u_X(r)$ for each segment type X. Conjugated to these profiles there are computable segment volume fraction profiles $\varphi_X(\mathbf{r})$. The mean field "machinery" may be summarized by

$$\varphi[u(\mathbf{r})] \leftrightarrow u[\varphi(\mathbf{r})] \tag{7.1}$$

Table 7.1: *Flory-Huggins interaction parameters (χ) between various pairs of segments at 283 K. Here D is the monomer in CO_2, W is the monomer in water, V is the empty site, C is the CH_2 segment, C3 is the alkyl segment at the (branched) hydrocarbon end of the surfactant and O is the head group oxygen of the surfactant. We assume a $1/T$ dependence for these interaction parameters. The set of parameters has more rounded values for $T = 300K$.*

χ	D	W	V	C	$C3$	O
D	0	1.65	1.65	0.99	0.4	1.66
W	1.65	0	3.87	0.99	1.55	-0.55
V	1.65	3.87	0	1.77	1.55	3.87
C	0.99	0.99	1.77	0	0.55	1.77
$C3$	0.4	1.55	1.55	0.55	0	2.21
O	1.66	-0.55	3.87	1.77	2.21	0

In words, the SCF algorithm specifies how the volume fraction profiles must be computed from the segment potentials (left hand side of the equation: here the mean field approximation is implemented) and how the potentials follow from the volume fraction profile (right hand side of the equation: here is where the FJC approximation is implemented). The spatial coordinate $\mathbf{r}$ in these functions is the coordinate "perpendicular" to the mean-field directions. For example, for self-assembled bilayers a planar lattice is used wherein the mean field approximation is applied in the x-y planes and the gradient direction is in the z-direction so that $z \equiv \mathbf{r}$. For spherical micelles the gradient direction is in the radial direction and the mean field averaging is over spherical shells of lattice sites. More information about the coordinate systems is given in the appendix.

The short-range attractive and repulsive interactions between various segments of water, CO_2, surfactants and free volume are accounted for by the segment potentials. Each contact (i,j) contributes a (free) energy $\chi_{ij}kT/z$. A positive χ parameter indicates repulsion between unlike segments and a negative value signals attraction. The entropic contributions (translational and conformational entropy) are implemented by the chain model (FJC in our case). Once the fixed point of the equations is reached, usually referred to as the self-consistent solution (cf Equation 7.1), it is possible to evaluate the thermodynamic properties of the system. The thermodynamic quantities in turn give information about the feasibility of various options for the self-assembled structures, that is, (reverse) micelles versus planar bilayers.

Segments W, D and V already occurred in our previous study of the water /CO_2 system. We retain the parameters that we used there. Here we add new parameters for the segments C, $C3$ and O. The interaction of these segments with water were taken from previous modelling studies of (nonionic) surfactants in aqueous solutions.[11] The head group oxygen (O) is naturally the most hydrophilic one with $\chi_{WO} = -0.55$ and the tail group segments ($C3$) are most hydrophobic, having $\chi_{C3W} = 1.55$. The value for χ_{CW} (0.99) was found by fitting CMCs of surfactants in aqueous solutions as a function of the tail length. For more insight, we varied χ_{WO} to see the influence of this para-

meter on the self-assembly in both water and liquid CO_2. The temperature dependence of non-ionic surfactant assemblies can be implemented by making this parameter temperature dependent, while keeping others constant. Here we take a slightly different approach: we implemented a $1/T$-dependence for all χ parameters. We know from previous studies that we need a significant repulsion between the head and tail segments. This is achieved by taking $\chi_{OC} = 1.77$ and $\chi_{OC3} = 2.21$.

We needed to make educated guesses for the χ parameters between D (the segment of CO_2) and the two different carbon segments and between D and O. One of the arguments that we use, is based on the similarity between heptane (modelled as $(C)_7$) and CO_2 (modelled as D_2). Heptane has a (small) solubility gap with CO_2.[17] In our model the χ^{cr}_{DC} for the C_7 - D_2 system i.e. the critical χ parameter below which C_7 and D_2 are still miscible is 0.95 and we assume a slightly higher value of 0.99 between D and C to ensure a solubility gap.[10] The miscibility of the CH_3 (modelled as $C3$) and D_2 is expected to be significantly better. As a default value we choose for $\chi_{C3D} = 0.4$. We vary this parameter to investigate how critical the actual value is for the feasibility of (reverse) micelles in CO_2 and bilayers (in water). Finally, we select a strong repulsion between CO_2 and the oxygen groups of the surfactant, $\chi_{OD} = 1.66$.

From above it is clear that there are several somewhat arbitrary choices for the new parameters. We therefore stress that the validity of the parameters has to be justified a posteriori. Moreover, the most critical parameters that affect the micellisation are easily identified and the response to changes of these parameters are presented in the results section.

7.6 Output parameters for surfactant self-assembly

One of the challenges in this study is to quantify the reverse micellization of the surfactant in liquid CO_2. For example, we would like to know when reverse micelles in liquid CO_2 were possibly stable and when these are preferred over liquid crystalline bilayers that might form in the water phase. From quite general considerations and exemplified by the thermodynamics of small

systems we know that for thermodynamic stability of association colloids there should be zero excess energy (grand potential) associated with the formation of such objects. That is why we need to compare the chemical potential of the surfactants in the presence of reverse micelles in CO_2 to that in the presence of bilayers in the aqueous phase, under similar conditions. The system with the lowest chemical potential is identified as the most favourable one.

Hence, we need to compute the chemical potentials of the components. Equations exist to evaluate the chemical potential[10] in terms of concentrations of the various components in one of the bulk phases. The SCF method guarantees that in the system there are no chemical potential gradients. We refer to Chapter 6 for details.

We also require that the grand potential Ω for the association colloids goes to zero. As long as the grand potential $\Omega < 0$ the system tries to create more micelles, and when $\Omega > 0$ the number of micelles will decrease. Only when $\Omega = 0$ an equilibrium situation is obtained.

To consider reverse micelles in bulk CO_2 we select a spherical coordinate system with its origin coinciding with the micellar centre, and lattice layers $r = 1, \cdots, M_r$ where the number of lattice sites, L grows quadratically, with coordinate r i.e., $L(r) \propto r^2$. The primary result of the SCF calculations is the radial volume fraction profile for each molecule type i, $\varphi_i(r)$.

From the radial distribution function it is straightforward to evaluate the excess number of molecules of type i in the small system

$$n_i^\sigma = \frac{\sum_r L(r) \left[\varphi_i(r) - \varphi_i^b\right]}{N_i} \tag{7.2}$$

N_i being the number of segments of species i. For example, when i refers to the surfactant species, $n_{\text{surf}}^\sigma = g$, that is the aggregation number of surfactants in the (reverse) micelle.

The relation between the bulk volume fraction φ_i^b and the molar concentration C_i of a species i, is given by

$$C_i = \frac{\varphi_i^b}{N_a a^3 N_i} \tag{7.3}$$

a the size of one lattice site and N_a Avogadro's number.

Once the density and segment potential profiles are found in a self-consistent manner, the free energy follows and from that all other thermodynamic potentials. More specifically, we can evaluate the grand potential Ω_s as a function of the volume fraction and segment potential profiles.[10] The lower index s is added to indicate that we deal with a translationally restricted grand potential which differs from the overall grand potential by an entropic contribution. For dilute solutions of micelles we can estimate the ignored translational entropy of the micelle by $S_{\text{trans}} = -k_B \ln \phi_m$ where the volume fraction of micelles is found by $\phi_m = V_m/V_s$, with V_s the total volume of the system available per micelle and V_m the volume of a single micelle (which can be approximated by $g \times N_{\text{surf}}$). k_BT has its usual meaning. Then we have as a condition:

$$\Omega = \Omega_s - TS_{\text{trans}} = \Omega_s + k_BT \ln \frac{V_m}{V_s} = 0 \tag{7.4}$$

From this equation we see that $\Omega_s > 0$ as $k_BT \ln \frac{V_m}{V_s}$ is always negative. In our calculations we generate micelles with various aggregation numbers g yielding the function $\Omega_s(g)$. It can be shown that $-\partial\Omega_s/\partial g$ is inversely related to fluctuations in the micelle size. In other words, the stronger $\Omega_s(g)$ depends on the aggregation number, the more narrow is the size distribution of the reverse micelles. As negative size distributions cannot exist, for thermodynamic stability it is required that

$$\partial\Omega_s/\partial g < 0 \tag{7.5}$$

Spherical micelles are typically small so the translational entropy plays a significant role. For planar bilayers, on the other hand, this is not the case; we typically consider the cross-section of the bilayer only and normalise all properties by the area of the bilayer. Although the overall bilayer has some translational entropy, per unit area the entropy can safely be ignored. In this case the grand potential can be identified by the membrane tension, and thus $\Omega = \Omega_s = 0$ or, in other words, the membrane tension of equilibrated bilayers is zero.

For a macroscopic planar interface, such as the water - vapour interface, the interfacial tension (γ) is of course finite. Since we consider only the properties across the interface, we normalise all quantities by the area of the interface. Hence, the grand potential (Ω) is directly related to the interfacial tension γ as

$$\gamma = \frac{\Omega k_B T}{a^2} \tag{7.6}$$

This quantity is used below to evaluate the surface tension of the water - vapour interface as a function of the surfactant concentration.

7.7 The relation between adsorption and wetting

For obvious reasons our interest is drawn to the adsorption behaviour of CO_2 at the water - vapour interface, and how this adsorption is affected by the presence of surfactants. We already showed[10] that the adsorption isotherm of CO_2 on the water - vapour interface is a monotonically increasing function of the chemical potential of CO_2. The adsorbed amount Γ_{CO_2} (specified below) diverges as the chemical potential approaches the binodal value. The interpretation of this finding is that CO_2 completely wets the water - vapour interface.

Below we generate again a planar $W - V$ interface and compute an adsorption isotherm $\Gamma_{CO_2}(\mu_{CO_2})$ but now in the presence of surfactant. To find the isotherm we increased the amount CO_2 in the system at a fixed volume fraction of surfactant in the bulk of the water phase. Unlike in the absence of surfactant, it turned out that it was possible to find conditions for which the isotherm crossed the binodal condition $\mu_{CO_2} = \mu^{\#}_{CO_2}$ at finite adsorbed amount, $\Gamma_{CO_2} = \Gamma^{\#}_{CO_2}$. Only when much more CO_2 was forced to be in the interface, the chemical potential relaxed to the bulk binodal value. Such isotherms are typical for cases where CO_2 does not wet the water - vapour interface completely. We say that such a surface is partially wet by CO_2. Hence, the surfactant induces a wetting (phase) transition.

It is well-known that wetting transitions can be either first or second order. The distinction between the two can easily be made by recording $\Gamma^{\#}_{CO_2}$ as a

function of the control parameter, that is by recording $\Gamma^{\#}_{CO_2}(\varphi^b_{surf})$, where φ^b_{surf} is the bulk concentration of the surfactant (in the water phase). In the case where the adsorbed amount (at coexistence) $\Gamma^{\#}_{CO_2}(\varphi^b_{surf})$ smoothly increases and diverges at the wetting transition, this transition is second order.[18] If, at the wetting transition, this quantity diverges jump-like we have a first-order transition case.[18]

From the above it is clear that we need to evaluate Γ_{CO_2}. By choosing the phase rich in water as the bulk, we can evaluate the excess amount of each component θ^σ_i from:

$$\theta^\sigma_i = \sum_{z=1}^{M} \left(\varphi_i(z) - \varphi^b_i \right) \tag{7.7}$$

The excess number of molecules n^σ_i is then computed by

$$n^\sigma_i = \frac{\theta^\sigma_i}{N_i} \tag{7.8}$$

In order to define a surface excess, we need to choose a Gibbs reference plane, z^{Gibbs}. This is taken with respect to water,

$$z^{\text{Gibbs}} = \frac{\theta^\sigma_W}{\varphi_W(1) - \varphi_W(M)} \tag{7.9}$$

where $\varphi_W(1)$ is the volume fraction of water in the vapour phase and $\varphi_W(M)$ is the volume fraction of water in the water rich phase. Now the Gibbs excess of each component is given by

$$\Gamma_i = \frac{\theta^\sigma_i - z^{\text{Gibbs}} \left(\varphi_i(1) - \varphi_i(M) \right)}{N_i} \tag{7.10}$$

7.8 Results and discussion

7.8.1 The water - liquid CO_2 interface

The experimentally determined water - liquid CO_2 interfacial tension (IFT) as a function of time, for different bulk concentrations (between 0.01 and 1.2 %

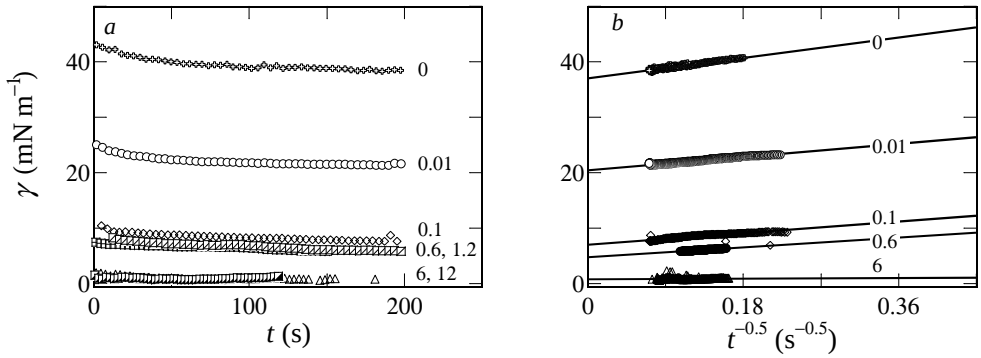

Figure 7.2: *(a) Dynamic interfacial tension between water and liquid* CO_2 *at 50 bar and 283 K for different surfactant concentrations in bulk liquid* CO_2 *as indicated (in (v/v)%). (b) The same IFT data plotted as a function of* $t^{-0.5}$*. The IFT data points are extrapolated to* $t \to \infty$*.*

v/v) of Igepal CA520 in CO_2, is depicted in Figure 7.2(a). The measurements were continued upto 200 s. The temperature and pressure ranges are selected based on the conditions used in liquid CO_2 dry-cleaning,[4] which are ~ 50 bar (i.e. $P/P_{\text{sat}} \approx 1.2$) and 283 K.

The densities of the CO_2 rich and CO_2 saturated water phases at the experimental pressures and temperatures were calculated using the equation of state of Span and Wagner[19] and Equations (3) and (4) in.[20] Further details can be found in[10] and the references therein.

The water - CO_2 IFT clearly depends on the bulk concentration of the surfactant in liquid CO_2: the higher the concentration, the lower is the interfacial tension. This is the expected behaviour.

To obtain the equilibrium interfacial tension (γ_{eq}) corresponding $t \to \infty$, we re-plotted the data (γ_t) of Figure 7.2a against $t^{-0.5}$ and extrapolated to zero (Figure 7.2b) following the well-known Ward and Tordai long-time approximation[21] as given by

$$\gamma_t = \gamma_{\text{eq}} + k \left(\frac{1}{\pi D t} \right)^{0.5} \tag{7.11}$$

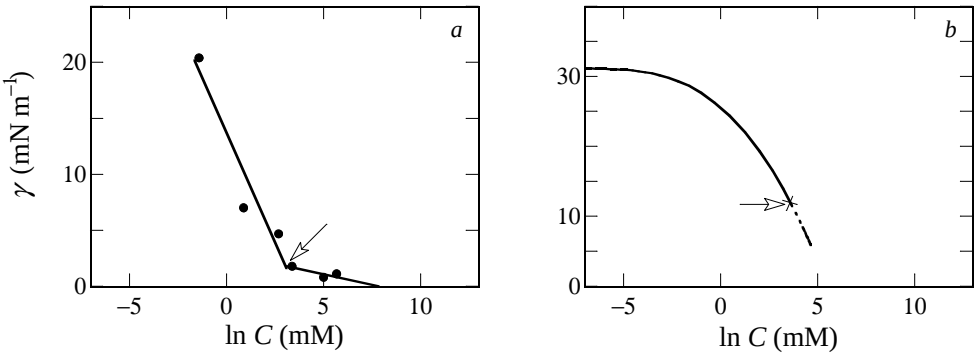

Figure 7.3: *(a) Equilibrium water - liquid* CO_2 *interfacial tension as a function of* $\ln C$*, the bulk concentration of surfactant in liquid* CO_2 *at 50 bar and 283 K. The experimental reverse micellar concentration of* $\sim$ *50 mM is indicated. The two solid lines are linear fits of the experimental data points (b) Water - liquid* CO_2 *IFT calculated from SF-SCF theory (at* $P/P_{\mathrm{sat}} = 1.2$*). The theoretical reverse CMC is* $\sim$ *40 mM and indicated in the figure.*

In Equation 7.11, k is an experimental constant and D is the diffusion coefficient of the surfactant in liquid CO_2. The intercepts obtained on the y-axis in Figure 7.2b correspond to the equilibrium IFT data (γ_{eq}) for each bulk concentration. Although the interfacial tensions were measured for six different bulk concentrations, for clarity, only four surfactant concentrations are shown.

The γ_{eq} values obtained from Figure 7.2b are plotted against the natural logarithm of the bulk concentration ($\ln C$) in Figure 7.3a. We notice a CMC like behaviour, i.e. a change in slope of γ_{eq} *versus* $\ln C$ beyond a concentration of $\sim$ 50 mM. We take this value as the critical reverse micellar concentration (CRMC) of Igepal CA520 in liquid CO_2.

The IFT - $\ln C$ curve obtained from self-consistent field modelling is presented in Figure 7.3b. The calculations were done at $P/P_{\mathrm{sat}} = 1.2$ and $T = 283$ K. In our model the value of P_{sat} is $\sim$ 110 bar[10] at 283 K.

The match between the experiment and model is reasonable, keeping in mind that no *a posteriori* parameter fitting was attempted to match these two

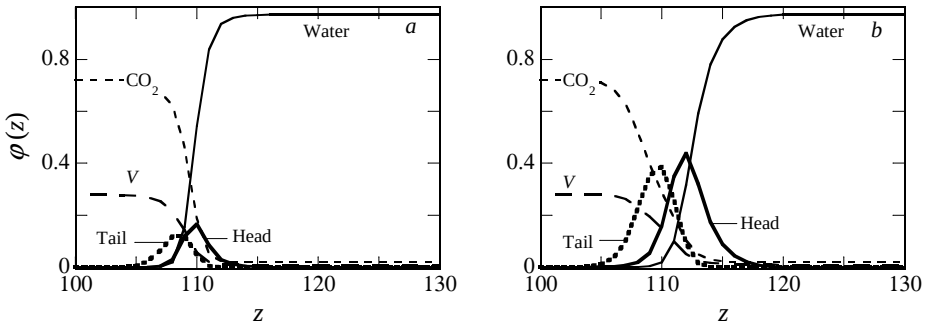

Figure 7.4: *SCF volume fraction profiles of various molecular species at the water - liquid* CO_2 *interface for a* φ^b_{surf} *of (a)* 1×10^{-8} *and (b)* 1×10^{-6} *in the water phase. The bulk* CO_2 *and water phases are situated at the left and the right side of the figures, respectively. The layer numbers* z *are arbitrary.* $P/P_{\text{sat}} = 1.2$ *and* $T = 283$ *K.*

values. According to the model, the CRMC appears at ~ 40 mM, as indicated in Figure 7.3b while the experimentally measured reverse CMC was ~ 50 mM (Figure 7.3a).

The theoretical IFT - $\ln C$ curve does not display a CMC like cusp. This was expected as the experimental "cusp" is in fact an experimental "artefact". In the IFT calculation involving the water - CO_2 interface, the model assumes the surfactant chemical potential to simply increase; it does not take into account the self-assembly process taking place in the bulk and the presence of micelles must be inferred from complementary calculations; we discuss this in section 7.8.3.

Next we looked at the adsorption of the surfactant at the water - CO_2 interface with increasing φ^b_{surf} in the water phase (Figure 7.4). Figures 7.4a and 7.4b correspond to a φ^b_{surf} of 10^{-8} and 10^{-6}, respectively. We clearly see an accumulation of surfactant at the water - liquid CO_2 interface. This excess surfactant at the interface lowers the water - CO_2 interfacial tension as found experimentally (Figure 7.2). The surface excess increases with increasing bulk concentration. Moreover, we see that the hydrophilic head and the hydrophobic tail groups are disposed towards the water and the CO_2 phases, respectively. At the water - CO_2 interface we also notice an accumulation of

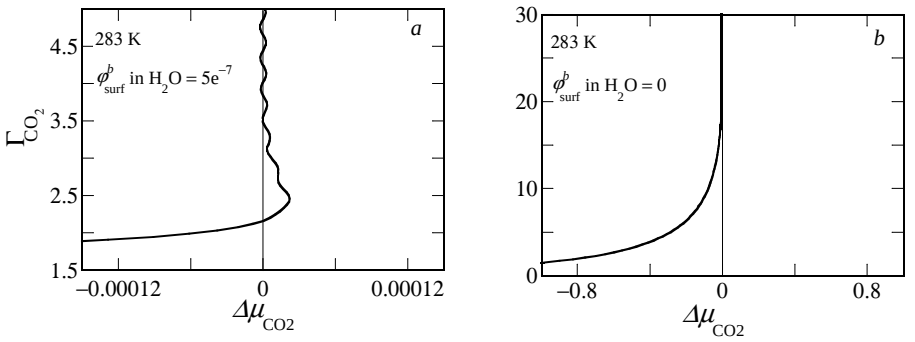

Figure 7.5: *Gibbs excess of* CO_2 *at the water - vapour interface as a function of* $\Delta\mu_{CO_2} = \mu_{CO_2} - \mu^{\#}_{CO_2}$*, where* $\mu^{\#}$ *is the chemical potential at coexistence, that is, at the binodal (a) in presence of a volume fraction of* 5×10^{-7} *surfactant in the water phase and (b) in absence of the surfactant. The adsorption isotherm in (a) indicates that the* W *-* V *interface is partially wet by* CO_2*, whereas in case of (b)* CO_2 *completely wets the* W *-* V *interface.*

the free volume, that is, a reduction in density.

7.8.2 Wetting transitions

In the previous result we focussed on the interface between water and CO_2. Such interfaces naturally develop when the pressure increases to values beyond saturation, so that liquid CO_2 is present in macroscopic amounts. However, at lower amounts of added CO_2 we have a water - vapour interface. We saw before that with increasing CO_2 concentration, liquid CO_2 appears at the water - vapour interface, or equivalently that the water - vapour interface is wet by liquid CO_2.[10]

We now consider what happens in the presence of the surfactant. As already explained, this involves the construction of adsorption isotherms of CO_2 at the W - V interface at a fixed concentration of surfactant in the bulk; in this context the bulk is the water-rich phase. The Gibbs excess of CO_2 (Γ_{CO_2}) is given as a function of the chemical potential of CO_2 in Figure 7.5a. The surfactant concentration in water (φ^b_{surf}) in this case is fixed at 5×10^{-7}. For comparison, we reproduce the result for $\varphi^b_{\text{surf}} = 0$ in Figure

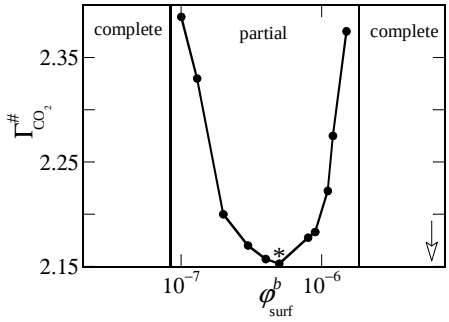

Figure 7.6: *Gibbs excess of* CO_2 *at the water - vapour interface when the isotherms crosses the bulk coexistence value for the first time,* $\Gamma^{\#}_{CO_2}$*, as a function of the surfactant concentration in water. For all surfactant concentrations* $\Gamma^{\#}_{CO_2}$ *was finite and thus we have partial wetting. The two vertical lines indicate estimates for the lower and the upper bounds of the surfactant concentrations at which* $\Gamma^{\#}_{CO_2}$ *diverges, that is where the two wetting transitions occurred. The arrow indicated the surfactant concentration in the water phase at which the first reverse micelles appear in the* CO_2 *phase. The density profile of the point indicated by the* $*$ *is given in Figure 7.7.*

7.5b. From the shape of the adsorption isotherm in Figure 7.5a, namely with an intersection of the line $\Delta\mu_{CO_2} = 0$ (saturation), we conclude that for this surfactant concentration the water - vapour interface is partially wet by CO_2. This implies that experimentally one expects the CO_2-phase to appear as a drop with a finite contact angle at the water - vapour interface.[22] The adsorbed amount, when the isotherm first crosses the coexistence condition, $\Gamma^{\#}_{CO_2}$, is finite.

Following this observation, we studied the surface phase diagram presented in Figure 7.6. In this figure we plotted the Gibbs excess (the excess surface density) of CO_2 at the binodal (i.e. at co-existence), denoted by $\Gamma^{\#}_{CO_2}$ as a function of φ^b_{surf}, which appears to be a control parameter to tune the wetting behaviour.

Without any surfactant or at extremely low surfactant concentration ($\varphi^b_{\text{surf}} < 10^{-7}$), liquid CO_2 is present as a macroscopic thick film at the W - V interface. As the surfactant concentration in the bulk increases, $\Gamma^{\#}_{CO_2}$ becomes finite and

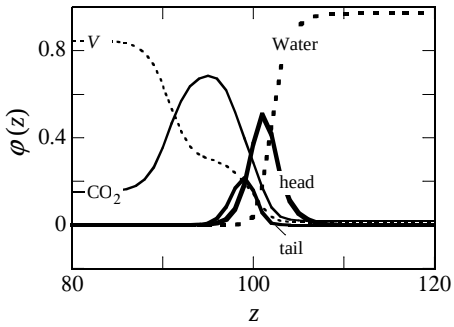

Figure 7.7: *Volume fraction profile of various molecular species at the three-phase co-existence of W, V and liquid* CO_2 *for a* φ^b_{surf} *of* 5×10^{-7} *in the water phase. The profiles correspond to the point in Figure 7.6 indicated by the asterisk. The layer numbers (z) are arbitrary.*

a phase transition takes place from complete wetting to partial wetting. Upon further increase of the surfactant concentration, $\Gamma^{\#}_{CO_2}$ goes through a minimum and increases again to a second divergence corresponding to a second wetting transition.

In summary, Figure 7.6 illustrates that there is re-entrant wetting behaviour: a window of surfactant concentrations for which the adsorbed amount of CO_2 remains finite and thus for which the water - vapour interface is not wet by CO_2. It was never observed that $\Gamma^{\#}_{CO_2}(\varphi^b_{\text{surf}})$ diverges jump-like when the wetting conditions are approached; this indicates that both transitions from partially wet to complete wet are most likely continuous, that is, they are of second order type. This is not too surprising because the CO_2 - vapour system is relatively close to its critical point. Wetting transitions near critical points tend to be of second order type.[23]

Density profiles of the various species in the co-existence region at which $\Gamma^{\#}_{CO_2}$ is minimum are shown in Figure 7.7. The profiles show that both CO_2 and the surfactant are present in excess at the W - V interface. The association of a finite amount of CO_2 with the surfactant layer is in line with the partial wetting of the W - V interface by CO_2, as explained above. We further notice that the surfactant head and tail groups reside in the water-rich and CO_2-rich

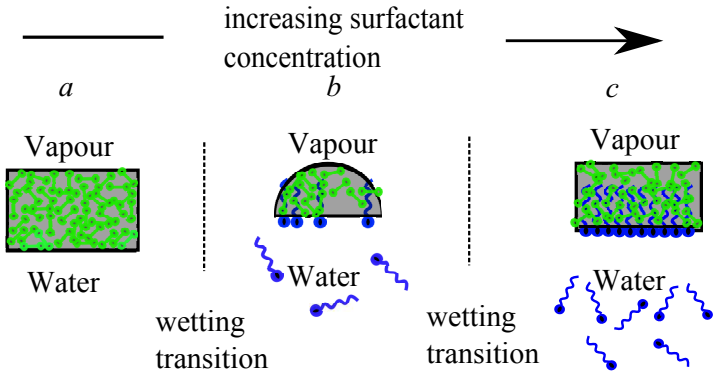

Figure 7.8: *Schematics of re-entrant wetting of* CO_2 *at the water - vapour interface. (a) A macroscopically thick* CO_2 *layer at the* W *-* V *interface without any surfactant (b) A drop of* CO_2 *at the* W *-* V *interface at a low concentration of surfactant and (c) Re-appearance of a macroscopically thick layer of* CO_2 *upon further increase of surfactant concentration.*

phases, respectively. Moreover, the density of the CO_2 layer at the interface does not reach the bulk value, but is associated with a high V content. Hence, a shoulder is found in the V profile.

The re-entrant wetting can be rationalised based on the following argument: without any surfactant a thick layer of CO_2 spreads at the W - V interface as shown in Figure 7.8a. This is in line with the critical point wetting as explained above. At low φ^b_{surf} when the interface is starved of surfactant monomers, CO_2 associates with the surfactant to form a less polar complex. This complex does not wet the $W-V$ interface (Figure 7.8b). CO_2 prefers to remain associated with the surfactant-rich islands. At higher φ^b_{surf}, the $W-V$ interface has a fully developed monolayer of surfactant spreading at the interface, which helps CO_2 to spread at the interface as well. This scenario is depicted in Figure 7.8c.

7.8.3 Self-assembly in bulk

Above we have discussed the calculations showing the effect of surfactant concentration on the water/CO_2 interfacial tension and wetting of the water - vapour interface by CO_2. In these calculations we used the surfactant concen-

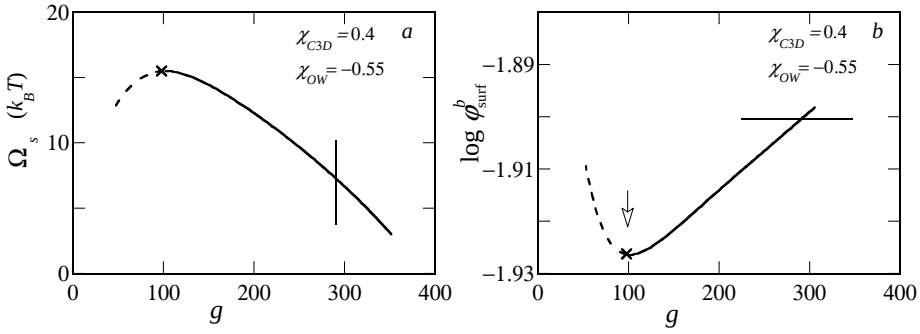

Figure 7.9: *(a) The grand potential Ω_s as a function of the surfactant aggregation number (g) for a spherical micelle with its center pinned to the center of the spherical coordinate system. (b) Corresponding $\log \varphi^b_{\text{surf}}$ as a function of the aggregation number g. The bulk volume fraction of water and free volume were taken to be consistent with three-phase co-existence conditions. The asterisks in (a) and (b) indicated the appearance of the first stable reverse micelles. The dashed regions of the curves indicated thermodynamically unstable reverse micelles. In panel (b) the horizontal line is drawn at the chemical potential above which surfactant bilayers appear in the water phase. In panel (a) the corresponding limit in the aggregation number g is indicated by the vertical line.*

tration (in the water-phase) as the control parameter. Until now we assumed that this concentration could be imposed arbitrarily. We realize that this is possibly flawed, because of the possibility that association colloids are formed in either the water or the CO_2-rich phases or even both. The occurrence of such phenomena puts an upper limit to the (free) surfactant concentrations that can exist in the (water) phase. In the following sections we study the formation of surfactant mesophases in both bulk liquid CO_2 (reverse micelles) and water (bilayers) phases individually.

Reverse micelles in liquid CO_2

For any micellization to occur there must be a driving force and a stopping mechanism in order to have stable micelles. This holds true for both common and reverse micelles. The moieties that form the core of the micelles necessarily provide the driving force, and the moieties that end up in the corona of the

micelles give the stopping force. The energy gain of the surfactant heads, which escape from the CO_2-rich phase, drives the assembly. Water co-assembles in the core, so the assembly is mediated by water. The loss in translational entropy of the chains goes against the micellization, and the hydrocarbon tails that want to remain solvated by CO_2 provide the stopping mechanism.

The grand potential (Ω_s) of a spherical micelle in the phase rich in CO_2 is plotted as a function of the surfactant aggregation number g (refer Equation 7.2) in Figure 7.9a in the phase rich in CO_2. The bulk volume fractions of water and free volume in the CO_2 rich phase correspond in this case to the three-phase co-existence conditions ($P = P_{\text{sat}}$).

Micelles in this phase are referred to as reverse micelles for obvious reasons. From Figure 7.9a we notice that Ω_s becomes more positive with increasing aggregation number and then goes through a maximum. As argued already, below the maximum (represented by the dashed part of the curve in Figure 7.9a), the micelles are not thermodynamically stable.[24] Micelles for which $\partial\Omega_s/\partial g < 0$, are thermodynamically stable. The smallest micelles that are stable (corresponding to the maximum) may be identified as the micelles at the theoretical (reverse) CMC.

The equilibrium bulk concentration of the surfactant as a function of the number of surfactant molecules in the micelles is presented in Figure 7.9b. The equilibrium concentration goes through a minimum at the same aggregation number where Ω_s shows a maximum. The value of φ^b_{surf} corresponding to the minimum can be identified as the reverse CMC and is found to be ~ 33 mM (indicated by the asterisk). The relevant part of Figure 7.9b (the solid curve) shows that with increasing size of the micelles the chemical potential increases slowly. We discuss below that there is a limit to this increase of the chemical potential, as surfactant bilayers may form in the water phase.

We also consider the effect of pressure (beyond P_{sat}) on self-assembly in CO_2. Pressure is varied by varying the volume fraction of the free volume in CO_2. The reverse micelles become smaller and the critical reverse micellar concentration (CRMC) shifts to higher concentration with increasing pressure (Figure 7.10). Apparently, liquid CO_2 becomes a better solvent for the

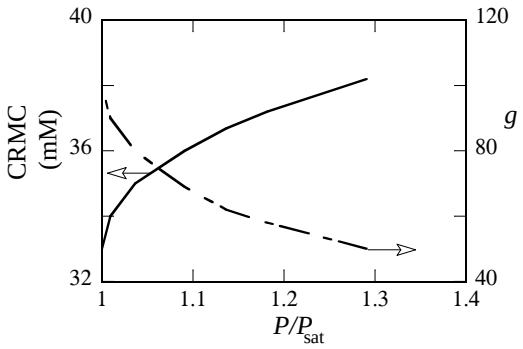

Figure 7.10: *SCF predictions for the reverse micellar concentration (left ordinate, solid curve) and aggregation number (right ordinate, dashed curve) as a function of (reduced) pressure* P/P_{sat}.

surfactant with increasing pressure and the stopping mechanism for reverse micellization becomes stronger due to better solvation of the surfactant tails, leading to smaller reverse micelles and a higher CRMC. The theoretical CRMC at $P/P_{\mathrm{sat}} = 1.2$ and temperature $T = 283$ K is ~ 40 mM. For the purpose of interpreting interfacial tensions, this value is indicated by the arrow in Figure 7.3b. The match between the experimentally determined CRMC (~ 50 mM, see Figure 7.3a) and the theoretically calculated one was reasonable taking into account that our model has not been fine-tuned. This is an interesting moment to assess the effects of two of the key parameters, namely, χ_{C3D} and χ_{OW} on the thermodynamics of micellization. The first one controls the solubility of the alkyl chain end in CO_2: it mediates the stopping mechanism. The second term expresses the tendency to co-assemble water in the reverse micelle: the more negative this value, the more water is taken up in the micelles. For this assessment, we return to the case of three-phase coexistence ($P/P_{\mathrm{sat}} = 1$). Results are shown in Figure 7.11a and Figure 7.11b.

In Figure 7.11a it is seen that with increasing repulsion between the methyl groups in the tail segment and CO_2, i.e. with increasing χ_{C3D}, decreasing the solvent quality, micelles with higher aggregation numbers are formed. This is seen by the shift of the maxima to higher aggregation numbers. Our interpret-

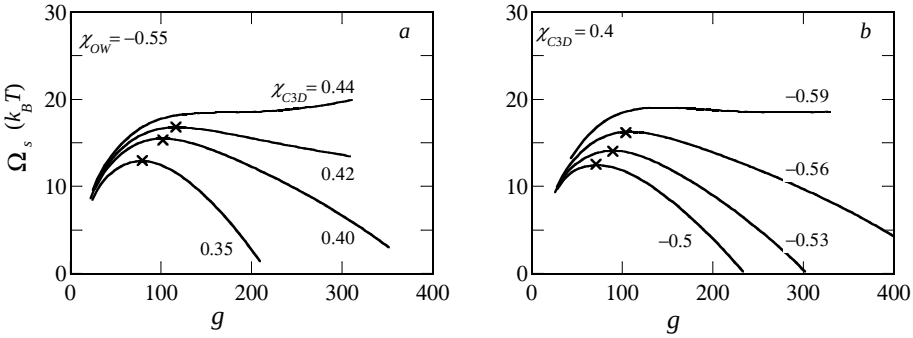

Figure 7.11: *Grand potential Ω_s as a function of aggregation number g for a spherical micelle (a) for various values of χ_{C3D} at fixed $\chi_{OW} = -0.55$ and (b) for various values of χ_{OW} at fixed $\chi_{C3D} = 0.4$. The volume fractions of water and free volume were taken to be consistent with three-phase coexistence i.e. at $P/P_{\rm sat} = 1$.*

ation is that the stopping mechanism becomes weaker with increasing χ_{C3D}, the tail segments reduce their contacts with CO_2 by forming larger reverse micelles, and they repel each other less. Moreover, we notice that $\partial\Omega_s/\partial g$ becomes less negative with higher χ_{C3D}, indicating more polydisperse (wider size distribution) reverse micelles.[16] Beyond $\chi_{C3D} = 0.42$ stable reverse micelles cannot be formed as $\partial\Omega_s/\partial g$ is no longer negative. This sets the upper limit of χ_{C3D} for having spherical reverse micelles in the CO_2-rich phase. Favourable tail-CO_2 interactions (lower χ_{C3D}) result in reverse micelles with lower aggregation number indicating a stronger stopping mechanism.

The effect of χ_{OW} can be seen from Figure 7.11b. An increase in attraction between the oxygen of the surfactant and with water, increases the driving force for reverse micellisation. Hence, the more negative χ_{OW}, the larger reverse micelles are formed, as evident from the shift of the maxima to higher aggregation number. Of course, with more driving force for self-assembly one should also provide a stronger stopping mechanism. In fact by fixing $\chi_{C3D} = 0.4$ the stopping force becomes gradually insufficient to limit the growth of the micelles. As a result we see a gradual growth of the micelle size distribution with more negative χ_{OW}-values, and beyond $\chi_{OW} = -0.56$ the spherical micelles lose stability ($\partial\Omega_s/\partial g$ is no longer negative). Hence,

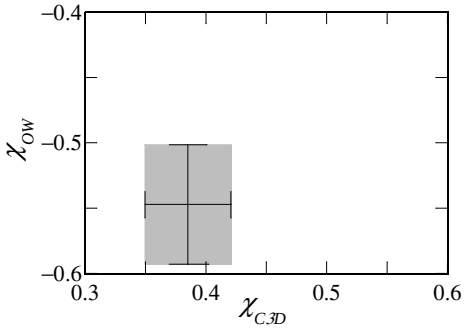

Figure 7.12: *The stability window (shaded area) for spherical reverse micelles with respect to two key interaction parameters, χ_{C3D} and χ_{OW} at $P/P_{\mathrm{sat}} = 1$. The volume fractions of water and free volume were taken to be consistent with three-phase coexistence, i.e. at $P/P_{\mathrm{sat}} = 1$.*

increasing attraction between water and the head group oxygen leads to reverse micelles with higher aggregation numbers, and eventually an insufficient stopping mechanism then leads to disappearance of spherical micelles.

Now that the window of stability of the spherical reverse micelles in the CO_2-rich phase (Figure 7.12) has been identified, it is worth to discuss the SCF prediction for the radial volume fraction distribution of the various segments in a typical reverse micelle having an aggregation number 150 (Figure 7.13a) . All interaction parameters have their default values (Table 1). The radial volume fraction profiles of a reverse micelle clearly prove the presence of significant amounts of water inside the core. In the corona the volume fraction of CO_2 is relatively high, which is consistent with the fact that the alkyl part of the surfactant is solvated by CO_2. In the corona some free volume is also present, imparting a reduced density to the tails.

Surfactant bilayers in the water phase

We saw that spherical reverse micelles can be thermodynamically stable, but that the parameter space with respect to χ_{OW} and χ_{C3D} is not particularly wide. In principle, we should also further analyse the stability of cylindrical

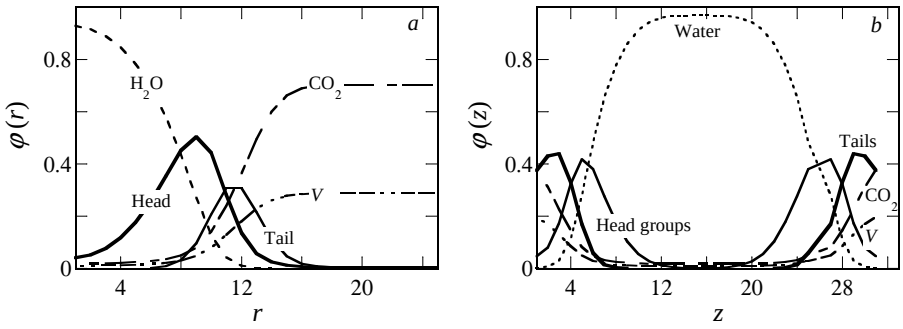

Figure 7.13: *Volume fraction distributions of various molecular species, (a) Radial distribution for a spherical micelle in the* CO_2 *rich phase with* $g = 150$ *and (b) Volume fraction distribution of molecular species for two halves of two tensionless bilayers situated at a center-to-center distance* $d = 30$ *in water. At the centre of both bilayers reflecting boundary conditions were applied implying an infinite array of bilayers. Both systems are at the three phase co-existence of water,* V *and* CO_2 *at 283 K. All parameters have the default values (Table 1).*

or lamellar structures in the CO_2-rich phase. For the moment we skip such an analysis and only mention that the competing association colloid that is identified in this system is a bilayer structure (lamellar) that may form in the water-rich phase, although we can not fully exclude that non-spherical micelles may form at elevated surfactant concentrations.

Turning our attention to the water phase, we performed calculations in which the bulk volume fractions of CO_2 and free volume in water were fixed to the values corresponding to the three-phase co-existence condition and 283 K. Considering the molecular architecture of the surfactant we note a relatively bulky apolar moiety (the alkyl and the benzene ring) and a relatively short ethylene oxide head group. This suggests a packing parameter of order unity. Therefore it is natural to consider the relative stability of bilayer membranes in the water-rich phase.

To study bilayers we select a planar lattice and pin the bilayer with its symmetry-plane to the edge of the lattice where we impose reflecting boundary conditions. In such a way we are able to remove the translational entropy of the

bilayer. Again we compute Ω_s, now as a function of the number of surfactants per unit area (g). We vary the number of surfactants in the bilayer until we find the condition that the bilayer is free of tension, that is when $\Omega_s = \gamma = 0$. We do not present the $\Omega(g)$ curve here. Instead, we directly discuss the structure of the bilayers found by this procedure. We notice that the chemical potential (i.e. $\log \varphi^b_{\text{surf}}$) associated with the reverse micelle formation in the CO_2-rich phase is lower than that associated with the formation of the bilayer in the water phase (-1.93 for the formation of reverse micelle *versus* -1.9 for the bilayer formation in water). Hence, the reverse micelles in the CO_2-rich phase comes first. As the surfactant concentration in the CO_2-rich phase increases further, the aggregation number of the reverse micelles increases and the chemical potential starts rising (as indicated in Figure 7.9b). This is not a favourable situation and the system can lower its free energy by forming bilayers in the water phase instead. In Figure 7.9b this is indicated by a horizontal line at the chemical potential at which the bilayers form. The aggregation number of micelles is therefore limited to $g \approx 290$. Accordingly, a vertical line in Figure 7.9a has been placed.

In Figure 7.13b we present the volume fraction profiles of the molecular components in the tensionless bilayer. Here we choose to plot the distributions over two bilayers which are separated by a core-to-core distance $d = 30$ (in lattice units). As reflecting boundary conditions were applied between layers $z = 0$ and $z = 1$ and between layers $z = 30$ and $z = 31$, it suffices to give only the distributions of half the bilayers. In between the bilayers there is a (bulk) water phase. The volume fractions of the free volume and CO_2 in this water phase are fixed according to the three-phase co-existence conditions.

We see that the head groups are associated with a finite fraction of water, whereas the tails are well shielded from water. We also notice that there are finite amounts of free volume ($\varphi_z \sim 0.2$) and CO_2 ($\varphi_z \sim 0.4$) accumulated in the tail region of the bilayer, making the bilayers quite compressible. It is rather important for the stability of these bilayers that there is just a finite amount of these "solvents" in the core. An unlimited swelling of the bilayers with CO_2 (and /or V) will hinder the stability of these mesophases. Appar-

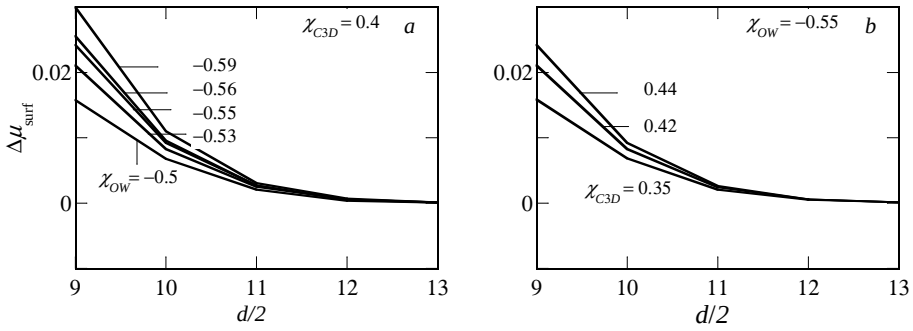

Figure 7.14: *Change in chemical potential ($\Delta\mu_{\rm surf}$) as a function of (half) the core-core distance between two bilayers with varying (a) for various χ_{OW} and fixed $\chi_{C3D} = 0.4$ and (b) for various χ_{C3D} at fixed $\chi_{OW} = -0.55$. The chemical potentials of CO_2 and free volume were chosen to represent three-phase coexistence ($P/P_{\rm sat} = 1$).*

ently there is a free energy barrier against the unbounded growth of the CO_2 and/or free volume phase in the bilayers, even though the chemical potentials allow for the formation of such phases. The finding that the swelling of the bilayers remain finite is in some respect surprising. As one might expect, when a V-phase would form in the bilayer, the CO_2 layer should spontaneously develop as well and grow without bounds: this is because the wetting study proved the absence of a barrier in this case. However, the V-phase cannot form in the absence of sufficient CO_2. Apparently, as a result there existed a barrier against the growth of the phases inside the bilayers. By which exact mechanism this barrier is put in place by the surfactant molecules remains unexplained.

The colloidal stability of the bilayers is further investigated by studying the inter-bilayer interactions as a function of distance (Figure 7.14). We follow the change in $\mu_{\rm surf}$ for the tensionless bilayers as a function of an imposed core-to-core distance between two bilayers d. More specifically, we focus on $\Delta\mu(d)$, which is the difference in chemical potential of the surfactants when two bilayers are at a certain distance d and when they are far apart, i.e. $d = \infty$. Physically, with decreasing d we mimic an increase of the total surfactant concentration in the water phase.

In Figure 7.14 interaction curves $\Delta\mu_{\text{surf}}$ are given for various values of the key interaction parameters χ_{C3D} and χ_{OW}. We observe that $\Delta\mu$ decreases with increasing d. Physically this means that the bilayers are repulsive. At large distances ($d/2 > 11$) we do not see any interaction between the bilayers, simply because the bilayers are not in contact with each other. The origin of the repulsion is not easily identified. Several phenomena occur simultaneously upon compression of the bilayers. As the membranes remain free of tension, the area per surfactant molecule adjusts itself. This implies some deformation of the surfactant layer, that is, the corona may be compressed or the tails may be squeezed.

As can be seen in Figure 7.14a, with increasing favourable interactions between O and W (more negative χ_{OW}), the repulsion between the bilayers increases. This was expected, as more favourable interactions between the head group oxygen and water means more resistance towards compression, leading to higher repulsion and more stable bilayers.

Similar behaviour is noticed when the parameter χ_{C3D} is varied keeping a constant χ_{OW} (Figure 7.14b). The higher χ_{C3D}, the stronger is the repulsion between the $C3$ and D segments, and the less CO_2 (and free volume) accumulate in the cores of the bilayers. Hence, it becomes more difficult to compress the bilayers. In this context, the molecular composition of the bilayers during compression is of interests. We consider the ratio between the number of CO_2 molecules and the number of surfactants in the bilayer, defined by the variable $x = \theta_{CO_2} N_{\text{surf}} / \theta_{\text{surf}} N_{CO_2}$. In Figures 7.15a and 7.15b we report x as a function of (half) the inter-bilayer spacing for varying χ_{OW} and χ_{CD}, respectively. We see that as the bilayers are compressed, for both the cases (varying χ_{OW} and χ_{CD}) the value of x decreases. Hence, the repulsion is in part due to the loss of CO_2 i.e., reduction of x. The number of surfactant molecules per unit area also decreases (not shown). This means that during compression the total membrane area increases. Nevertheless, the bilayer remains thermodynamically stable.

We further notice that the higher the attraction between the head group oxygen and W, the stronger is the decrease of x upon compression. This is

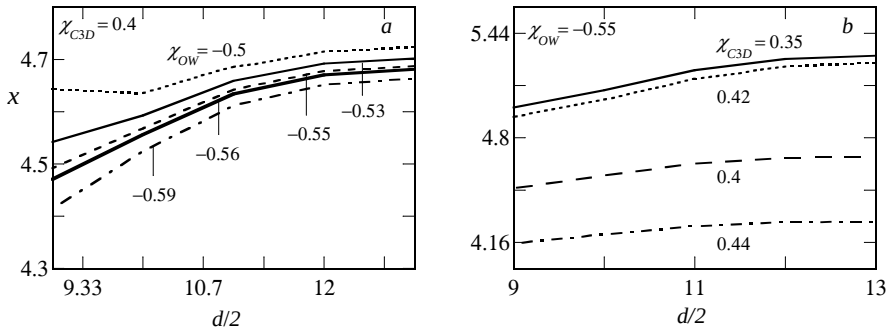

Figure 7.15: *Ratio x between the excess number of CO_2 molecules and the excess number of surfactant molecules in the bilayers as a function of compression for varying (a) χ_{OW} and (b) χ_{CD}. The volume fraction of water and free volume were taken to be consistent with three-phase coexistence ($P/P_{\mathrm{sat}} = 1$).*

because for more negative χ_{OW}, the increase of the excess surfactant molecules in the bilayers becomes energetically more favourable. Similarly, the penalty in energy to push out CO_2 molecules out of the bilayers becomes higher with increasing repulsion between the methyl groups of the tails and CO_2. The higher χ_{C3D}, the lower is the amount of CO_2 in the surfactant tail regions and the less compressible are the bilayers.

Above we noticed that the bilayers in the water phase are colloidal stable: they do not attract each other. In other words we do not see the formation of a lamellar phase. However, it must be mentioned that we do not account for attractive van der Waals interactions between bilayers. These interactions should be added to the pair potentials *a posteriori*.

7.8.4 Conclusion and outlook

We experimentally verified the interfacial activity of a branched hydrocarbon surfactant, Igepal CA520, at the water- CO_2 interface at 50 bar and 283 K. The IFT between water and liquid CO_2 decreases with increasing surfactant concentration in the bulk CO_2 phase. The experimental IFT - ln C curve shows a CMC like cusp and from this curve the onset of self-assembly in the

bulk was found to be $\sim$ 50 mM. These measurements were complemented by SCF modelling. Although the model needs many parameters, which are still subject to further optimisation, it is satisfying to mention that the model semi-quantitatively predicted the correct CRMC of $\sim$ 40 mM. The modelling results also deepened our understanding behind the molecular processes of wetting, adsorption and self-assembly in these systems.

Using the surfactant concentration as the control parameter, we predict a pair of wetting transitions for the CO_2 phase at the water - vapour interface. Both in the absence of surfactant and at high surfactant concentrations the water vapour interface is wet by CO_2. At intermediate surfactant concentrations, yet below the CRMC, the water - vapour interface is wet partially by CO_2. Intuitively we expected that this would affect the stability of the bilayers in the water phase, but this is not the case. Both wetting transitions, that is the wetting transition from complete to partial at the re-entrant wetting transition, are of the second order type. We are not too surprised by this, because the system is close to the critical point. Again, both wetting transitions occur below the critical reverse micellar concentration and therefore also below the bulk volume fraction of surfactant that is in equilibrium with the surfactant bilayers in the water phase.

The reverse micelles in liquid CO_2 are stable for a narrow range of χ_{OW} and χ_{C3D} at $P/P_{\text{sat}} = 1$. With increasing pressure the stopping force for micellisation becomes stronger. Hence, with increasing pressure the parameter window for the micellisation widens a bit. Nevertheless we found that the thermodynamic stability of the micelles is easily lost. This might explain in part why in practise the search for proper surfactants in liquid CO_2 systems has been so frustrating. Our results may pave the way to study the roles of various structural units, such as the length of the EO groups, the degree of branching and the number of $C3$ or C in the surfactant tail region, on the process of reverse micellization. The understanding emerging from these studies would provide guidelines for the design of surfactants for liquid CO_2.

We used the self-consistent field theory to compare the self-assemblies in the bulk CO_2 and in water. More specifically, we determined the chemical

potential needed for the formation of reverse micelles in the CO_2 rich phase and bilayers in the water phase. From this it follows that with increasing surfactant concentration first reverse micelles form in CO_2 followed by bilayers in water. These findings should be verified by X-ray or neutron scattering studies. Preliminary X-ray scattering data in a ternary system of Igepal CA520, liquid CO_2 and water show the signature of surfactant reverse micelles. These results can be found in Chapter 8.

Bibliography

[1] R. Nagarajan and E. Ruckenstein. Molecular Theory of Microemulsions. *Langmuir*, 16(16):6400–6415, 2000.

[2] R. Nagarajan and E. Ruckenstein. Theory of Surfactant Self-assembly: A Predictive Molecular Thermodynamic Approach. *Langmuir*, 7(12):2934–2969, 1991.

[3] W. Ryoo, S. E. Webber, and K. P. Johnston. Water-in-Carbon Dioxide Microemulsions with Methylated Branched Hydrocarbon Surfactants. *Ind. Eng. Chem. Res.*, 42(25):6348–6358, 2003.

[4] S. Banerjee, S. Sutanto, J. M. Kleijn, and M. A. Cohen Stuart. Towards Detergency in Liquid CO_2- A Surfactant Formulation for Particle Release in an Apolar Medium. *Colloids Surf. A Physicochem. Eng. Asp.*, 415(0):1–9, 2012.

[5] R. G. Larson, L. E. Scriven, and H. T. Davis. Monte Carlo Simulation of Model Amphiphile–Oil–Water Systems. *J. Chem. Phys.*, 83(5):2411–2420, 1985.

[6] M. Lísal, Carol K. H., Keith E. G., and A. Z. Panagiotopoulos. Self-Assembly of Surfactants in a Supercritical Solvent from Lattice Monte Carlo Simulations. *J. Chem. Phys.*, 116(3):1171–1184, 2002.

[7] S. Salaniwal, S. T. Cui, P. T. Cummings, and H. D. Cochran. Self-Assembly of Reverse Micelles in Water/Surfactant/Carbon Dioxide Systems by Molecular Simulation. *Langmuir*, 15(16):5188–5192, 1999.

[8] S. Salaniwal, S. Cui, H. D. Cochran, and P. T. Cummings. Molecular Dynamics Simulation of Reverse Micelles in Supercritical Carbon Dioxide. *Ind. Eng. Chem. Res.*, 39(12):4543–4554, 2000.

[9] S. Salaniwal, S. T. Cui, H. D. Cochran, and P. T. Cummings. Molecular Simulation of a Dichain Surfactant/Water/Carbon Dioxide System. 1. Structural Properties of Aggregates. *Langmuir*, 17(5):1773–1783, 2001.

[10] S. Banerjee, E. Hassenklöver, J. M. Kleijn, M. A. Cohen Stuart, and F. A. M. Leermakers. Interfacial Tension and Wettability in Water-Carbon Dioxide Systems: Experiments and Self-consistent Field Modeling. *J. Phys. Chem. B*, 117(28):8524–8535, 2013.

[11] B. R. Postmus, F. A. M. Leermakers, and M. A. Cohen Stuart. Self-Consistent Field Modeling of Non-ionic Surfactants at the Silica–Water Interface: Incorporating Molecular Detail. *Langmuir*, 24(8):3960–3969, 2008.

[12] Y. Sutjiadi-Sia, P. Jaeger, and R. Eggers. Interfacial Phenomena of Aqueous Systems in Dense Carbon Dioxide. *J. Supercrit. Fluids*, 46(3):272–279, 2008.

[13] A. Georgiadis, G. Maitland, J. P. M. Trusler, and A. Bismarck. Interfacial Tension Measurements of the (H_2O + CO_2) System at Elevated Pressures and Temperatures. *J. Chem. Eng. Data*, 55(10):4168–4175, 2010.

[14] P. Chiquet, J.-L. Daridon, D. Broseta, and S. Thibeau. CO_2/Water Interfacial Tensions Under Pressure and Temperature Conditions of CO_2 Geological Storage. *Energ. Convers. Manage.*, 48(3):736–744, 2007.

[15] O. A. Evers, J. M. H. M. Scheutjens, and G. J. Fleer. Statistical Thermodynamics of Block Copolymer Adsorption. 1. Formulation of the Model and Results for the Adsorbed Layer Structure. *Macromolecules*, 23(25):5221–5233, 1990.

[16] F. A. M. Leermakers and J. M. H. M. Scheutjens. Statistical Thermodynamics of Association Colloids: V. Critical Micelle Concentration, Micellar Size and Shape. *J. Colloid Interface Sci.*, 136(1):231–241, 1990.

[17] M. J. Hollamby, K. Trickett, A. Mohamed, Rogers S. E. Eastoe, J., and R. K. Heenan. Surfactant Aggregation in CO2/Heptane Solvent Mixtures. *Langmuir*, 25(22):12909–12913, 2009.

[18] M. Schick. *Liquids at Interfaces, Proc. Les Houches Session XLVIII, 1988*, page 416, 1990.

[19] R. Span and W. Wagner. A New Equation of State for Carbon Dioxide Covering the Fluid Region from the Triple–Point Temperature to 1100 K at Pressures up to 800 MPa. *J. Phys. Chem. Ref. Data*, 25(6):1509–1596, 1996.

[20] A. Hebach, A. Oberhof, and N. Dahmen. Density of Water+Carbon Dioxide at Elevated Pressures: Measurements and Correlation. *J. Chem. Eng. Data*, 49(4):950–953, 2004.

[21] P. Joos and V. B. Fainerman. Dynamic Surface Phenomena. 1999.

[22] B. V. Derjaguin, N. V. Churaev, and V. M. Muller. *Surface Forces*. New York: Plenum Press, 1960.

[23] J. W. Cahn. Critical Point Wetting. *J. Chem. Phys.*, 66(8):3667–3672, 1977.

[24] P. N. Hurter, J. M. H. M. Scheutjens, and T. A. Hatton. Molecular Modeling of Micelle Formation and Solubilization in Block Copolymer Micelles. 1. A Self-Consistent Mean-Field Lattice Theory. *Macromolecules*, 26(21):5592–5601, 1993.

[25] J. M. H. M. Scheutjens and G. J. Fleer. Statistical Theory of the Adsorption of Interacting Chain Molecules. 1. Partition Function, Segment Density Distribution, and Adsorption Isotherms. *J. Phys. Chem.*, 83(12):1619–1635, 1979.

[26] O. A. Evers, J. M. H. M. Scheutjens, and G. J. Fleer. Statistical Thermodynamics of Block Copolymer Adsorption. Part 2.–Effect of Chain Composition on the Adsorbed Amount and Layer Thickness. *J. Chem. Soc., Faraday Trans.*, 86(9):1333–1340, 1990.

[27] L. A. Meijer, F. A. M. Leermakers, and J. Lyklema. Self-Consistent-Field Modeling of Complex Molecules with United atom Detail in Inhomogeneous Systems. Cyclic and Branched Foreign Molecules in Dimyristoylphosphatidylcholine Membranes. *J. Chem. Phys.*, 110(13):6560–6579, 1999.

Appendix

SCF formalism for planar geometry

The water - liquid CO_2 and water - vapour interfaces as well as the bilayer formation in the water phase have been modelled using planar lattices. Calculation of the volume fraction of segments s of chain i containing N segments follows from the chain segment weighting factors, $G_i(z, s|1; N)$. The notation implies that for a chain there are two complementary walks that begin from opposite ends, one from segment 1 and the second from the other end, N. Both these walks terminate at s, which is at coordinate z. The composition law combines the two walks consisting of $s-1$ and $N-s$ steps, respectively.[15,25,26]

$$G_i(z, s|1; N) = \frac{G_i(z, s|1)G_i(z, s|N)}{G_i(z, s)} \tag{7.12}$$

The term in the denominator, which is the statistical weight of a free segment s at coordinate z, is included in both the walks and corrects for double counting. The summation over all segments $s = 1, \cdots, N_i$ of all these distribution functions results in the volume fraction of molecule i in layer z and is given by,

$$\varphi_i(z) = C_i \sum_{s=1}^{N_i} \frac{G_i(z, s|1)G_i(z, s|N)}{G_i(z, s)} \tag{7.13}$$

C_i is a normalization factor and is given by,

$$C_i = \frac{\theta_i}{N_i G_i(N|1)} \tag{7.14}$$

where the single chain partition function

$$G_i(N|1) = \sum_z G_i(z, N|1) \tag{7.15}$$

and

$$\theta_i = \sum_i \varphi_i(z) \tag{7.16}$$

The end point distribution functions are calculated using a propagator scheme. We gave the propagator formalism of small molecules such as CO_2 and water in our previous publication[10] and in this section we deal with the surfactant, which is a chain like molecule.

The free segment distribution function for segments at layer z, is $G_i(z,s)$. This quantity is related to the free segment distribution function of a segment type X at co-ordinate z, $G_X(z)$, while segment s is of type X. Mathematically,

$$G_i(z,s) = \sum_X \delta_{i,s}^X G_X(z) \tag{7.17}$$

Here X represents the segment types ($C3$ or C or O) and the summation is over all segment types. $\delta_{i,s}^X$ is unity if the segment s of molecule i is of type X and zero for all other types of segments. The forward and backward propagators read

$$\begin{aligned} G_i(z,s|1) &= G_i(z,s) \sum_{z'=z-1,z,z+1} \lambda_{z-z'} G_i(z^{'}, s-1|1) \\ &= G_i(z,s) \left\langle G_i(z,s-1|1) \right\rangle \end{aligned} \tag{7.18}$$

$$\begin{aligned} G_i(z,s|N) &= G_i(z,s) \sum_{z'=z-1,z,z+1} \lambda_{z-z'} G_i(z^{'}, s+1|N) \\ &= G_i(z,s) \left\langle G_i(z,s+1|N) \right\rangle \end{aligned} \tag{7.19}$$

The angular parentheses stand for an average over three layers and $\lambda_{z-z'}$ is the *a priori* step probability to go from a layer $z^{'}$ to z. The propagators are started realizing that $G_i(z,1|1) = G_i(z,1)$ and $G_i(z,N|N) = G_i(z,N)$.

The segmental weighting factor for segment type X has already been discussed at length in our previous publication[10] and is given by

$$G_X(z) = \exp\left(\frac{-u_X(z)}{k_B T}\right) \tag{7.20}$$

where,

$$u_X(z) = \alpha(z) + k_B T \sum_Y \chi_{XY}(\langle\varphi_Y(z)\rangle - \varphi_Y^b) \tag{7.21}$$

$G_X(z)$ is the probability of finding a free segment X in layer z relative to that of finding it in a layer in the homogeneous bulk solution.[10]

The first term in Equation Equation 7.21 is the Lagrange parameter, an entropic term, which represents the excluded volume interactions with respect to the bulk solution and is independent of the segment type; $\alpha(z)$ is an adjustable parameter, which ensures the the incompressibility condition $\sum_i \varphi_i(z) = 1$ in each layer. The second term is an enthalpic term and arises from interactions between segments X and Y; $\langle\varphi_Y(z)\rangle$ is the site average volume fraction of Y in layer z and contains contact contributions from neighbours in layer $z-1$, z and $z+1$. The site volume fractions, which are an average over three consecutive layers are given by,

$$\langle\varphi_X(z)\rangle = \lambda_{-1}\varphi_X(z-1) + \lambda_0\varphi_X(z) + \lambda_1\varphi_X(z+1) \tag{7.22}$$

where $\lambda_{z'-z}$ is the fraction of contacts of a site in layer z with sites in layer z' with z' equal to $z-1$, z or $z+1$. The first term inside the summation in Equation 7.21) is the Flory-Huggins interaction parameter (χ) and takes into account the short range attractive and repulsive interactions between molecules at segment levels. The final term in Equation 7.21 is the excess volume fraction of segment Y in layer z (averaged over three consecutive layers) with respect to the bulk volume fraction of Y, φ_Y^b.

We have so far given the expressions for linear molecules having different segments in their backbone. The surfactant molecule that we used in our model contains $C3$ branching and also the benzene ring was represented as a branched moiety. The propagators for this type of molecule can be found in.[27] In the next section we delineated the differences between the flat and spherical lattices.

Details for spherical lattice

The formation of spherical self-assembled objects was studied by placing the molecules inside a spherical lattice and the SCF machinery was adjusted accordingly. In a spherical lattice we specified $r = 1, \cdots, r_M$ layers, the first layer being at the centre of the lattice. At the other end, i.e. right after layer r_M, a mirror like boundary condition was imposed. Unlike in the planar lattice, the number of lattice sites, $L(r)$ is a non-trivial function of the coordinate r. More specifically for spherical geometry $L(r) = V(r) - V(r-1)$, where, $V(r) = \frac{4}{3}\pi r^3$ is the volume of the layer r. The key difference with the planar lattice is that the number of lattice sites is different in each layer and hence λ_{-1}, λ_0 and λ_1 are functions of the radial coordinate r. The "inversion symmetry" dictates

$$\lambda_{-1}(r)L(r) = \lambda_1(r-1)L(r-1) \tag{7.23}$$

As $L(r)$ is an increasing function of r, the transition probabilities λ also become r-dependent. The expressions are given below.

$$\lambda_1(r) = \lambda_1^b \frac{S(r)}{L(r)} \tag{7.24}$$

and

$$\lambda_{-1}(r) = \lambda_{-1}^b \frac{S(r-1)}{L(r)} \tag{7.25}$$

and

$$\lambda_0(r) = 1 - \lambda_1(r) - \lambda_{-1}(r) \tag{7.26}$$

The λ_1^b and λ_{-1}^b in the above equations are the correcting factors pertaining to the equivalent planar lattice and $S(r) = 4\pi r^2$ is the contact area.

The total amount of molecule i, θ_i, is related to the volume fraction of molecule i in layer r by

$$\theta_i = \sum_i L(r)\varphi_i(r) \tag{7.27}$$

and the single chain partition function, $G_i(N|1)$ reads in this geometry:

$$G_i(N|1) = \sum_i L(r) G_i(r, N|1) \tag{7.28}$$

The notations have the same meaning as those explained for the planar lattice case.

Chapter 8

Is Igepal CA520 Soluble in Liquid CO_2? And Does it Form Mesophases?

Surfactants for liquid CO_2 at 45-60 bar and 10 °C are rare to find. Even more difficult is to find soluble surfactants of hydrocarbon origin for this medium. In Chapter 4 and Chapter 6 we have introduced a branched non-ionic surfactant of C_iEO_j type, which gives detergency benefit in liquid CO_2 and is interfacially active at the water-liquid CO_2 interface. Numerical self-consistent field modeling has indicated that this surfactant can form self-assembled mesophases in liquid CO_2 in the presence of water. In this chapter, we first show conclusively by bubble point measurements that Igepal CA520 is soluble in liquid CO_2 at 45-60 bar and 5-10 °C. Secondly, we show by small angle X-ray scattering that it forms mesophases with or without water. In absence of water the surfactant forms a reverse micellar phase (L_2) and with the addition of water a phase transition to lamellar (L_α) liquid crystalline phases takes place. These studies indicate that water can be used as a mesogen (self-assembly promoter) in liquid CO_2.

The X-ray scattering curves show that a well-defined structure evolves beyond a critical water amount. The preliminary fitting of the data suggest

that the aggregates are of rod or disc like shape with a cross-section of ~ 4.6 nm, indicative of a bilayer arrangement. For the surfactant concentration of 0.3 and 0.67 M, the lamellar periodicity increases from $\sim$ 4 to 12 nm with increasing amounts of water.

8.1 Introduction

The state-of-the-art of surfactant research in liquid and supercritical CO_2 is given in detail in Chapter 2. Past research has shown that fluorinated surfactants are soluble in liquid CO_2 and in some of the cases they have been shown to form mesophases. But since fluorinated surfactants are not environmentally friendly, there was a need to find CO_2 soluble hydrocarbon surfactants. Branched hydrocarbon surfactants were found to be soluble in supercritical CO_2. Very recently it was shown by solubility measurements that linear polyoxyethylene non-ionic surfactants are soluble in liquid CO_2 at 45 - 60 bar and 10 °C.[1,2] However, it was not reported anywhere if these surfactants self-assemble in liquid CO_2. Although literature on self-assembly in liquid CO_2 is extremely rare to come across, self-assembly in supercritical CO_2 has been reported earlier[3–7]

In Chapter 4 we have introduced a branched, low molar mass, non-ionic surfactant of hydrocarbon origin, Igepal CA520 and tested its soil removal efficiency in a pilot scale dry-cleaning set up using liquid CO_2. A formulation was designed in hexane using Igepal and water and used as a pretreatment on fabrics. These fabrics were then cleaned in liquid CO_2. The formulation has shown benefit compared to the control. The control for this test were fabrics cleaned in liquid CO_2 without the pretreatment. In Chapter 6 we have presented the interfacial behavior of Igepal CA520 at the water-liquid CO_2 interface. The surfactant is interfacially active and the interfacial tension as a function of the surfactant concentration shows a CMC like cusp indicating the formation of self-assembled structures at higher surfactant concentrations. Our modeling results (Chapter 7) indicate that in a biphasic system of water and liquid CO_2, Igepal type of molecules can self-assemble. In Chapter 3,

we have argued that even though the presence of water is necessary for dry-cleaning, water can hinder the removal of particulate soil by forming capillary bridges between soil and fabric. However, Igepal CA520 can reduce the capillary force by an order of magnitude, as shown in Chapter 5. We hypothesized that the self-assembled structures of the surfactant play a crucial role in the reduction of the adhesion. Nevertheless, experimental evidences of solubility and mesophase formation of Igepal type of surfactants do not exist. Hence the aim of the work described in this chapter is to determine experimentally if Igepal CA520 is soluble in liquid CO_2 under dry-cleaning conditions, and if so, does it form mesophases? Moreover, we investigated the role of surfactant to water ratio in driving self-assembly in liquid CO_2.

8.2 Materials and methods

8.2.1 Cailletet apparatus

A Cailletet apparatus in the Process and Energy Laboratory of TU Delft was used to measure the solubility of Igepal CA520 in liquid CO_2. The pressure and temperature range of the apparatus is 1 to 150 bar and -18 to 197 °C, respectively. The operating principle is based on bubble point measurements. Measurements start at a fixed temperature with a phase separated sample and then pressure is increased so that one of the phases disappears upon solubilization. The apparatus consists of a glass tube of known dimension in which the liquid surfactant was dosed at atmospheric pressure. Subsequently the tube was connected to a gas rack followed by injection of gaseous CO_2. The mole of CO_2 is calculated from the equation of state of an ideal gas with the known values of volume, temperature and pressure. After this step the sample is de-aerated and sealed with mercury. The mercury transmits the pressure to the sample from the pressure generating device (see Figure 8.1). Pressure is changed by a hand pump and a dead weight pressure gauge measures the pressure inside the autoclave. The accuracy of the pressure measuring device is extremely high, of the order of $\pm$ 0.03 bar. A thermostatic liquid runs outside the tube to maintain the temperature of the sample. At

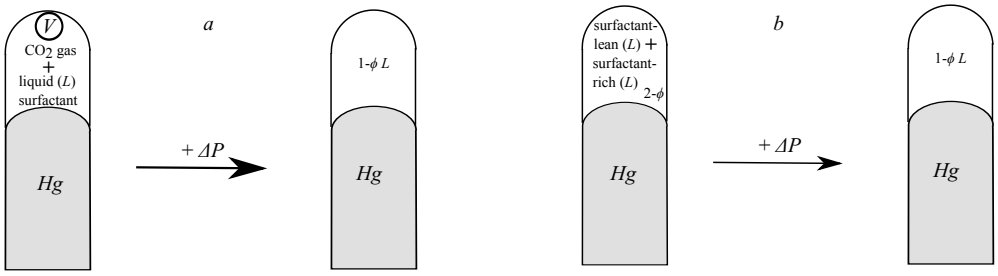

Figure 8.1: *Schematics showing the principle of bubble point measurement using the Cailletet apparatus. (a) (left) Two-phase L-V sample where the V phase is the* CO_2 *gas residing at the top of the Cailletet tube. (right) Upon increase of the pressure the vapour phase is converted into liquid and since there is no solubility gap between the surfactant and the liquid* CO_2*, one single liquid phase is obtained. (b) (left) Two immiscible liquid phases, one lean in surfactant and the other rich in surfactant. (right) With an increase of pressure both phases gets solubilized into each other resulting in one single liquid phase.*

a certain temperature, the pressure in the tube is increased so that gaseous CO_2 becomes liquid, its solvency power is improved and one liquid phase is formed with the surfactant (Figure 8.1). Mixing between the sample and the CO_2 gas bubble is provided by a stainless steel ball housed inside the tube. The ball is driven by reciprocating magnets.

After the attainment of one liquid phase, the sample is decompressed until the system phase separates again into gas and liquid. These steps are repeated until the phase separation is obtained within the accuracy of the Cailletet apparatus , i.e. $\pm$ 0.03 bar. These steps lead to one point on the liquid-vapour line of the *P-T* phase diagram. To get the next data point, the temperature is changed and the procedure is repeated.

Generation of the liquid-liquid line is done in a similar same way. In this case the phase separated sample consists of two liquid compositions, (Figure 8.1*b*) liquid CO_2 and liquid surfactant and it undergoes a phase transition to a single liquid phase. The disappearance and reappearance of the phases are detected by visual observation and hence analysis of the phase separated compositions is not possible in this type of measurements.

The solubility measurements were performed for a surfactant mole fraction

Figure 8.2: *The high pressure cell, fitted with two diamond windows, used to perform SAXS experiments in liquid* CO_2.

(n_S) of 0.2.

8.2.2 High-pressure cell

Small angle X-ray scattering (SAXS) experiments were performed using a high pressure cell (Figure 8.2). The cell has been designed and built in a collaboration between NWO (the Dutch Science Organization) and DPI (Dutch Polymer Institute) to perform *in situ* X-ray and neutron scattering measurements using liquid or supercritical CO_2.

The cell is made out of stainless steel and fitted with two single crystal diamond (type III) windows. The diameter and thickness of these windows are 6 mm and 0.4 mm, respectively. Mixing in the cell is provided by a magnetically coupled overhead stirrer. The volume of the cell is 54 ml.

A pressure transducer and a heating jacket with a CAL 3300 temperature controller are used to monitor and control the pressure and temperature inside the cell. The set-up is connected to a high pressure PM101 pump (New Ways of Analytics, Lörrach Baden-Württemberg, Germany) to charge CO_2 into the cell. The cell can handle pressure and temperature up to 300 bar and 120 °C,

respectively.

Our measurements were performed at 65 ± 4 bar and 11 ± 4 °C. Liquid CO_2 at these conditions has the same density (∼ 850 - 900 kg/m^3) as under industrial dry-cleaning conditions (refer Chapter 2). The temperature was maintained using an external thermostat fluid. After each measurement, the cell was depressurized and cleaned for subsequent experiments.

8.2.3 Small angle X-ray Scattering (SAXS)

SAXS experiments were performed at the Dutch-Belgian Beamline (DUBBLE, BM26-B) of the European Synchrotron Radiation Facility (ESRF) in Grenoble, France. The wavelength of the X-ray was 0.6526 Å and the sample to detector (Dectris-Pilatus 1M) distance was 3 m. Scattering patterns (2D) were recorded using the detector resolution of 981 * 1043 pixels and pixel size of 172 μm * 172 μm. The spectra were radially averaged and corrected for absorption, background scattering and primary beam intensity fluctuations. For the calibration of the wave-vector (q) scale of the scattering curve, the scattering patterns of silver behenate were used. In most of the cases, the intensities of the scattering curves were converted from an arbitrary to an absolute scattering cross-section using water as a secondary calibration standard. The scattering cross-section, $d\sigma(q)/d\Omega$ describes the number of scattered photons per unit time, relative to the incident photon flux, per unit solid angle at q, per unit volume of the sample and describes the intensity of the scattered photons at a certain angle i.e. $I(q)$.

$$\frac{d\sigma(q)}{d\Omega} = I(q) = n\Delta\rho^2 V^2 P(q) S(q) \tag{8.1}$$

where n is the number density of the aggregates, $\Delta\rho$ is the excess scattering length density, given by the difference in the electron density. The latter can be calculated from the partial specific density and composition. The volume of the aggregates is given by V. The form factor, which describes the shape of the aggregates and the structure factor, which describes the inter-aggregate interactions, are given by $P(q)$ and $S(q)$, respectively. The experimental $I(q)$

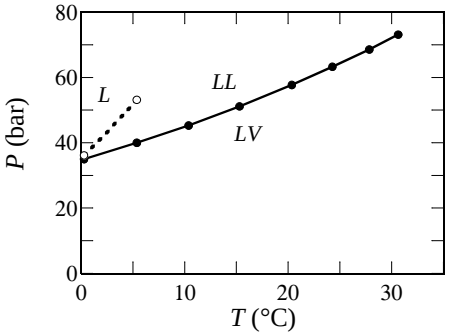

Figure 8.3: *P-T phase diagram of Igepal CA520 in liquid* CO_2 *at* $x_S = 0.2$ *as determined by bubble point measurement. L and V stand for liquid and vapour phases respectively. LL corresponds to two co-existing liquid phases, one surfactant-rich and the other surfactant-lean.*

vs q curve were fitted with the form factor of both a core-shell rod[8] or a disc-like[9,10] aggregate.

8.2.4 Sample preparation

Required amounts of surfactant and water were dosed in the cell at atmospheric pressure and the cell was then pressurized. After the desired pressure was reached, the stirrer was turned on and the samples were homogenized for 30 minutes and subsequently the spectra were collected.

The ternary compositions are represented by the mole ratio of water to surfactant, represented by x, and the concentration of the surfactant in M (moles/L).

8.3 Results and discussion

8.3.1 Solubility study: P-T phase diagram

We have used bubble point measurements to determine the solubility of Igepal CA520 in liquid CO_2. The P-T phase diagram of Igepal CA520 and CO_2 is given in Figure 8.3. The mole fraction of the surfactant, n_S, is 0.2. Two

types of phase transitions, liquid-vapour (LV) to liquid-liquid (LL) and liquid-liquid (LL) to single liquid (L) can be noted in Figure 8.3. The former phase transition is the solid curved line and the black dots are the experimental data points. The dashed line represents the LL to L transition. The open circles are the experimental data points.

Table 8.1: *Compositions of the ternary Igepal/ liquid* CO_2*/ water systems studied by SAXS. For explanation of the symbols, see the text.*

S	W	L_{CO_2}	n_S	n_W	$n_{L_{CO_2}}$	x	$\frac{mol_{H2O}}{mol_{EO}}$	C_S/CRMC	C_S (M)
1.7	0	98.3	0.01	0	0.99	0	0	0.8	0.04
10	0	90	0.09	0	0.91	0	0	5.4	0.27
10	5	85	0.05	0.52	0.44	11	2	5.7	0.29
10	10	80	0.03	0.69	0.28	25	4.5	6	0.31
10	20	70	0.02	0.84	0.15	45	9.1	9	0.35
20	5	75	0.09	0.52	0.39	6	1	13	0.65
20	10	70	0.06	0.70	0.24	11	2	14	0.7

Below the solid line the system is phase-separated into two phases, a gaseous CO_2 phase and a liquid surfactant phase. As the pressure is increased at a fixed temperature, the gaseous CO_2 undergoes a phase transition into liquid CO_2 and a composition consisting of two liquid phases results, one surfactant-rich and the other surfactant-lean. The partition of liquid CO_2 in both the liquid phases cannot be ascertained from these measurements.

At 0.28 °C and 36 bar, the system forms one single liquid from a liquid-liquid phase separated sample. This phase transition is important as here the surfactant and the liquid CO_2 become completely miscible. As the temperature is increased to 5 °C, the transition pressure from L-L to a single L phase also increases to 53 bar. This means that Igepal CA520 is soluble at 5 °C and 53 bar. Industrial dry-cleaning happens at 45-60 bar and between 5 and 10 °C. Hence around these conditions, Igepal CA520 will be above the cloud point.The LL to L phase transition line does not stop at 5 °C and 53 bar, but this is the highest point that has been determined in the present case.

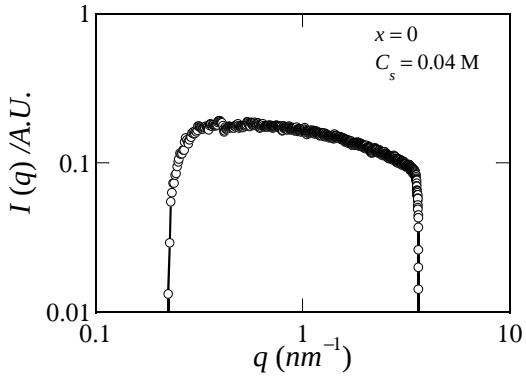

Figure 8.4: *SAXS curve for binary Igepal CA520/liquid* CO_2 *system. The concentration of the surfactant is 0.04 M. The ratio, x, which stands for the ratio of moles of water to moles of surfactant, is indicated in the figure.*

8.3.2 Determination of the phase behaviour: Small angle X-ray scattering

The phase behavior of the Igepal CA520/water/liquid CO_2 as a function of composition was probed by small angle X-ray scattering at 65 ± 4 bar and 11 ± 4°C. The ternary compositions used for scattering experiments are summarized in Table 8.1. The first three columns of Table 8.1 represent the concentration of the surfactant (S), water (W) and liquid CO_2 (L_{CO_2}) in volume %. Mole fractions of surfactant water and liquid CO_2 in the mixture are n_S, n_w and n_{LCO2}. The ratio of the moles of water to the moles of the surfactant is x and the ratio of the moles of water to the moles of EO is $5x$. The concentration of surfactant relative to the reverse micellar concentration (CRMC) is given as C_S/CRMC. The CRMC of the surfactant in liquid CO_2 at similar conditions is $\pm$ 50 mM (Chapter 7). The last column of Table 8.1 lists the concentration of Igepal CA520 in liquid CO_2 in M.

The surfactant concentration varies about the $\sim$ CRMC to 14 times above the CRMC. So when the surfactant concentration is below or just about at the CRMC, there should be either monomeric surfactant or reverse micellar aggregates in liquid CO_2. For this range of surfactant concentration we do not

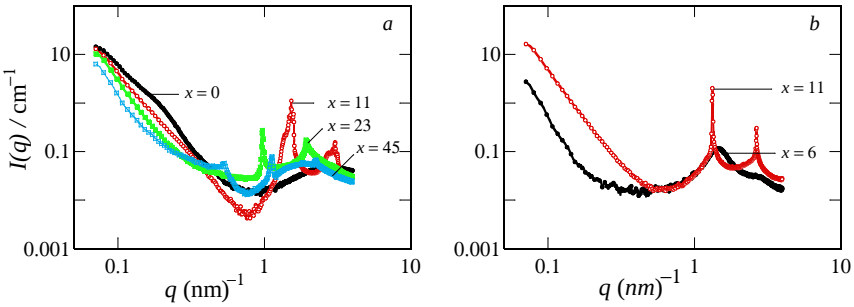

Figure 8.5: *SAXS curves of ternary systems containing Igepal CA520/water/liquid* CO_2*. (a) The surfactant concentrations,* C_S *are 0.27 M (black), 0.29 M (red), 0.31 M (green) and 0.25 M (blue). (b) The surfactant concentrations,* C_S*, are 0.65 M (black) and 0.7 M (red). The ratio, moles of water to moles of surfactant,* x*, is indicated for each curve.*

expect a phase transition in the binary system of liquid CO_2 and surfactant. In a ternary system where water is present as the third component, phase transition can be brought about by varying the amount of water alone. This is because water is known to drive the self-assembly of non-ionic surfactants with EO head groups in apolar solvents.[11–14] Hence, we analyzed the results in terms of the water to surfactant mole ratios (x) as we expect the phase diagram to scale with this particular ratio.

The intensity ($I(q)$) versus wave vector (q) for $C_S = 0.04$ M and $x = 0$ is presented in Figure 8.4. Since at this surfactant concentration the surfactant is not above the CRMC (C_S/CRMC = 0.8, Table 8.1), we do not see any significant scattering in the SAXS curve and this is in line with our expectations. This verifies the accuracy of our experimentally determined CRMC (Chapter 7) and gives confidence in the numerical modeling that augmented this.

SAXS results at 65 bar and 11 °C for the ternary system with $C_S \approx 0.3$ M and $x = 0$, 11, 23 and 45 are shown in Figure 8.5*a*. The SAXS pattern for the binary system ($x = 0$) shows the signature of isotropic mesophases (L_2). The $I(q)$ vs q curve shows a power law regime for $q > 0.2$ nm^{-1}. This indicates the presence of aggregates. In this case, we expect reverse micelles.

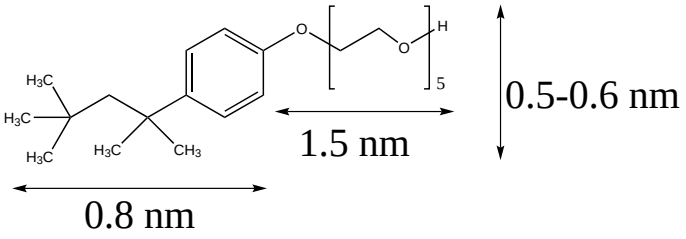

Figure 8.6: *Chemical structure and dimensions of Igepal CA520.*

The experimental $I(q)$ vs q curve could be fitted with the form factor of both a core-shell rod[8] or a disc-like[9,10] aggregate. Since the data at lower q range is not available, the presence of the rod could not be ascertained with a power law scaling of -1. Hence, from the fit we can only get the cross-sectional dimension, which indicates a thickness of ~ 4.6 nm. This implies a bilayer arrangement, the dimension being two times the length of the surfactant molecule (Figure 8.6). From the shoulder at low $q \sim 0.2$ nm^{-1}, we obtained the average distance between the aggregates as ~ 30 nm.

With the addition of water a different scattering pattern emerges, which can be clearly seen from the 2D diffraction pattern shown in Figure 8.7*a* - *e*. For $x = 11$ and 23 two peaks appear between $0.1 < q < 10$ with a q ratio of 1:2. This ratio is typical of ordered lamellar liquid crystalline phases (L_α). The lamellar periodicity, $d_{L\alpha}$ (Figure 8.7), can be obtained from the relation $q^* = 2\pi/d$ where q^* is the position of the diffraction peak of the highest intensity.[15]

We note that the peak with the highest intensity shifts to lower q values with increasing x, i.e. with higher water concentration. As the water amount increases (x from 11 to 23) $d_{L\alpha}$ increases from $\sim 4 - 4.5$ nm to ~ 6.5 nm, while the bilayer thickness remains constant at ~ 4.6 nm (see Figure 8.7*b* and *c*). The SAXS profile for $x = 23$ shows a well defined lamellar structure with a high order stacking as evident from the narrow and intense peaks of the first and second order.

For $x = 11$ and 23, the first peak is the highest intensity peak. However, for $x = 45$, the second peak is the highest one. At this stage we are unable to

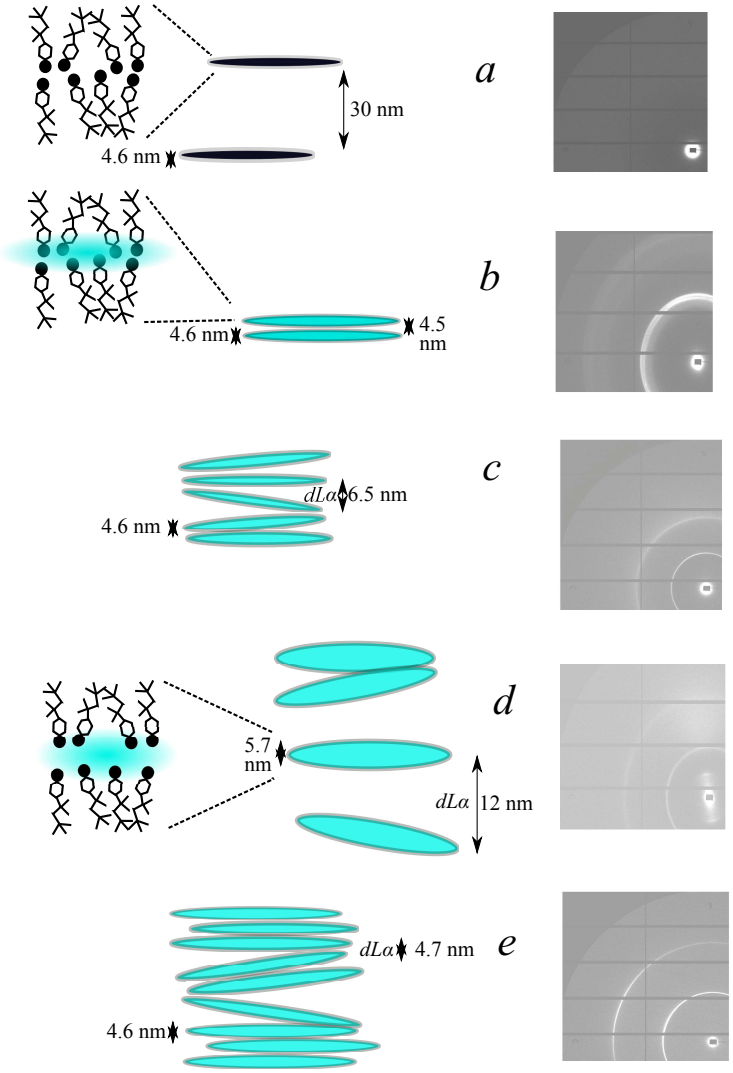

Figure 8.7: *Schematics showing the evolution of the lamellar liquid crystalline phase from the disc/rod like reverse micellar phase with the addition of water (a to e). On the right hand side of the figures the 2D diffraction patterns are also shown for each of the cases. The blue regions represent water. The lamellar periodicities ($d_{L\alpha}$) and the bilayer thickness (of the discs or cross-sections of the rods) are indicated.*

decipher from this the structure of the mesophase formed at this composition. There could be a co-existence of different liquid crystalline phases and then the $I(q)$ *versus* q pattern would result from of all the scattering contributions of the various mesophases. Further investigation is needed in order to ascertain the phase behaviour at or beyond this composition. Nevertheless, the bilayer thickness and the d-spacing, as obtained from the fit, were $\sim$ 5.7 nm and 12 nm respectively (Figure 8.7*d*). The increased d-spacing of the aggregates at $\sim$ 12 nm is clearly seen from the peak centred at around 0.5 nm^{-1}. An increase of the bilayer thickness from 4.6 nm to 5.7 nm may stem from the swelling of the bilayer with excess water.

In Figure 8.5b the SAXS curves for a higher surfactant concentration ($C_S \approx$ 0.7 M) and $x = 6$ and 11 are plotted. The $I(q)$ curve for $x = 6$ indicates a number of peaks at higher q values. The highest intensity peak is at $q = 1.47$ nm^{-1} and a small shoulder peak at $q = 2.84$ nm^{-1}. The peaks for $x = 6$ and 11 also obey a 1:2 ratio. For $x = 11$, the peaks are more intense and narrower indicating a well-defined lamellar structure and are slightly shifted to lower q values, corresponding to a slight increase in $d_{L\alpha}$ from 4.3 nm to 4.8 nm with the increase of water content from $x = 6$ to $x = 11$, respectively (Figure 8.7*d* and *e*). The fitted form factor reveals a bilayer thickness of $\sim$ 4.6 nm similar to the other composition.

These findings are summarized in the partial ternary phase diagram in Figure 8.8. The three axes represent surfactant, water and liquid CO_2 concentration in volume %. The symbols L_2 and L_α stand for reverse micellar and lamellar phases respectively. The dashed lines are water dilution lines. The question mark represent the un-identified phase at $C_S = 0.35$ M and $x =$ 45. The grey area encloses the region at which the systems contain L_α phases. Of course, the L_α region is not necessarily limited to the region between the measured compositions. The experimentally investigated compositions are indicated as black dots.

Our results are in line with the studies conducted by Pacynko *et al.* for C_iEO_j type non-ionic surfactants in heptane.[16] They showed that water can act as a promoter of self-assembly, i.e. as a mesogen in non-aqueous solvents.

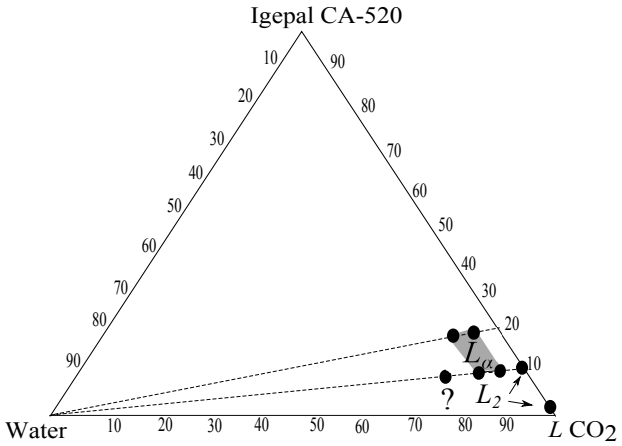

Figure 8.8: *The partial ternary phase diagram of Igepal CA520/water/liquid* CO_2 *at* 65 ± 4 *bar and* $11 \pm 4\,^\circ C$. L_2 *and* L_α *stand for reverse micellar and lamellar phases respectively. The dashed lines are water dilution lines. The question mark represents an un-identified phase. The grey area encompasses the region at which the composition is of* L_α *type. The black dots are the compositions chosen for SAXS experiments.*

They reported the aggregation of ethoxylated non-ionic surfactants in heptane and related the number of hydrophilic (EO) groups to the tendency of self-assembly and suggested the role of short-range interactions such as dipole-dipole, dipole-induced-dipole and dispersion interactions.[16] This implies that increasing the EO number results in a stronger driving force and a larger tendency for the aggregate formation in apolar media.

We also notice that qualitatively the phase behaviour of the Igepal CA520/liquid CO_2/water system is similar to that of the Igepal/hexane/water system. The latter system was introduced in Chapter 4 where a similar phase transition from the L_2 to the L_α phase was noted with the addition of water.

8.4 Conclusion and Outlook

It can be concluded from this chapter that Igepal CA520 is soluble in liquid CO_2 and it self-assembles in liquid CO_2 with added water. The phase behavior shows a classical pattern with increasing water to surfactant ratio, i.e. a transition from an isotropic, reverse micellar phase to an ordered liquid crys-

talline phase. Water promotes the self-assembly by acting as a mesogen i.e. it increases the driving force for the assembly of EO groups. The concentration of water is a key parameter, and beyond a critical water mole fraction the aggregates become well defined in shape. From the dry-cleaning perspective this means that the extra water that is added in the formulation can be successfully utilized in presence of Igepal type of surfactants by forming water induced mesophases. In this way, the detrimental effect of water towards the detergency of the particulate soil can be prevented and yet the water pool can be used for the enhanced removal of the polar soil. Moreover, based on the resemblance between the two ternary systems, IgepalCA520/liquid CO_2/water and IgepalCA520/hexane/water, it is noteworthy that hexane is a good model solvent for liquid CO_2. This finding can open up new possibilities not only for further research on amphiphiles but also for measurements, which are impossible to carry out in liquid CO_2 at this stage. Experimentation in liquid CO_2 system is not easy as it requires high pressure instrumentation. Moreover, even if high pressure equipment are available, generation of data is time consuming and difficult. Hence, an initial screening in a model solvent can be a good first step forward, as exemplified by this thesis.

Bibliography

[1] T. E. Sandoval and M. P. Gárate. Measurement of the Phase Behaviour of the Binary Systems Carbon Dioxide (CO_2 + Non-Ionic Surfactants (C_iEO_j). *J. Chem. Thermodyn.*, 45(1):109–113, 2012.

[2] T. E. Sandoval, M. P. Gárate, J. Scavia, L. J. Florusse, and C. J. Peters. Effect of the Ethoxy Groups Distribution on the Phase Behaviour of the Binary Systems Carbon Dioxide CO_2 with Industrial Non-Ionic Surfactants (C_iEO_j). *J. Chem. Thermodyn.*, 57:224–229, 2013.

[3] X. Dong, C. Erkey, H.-J. Dai, H.-C. Li, H. D. Cochran, and J. S. Lin. Phase Behavior and Micelle Size of an Aqueous Microdispersion in Supercritical CO_2 with a Novel Surfactant. *Ind. Eng. Chem. Res.*, 41(5):1038–1042, 2002.

[4] J. L. Fulton, D. M. Pfund, J. B. McClain, T. J. Romack, E. E. Maury, J. R. Combes, E. T. Samulski, J. M. DeSimone, and M. Capel. Aggregation of Amphiphilic Molecules in Supercritical Carbon Dioxide:A Small Angle X-ray Scattering Study. *Langmuir*, 11(11):4241–4249, 1995.

[5] J. Eastoe, A. Dupont, and D. C. Steytler. Fluorinated Surfactants in Supercritical CO_2. *Curr. Opin. Colloid Interface Sci.*, 8(3):267–273, 2003.

[6] J. Liu, J. Zhang, T. Mu, B. Han, G. Li, J. Wang, and B. Dong. An Investigation of Non-fluorous Surfactant Dynol-604 based Water-in-CO_2 Reverse Micelles by Small Angle X-ray Scattering. *J. Supercrit. Fluids*, 26(3):275–280, 2003.

[7] F. Triolo, A. Triolo, R. Triolo, J. D. Londono, G. D. Wignall, J. B. McClain, D. E. Betts, S. Wells, E. T. Samulski, and J. M. DeSimone. Critical Micelle Density for the Self-Assembly of Block Copolymer Surfactants in Supercritical Carbon Dioxide. *Langmuir*, 16(2):416–421, 2000.

[8] P. Lindner and T. Zemb. *Neutrons, X-rays and Light: Scattering Methods Applied to Soft Condensed Matter*. Elsivier Science, London, 2002.

[9] A.E. Blaurock. Evidence of Bilayer Structure and of Membrane Interactions from X-ray Diffraction Analysis. *Biochimica et Biophysica Acta (BBA) - Reviews on Biomembranes*, 650(4):167–207, 1982.

[10] M. R. Brzustowicz and A. T. Brunger. X-ray Scattering from Unilamellar Lipid Vesicles. *Journal of Applied Crystallography*, 38(1):126–131, 2005.

[11] K. Shinoda and H. Saito. The Effect of Temperature on the Phase Equilibria and the Types of Dispersions of the Ternary System Composed of Water, Cyclohexane, and Nonionic Surfactant. *J. Colloid Interface Sci.*, 26(1):70–74, 1968.

[12] M. Kahlweit, E. Lessner, and R. Strey. Influence of the Properties of the Oil and the Surfactant on the Phase Behavior of Systems of the Type Water-Oil-Nonionic Surfactant. *J. Phys. Chem.*, 87(24):5032–5040, 1983.

[13] R. Aveyard, B. P. Binks, and P. D. I. Fletcher. Interfacial Tensions and Aggregate Structure in Pentaethylene Glycol Monododecyl Ether/Oil/Water Microemulsion Systems. *Langmuir*, 5(5):1210–1217, 1989.

[14] S. Banerjee, S. Sutanto, J. M. Kleijn, and M. A. Cohen Stuart. Towards Detergency in Liquid CO_2 - A Surfactant Formulation for Particle Release in an Apolar Medium. *Colloids Surf. A Physicochem. Eng. Asp.*, 415(0):1–9, 2012.

[15] P. Alexandridis, U. Olsson, and B. Lindman. A Record Nine Different Phases (Four Cubic, Two Hexagonal, and One Lamellar Lyotropic Liquid Crystalline and Two Micellar Solutions) in a Ternary Isothermal System of an Amphiphilic Block Copolymer and Selective Solvents (Water and Oil). *Langmuir*, 14(10):2627–2638, 1998.

[16] Witold F. Pacynko, Jack Yarwood, and Gordon J. T. Tiddy. Infrared Spectroscopic Studies on the Aggregation of Polyoxyethylene Surfactants in hydrocarbon solvents. *J. Chem. Soc., Faraday Trans. 1*, 85:1397–1407, 1989.

Chapter 9

General Discussion and Outlook: From Surface Forces to Surfactant Design

In this final chapter we connect the major findings of this thesis and add some observations that did not get a place in one of the previous chapters. By making these connections, we can provide a fundamental picture of the physico-chemical aspects of the removal of particulate soil from textiles in liquid CO_2, which was one of the main goals of the work. In particular, surface forces in non-polar media are addressed, considering the effects of the additives water and alcohol, the nature of the surfaces (roughness and softness, hydrophobicity), and the mode of action of a surfactant (Igepal CA520), which was rationally chosen after thorough analysis of the detergency challenges in CO_2 dry-cleaning. Based on the obtained insights from experiments and numerical modelling, we further provide guidelines for the design of a suitable surfactants for liquid CO_2, thus meeting the other major goal of this thesis as well. Finally, remaining questions are identified and an outlook is given.

9.1 Introduction

As expounded in Chapters 1 and 2, colloidal interactions in liquid CO_2 from the perspective of dry-cleaning have hardly been addressed so far. This thesis is aimed at bridging this gap. In dry-cleaning industry, using liquid CO_2 as the medium of cleaning, a number of additives are used to aid the particle removal process. Among these additives water, surfactant and alcohol are the most important ones. To determine their effects, only phenomenological detergency tests were available, expressing the results in terms of the cleaning performance index (CPI). Therefore it remained unclear at a fundamental level why and how these additives work. Especially on the surfactant front the clarity was lacking. For example, an amine based surfactant (Amihope LL) was chosen in a quite ad hoc manner and was shown to improve the detergency; however, it was not even clear to which extent this surfactant is soluble in the medium, if it lowers the interfacial tension and if it forms self-assembled structures, let alone why it gave rise to a better cleaning performance.

This is where this work began. We started out with a thorough physico-chemical analysis of the causes of the existing problems in liquid CO_2 dry-cleaning and directions to solve them, which resulted in Chapter 2 of this thesis. We then introduced a systematic approach by measuring the interaction forces between a model fabric (cellulose) and a model soil particle (silica) in a non-polar model solvent (n-hexane) and investigating the effect of additives. This comprises the first part of the thesis (Chapters 3 to 5). The experimental work was extended to liquid CO_2 systems and these studies are captured in the second part of the thesis (Chapters 6 to 8).

In both the model solvent and in liquid CO_2 systems we studied the (phase) behaviour and effect of a surfactant prototype (Igepal CA520). We further built our understanding with the help of a numerical molecularly detailed mean-field model. This model helped us understand wetting phenomena at the water - CO_2 interface without or with surfactant, the bulk self-assembly behaviour of the surfactant in liquid CO_2 in the presence of water, and what details of the surfactant architecture are important to make it suitable for

liquid CO_2.

In this chapter we will summarize our findings, highlighting some of the key results. Some aspects which we could not discuss in previous chapters, but are deemed important, will also be outlined in this part. Based on experimental and modelling results, we will end the story with design rules for effective surfactants for liquid CO_2 and an outlook.

9.2 Surface forces in low dielectric media

Liquid CO_2 has an extremely low dielectric constant (1.6 at 60 bar and 10 °C) and this has major implications for the interaction forces between colloidal bodies through this medium. Generally, surface forces in low dielectric media are much less understood than those in aqueous solutions. For interactions in aqueous solutions experimental interaction curves are commonly interpreted using classical DLVO (Derjaguin-Landau-Verweij-Overbeek) theory, i.e., in terms of electrostatic interactions and van der Waals forces. It has been generally found that DLVO theory provides a good description for the interactions between surfaces at separations above, say 5 nm (at close separation so-called non-DLVO interactions, like hydration forces, hydrophobic attraction and steric interactions, play a substantial role). However, in ultra-low dielectric media like liquid CO_2 the charge density on any surface is low, Debye lengths are high (up to the micron scale) and salts hardly dissociate. On the other hand, van der Waals forces through liquid CO_2 can be much stronger compared to those across water, as shown in Chapter 2 for the interaction between a model soil particle (silica) and a model fabric surface (cellulose). Both the absence of charge on surfaces and the high van der Waals forces contribute to the problematic removal of soil particles from fabrics and their undesired redeposition in liquid CO_2 dry-cleaning. The presence of small amounts of water (without a suitable surfactant) increases these problems, as outlined below.

At the start of this project we chose n-hexane as a model for liquid CO_2, since it was very difficult or even impossible to perform all experiments that we

planned in liquid CO_2 (e.g., an atomic force microscope that operates under high pressure is still non-existing). The dielectric constant of n-hexane is very close to that of liquid CO_2, and like in liquid CO_2, trace amounts of water can be dissolved in it. In addition, n-hexane and liquid CO_2 are miscible in all proportions, illustrating their compatibility. In retrospect, the selection of n-hexane as a model for liquid CO_2 turned out to be an excellent choice indeed. We will come back to this in section 9.4.

9.3 The role of water

Chapter 3 is dedicated to the role of water in mediating the surface forces between a model fabric and soil particle. In CO_2 dry-cleaning, water is inherently present as a minor component in the medium. Moreover, extra water is added to liquid CO_2 to enhance the detergency of polar soils. It was known from previous detergency experiments that although extra water improves the detergency of polar soil, detergency of particulate soil deteriorates. The reason for this was unclear. We employed an atomic force microscope (AFM) to quantify the forces of interactions between a spin-coated cellulose layer and a silica particle (3 μm radius) immersed in n-hexane without and in the presence of water. The adhesion force in wet hexane was found to be much (five times) higher than in dry hexane and we attributed this higher force to the formation of water capillary bridges between the interacting surfaces in n-hexane. However, the measured capillary forces were still considerably lower than predicted by the theory of capillary condensation. This suggested that there was not one capillary bridge spanning the whole interaction area between the particle and the surface, but multiple smaller bridges, resulting from the roughness of the surfaces.

9.4 Roughness and softness of the surface

The roughness and the softness of interacting surfaces are both important factors determining the capillary adhesion due to the presence of water in

nonpolar media.

To obtain more insight into the effect of surface roughness, the kinetics of capillary bridge formation was further investigated. It was found that the adhesion force slowly increases in time (up to 200 s), in a logarithmic fashion. From the relation between the maximum adhesion force and the condensate volume it was concluded that our system falls into the asperity regime, meaning that multiple tiny water bridges are formed between the closest asperities at either of the surfaces. Both the slow kinetics and the asperity regime are in line with the roughness argument. These aspects are described in detail in Chapter 3.

We have quantified the softness of the cellulose surface by measuring its Young's modulus in water as well in n-hexane, using the quantitative nanomechanical mode of the AFM. The cellulose surface is three orders of magnitude softer in water than in hexane. This essentially implies that when the silica particle is pressed against the cellulose surface in water, the contact area increases and the resulting adhesion force can be much higher than in hexane. We hypothesized that the two very different Young's moduli of wet and dry cellulose pose different barriers towards the retraction of the silica particle from the cellulose surface.

We expect the formation of similar capillary bridges in water-saturated liquid CO_2. Liquid CO_2 can solubilize $\sim$ 1000 ppm of water at the relevant pressure and temperature conditions (see Chapter 2). Moreover, in reality the fabric surfaces are also rough and hence the detrimental effect of water on particulate soil removal as seen in detergency experiments is most probably due to water capillary bridge formation (hydrophilic) soil particles and fabric surfaces (complete wetting of water).

9.5 Hydrophobicity / hydrophilicity of the surfaces

In practice the soil mix and the fabric types can have any surface energy ranging from hydrophilic to hydrophobic. This topic has not been addressed yet in this thesis. To investigate the adhesion forces as function of varying sur-

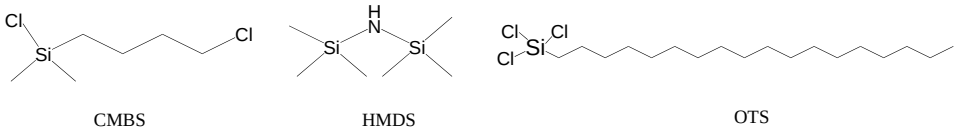

CMBS HMDS OTS

Figure 9.1: *Agents used for hydrophobic modification of silica surfaces. CMBS: cis-β-methylstyrene: HMDS: hexamethyldisilazane; OTS: octadecyltrichlorosilane.*

face energies, we chemically modified silica surfaces with various hydrophobic agents and characterized them by measuring the water contact angle. The hydrophobic agents are depicted in Figure 9.1. The silica particle was kept unmodified.

Again we measured the surface forces between the SiO_2 particle and the modified surface through water-saturated hexane and the results are summarized in Figure 9.2. As expected a clear decrease of capillary adhesion force is found with increasing water contact angle, i.e. with increasing surface hydrophobicity. Indeed, in practical detergency tests it has been found that in liquid CO_2 the removal of particulate soil from hydrophobic surfaces such as wool is better than from hydrophilic surfaces such as cellulose.[1]

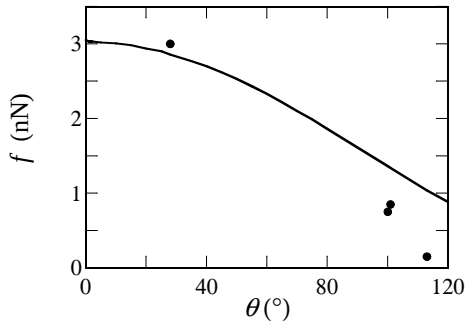

Figure 9.2: *Maximum capillary adhesion force between modified silica surfaces and an unmodified silica particle as a function of advancing water contact angle of water on the surfaces. The experimental data are represented by black dots. The solid curve is a fit of the model for capillary adhesion.*[2]

9.6 Effect of alcohol

Now that we have established the effect of water in relation to the properties of the surface and the particle, it is relevant to discuss the effect of alcohol on the interaction force. In CO_2 dry-cleaning alcohols, more specifically 2-propanol, are added as a co-solvent at a concentration of ≈ 5 % (w/w) as a detergency aid. van Roosmalen *et al.*[3] have studied the effect of the addition of 1 and 2-propanol, methanol, ethanol, 1 and 2-butanol, 1-pentanol and 1-hexanol on the cleaning performance. It was found that the addition of co-solvents can lead to a significant enhancement of the detergency. However, hardly any difference in the CPI was found among the various alcohols tested, apart from 1-butanol and 1-pentanol, which were detrimental to the cleaning. Out of the various alcohols tested, 1 and 2-propanol stood out to be the better candidates and at the end 2-propanol was chosen as the most suitable co-solvent since it is cheaper and less harmful than 1-propanol.

Based on these preliminary detergency results, we studied the effect of 1 and 2-propanol on the interaction forces between cellulose and silica through dry as well as wet hexane. In Figure 9.3 we show force-distance curves between cellulose and silica through water-saturated hexane with or without 2-propanol. The amount of 2-propanol was 5.3 % (w/w). The effect of adding 2-propanol is quite dramatic: it reduced the adhesion force and the range of interactions to virtually zero.

This finding can be directly correlated to the detergency results obtained by van Roosmalen. Our explanation is that the presence of alcohol lowers the water-hexane interfacial tension, as the alcohol is soluble in both water and hexane, resulting in a dramatic lowering of the capillary adhesion between cellulose and silica.

We further studied the effect of the concentrations 1-propanol and 2-propanol on the force of interactions in dry as well as wet hexane and the results are shown in Figure 9.4. No effect of the surface delay time has been observed.

For dry hexane we do not see significant differences between the two al-

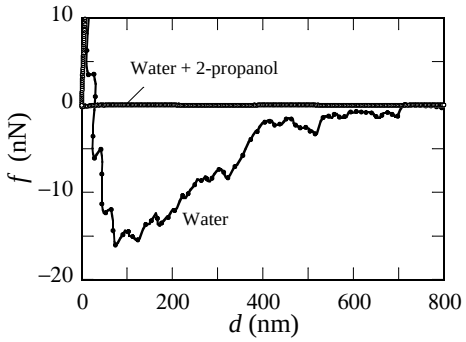

Figure 9.3: *Retraction curves between cellulose and silica after 200 s surface delay in water-saturated n-hexane without and with added 2-propanol (5.3 % (w/w). Tip velocity 2 um/s.*

cohols. The maximum adhesion force decreases with increasing concentration of alcohol. Also for water-saturated hexane at an alcohol concentration of ∼5 % (w/w) not much difference in the adhesion forces for 1 and 2-propanol was observed. For 1-propanol the force decreases with increasing concentration of alcohol, as in the case of dry hexane. However, for 2-propanol at ∼ 0.7 % the adhesion force is much lower than for 1-propanol, while at ∼ 2.7 % it is considerably higher. The reason for this is not clear.

The (small) adhesion force of in case of alcohols in dry hexane may be due to the formation of H-bonded alcohol clusters at the solid-hexane interface.[4] The -OH groups of the cluster are exposed to the apolar hexane resulting in a higher interfacial tension and hence a higher adhesive force. As the alcohol concentration is increased, the interfacial tension between the cluster moiety and the bulk hexane (as the bulk also solubilizes more alcohol) is lowered, resulting in a lower adhesive force between the interacting surfaces. Kurihara *et al.*[4] have shown by ATR-IR spectroscopy that 1-propanol forms linear and 2-propanol forms cyclic clusters at the interface. In the cyclic cluster the OH groups are sequestered from the bulk hexane and hence the adhesion force in case of 2-propanol should be less than that of 1-propanol. However, Kurihara *et al.*[4] also pointed out that beyond 0.3 % (w/w) alcohol the difference between

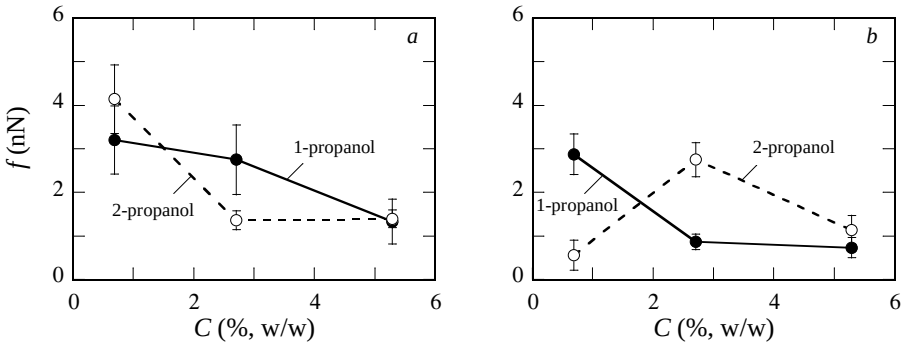

Figure 9.4: *Adhesion force between cellulose and silica in (a) dry and (b) wet hexane as a function of the concentration alcohol (1-propanol and 2-propanol as indicated). Surface delay 50 s.*

1-propanol and 2-propanol vanishes. In our measurements the lowest amount of alcohol was 0.7 % and hence we did not see any significant differences between 1 and 2-propanol in dry hexane.

9.7 Igepal CA520 as a prototype surfactant for liquid CO_2

Four years back when this project was started, most of the work on surfactants for CO_2 reported in literature, if not all, was for supercritical conditions and this situation has hardly changed. A review of these studies can be found in Chapter 2 of this thesis. One finds examples of stubby (methyl-branched), high molecular weight surfactants, fluorinated surfactants, block copolymeric surfactants, and peracetylated sugar derived surfactants that have shown promise in supercritical conditions. Compared to liquid CO_2, supercritical CO_2 has the advantage of superior solvency power owing to the higher density and diffusivity.

However, CO_2 dry-cleaning is based on liquid CO_2 and not on supercritical CO_2. There is hardly any surfactant which is soluble at 45 - 60 bars and 10 °C and the dry-cleaning industry is craving for one to promote this environment-

ally friendly technology. So where should one start? From the very beginning we were keen on doing a systematic hypothesis driven research instead of a trial-and-error based screening. Following our comprehensive review (Chapter 2), we hinged on the idea of having a branched surfactant as first proposed by Ryoo *et al.*[5] For the rest our approach (described in Chapter 4 in detail) was different as we emphasized on having a low molecular weight, commercially available non-ionic (C_iEO_j type) surfactant. Based on our knowledge on apolar media we restricted the EO numbers to within 5 and a short carbon chain length of 8 and arrived at Igepal CA520. An ideal starting point would have been to check the solubility of this surfactant in liquid CO_2 under dry-cleaning conditions. Unfortunately, this could not be achieved at the very outset due to the unavailability of suitable instrumentation. Hence, the initial solubility check was performed in the model solvent, n-hexane. Other than Igepal CA520, we also tested the EO_3 variety. Whereas the Igepal CA520 formed a turbid solution in n-hexane, the EO_3 variety completely remained phase separated and hence we decided to do further experiments on Igepal CA520.

Since it was imperative to have water in the system we decided to drive the self-assembly of this surfactant in n-hexane using water. Water is known as a mesogen since it drives the formation of liquid crystalline phases in apolar media and this idea was utilised in the study described in Chapter 4. We hypothesized that to prevent water capillary condensation between the fabric and particulate soil surfaces, the added water has to be encapsulated inside surfactant mesophases.

The next step consisted of mapping out the relevant part of the phase diagram for the ternary system of surfactant, n-hexane and water. In this way, two compositions were identified for detergency tests, one containing an isotropic L_2 reverse micellear phase and the other a co-existence of L_2 + L_α mixture. The choice of the latter was based on the hypothesis that a lamellar phase would adsorb more effectively on a flat fabric interface, thereby improving the particle release process over the L_2 composition.

Detergency tests were performed in n-hexane, but also in the pilot CO_2 dry-

cleaning set-up in the Process and Energy Laboratory at Delft University. To this end the Igepal/hexane/water formulations were applied as pre-treatment in the CO_2 dry-cleaning process. Although the detergency results remained inconclusive of proving or disproving the above-mentioned hypothesis, both the formulations gave detergency benefit over cleaning tests using only liquid CO_2. The reasons that we did we not see the positive effect of having an L_α phase in the formulation may be manifold. A detergency test is a complex experiment, a culmination of many processes occurring at the same time.

Nevertheless this was the first clue that we obtained in a real CO_2 system that this surfactant might work. Although the formulations contained n-hexane and were applied as a pre-treatment we were getting hopeful at this stage.

Again we employed the AFM to measure the interaction forces between the silica particle and cellulose surface in the presence of the surfactant formulations. These measurements are the basis of Chapter 5. We showed that irrespective of the type of mesophases the adhesive force between cellulose and silica was significantly lower in the surfactant formulations than in water-saturated hexane. We hypothesized that the small remaining attraction could stem either from wetting of the surfaces by the lamellar phase, followed by condensation of water from the bulk,[6] or from a confinement induced transition of micelles (L_2) to lamellar (L_α) structures, followed by water condensation.[7] In either case, the (small) attraction would be a result of wetting of the surfaces and the (low) interfacial tension between water and hexane in the presence of the surfactant.

Although the AFM measurements nicely augmented the detergency results, there is scope for further understanding. We here pose some questions for further investigation. Is it possible to decouple the role of the adsorbed surfactant films and the meniscus formed at the confined spaces in the adhesion force? In other words, can the interaction be viewed as capillary condensation of water in presence of the surfactant or is there a contribution of the attraction between the adsorbed surfactant layers? If so, does one become dominant over the other as function of the separation distance? There are

models by Derjaguin and Churaev[8] for polymolecular adsorption and capillary condensation in narrow slit pores, where the relative strengths of adsorbate-adsorbate and adsorbate-adsorbent interactions play a role. In the case of strong adsorbate-adsorbate interaction, the co-existence of the capillary meniscus and the adsorbed films is not possible below a critical width of the slit, whereas for strong adsorbent-adsorbate interactions the co-existence is possible for any slit width. Can these theories be extended to the amphiphile systems at confined spaces?

In Chapter 3, where we studied capillary condensation of water in narrow confined spaces, we assumed the presence of an adsorbed water film at all distances. Water - silica or water - cellulose interactions should fall under the category of strong adsorbent-adsorbate interaction owing to the H-bonded interactions. We assumed dispersion type interactions between the surrounding hexane and surfaces through the water film and estimated the thickness of the film as 7 nm. Can this estimate be verified experimentally, for example by ellipsometry?

9.8 Interfacial behaviour and self-assembly of Igepal CA520 in the water - liquid CO_2 system

To understand how Igepal CA520 behaves in water - liquid CO_2 systems, it is necessary to know the interfacial behaviour of Igepal CA520 at the water - CO_2 interface as well as its ability to form mesophases such as (reverse) micelles and lamellar phases.

As a reference the properties of the bare water - CO_2 interface had to be investigated first. Not only were we interested in the interfacial tension, but we also wanted to have an insight in the wetting and adsorption phenomena at the interface. This was achieved partly through experiments and partly by numerical modeling, using the self-consistent field model of Scheutjens and Fleer (SF-SCF). The experiments were done in the laboratory of Heat and Mass transfer in the Technical University of Hamburg-Harburg, Germany. We showed that the water - CO_2 interfacial tension decreases and the water contact

angle on a hydrophilic surface in CO_2 increases with increasing pressure. The first phenomenon was explained from the increasing Gibbs excess of CO_2 at the water - vapour interface. The increase in contact angle was shown to result from the adsorption of CO_2 on the -OH populated surfaces with increasing pressure. The model further predicted complete wetting of the water - vapour interface by a CO_2 layer, which was in line with the fact that the system conditions were chosen not far from criticality. These phenomena are captured in Chapter 6.

The model delineated in Chapter 6 was extended further in Chapter 7 for studying the interfacial and bulk phase behaviour of Igepal CA520 in water - liquid CO_2 system. The experimental water - CO_2 interfacial tension data in presence of the surfactant indicates that the surfactant is interfacially active. By implementing these experimental findings into our numerical model, we investigated the self-assembly of Igepal CA520 in the bulk CO_2 or water. The model predicted formation of reverse micelles both at three-phase coexistence (at $P/P_{\text{sat}} = 1$) and for $P/P_{\text{sat}} > 1$. The effect of pressure on the formation of reverse micelles was predicted: with increasing pressure the critical reverse micellar concentration (CRMC) increases and the critical aggregation number decreased. The physical explanation is that a higher pressure leads to a stronger stopping mechanism for reverse micellization due to the better solvation (better solvency power of liquid CO_2) of the surfactant tails by CO_2.

In the water phase bilayer formation was predicted to occur beyond a critical surfactant chemical potential. Apart from the bulk phase behaviour, the presence of the surfactant gives rise to interesting wetting phenomena at the water - vapour interface. Partial wetting by CO_2 was noted, followed by a re-entrant wetting transition as the surfactant chemical potential in the bulk water phase was increased.

The theoretical phase behaviour presented in Chapter 7 was validated in Chapter 8 by small angle X-ray scattering experiments (SAXS) on Igepal/water/liquid CO_2 ternary systems. The SAXS results indicated conclusively the presence of self-assembled aggregates. The role of water in driving the self-assembly has been mapped and it was concluded that water acts as a

mesogen (promoter of liquid crystals) in C_iEO_j type surfactant - liquid CO_2 systems. In the absence of water, at a particular range of surfactant concentrations, the system contains isotropic reverse micellar mesophases (often termed as L_2) and with the addition of water L_2 undergoes a phase transition to L_α. The lamellar repeat distance increases with increasing water content. Following these findings, a partial phase diagram in liquid CO_2 has been generated in Chapter 8. In Chapter 4 one finds the phase diagram of the Igepal/water/hexane ternary system. Comparing these two phase diagrams it is clear that water plays similar roles in the two systems. With this knowledge we can now say with conviction that for our studies n-hexane has proven to be a very well-chosen model solvent for liquid CO_2.

9.9 Design rules for a surfactant for liquid CO_2

The molecular pictures that emerged from the SF-SCF modelling are rich and proved to be valuable for studying the interfacial behaviour and self-assembly of surfactants in a complex fluid system. We did not stop at clarifying the underlying physics, but also applied the model to provide pragmatic design guidelines for surfactant architecture in liquid CO_2. These guidelines are presented in this section.

In Chapter 7 we pointed out that the stability window for reverse micelles in liquid CO_2 with respect to the two key Flory-Huggins interaction parameters, namely the χ_{C3D} and χ_{OW} (between methylgroups in the surfactant tail and CO_2, and between the head group oxygens and water, respectively), was rather narrow. The first interaction parameter dominates the stopping mechanism for micellisation, while the latter determines the driving force for this process. The fact that this window is narrow essentially points out the difficulties involved in designing amphiphiles for liquid CO_2. This finding is a good starting point to study the effect of surfactant architecture on the process of reverse micellization.

Surfactant architecture is a broad term; there are many structural properties that can be varied. In the following we will focus on the effects on the

self-assembly of the surfactant in liquid CO_2 of branching, tail length, EO chain length and CH_3 or CH_2 type interactions on the backbone.

In Figure 9.5 we have plotted the grand potential of translationally restricted spherical micelles, Ω_s, against the aggregation number g. The interpretation of Ω_s is given in detail in Chapter 7. Here we will only discuss the gist of the main findings.

The default surfactant molecule is same as in Chapter 7 and is schematically presented in Figure 9.6. The linear counterpart of this default molecule is represented by C_8 - b - linear - EO_5. Here b stands for the benzene ring. For this molecule Ω_s increases monotonically with increasing g and therefore does not satisfy the thermodynamic criterion of $d\Omega_s/dg < 0$ for any g. This indicates that spherical reverse micelles are not the preferred shape for this linear surfactant in liquid CO_2. This is an interesting finding since we have seen before and also from Figure 9.5 that if branching is introduced C_8 - b - EO_5 surfactants do form stable reverse micelles. However, if the length of the alkyl tail of the linear variant is increased, stability of the spherical reverse micelles is regained. This is exemplified by the curves for the C_{10} - b - linear - EO_5 and the C_{12} - b - linear - EO_5 molecules in Figure 9.5a. From these observations we conclude that for smaller molecules ($< C_{10}$), branching is important and for longer molecules (C_{10} and above), CH_3 type interactions are more important over branching. This can be explained from the packing parameter v/a_0l (i.e., the ratio between the apparent cross section of the surfactant tail v/l and the head group area a_0). In order to form reverse micelles, the packing parameter has to be larger than 1. This can be achieved by incorporating branching (more excluded volume) in the tail or by increasing the tail length. Moreover, we have seen that having more methyl groups, implies a stronger stopping mechanism for the self-assembly, while the driving force remains constant. This leads to a lower critical reverse micellar concentration (CRMC), a higher volume fraction of reverse micelles and a lower aggregation number at the CRMC (compare e.g. the curves for the default molecule and C_{12} in Figure 9.5a.)

The results of introducing branching at the benzene ring or more branching

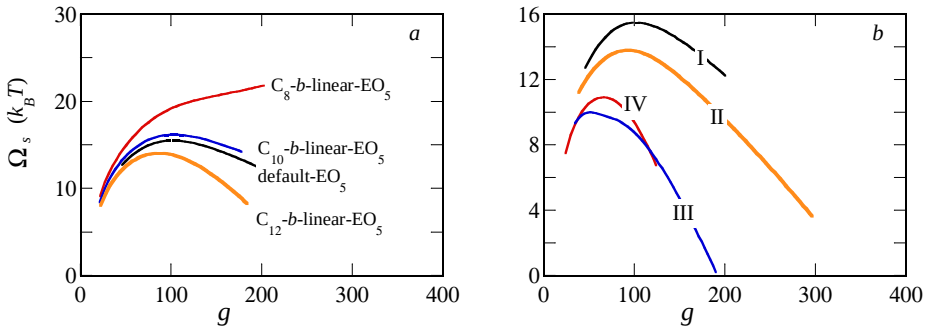

Figure 9.5: *Grand potential of translationally restricted spherical reverse micelles in liquid CO_2 as a function of aggregation number. a) Effect of the number of methyl groups in the surfactant tail. b) The role of branching in the tail.*

on the alkyl tail are summarised in Figure 9.5b.

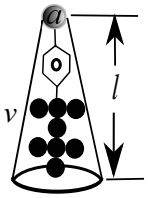

Figure 9.6: *The default molecule (representing Igepal C520, Chapter 7) and schematics of its packing parameter.*

The branch points on the benzene ring were varied (see Figure 9.7): in type II, the branch points are further from the head groups and in type III , the branch points are adjacent to the head groups. As can be seen from Figure 9.5b, for type III, the reverse micelles are more robust, their aggregation number at the CRMC is lower and there is a higher number of reverse micelles at the CRMC compared to the default (type I) or the type II molecule.

These results can also be explained in terms of the packing parameter (Figure 9.8). When the branch points are adjacent to the head groups (type III), the wedge shape effect is immediate, whereas, in case of type II, the wedge starts off farther down the chain leading to less-efficient packing of the molecules in the reverse micelles. Introduction of more branching (type IV,

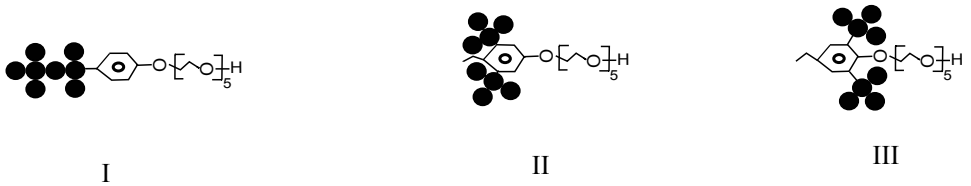

I II III

Figure 9.7: *(I) The default surfactant molecule (II) Molecules having branch points on the benzene ring, further away (III) Molecules having branch points on the benzene ring close to the head group.*

Figure 9.9) on the alkyl tail farther from the benzene ring brings in the same effect as in III.

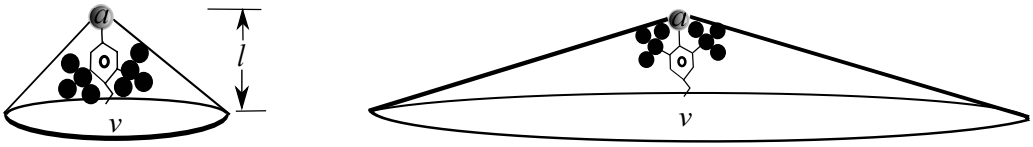

Figure 9.8: *Schematics of packing parameter for molecules with type II branching (a) and type III branching (b).*

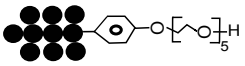

Figure 9.9: *Surfactant with more branching (type IV) on the alkyl tail than the default molecule.*

The effects of tail and head group chain lengths on the CRMC and critical aggregation number are presented in Figure 9.10. In these cases the molecules considered are linear. The CRMC goes up with increasing carbon numbers for both EO_5 and EO_6, because the higher the number of CH_3 groups in the tail, the higher is the solubility of the surfactant in liquid CO_2. With increasing length of the EO chain, the driving force for self-assembly increases and hence the CRMC is lower for EO_6 than for EO_5.

The aggregation number is practically constant with tail length up to C_{10} and then decreases for both EO_5 and EO_6. More CH_3 groups implies a stronger stopping force and hence the aggregates become smaller. The aggregation

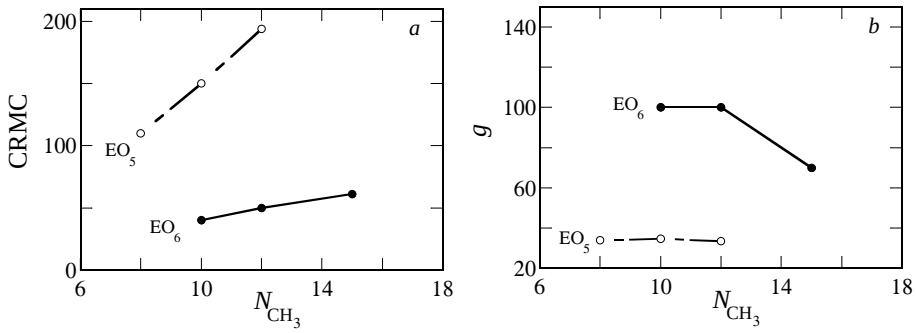

Figure 9.10: *Dependence of the critical reverse micelle concentration (a) and the corresponding aggregation number (b) for linear surfactant molecules on the number of carbons in the alkyl tail, N_{CH3}, for two different lengths of the head group EO chain.*

number is lower for EO_5 than for EO_6 since there is less water associated with the polar core.

9.10 Outlook

We have shown experimentally that a small branched surfactant molecule such as Igepal CA520 is soluble in liquid CO_2 and water can be used to promote its self-assembly in this medium. In general we found that the knowledge on self-assembly in apolar media also holds for liquid CO_2. Our theoretical analysis and design attempt throws a number of possibilities for future experiments. We conclude that branching is important for small molecules (less excluded volume). For longer molecules there must be CO_2-philic groups attached to the tail part of the surfactant, while the number of EO groups should be limited to five or six. Moreover, the Igepal molecule can be modified by incorporating CH_3 branching at the benzene rings ortho to the head groups to further improve the self-assembly.

Now that we have predicted the CRMC and aggregation numbers of a C_iEO_j type of non-ionic surfactant in liquid CO_2, these concepts should be tested further experimentally by X-ray/neutron scattering.

We have used so far a spherical geometry in our model. However, other micellar shapes, such as rod or disc, are also possible. Thermodynamics of these systems can also be studied in future using the same self-consistent field approach. In addition, the mean field approach can be improved further by incorporating atomistic details and the effect of insertion of other CO_2-philic groups can also be studied in future.

Moreover, the effect of alcohol on the phase behaviour of the Igepal CA520 /water/liquid CO_2 can be the subject of SAXS studies in future. In Chapter 2 we have mentioned that alcohol is also used as an additive in dry-cleaning formulations. In the present chapter we discussed the effect of adding alcohol in the water-saturated hexane to reduce the adhesion force between cellulose and a silica particle. Therefore, it would also be interesting to study the effect of alcohol content on the phase behaviour of the quaternary system as well. Furthermore, other compositions of the ternary phase diagram can be mapped in future by systematically varying the surfactant concentration and water to surfactant ratios.

The incentive of this project was to find ways to improve the perspectives of liquid CO_2 as a dry-cleaning solvent, to replace the environmentally harmful and toxic solvents that are commonly used at present. Our results show that Igepal CA520 is a CO_2 soluble surfactant with obvious potential to aid the process of particulate soil removal in liquid CO_2. More surfactants may be synthesized according to our selection criteria and design rules. An additional and not unimportant advantage of Igepal CA surfactants is that they are biodegradable and not very toxic.[9]

Of course, the effectiveness of Igepal CA520 as a surfactant in liquid CO_2 dry-cleaning has to be proved in systematic detergency tests in comparison to other dry-cleaning methods and in relation to specific target specifications. We expect a composition of the washing liquid in which both reversed micelles and lamellar phases are present, to be the most favourable. The presence of water in the washing liquid would then serve two purposes: to drive the reverse micellar and lamellar phase formation which would promote particle removal, and to enhance the removal of polar (water soluble) soil for which the addition

water was originally intended.

At the moment, dry-cleaning using CO_2 has been commercialized on a small scale only. We expect that if detergency tests using Igepal or other candidate surfactants indeed show a significant enhancement of the cleaning performance, this will contribute to a break-through of this form of environmentally friendly dry-cleaning.

The learning from this thesis is manifold and can also be beneficial to other research domains where CO_2 is in burgeoning demands such as enhanced oil recovery, polymer synthesis in CO_2 and extraction of polar compounds. Besides, behaviour of the CO_2 - water interface and wetting of various surfaces by CO_2 are required for addressing problems involved in geological storage of CO_2.

In enhanced oil recovery using CO_2, the high mobility of CO_2 is a concern.[10–12] CO_2 is more mobile than oil or water, owing to its low viscosity. This high mobility causes fingering through the oil retained in the porous media and as a result CO_2 comes out of the oil well, leaving the oil behind.[12,13] One way to tackle this problem is to enhance the viscosity of CO_2 by thickening agents. Apart from using polymeric associative thickeners, surfactant self-assembly has also been employed to modify the viscosity of CO_2[12,13] . It has been shown that the viscosity of CO_2 can be increased by 20 - 90 % using 6 - 10 wt % of CO_2 compatible di-chain fluorinated surfactants.[13] This is indeed a promising result not only for oil recovery problems but also for any processes involving CO_2 where mechanical action plays a role. In Chapter 2 we have discussed the challenges involved in generating momentum in liquid CO_2 and in this context the findings described in Chapter 4 and 8 are noteworthy. An important lead is the possibility of steering the phase diagram of Igepal CA520/water/liquid CO_2 towards the lamellar phase by the addition of water. The viscosity of the lamellar phase is higher than the isotropic reverse micellar phase. Hence, Igepal CA520 with added water could be tested for viscosity modification of CO_2 in future.

Although the fluorinated surfactants have been shown to be able to thicken CO_2, the increase in viscosity is too small to be effective in enhanced oil

recovery.[13] Moreover, the need for hydrocarbon analogues to do the job is ever increasing.[12] Realizing that a lamellar phase formulation has never been deployed to increase the viscosity of CO_2, we see an opportunity to put this idea forward for future research. Of course, the phase diagram of Igepal in supercritical CO_2 has to mapped for this purpose.

In the same context, CO_2-in-brine mobility control foams are also getting much attention.[12] Several hydrocarbon surfactants have been suggested as foam stabilizers. Siloxane based surfactants with added co-solvents or ethoxylated alkyl-aryl (alkyl phenol) hydrocarbons.[12] It has been realized that CO_2-in-water or CO_2-in-brine emulsion are good as foaming formulations, though mention of water-in-CO_2 emulsion have also been found.[12] However, poor solubility of these surfactants in CO_2 was again the road block. Towards this end we can think of using the same alkyl-aryl, methyl branched backbone of Igepal CA520 with higher EO chain lengths to form CO_2-in-water emulsions. To form water-in-CO_2 emulsions, Igepal CA520 can be tried as it is.

Extraction of polar compounds using reverse micelles in CO_2 is another domain that is flourishing. One can think of several applications such as mitigation of water contamination, extraction of pharmaceutical products from fermentation vessels, selective encapsulation of drugs for targeted delivery[14] and the transport of reagents for chemical reactions (polymerization) in CO_2.[15] Fluorinated dendrimers have been shown to be soluble and form reverse micelle type structures in liquid CO_2[15] and can extract polar molecules into their core. However, they suffer from the same undesirability i.e. having fluorine in their structure. In future, the suitability of reverse micelles of Igepal CA520 in liquid CO_2 can be investigated.

In case of the geological storage of CO_2 in deep saline aquifers or depleted hydrocarbon reservoirs, rapid leakage of CO_2, caused by the failure of the capillary rock is a nuisance and the water - CO_2 or Brine - CO_2 interfacial tension is known to be one of the factors to control this leakage.[16,17] We have demonstrated in Chapter 6 and 7 that a numerical self-consistent field modeling can predict the water - CO_2 interfacial tension quite well. Hence, for

further research this kind of modeling can be employed to gain insight into the interfacial and wetting behaviour of these complex fluid systems at a shorter time scale. This is important since measurements at high pressure are difficult and time consuming and in certain real life situations may be even impossible to perform.

Bibliography

[1] van Roosmalen M. J. E. *Dry-cleaning with High Pressure Carbon Dioxide*. PhD thesis, TU Delft, 2003.

[2] L. Sirghi, M. Nakamura, Y. Hatanaka, and O. Takai. Atomic Force Microscopy Study of the Hydrophilicity of Tio_2 Thin Films Obtained by Radio Frequency Magnetron Sputtering and Plasma Enhanced Chemical Vapor Depositions. *Langmuir*, 17(26):8199–8203, 2001.

[3] M. J. E. van Roosmalen, G. F. Woerlee, and G. J. Witkamp. Dry-cleaning with High-pressure Carbon Dioxide–the Influence of Process Conditions and Various Co-solvents (Alcohols) on Cleaning-results. *J. Supercrit. Fluids*, 27(3):337–344.

[4] M. Mizukami and K. Kurihara. Hydrogen-Bonded Macrocluster Formation of 1-Propanol and 2-Propanol on Silica Surfaces. *Aust. J. Chem.*, 56(10):1071–1080.

[5] W. Ryoo, S. E. Webber, and K. P. Johnston. Water-in-Carbon Dioxide Microemulsions with Methylated Branched Hydrocarbon Surfactants. *Ind. Eng. Chem. Res.*, 42(25):6348–6358, 2003.

[6] P. Petrov, U. Olsson, and H. Wennerström. Surface Forces in Bicontinuous Microemulsions: Water Capillary Condensation and Lamellae Formation. *Langmuir*, 13:3331–3337, 1997.

[7] P. Petrov, S. Miklavcic, U. Olsson, and H. Wennerström. A Confined Complex Liquid. Oscillatory Forces and Lamellae Formation from an L3 Phase. *Langmuir*, 11:3928–3936, 1995.

[8] B. V. Derjaguin and N. V. Churaev. Polymolecular Adsorption and Capillary Condensation in Narrow Slit Pores. *J. Colloid Interface Sci.*, 54(2):157–175, 1976.

[9] http://www.stepan.com/products/surfactants/igepal%c2%

[10] Holm L.W. Bernard, G.G. and C.P. Harvey. Use of surfactant to reduce CO_2 mobility in oil displacement. *Soc. Pet. Eng. J.*, 20(8):281–292, 1980.

[11] J. P. Heller, C. L. Lien, and M. S. Kuntamukkula. Foam-like Dispersions for Mobility Control in CO_2 Floods. *Soc. Pet. Eng. J.*, 25(8):603–613, 1985.

[12] D. Xing. *CO_2 Mobility Control using Direct Thickeners and Foaming Agents*. PhD thesis, Swanson School of Engineering, University of Pittsburgh, 2012.

[13] K. Trickett, D. Xing, R. Enick, J. Eastoe, M. J. Hollamby, K. J. Mutch, S. E. Rogers, R. K. Heenan, and D. C. Steytler. Rod-Like Micelles Thicken CO_2. *Langmuir*, 26(1):83–88, 2010.

[14] S. Stevelmans, J. C. M. van Hest, J. F. G. A. Jansen, D. A. F. J. van Boxtel, E. M. M. de Brabander-van den Berg, and E. W. Meijer. Synthesis, Characterization, and Guest-Host Properties of Inverted Unimolecular Dendritic Micelles. *J. Am. Chem. Soc.*, 118(31):7398–7399, 1996.

[15] A. I. Cooper, J. D. Londono, G. Wignall, J. B. McClain, E. T. Samulski, J. S. Lin, A. Dobrynin, M. Rubinstein, A. L. C. Burke, J. M. J. Frechet, and J. M. DeSimone. Extraction of a hydrophilic compound from water into liquid co2 using dendritic surfactants. *Nature*, 389:368–371, 1997.

[16] P. Chiquet, J. L. Daridon, D. Broseta, and S. Thibeau. CO2/water Interfacial Tensions under Pressure and Temperature Conditions of CO2 Geological Storage. *Energ. Convers. and Manage.*, 48:736–744, 2007.

[17] L. C. Nielsen, I. C. Bourg, and G. Sposito. Predicting CO_2-Water Interfacial Tension Under Pressure and Temperature Conditions of Geologic CO_2 Storage. *Geochim. Cosmochim. Ac.*, 81(0):28–38, 2011.

Summary

This thesis aims at gaining fundamental insight on colloidal interactions in two types of apolar media, namely, liquid CO_2 and (as a model for liquid CO_2) n-hexane. The other components playing major roles are surfactants and water. The background of the work was to address the challenges met in the use of liquid CO_2 as a dry-cleaning solvent, in particular the insufficient removal of particulate soil.

Since the dielectric constant of liquid CO_2 is extremely low (1.6 at 60 bar and 10 °C), it has a low individual Hamaker constant. This in turn leads to a many orders of magnitude higher van der Waals force between interacting surfaces through liquid CO_2 as opposed to traditionally employed solvents like perchloroethylene (PERC), which are toxic and environmentally unfriendly. Both the absence of charge on surfaces and the high Van der Waals force mean that a high solvodynamic force (high Reynolds number) is required to dislodge particles from fabrics.

The situation becomes worse in the presence of water (without a suitable surfactant), which is a minor component in any dry-cleaning formulation. Our atomic force microscopy results indicate that water-mediated capillary bridges can lead to higher adhesion forces between the interacting surfaces. The roughness and softness of the surfaces were found to affect the kinetics, magnitude and range of the interaction force.

Further, we have shown that using suitable surfactants these forces can be reduced. Following a systematic selection approach based on the hypothesis that a hydrocarbon surfactant for liquid CO_2 should have a low molecular

weight and a branched t-butyl tail in its alkyl part, Igepal CA520 was chosen. This surfactant has an ethylene oxide (EO) chain as a headgroup (C_iEO_j type surfactant). The surfactant solubility was tested first in the model solvent, followed by measuring its cloud point in the liquid CO_2 system, which showed that the surfactant is soluble at $\sim$ 50 bar and 5 - 10 °C (CO_2 dry-cleaning conditions). Furthermore, we found that Igepal CA520 was surface active at the water - liquid CO_2 interface. Igepal CA520 was further tested in a pilot scale dry-cleaning apparatus, where it showed marked improvement in detergency of particulate soil.

The interfacial behaviour of the surfactant - water - liquid CO_2 system was also studied using the self-consistent field theory of Scheutjens and Fleer (SF-SCF). We showed that the interfacial tension of bare water - CO_2 interface decreases with increasing pressure and becomes invariant of pressure beyond the saturated vapour pressure. The water contact angle on a hydrophilic surface in CO_2 increases with increasing pressure. The first phenomenon was explained from the increasing Gibbs excess of CO_2 at the water - vapour interface. The increase in contact angle was shown to result from the adsorption of CO_2 on the -OH populated surfaces with increasing pressure. The model further predicted complete wetting of the water - vapour interface by a CO_2 layer, in line with the fact that the system conditions were chosen not far from criticality.

The model was further extended to describe and predict the interfacial and bulk properties of the liquid CO_2/surfactant/water system. The experimental water - CO_2 interfacial tension data and the SF-SCF modeling of the Igepal/water/liquid CO_2 system indicated that Igepal adsorbs at the water - liquid CO_2 interface. The model also predicted the formation of reverse micelles both at the three-phase (water/liquid CO_2/gaseous CO_2) coexistence (at $P/P_{\mathrm{sat}} = 1$) and for $P/P_{\mathrm{sat}} > 1$. With increasing pressure the critical reverse micellar concentration (CRMC) increases and the aggregation number at the CRMC decreases. A higher pressure leads to a stronger stopping mechanism for reverse micellization due to the better solvation (better solvency power of liquid CO_2) of the surfactant tails by CO_2.

Apart from the bulk phase behaviour, the presence of the surfactant gives rise to interesting wetting phenomena at the water - vapour interface. Partial wetting by CO_2 was noted, followed by a re-entrant wetting transition as the surfactant concentration in the bulk water phase was increased.

The theoretical phase behaviour was validated by small angle X-ray scattering experiments (SAXS) on Igepal/water/liquid CO_2 ternary systems. The SAXS results indicated conclusively the presence of self-assembled structures. The role of water in driving the self-assembly has been mapped and it was concluded that water acts as a mesogen (promoter of liquid crystals) in C_iEO_j type surfactant - liquid CO_2 systems. In the absence of water, at a particular range of surfactant concentrations, the system contains isotropic reverse micellar mesophases (often termed as L_2) and with the addition of water L_2 undergoes a phase transition to a lamellar phase, L_α. The lamellar repeat distance increases with increasing water content. Following these findings, a partial phase diagram in liquid CO_2 has been generated. Comparing the phase diagrams of Igepal CA520/water in liquid CO_2 and in n-hexane it is clear that water plays similar roles in the two systems. Based on this we also conclude that n-hexane is a good model for liquid CO_2.

The model was used to arrive at design guidelines for surfactants for liquid CO_2. It is interesting to note that the stability window for reverse micelles in liquid CO_2 is rather narrow with respect to the two key Flory-Huggins interaction parameters, namely the χ_{C3D} and χ_{OW}, characterizing the interaction between methyl groups in the surfactant tail and CO_2, and between the head group oxygen and water, respectively. The first interaction parameter dominates the stopping mechanism for micellization, while the latter determines the driving force for this process. The fact that this window is narrow essentially points out the difficulties involved in designing amphiphiles for liquid CO_2. The design criteria emerging from modeling are based on the numerical results that for smaller molecules ($< C_{10}$), branching is important and for longer molecules (C_{10} and above), CH_3 type interactions are more important over branching.

Apart from CO_2 dry-cleaning, the knowledge gained in this thesis can

be beneficial to many other environmentally friendly industrial processes involving liquid CO_2, such as enhanced oil recovery and extraction of polar compounds. The outcome of this thesis can also be extended to alleviate the problems associated with the geological storage of CO_2 at high pressure under the ocean floor (deep saline aquifers).

Samenvatting

Dit proefschrift beoogt fundamentele kennis te verschaffen over colloïdale wisselwerkingen in twee apolaire media, namelijk vloeibaar kooldioxide (CO_2) en, als model voor vloeibaar CO_2, n-hexaan. De andere componenten die een belangrijke rol spelen in het beschreven onderzoek, zijn surfactanten (oppervlakteactieve stoffen) en water. De achtergrond van dit werk is het chemisch reinigen van textiel met behulp van vloeibaar CO_2, waarbij met name de verwijdering van deeltjesvuil zoals zand, klei en roetdeeltjes, nog onvoldoende is. Het doel van dit project was om de mechanismen op te helderen die een rol spelen bij het verwijderen van deeltjesvuil, en met dit inzicht richtlijnen te formuleren voor het ontwerpen van geschikte surfactanten. De diëlektrische constante van vloeibaar CO_2 is extreem laag (1,6 bij een druk van 60 bar en een temperatuur van 10 °C) en daardoor heeft de stof een lage Hamakerconstante. Dit betekent dat Vanderwaalskrachten tussen materialen in vloeibaar CO_2 ordes groter zijn dan in de oplosmiddelen die traditioneel worden gebruikt voor chemisch reinigen van textiel, zoals tetrachloorethyleen (oftewel perchloorethyleen, PERC), en die giftig en milieuonvriendelijk zijn. Zowel de afwezigheid van lading op het oppervlak van deeltjes en textiel als de hoge Vanderwaalskrachten leiden er toe dat er in vloeibaar CO_2 grote mechanische (solvodynamische) krachten nodig zijn om het deeltjesvuil te verwijderen. De situatie verslechtert nog als er in het vloeibaar CO_2 wat water aanwezig is zonder dat een geschikte surfactant is toegevoegd. In elke detergentformulering voor chemisch reinigen zit waterals een van de additieven. Uit onze metingen van de wisselwerking tussen een silica deeltje (model voor vuil) en cellulose (model voor textiel) met

de atomic force microscoop blijkt dat in apolaire media water capillaire bruggen kan vormen die leiden tot hoge adhesiekrachten. De grootte en het bereik van deze krachten worden beïnvloed door de oppervlakteruwheid van de materialen en de elasticiteit (zachtheid) van het celluloseoppervlak. Het gebruik van een geschikte oppervlakte-actieve stof kan deze krachten verminderen. Op grond van de hypothese dat een geschikte, milieuvriendelijke surfactant voor vloeibaar CO_2 een laag moleculair gewicht moet hebben en een vertakte alkylstaart, hebben we Igepal CA520 gekozen voor verdere studie. Deze stof heeft een t-butylstaart en een ethyleenoxide (EO) keten als kopgroep (C_iEO_j-type surfactant). De oplosbaarheid van Igepal CA520 werd eerst getest in het modeloplosmiddel, en vervolgens werd het troebelingspunt ("cloud point") in vloeibaar CO_2 bepaald als functie van de druk. Hieruit werd gevonden dat Igepal CA520 oplosbaar is in vloeibaar CO_2 rond 50 bar en tussen 5 en 10 °C, overeenkomend met de condities die gebruikt worden bij chemische textielreiniging. Ook vonden we dat de stof de oppervlaktespanning verlaagd tussen water en vloeibaar CO_2. De surfactant werd verder getest in een proefopstelling voor textielreiniging, waar het een opmerkelijke verbetering liet zien in de waskracht van vloeibaar CO_2 wat betreft deeltjesvuil. De karakteristieken van het grensvlak tussen CO_2 en water werden bestudeerd met behulp van de zelf-consistente veld theorie van Scheutjens en Fleer (SF-SCF). We lieten hiermee zien dat de grensvlakspanning tussen water en CO_2 afneemt met toenemende druk en onafhankelijk wordt van de druk boven de verzadigde dampspanning van CO_2 (Psat). De contacthoek van water op een hydrofiel oppervlak in CO_2 neemt toe met toenemende druk. Deze resultaten zijn in overeenstemming met experimentele data. De afname in grensvlakspanning is het resultaat van een toenemend overschot aan Gibbs-energie van CO_2 in het water/damp-grensvlak. De toename in de contacthoek wordt veroorzaakt door adsorptie van CO_2 aan het grensvlak. Het model voorspelt verder complete bevochtiging van het water/damp-grensvlak door een CO_2 laagje, in overeenstemming met het feit dat de condities niet ver van het kritische punt waren gekozen. Het model werd uitgebreid om de grensvlak- en bulkeigenschappen van het vloeibaar CO_2/surfactant/water-systeem te beschrijven en te voorspel-

len. De experimenteel bepaalde grensvlakspanningen tussen water en CO_2 in aanwezigheid van Igepal en de SF-SCF modelering van dit systeem toonden aan dat Igepal adsorbeert aan het water/vloeibaar CO_2 grensvlak. Het model voorspelt verder dat er omgekeerde micellen worden gevormd zowel bij de driefasencoexistentie (water/vloeibaar CO_2/CO_2 damp), waarvoor geldt dat $P/P_{\mathrm{sat}} = 1$, als voor $P/P_{\mathrm{sat}} > 1$. Met toenemende druk neemt de kritische omgekeerde-micelvormingsconcentratie (CRMC) toe en het aggregatiegetal bij de CRMC neemt af. Een hogere druk leidt namelijk tot een sterker stopmechanisme voor de vorming van omgekeerde micellen door een betere solvatatie van de staarten (sterker oplossend vermogen van CO_2). Behalve het fasengedrag in de bulk, geeft de aanwezigheid van de surfactant aanleiding tot interessante bevochtigingsverschijnselen aan het water/CO_2 damp-grensvlak. Als functie van de surfactantconcentratie werd een venster gevonden waarin partiële bevochtiging door CO_2 plaats vindt, terwijl daarbuiten volledige bevochtiging optreedt. Het fasengedrag zoals gevonden uit de modelberekeningen, werd gevalideerd door SAXS-experimenten (kleine-hoek röntgenverstrooiing). De SAXS-resultaten voor het Igepal/water/vloeibaar CO_2 systeem toonden de aanwezigheid van zelf-geassembleerde structuren overtuigend aan. De rol van water bij de vorming van deze structuren werd in kaart gebracht en de conclusie was dat water optreedt als mesogeen (promotor van de vorming van vloeibare kristallen) in mengsels van C_iEO_j-type surfactant en vloeibaar CO_2. Zonder water bevat het systeem in een bepaald gebied van surfactantconcentraties isotrope omgekeerde micellen (deze fase wordt vaak aangeduid als L_2) en met de toevoeging van water gaat L_2 over in een lamellaire fase, L_α. De periodieke afstand tussen de surfactantbilagen neemt toe met toenemend watergehalte. Op grond van deze resultaten werd een partieel fasendiagram geconstrueerd voor vloeibaar CO_2/ Igepal/water. Als we dit vergelijken met het fasendiagram voor n-hexaan/water/Igepal, is het duidelijk dat water in de twee systemen een zelfde rol speelt. Dit bevestigt dat n-hexaan een goed model is voor vloeibaar CO_2. Het SF-SCF model werd gebruikt om richtlijnen op te stellen voor het ontwerpen van surfactanten voor vloeibaar CO_2. Interessant hierbij is dat het stabiliteitsvenster voor omgekeerde micellen in vloeibaar CO_2

nogal klein is wat betreft de twee sleutelparameters in het model, namelijk de Flory-Hugginsparameters χ_{C3D} en χ_{OW}. Deze karakteriseren respectievelijk de wisselwerking tussen de methylgroepen in de surfactantstaart en CO_2 en die tussen de zuurstof in de kopgroep en water. De eerste interactieparameter domineert in het stopmechanisme voor micelvorming, terwijl de tweede de drijvende kracht voor dat proces bepaald. Het feit dat dit venster zo klein is, geeft in essentie de moeilijkheden weer om geschikte surfactanten te vinden voor vloeibaar CO_2. De ontwerpcriteria die voortkomen uit het model, zijn gebaseerd op de numerieke resultaten dat voor kleinere moleculen ($< C_{10}$) vertakking in de staart belangrijk is en voor langere moleculen (C_{10} en groter) CH_3-type wisselwerkingen belangrijker zijn dan vertakking. Behalve voor het gebruik van vloeibaar CO_2 in de textielreiniging, kan de kennis die vergaard is in dit project ten goede komen van andere milieuvriendelijke industriële processen waarbij vloeibaar CO_2 wordt gebruikt, zoals derde-generatie oliewinning en extractie van polaire stoffen. De uitkomsten van dit kunnen ook worden uitgebreid om de problemen aan te pakken die samenhangen met de geologische opslag van CO_2 onder hoge druk in diepe zoutwaterlagen.

List of publications

- S. Banerjee, S. Sutanto, J. M. Kleijn, M. J. E. van Roosmalen, G.-J. Witkamp, M. A. Cohen Stuart: *Colloidal Interactions in Liquid* CO_2 – *A Dry-Cleaning Perspective*, Adv. Colloid Interface Sci., 175, (2012), 11–24.
- S. Banerjee, P. Mulder, J. M. Kleijn and M. A. Cohen Stuart: *Effect of Surface Roughness and Softness on Water Capillary Adhesion in Apolar Media*, J. Phys. Chem. A, (2012), 116, 6481–6488.
- S. Banerjee, S. Sutanto, J. M. Kleijn and M. A. Cohen Stuart: *Towards Detergency in Liquid* CO_2 *- A Surfactant Formulation for Particle Release in an Apolar Medium*, Colloids Surf. A Physicochem. Eng. Asp., 415, (2012), 1–9.
- S. Banerjee, P. Mulder, J. M. Kleijn, and M. A. Cohen Stuart: *Ternary Fluid Mixture Confined Between Surfaces: Surface-Induced Phase Transition and Long-Range Oscillatory Forces*, Chem. Lett., (2012), 41, 1113–1115.
- S. Banerjee, E. Hassenklöver, J. M. Kleijn, M. A. Cohen Stuart and F. A. M. Leermakers: *Interfacial Tension and Wettability in Water - Carbon Dioxide Systems: Experiments and Self-consistent Field Modeling*, J. Phys. Chem. B (2013), 117, 8524–8535.
- S. Banerjee, J. M. Kleijn, M. A. Cohen Stuart and F. A. M. Leermakers: *A Liquid* CO_2 *- Compatible Hydrocarbon Surfactant: Experiment and Modeling* , J. Phys. Chem. Chem. Phys. Accepted, 2013.
- S. Banerjee, D. H. Merino, G. Portale, J. M. Kleijn, and M. A. Cohen Stuart: *Is Igepal CA520 Soluble in Liquid* CO_2*? And Does it Form Mesophases?* In preparation.

Acknowledgement

Over these four years I have met some wonderful people leaving indelible marks in my life. This page is dedicated to them. I will start at the very beginning when I came to FYSKO from Manchester.

There is surely one person in this world, without whose persuasion, I would have surely gone to Cambridge to earn my PhD degree and that person is Gordon. When I got the offer from Christ College, Cambridge, I thought this was it. Names like Charles Darwin, John Milton and J. C. Bose whizzed past my thoughts. Well, leaving that option was surely difficult for me, but now I hardly have any regret because of the training, exposure and freedom I have been entrusted with at FYSKO.

Martien, you, pushed my bike (I was on it too) on my very first bike trip for quite some stretch while I was still trying to understand why am I doing this?! *Dank u* for all those rides to Delft, Twente and other places by your car. It would be unfair if I don't thank you for encouraging me to participate in the AkzoNobel young scientist contest and putting me up as one of the organizers of the PhD trip of 2011. Both gave me a gamut of exposure. I would also like to thank you for the Grenoble contact for the high pressure SAXS. While working with you I realized that you are gifted with an ability of explaining complex things in a very lucid and simple language. Another striking thing about you is that no matter how busy you are, you are right on time to give your comments back on manuscripts. Every Fyskolese knows that you are a great speaker; we know that you are a good listener too. Thanks.

Mieke, you came to collect me from Ede-Wageningen station by your car

on a cold and rainy day of March 2009. You were a great help in giving us information about the possible MSc courses that Surender did afterwards. We had some great time together in Basel, Japan, Hamburg and Den Haag. Thanks for those *candies*! I liked the freedom and independence that you bestowed on me throughout these four years. You are very approachable, I never needed an appointment to talk to you. Your questions on my articles always had been very subtle and difficult to tackle. I would be glad if I can one day become a reviewer as critical as you. Thanks.

Frans, though your addition to the project happened at the fag end but that we had a fruitful collaboration is due to your relentless enthusiasm and patience. Thanks for agreeing to the crazy idea of having you as one of my Para nymphs. I will never forget our nocturnal booze-hunting car ride during our PhD trip in US. The dinner parties and the very interesting thread making exercise using the indigenous Gandhian charkha can never be erased from my memory. Thanks to Roelfike for putting up with all those craziness. Frans, you are a great teacher with a commitment to nurture students with thinking minds. Teachers like you not only work with students but also rear them. Thanks.

I would not have met Pieter had I not gone to that *don't tell your mom* party one chilly night at Junushoff. And the rest is history. I thank you for your tremendous patience with the QNM-AFM and the notorious hexane system. Leonie, Carel, Quirijn and Tim you guys were so full of enthusiasm that we could achieve much more than what I initially thought of. Among other things I would like to thank you for coming up with a good report in such a short time that when I wanted to write a paper out of it I could do that with ease. Yuval, I used to enjoy the long email exchanges between us. I hope you are having a memorable time in Israel. I am still at awe that you could actually speak that fast.

Daniel, because of you, the tiring Grenoble days became tolerable. The time that you spent helping me with the experiments is also unforgettable; we were almost living at FYSKO for seven long days. Unfortunately we could not make many things working but we could not have given more of ourselves

to make things better. I would also like to thank Giuseppe Portale for his involvement in the project.

Eveline, my Hamburg days would have been much more difficult without you. How could I ever forget you accompanying me in the doctor's chamber during the freezing cold winter of 2012? My solitary days in the Hamburg lab used to come alive with your help. Thanks for arranging so many things for me during that one month. Philip, in the supercritical conference in Den Haag I was carrying not even a poster but I walked out of it with an extremely fruitful collaboration. In fact, the experiments that I did in your lab paved the way for the numerical modeling that I did later. You were very co-operative together with Prof. Eggers for letting me do those studies using the facilities of TUHH.

Thao, Lennart, Harke, Junyou, Dmitry, Monika, Emilia, Yunus, Armando, Liyakat, Huanhuan, the entire batch of 2009, we always shared a special bond between us. The experience during our 2011 PhD trip was something special. Thanks for being such wonderful colleagues and friends. The mention of the PhD trip brings some other people in the scene, particularly Yuan and Evan. Although the hostel in Singapore was the worst among the three places that we stayed in, but the warmth of togetherness compensated the unavailability of comfort. How can I ever forget the white mask, the belly dance at midnight and the mad discussion that you, Thao and me had during those days and nights. Yuan you are the reason I ate jelly fish head and have a bag full of *Lajiao mian* at home. Thanks. Evan thanks for turning the T-shirt idea into a reality and picking me up quite late while I was returning from my cousins' place in Singapore. Thanks also for organizing the sailing trip in Grow. Harke and Lennart we are like a nuclear family. It is hard to imagine that such diverse personalities can coexist with peace in a single room. You guys never complained about me keeping a tropical micro-climate inside our office. I have many stories to share with my future grandchildren because of you two. Dmitry I enjoyed the philosophical discussion that we had while doing confocal. There's no one to greet me with *lal salaam* at FYSKO these days. I got enriched with Pascal's passion about gaming. Thanks for helping

me in taking my very first AFM image. Christine (Henry) thanks for all those books and the lawn tennis racket. Katarzyna, thanks for the *Zubrówka* with the grass and agreeing to become my Para nymph. Kathelijne, Liyakat and Emilia because of you guys I now hold a record of being para nymph the most number of times. Thanks. Gosia & Gosia, Maria, Hande, Helen, Nadia, Celine, Sabine, Stevia, Diane, Jeroen, Rahim, Jacob, Juan & Ran, Rui, Christian, Jacob, Natalia, Maarten, Merve, Inge, Antsje, Cecilia, Johan, Wiebe and Saskia and Petya each one of you is a short story in my life. Kamuran thanks for dropping me home in your car when I fell down from my bike.

Renko and Hanneke I loved the experience of introducing my music to the Dutch kids. Thanks.

Remco you had been a great help on many occasions. Probably you are the only one, other than Daniel, who is aware of the fun with the high pressure measurements. Thanks. Josie, thanks for sharing all those obnoxiously funny jokes and taking care of things even if those required being awake at wee hours. You are a breath of fresh air in the department and no matter what, I just love your hair colour. Mara, my *loove*, thanks for taking the burden of looking nice on behalf of the whole nerdy crowd. Thanks for being patient and catering to our last minute urgent orders. Hope Josie, you and I will continue to have our mindless laughter fits in the coming year. Anita thanks for the money matters and the *girls' night out*s. Roelfina, you were a great help during the initial unsettling days. *Bedankt*. Ronald, apart from the help with the computers thanks for enlightening me about the lifestyles of chickens. Anton thanks for your very polite yet persistent requests of signing on the attendance book after 17:30. Thanks for those *candies* that you had behind the closed door and shared with us. I was also impressed with your response when you found me and Surender inside your room unexpectedly.....Bert, thanks for maintaining the candy cabinet, helping with the reimbursement claims, filling out the time-writing sheet a couple of times and bringing the earrings from Ethiopia.

Herman and Willem, I enjoyed our brief encounters at and outside (e.g.

Wageningen city centre) FYSKO. Paolo I still cherish those table tennis games that Huanhuan, Thao, you and I used to play at the basement of the microbiology department. I quite liked your bowling (cricket) style too. Hans, I always enjoyed your anecdotes. I also like you asking me *are you happy*? Thanks for keeping the FICS limited to five volumes only. Peter (Barneveld), from you I learnt *silence is golden*.

Geo & Sushmita and Johnson, Germany came alive with you all. Saurabh & Shruti, Nidhi & Manohar and Awan thanks for not letting me miss Desi food in Europe. Sidhu, Saurabh, Satish, Umesh and Nagendra thanks for those cricketing evenings. Sidhu you are a true monk, always smiling and willing to help. Satish, thanks for the MM2 force field calculation and Sidhu, thanks for your help with the IRRAS.

Andy (Li Ran), you did all the work to take me to Wimbledon 2010. I could watch, because of you, Sharapova howling live on Court no. 1 and the longest match in the history of Wimbledon, the Mahut-Isner epic, reaching a decision.

Sur, we never believed in what Susan Sontag said on marriage: "*is an institution committed to the dulling of feelings*"! It must have been quite a difficult task to put up with a domineering, opinionated, feminist, and omnivorous yet Gandhian and Tagorean wife but you are doing it with style. Thanks for all your love, care, support and encouragement. You are the best thing that has ever happened to me.

Maa, buba thanks for giving me the right shoes and agreeing to the idea of leaving a secure job and jumping into the world of uncertainties. I never met a tougher teacher than you, Maa, in my life. Buba, you are the one who instilled "question everything" mind-set in me. And then I bow to rest of my family members with whom I share a part of my heart.

Thanks to all those who call(ed) me "*Suomi*".

About the author

Soumi Banerjee was born on 24th of September, 1977 in Kolkata, India. She completed her secondary education from a special Hindu missionary discipline, RKSM Sister Nivedita Girls' School. In both secondary and higher secondary education she holds national scholarships. She studied B.Sc. (Honours) in Chemistry at Bethune College, Calcutta University. Later she did B. Tech. in Polymer Science and Technology from Science College, Calcutta University. In 2004 she joined Unilever Research India as a research associate. After working in the home and personal care division of Unilever research for two and a half years, she joined Haldia Petrochemicals Ltd. as an assistant manager and worked in their application research and development centre on polyolefins. In 2008 she went to the University of Manchester for the degree of M.Phil. in Colloids, Crystals, Interfaces and Materials. In 2009 she joined the Laboratory of Physical Chemistry and Colloid Science as a PhD student to work on colloids in apolar media with Prof. Martien A. Cohen Stuart and Dr J. Mieke Kleijn. She was the recipient of the AkzoNobel Young Scientist Award in 2010. At present, She is doing a L'Oréal sponsored post-doc with Prof. Frans Leermakers on polymer - surfactant interactions using self-consistent field modeling. Her other interests are music, reading, sports and gastronomy.

Netherlands Research School for the
Socio-Economic and Natural Sciences of the Environment

C E R T I F I C A T E

The Netherlands Research School for the
Socio-Economic and Natural Sciences of the Environment
(SENSE), declares that

Soumi Banerjee

born on 24 September 1977 in Kolkata, India

has successfully fulfilled all requirements of the
Educational Programme of SENSE.

Wageningen, 2 October 2013

the Chairman of the SENSE board

Prof. dr. Rik Leemans

the SENSE Director of Education

Dr. Ad van Dommelen

The SENSE Research School has been accredited by the Royal Netherlands Academy of Arts and Sciences (KNAW)

KONINKLIJKE NEDERLANDSE
AKADEMIE VAN WETENSCHAPPEN

The SENSE Research School declares that **Ms. Soumi Banerjee** has successfully fulfilled all requirements of the Educational PhD Programme of SENSE with a work load of 56 ECTS, including the following activities:

SENSE PhD Courses

- Environmental Research in Context
- Research Context Activity: Co-organizing PhD trip South East Asia for Laboratory of Physical Chemistry and Colloid Science, 12-28 February 2011, and Compiling Abstract Book
- Imaging science

Other PhD and Advanced MSc Courses

- Han-sur-Lesse Winterschool 2010
- Advance Soft Matter
- Statistical Thermodynamics
- PhD competence assessment

Management and Didactic Skills Training

- Supervising one MSc and one BSc thesis
- Supervising group work for the *Bachelor Completion Project*
- Practical assistant for the BSc course *General Chemistry for Life Sciences*

External training at a foreign research institute

- X-ray scattering at high pressure, ESRF, July 2012, Grenoble, France,
- High pressure experimentation 2, Technical University of Hamburg, February 2012, Harburg, Germany

Oral Presentations

- *Capillary Condensation in Apolar Media: Kinetics of Condensation and Quantitative Nano-mechanical Analysis by AFM.* IACIS 2012, 14-18 May 2012, Sendai, Japan
- *Meeting Tomorrow's Challenges through Science & Innovation.* Akzo Nobel Science Award, 7-8 October 2010, Haarlem
- *Surface Forces in Apolar Media.* PhD trip 2011, NUS, 14 February 2011, Singapore
- *Surface Forces and Self-assembly in Apolar Media.* Institute for Complex Molecular Systems, TU Eindhoven, 23 May 2012, Eindhoven
- *Colloids in Ultralow Dielectric Media.* AkzoNobel visit, 15 January 2013, Slough, UK
- *Surface Forces in Ultralow Dielectric Media.* PhD trip 2013, Bruker, 10 February 2013, San Francisco, USA

SENSE Coordinator PhD Education

Drs. Serge Stalpers

Enabling new technology

This research is supported by the Dutch Technology Foundation STW, which is the applied science division of the Dutch Scientic Organisation NWO, and the Technology Programme of the Ministry of Economic Affairs.

Cover design: Soumi Banerjee & Surender Dhayal
Software Utility: Harke Pera
Creative consultant: Shubhojit Sengupta

Printed by Wöhrmann Print Service, Zutphen